2011

Production and preservation of the Arctic sea ice diatom biomarker IP25

Brown, Thomas

PRODUCTION AND PRESERVATION OF THE ARCTIC SEA ICE DIATOM BIOMARKER IP25

THOMAS A. BROWN

PhD 2011

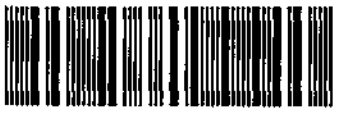

Production and preservation of the Arctic sea ice diatom biomarker IP_{25}

By

Thomas A. Brown

A thesis submitted to the University of Plymouth in partial fulfilment for the degree of:

DOCTOR OF PHILOSOPHY

Petroleum and Environmental Geochemistry Group

School of Geography, Earth and Environmental Sciences

University of Plymouth

February 2011

Production and preservation of the Arctic sea ice diatom biomarker IP_{25}

By
Thomas A. Brown

ABSTRACT

The presence of the sea ice biomarker IP_{25} in Arctic marine sediments has previously been used as a proxy measure of past sea ice conditions in the Arctic. Although the sea ice diatom origin of IP_{25} was established previously, the nature of its production within sea ice, along with its transport through the water column to underlying sediments and its short-term preservation therein, had not been investigated in any significant detail.

Variations in the concentration of the sea ice diatom biomarker IP_{25}, were measured in sea ice collected from the eastern Beaufort Sea and Amundsen Gulf from January to June 2008. Temporal and vertical changes in IP_{25} concentrations were compared against other established indicators of sea ice algal production to determine, for the first time, that approximately 90% of the total sea ice IP_{25} accumulation occurred coincident with the ice algal bloom period. It was further established that IP_{25} biosynthesis was restricted, by sea ice porosity, to within the lower few centimetres of the sea ice and specifically to where brine volume fractions were >5%.

Concentration differences of IP_{25} between sea ice and filtered seawater samples were also compared with those of established lipid indicators of algal production to estimate the dispersion of these lipids following seasonal sea ice melt. The largest concentration differences between sea ice and seawater samples were observed for IP_{25} and some other HBIs, consistent with a sea ice origin, while concentrations of fatty acids and sterols suggested contributions from both sea ice and phytoplankton. A novel analysis of a range of macrofaunal species revealed the presence of IP_{25} and other HBIs, with distributions somewhat resembling those observed in sea ice but more closely reflecting distributions of HBIs measured in sediments. As such, it is hypothesised that IP_{25} and HBI distributions in macrofaunal species reflect those of the sediments in which they live. The presence of IP_{25} and HBIs in macrofaunal species revealed, for the first time, a significant potential for biological cycling and storage of IP_{25} and other HBIs in the Arctic resulting from exposure during transport of the biomarker between sea ice and sediment. The observed presence of IP_{25} in 75% of the specimens investigated has presented important evidence for the potential of IP_{25} to act as a tracer of Arctic sea ice diet in the marine food web.

Measurement of the downcore profiles of IP_{25} in shallow marine sediments alongside other biogeochemical parameters provided new evidence for the early diagenesis of this biomarker. Statistical correlations between some IP_{25} and Mn/Ti profiles (Station 405b; $r = 0.89$), that aid determination of the oxygen penetration depth, provided novel evidence for the partial degradation of IP_{25} (and other HBIs) in the upper sediment sections considered to be oxic. As such, it is suggested here, for the first time, that reactions under oxic conditions could be responsible for degradation of HBIs in some Arctic marine sediments, with the supply of organic carbon influential on the depth of oxygen penetration.

The observations recorded in this thesis have therefore offered a much greater understanding of the concentration and distribution of IP_{25} and related lipids in a wide range of Arctic environments including sea ice, seawater, macrofauna and sediments, than was previously known. Since in most cases these observations represent the first of their kind, it is anticipated that the work carried out here will play an important role, forming the foundation of many important future studies.

Table of Contents

LIST OF FIGURES

LIST OF TABLES

ACKNOWLEDGEMENTS

I would like to thank my supervisors, Professor Simon Belt, Dr Guillaume Massé and Dr Xavier Crosta for their part in setting up the groundwork for this thesis and their invaluable patience, support and advice throughout.

I am especially grateful for the support and friendship of Dr Lindsay Vare in getting me started on this mammoth task and also Dr Paul Sutton for constant technical support (even when you were really busy!).

I would also like to thank the rest of PEGG, the school technical staff; Andy, Andrew, Claire and Ian and Graduate School administration; Debbie, for support and encouragement throughout.

I am also grateful to Dr Ian Bull and Mr James Williams at the Bristol University Organic Geochemistry Unit for having the patience to not 'fix' the GC/IRM/MS with a sledge hammer.

Considerable thanks is also owed to the scientists and crew onboard the *CCGS Amundsen* during my visit in 2008 for being so incredibly helpful and supportive of my needs.

On a more personal note, I wish to thank Dr Tim Hooker and Professor Frank Round for their unintentional inspiration of a young boy that has led to me achieving the unthinkable.

Finally, I cannot imagine being where I am now without the love and support of my family and of my very understanding wife, Katie. Thank you so much, you could never begin to realise how important you are to me.

AUTHOR'S DECLARATION

At no time during the registration for the degree of Doctor of Philosophy has the author been registered for any other University award.

This study was financed with the aid of a research studentship from the Natural Environmental Research Council (NERC)

A programme of advanced study was carried out, with relevant scientific seminars and conferences attended, at which work was often presented

Word count, 72778

Signed . . . . . .

Thomas A. Brown

Date. February 2011

PUBLICATIONS

Brown, T., Belt. S., Mundy, C., Philippe, B., Massé, G., Poulin, M. and Gosselin, M. (2011) Temporal and spatial growth trends of individual biomarkers from sea ice diatoms. *Polar Biology*. DOI: 10.1007/s00300-00010-00942-00305 (Chapters 4 & 5).

Brown, T., Belt, S. Detection of the sea ice diatom biomarker IP_{25} in Arctic macrofauna: A potential indicator of sea ice diatom diet. *Polar Biology*. (In preparation). (Chapter 6).

Brown, T., Belt, S., Isolation, purification and quantification of the chemical sea ice proxy IP_{25} from Arctic marine sediments. *Limnology and Oceanography: Methods*. (Submitted). (Chapter 7).

PRESENTATIONS AND CONFERENCES ATTENDED

2nd Annual Biogeochemistry Centre Conference University of Plymouth, Plymouth, U.K , 17 December 2010 Oral presentation. "IP_{25}. Problem or Progression".

21st Annual Meeting of the British Organic Geochemical Society, Manchester, **UK**, 6th - 7th July 2010. Oral presentation: "Moving Forwards by Looking Backwards: IP_{25}, the Next Instalment".

6th BEACh/ 1st Annual Biochemistry Research Centre Conference. Plymouth University, Plymouth, **UK**. 14th December 2009. Oral presentation: "IP_{25}. The specific sea ice indicator"

UK Sea Ice Group National Oceanographic Centre, Southampton, **UK**, 27th November 2009 Oral presentation: "IP_{25}: The specific sea ice indicator"

U K Sea Ice Group. Met Office, Exeter, **UK**, 7th – 8th September 2009. Oral presentation: "IP_{25}: The Specific Sea Ice Indicator".

20th Annual Meeting of the British Organic Geochemical Society, Bristol, **UK**, 7th – 8th July 2009. Oral presentation: "IP_{25}: The Specific Sea Ice Indicator" Awarded oral presentation prize

Gordon Research Conference, Polar Marine Science - Beyond IPY: Crossing Boundaries, Lucca (Barga), **Italy**. 15th – 20th March 2009. Poster presentation. "The IP_{25} Sea Ice Indicator. When is it Produced, . Where is it Preserved?"

Seminar, *CCGS* Amundsen, Canadian Arctic, **Canada**, 20th March 2008. Oral presentation: "Investigations into Novel Chemical Markers for Past Sea Ice".

Seminar, Tromsø, **Norway**, 22nd January 2008. Oral presentation. "Investigations into Novel Chemical Markers for Past Sea Ice".

Arctic Frontiers, Tromsø, **Norway**, 21st – 27th January 2008. Poster presentation: "Novel Highly Branched Isoprenoid Biomarkers as Indicators of Sea-Ice Diatoms: Implications for Historical Sea-Ice Records and Future Predictions".

LIST OF COMMON ABBREVIATIONS

CPI – Carbon preference index
EPS – Exopolymeric substances
GC – Gas chromatography
GC/MS – Gas chromatography – mass spectrometry
GC/IRM/MS – Gas chromatography – isotope ratio monitoring – mass spectrometry
HBI – Highly branched isoprenoid
HPLC – High performance liquid chromatography
ICP-MS – Induction coupled plasma – mass spectrometry
IP_{25} – C_{25} highly branched isoprenoid monoene
LM – Light microscopy
NSL – Non saponifiable lipid
NLR – Nonspecific lipid region
PAR – Photosynthetically active radiation
PCA – Principal components analysis
PLR – Planktonic lipid region
SEM – Scanning electron microscopy
SILR – Sea ice lipid region
SIM – Selective ion monitoring
TIC – Total ion current
TOC – Total organic carbon
TOE – Total organic extract

GLOSSARY OF TERMS

Benthic diatom - Non-planktonic diatom that lives attached to or resting on any solid substrate.

Centric diatom – Radially symmetrical diatom, usually planktonic diatoms with thin siliceous frustules, often with protrusions to increase their surface area. Commonly existing in long filamentous chains

Cod-end – Narrow end of a net that collects and concentrates material of interest.

Congelation ice – Sea surface ice which forms from congealing ice crystals in the upper water column in calm sea conditions, often coincident with a near coastal proximity.

Epontic - Organisms which inhabit both sea ice and the water column immediately beneath the sea ice.

Frazil ice – Sea ice that forms from a collection of randomly positioned plates of ice about 1 mm in diameter, normally forming in turbulent waters away from sheltered coastal areas

Lead flaw – An opening of water between drift ice and landfast ice

Pennate diatom – Bilaterally symmetrical diatom, usually benthic with siliceous frustules often more dense than planktonic varieties with fewer/no cellular protrusions

Polynya – Area of open water surrounded by sea ice that appears each year that usually remains free from ice.

Sympagic – An environment that consists of ice

CHAPTER ONE

1 Introduction

1.1 Climate change

Climate change is a major focus of scientific research. Significant deviation in the Earth's climate, in response to both natural and anthropogenic changes, such as solar radiation, ocean circulation and greenhouse gases, are being constantly monitored. Global warming itself, is, closely linked to decreasing polar sea ice in the Arctic (Polyak *et al.*, 2010). Scientists have become increasingly aware of the importance and contribution of polar oceans and the part they play in driving the Earth's climate (Stoll, 2006). The annual variation of polar sea ice extent influences not only the exchange, but also the distribution of moisture and solar energy (Dieckmann *et al.*, 2010). In addition, concentrated seasonal inputs of dense brine, following sea ice formation, contribute to driving ocean circulation (Dieckmann *et al.*, 2010). Of particular importance in exerting controls on energy distribution and circulation is the high albedo of ice and snow. The higher albedo of ice-covered water, in contrast to that of ice-free water, is capable of generating a greater variation in the degree of solar energy reflected than for other regions of the Earth (Robock, 1980). Therefore it is evident, that in order to better understand solar energy transfer and improve present and future climate variability predictions, the capacity to rapidly determine past sea ice extent and the associated climatic response is crucial.

The significance of global climate change is now better understood than ever before. The recent introduction of satellite observations (since 1979) is largely responsible for this increase in awareness. Satellites enable graphical representations to extend the

availability of vast arrays of meteorological and hydrological data, along with highly specific scientific data such as chlorophyll concentrations, atmospheric aerosol, irradiance and light attenuation (NASA, 2009), into the public forum High resolution data, such as up-to–the-day sea ice area and extent (Arctic-ROOS, 2009) is also highly valuable for operational decisions within organisations such as the coastguard and shipping industry. However, use of these short term data is clearly constrained in terms of historical climate monitoring prior to 1979. While high resolution data is preferable in generating predictions of future climate change, it is essential to also account for historical fluctuations to ensure, for example, that cyclic trends in variables, such as temperature, are exposed. One example of this is evidenced in the 'Hockey–stick' model (Mann *et al*, 1998) which depicts rapid rises in temperature and sea level over the last ca 200 years based on observation of just 1000 years. Comparison of the 'Hockey-stick' model against historical, glacial and inter-glacial cycles, exposes the importance of scale, where the latter demonstrates numerous climate fluctuations, when considering the significance of observed trends. Analysis of extended climate records employing more traditional techniques, in addition to modern high resolution techniques, is therefore essential in establishing the significance of these recent observations

For example, Mayewski and co-workers investigated published data from the analysis of ca. 50 globally distributed sediment cores (Mayewski *et al.*, 2004). Collectively, these cores provided data based on a wide range of proxy techniques including analysis of volcanic aerosols, glacial fluctuations, greenhouse gases and oxygen and carbon isotopes from glacial and cosmogenic sources. Geological minerals and biological transfer functions of diatoms, pollen and ostracods were also included in some of the analysis. Interpretation of the data led to claims of six Northern Hemisphere rapid climate fluctuations within the Holocene (Mayewski *et al*, 2004). Such observations

question the significance of anthropogenic climate forcing observed in recent data, whilst simultaneously emphasising the need for a reliable long term approach to establishing historical climate reconstructions.

1.2 Measures of past climate change

The inability to directly observe historical climate, beyond the limits of modern techniques, demands the use of indirect observations and measurements of a range of 'proxies' (Haslett, 2002b). Examination of physical artefacts as relics of palaeoenvironments enables scientists to predict the physical, chemical and climatic conditions of the past. Some of the most common approaches employed in high latitude regions involve the collection, separation and analysis of micropalaeontological specimens including, for example, foraminifera, radiolarians, dinoflagellates and diatoms.

Foraminifera are single-celled planktonic and benthic marine protists that construct a test (shell) that is often capable of prolonged sedimentary preservation (Murray, 2002). The relative distribution of species abundance, planktonic/benthic ratio or dissolution of foraminifera can be used to infer the palaeo-sea ice conditions of a particular region (Darby *et al.*, 1997; Smart, 2002; Schell *et al.*, 2008; Blasco *et al.*, 2009). Although foraminifera survive in a variety of habitats (as plankton and or in sediments), rather than sea ice itself, sea ice based assumptions may still be achievable (Schell *et al.*, 2008). For example, sea ice can retard the growth of planktonic species, adjusting the planktic/benthic distribution. Additionally, mathematical transfer functions can relate modern species distributions with environmental parameters of the modern day, enabling palaeo-sea conditions, such as sea surface temperature, to be determined (Smart, 2002). One 15 kyr palaeo sea ice reconstruction of the Mackenzie-Beaufort Sea

Slope and Amundsen Gulf adopted a variety of foraminiferal techniques, including increased dissolution, resulting from low sedimentation rates, as an indicator of sea ice conditions. In addition, identification of individual species and planktonic/benthic ratios were used to determine periods of open water and sea ice cover over the Holocene, concluding that, a recent period of open water with fluctuating periods of perennial and seasonal sea ice leading back to the last glacial maximum at ca 11.5 kyr existed (Blasco *et al*, 2009). However, the notion of calcareous dissolution as a reliable indication of perennial sea ice conditions has been disputed, since lower Arctic water temperatures can result in the undersaturation of water with regards to carbonate dissolution (Mudie *et al*, 2001a).

Some other useful microfossil indicators are studied in similar ways to foraminifera. Radiolarians are often incorporated into ecological studies involving foraminifera on the basis of their similarities (Haslett, 2002a) and are separated by classification based mainly on the siliceous opaline test of radiolaria *versus* the calcium carbonate test of foraminifera While radiolaria inhabit the water column from depths of thousands of metres to the surface (Yamashita *et al.*, 2002; Sakai *et al*, 2003), the vast number of extant species (ca. 500) reflects the niche-specific nature of these useful microfossils (Casey *et al.*, 1990), making ecological interpretations based on the faunal assemblage reasonably reliable. Adopting both foraminifera and radiolaria in palaeoenvironmental reconstruction is therefore considered beneficial, especially in terms of preservation; where calcium carbonate may dissolve, siliceous opal may persist The co-analysis of radiolaria and foraminifera has been carried out to determine the biostratigraphy, paleoenvironment and paleogeographic implications of the Queen Charlotte Islands, British Columbia, Canada (Kottachchi *et al.*, 2002). It was found that significant shifts in foraminiferal assemblages relating to sea level changes were closely represented in the radiolaria Radiolarians are commonly used as sea surface temperature indicators

(Haslett, 2002a), with a variety of statistical techniques available, such as recurrent group analysis (Nigrini, 1970) and factor analysis (Molina-Cruz, 1977), along with transfer functions, used to obtain absolute sea surface temperatures. Unlike some other sea surface temperature indicator species (e.g. coccolithophores), radiolaria are capable of representing sub-sea ice conditions (Morley *et al.*, 1984) with a representative assemblage reaffirming their usefulness in the reconstruction of sea ice conditions.

Other planktonic indicators of sea surface temperature include the dinoflagellates (Molina-Cruz, 1977; Matthiessen *et al.*, 1997; de Vernal *et al.*, 2005), where enumeration and identification of species is again used for temperature reconstruction (Mudie *et al.*, 2001a).

Dinoflagellates are commonly occurring motile cells, typically 20 – 200 μm in length and are capable of moving vertically in the water column to adjust for changes in temperature and salinity (Mudie *et al.*, 2001b). Approximately 10 – 15% of dinoflagellates produce a resting spore (cyst) capable of persisting in the fossil record (Rochon, 2009). However, the distribution and life cycles of Arctic species of dinoflagellate is complex, making palaeoenvironmental assumptions difficult. Reconstruction is usually governed by resting spore distribution and carried out in addition to established microfossil and geochemical reconstructions (Schell *et al.*, 2008). Studies in Antarctica suggest a degree of sea ice specificity with observation of some dinoflagellate cysts within sea ice (Kurt *et al.*, 1992), albeit in low abundance (10^3 – 10^4 cells L^{-1}). Further, de Vernal and co-workers established a quantitative palaeoceanographic reconstruction in the Arctic, sub-Arctic and northern North Atlantic Seas based on the dinoflagellate cysts found at over 600 sites (de Vernal *et al.*, 2001). While a number of limitations are discussed, such as morphological variation, large interannual variation and sparse hydrological data, reconstructions of a range of sea-surface parameters, including sea ice cover were proposed.

Where regions experiencing sea ice are concerned, diatoms (unicellular photosynthetic algae ranging, in size, from ca. 1 – 1000 μm) are considered the most specific microfossil (Poulin, 1990b), having a specific sea ice assemblage present in the Arctic. The ubiquitous nature of diatoms, in addition to their fairly robust siliceous opal frustules (for some species) and vast number of species (ca 100,000 extant in ca. 200 genera; Round *et al.*, 1990), provides scientists with a biological indicator organism for almost any marine or aquatic environment. Like foraminifera, diatoms consist of planktonic (centric) and benthic (pennate) varieties, dependent on their habitat. The sea ice habitat contains between 25 and almost 200 diatom species (Melnikov, 1997) with an 89% dominance of pennate varieties; within which Naviculoid varieties are commonly most abundant. Within the pennate assemblage, some species are considered ice endemic, existing only within Arctic sea ice, making their presence in the sedimentary fossil record good evidence of previous sea ice cover. The ability to distinguish between sea ice diatoms and planktonic species in sediments has been exploited previously for palaeo-sea ice reconstructions (e.g. Poulin, 1990b; Smith, 2002; Ruhland *et al.*, 2003; Brown, 2007). For example, transfer functions derived from the fossil diatom assemblage revealed an unstable Holocene climate (Koc *et al.*, 2004). Statistical analysis (factor analysis) identified eight distinctive diatom assemblages in diatoms isolated from four northern Atlantic sediment cores from which sea surface temperature was reconstructed, indicating historical shifts in ocean currents within the region.

Like all proxies, each of the microfossil approaches, e.g. foraminifera, dinoflagellate and diatom, possess caveats that share a common limitation; expertise. The reliable application of each microfossil-based proxy analysis relies, initially and heavily, on the correct identification of individual microscopic species and the ability to correctly

classify these, an ability of which increasingly few people are capable (Round, 2008). In addition, such microfossil methods require complex preparatory steps to isolate the microorganisms from various sediment matrices prior to observation. If this is not carried out correctly, it can lead to unreliable data, perhaps due to procedural losses through discrimination, for example. These limitations make the availability of more rapid, robust analytical approaches to palaeo sea ice reconstruction more desirable.

1.3 Biomarkers in marine sediments

Biomarkers are molecular fossils of historical living organisms (Eglinton *et al.*, 1967). The chemical composition of an organism often reflects the conditions in which it lives, so the individual molecules of some marine organisms can represent changes in their habitat or environment in various ways. For example, deficient carbon replenishment in a closed, or semi-closed, habitat can affect the carbon isotope distribution in lipids through biosynthesis (Gibson *et al.*, 1999; Kennedy *et al.*, 2002), while temperature can control the degree of unsaturation in the lipids of some organisms (Rowland *et al.*, 2001b). Measurement of these often distinctive chemical signatures is generally rapid, when compared to micropalaeontological approaches, employing established laboratory techniques such as solvent extractions and chromatographic techniques, familiar to many geochemists. As a result, numerous biomarker-based methods now exist for the detection of palaeo-sea surface conditions (Killops *et al.*, 1993; Peters *et al.*, 2007; Eglinton *et al.*, 2008; Rueda *et al.*, 2009).

For example, an unsaturation index (U^{K}_{37}) derived from the alkenone (C_{37} – C_{39}) composition of coccolithophores, reflects mean sea surface temperatures (Brassell *et al.*, 1986). The index, comprising comparison of di- and tri-unsaturated homologues, enables the determination of sea surface temperatures. However, the source organisms,

commonly *Emmiliania huxleyi*, favour temperate conditions in the range 8 – 25°C (Prahl *et al*, 1987; Prahl *et al*, 1988), while Arctic sea surface temperatures are typically colder (< 5°C) making the index better suited to warmer regions.

Sea surface temperature can also be determined by application of the TEX_{86} index, derived from the glycerol dialkyl glycerol tetraether (GDGT) composition of membrane lipids of archaea and bacteria (Rueda *et al*, 2009). TEX_{86} is based on the number of alkyl rings in tetraethers containing 86 carbon atoms; the number of rings formed responds to changes in temperature as the source organisms adapt to maintain cell membrane fluidity (Wuchter *et al.*, 2004).

GDGTs can also be used to determine the relative inputs, through time, of fluvial soil organic matter in marine environments (Schouten *et al.*, 2004, Rueda *et al*, 2009) This, so-called BIT index is based on a comparison of the proportion of branched GDGTs, derived from anaerobic bacteria living in soils and peat bogs, to quantify an unbranched marine GDGT, crenarchaeol.

In terms of more commonly occurring biomarkers, *n*-alkanes, fatty acids and sterols represent a significant proportion of the lipid content of many marine sediments. However, the ubiquity of these lipids is also a drawback, reducing their ability to act as specific biomarker indicators. From the analysis of the *n*-alkanes for example, the CPI, or carbon preference index, can be derived by measuring the different chain lengths of *n*-alkanes in marine sediments (Bray *et al*, 1961). Comparison of odd to even long chain ($nC_{25} - nC_{34}$) *n*-alkanes, formed by decarboxylation of the even-numbered fatty acids in terrestrial plants, is considered a measure of terrestrial sedimentary input in the marine environment (Riederer *et al.*, 2006).

Similarly, sterols may be derived from a variety of source organisms in the marine environment (Volkman, 1986). While phytosterols and zoosterols are reasonably distinct, the precise origins of individual sterols can often be difficult to ascribe.

Regardless, the relative abundances of different sterols can be used to indicate the relative inputs of terrestrial, planktonic and animal sources in marine sediments (Wen-Yen *et al.*, 1976; Volkman, 1986; Barrett *et al.*, 1995).

In summary, a range of biomarker techniques are available for reconstructing palaeo-sea temperatures, but very few of these are capable of reliably determining palaeo-sea ice conditions.

1.4 Highly branched isoprenoid alkenes and the IP_{25} biomarker

Highly branched isoprenoid (HBI) alkenes are ubiquitous biomarkers found in a wide range of marine sediments (Robson *et al.*, 1986; Rowland *et al.*, 1990; Belt *et al.*, 2000a; Sinninghe Damsté *et al.*, 2004) and occur mainly as C_{25} and C_{30} analogues, commonly exhibiting between two and six double bonds (Rowland *et al.*, 1990; Volkman *et al.*, 1994; Wraige *et al.*, 1997; Belt *et al.*, 2000a; Belt *et al.*, 2001b; Belt *et al.*, 2001d; Grossi *et al.*, 2004). In recent years, various structures and source organisms (all diatoms) have been reported (Volkman *et al.*, 1994; Belt *et al.*, 2001c; Grossi *et al.*, 2004) along with biosynthetic pathway exploration (Massé *et al.*, 2004b), reactivity studies (Belt *et al.*, 2000b) and factors affecting the specific distribution of HBI isomers within microalgae (Robson *et al.*, 1988; Wraige *et al.*, 1998a; Rowland *et al.*, 2001b; Belt *et al.*, 2002). Within the latter studies, a strong dependence of C_{25} HBI unsaturation was noted in *Haslea ostrearia* (Gallion) Simonsen, with the degree of unsaturation dependant on growth temperature (Rowland *et al.*, 2001b). For example, at 25°C the algae produced predominantly penta- and tetraenes, while at 15°C and 5°C, trienes and dienes were produced respectively. Since some species of the *Haslea* genus had previously been reported as being sea ice specific (Poulin, 1990b; Booth *et al.*, 1997), it

was hypothesised that an increased proportion of the more saturated HBI isomers may be present in sea ice diatoms (Robson *et al.*, 1986). It was further postulated that, if this was the case, the presence of similarly unsaturated HBI isomers in Arctic sediments might then act as a proxy for past sea ice occurrence (Belt *et al.*, 2007). Recent investigations established that indeed one HBI isomer, a C_{25} mono-unsaturated HBI alkene (**Error! Reference source not found.**) is present in Arctic sea ice and is ell preserved in Arctic sediments (Belt *et al*, 2007; Vare *et al*, 2009). This isomer, termed 'Ice Proxy 25' or IP_{25}, is probably attributable to a limited number of diatom species probably belonging to the *Haslea* genus (Belt *et al*, 2007) Since a number of *Haslea* diatoms are endemic to the underside of sea ice (Booth *et al.*, 1997), it has been proposed that the occurrence of the IP_{25} biomarker in Arctic marine sediments indicates the presence of overlying sea ice, providing scientists with a potential proxy for past sea ice.

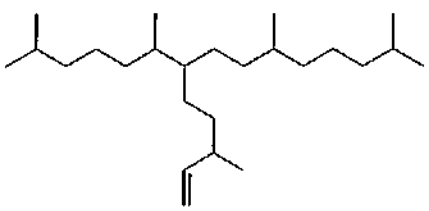

Figure 1.4-1. Structure of the C_{25} mono-unsaturated HBI alkene termed IP_{25} with unsaturation point at $\Delta^{23(24)}$.

One high resolution application of the IP_{25} biomarker on marine sediments obtained from northern Iceland illustrates the proxy's ability to accurately record palaeo-sea ice conditions. Massé *et al.*, (2008) compared the amount of IP_{25} derived sea ice presence to historical sea ice records, as well as diatom derived sea surface temperature, with exceptional agreement. New sea ice data were also produced for periods of previously unknown conditions, with longer term conditions, such as the Little Ice Age, also being resolved. Another recent study by Vare *et al.*, (2009), managed to successfully

reconstruct sea ice variations in the central Canadian Arctic Archipelago (CAA) based upon the extraction and analysis of sediment samples containing IP_{25}. Based primarily on the occurrence of IP_{25}, in addition to complementary proxy analysis of other biomarkers (stable isotope composition of bulk organic matter, benthic foraminifera, sediment particle size and inorganic geochemistry), researchers were able to present an interval based sea ice record for 10.0 – 0.4 cal. Kyr BP. The continuous reconstruction, based on ca. 600 sediment horizons, improved the understanding of sea ice variation in the CAA by providing a unique direct proxy approach in contrast to previous studies in the region that employed such proxies as bowhead whale remains (Dyke *et al.*, 1996b; Savelle *et al.*, 2000), marine molluscs (Dyke *et al.*, 1996a) and driftwood presence on raised beaches (Dyke *et al.*, 1997).

Application of the IP_{25} biomarker was further validated in sediments from the Fram Strait (Müller *et al.*, 2009). The abundance of IP_{25} was used, in addition to that of a marine phytosterol (brassicasterol), to establish a 30 kyr palaeo-sea ice record for the region. The use of brassicasterol, in addition to IP_{25}, provided the basis for distinction between sea ice conditions, ranging from open water, perennial and permanent sea ice cover, concluding that regional sea ice changes were linked to regional as well as global climate anomalies and oceanographic circulation in the North Atlantic.

Further analysis of three piston cores from the CAA (Barrow Strait, Victoria Strait and Dease Strait) improved the confidence in IP_{25} based palaeo-sea ice reconstructions. Striking similarities were observed in palaeo-sea ice conditions derived from the three separate sediment cores (Belt *et al.*, 2010). Data was complemented by particle size and mineralogical data which provided further evidence in support of the climatical changes observed in IP_{25} measurements.

In order to confirm the theoretical direct relationship of IP_{25} in terms of reconstructing sea ice through sedimentary analysis, it is necessary to test the hypothesis of production in Arctic sea ice to determine the specific temporal and spatial origin of its production. Furthermore it is necessary to observe IP_{25} passing from the sea ice, through the water column to the sea floor to establish the potential sedimentation route.

In summary, sea ice conditions are often based on reconstructions compiled from indirect proxies such as those used to derive sea surface temperatures; e.g. UK_{37}, TEX_{86} or from micro/macro-fossil analysis of species only indirectly related to sea ice The application of IP_{25} therefore, aims to provide an improved technique based on the direct proxy observations of this sea ice specific mono-unsaturated HBI

1.5 The present study

While a number of polyunsaturated HBIs have been successfully isolated from diatom cultures in laboratories (Massé, 2003), IP_{25} was previously only identified in a limited number of available sea ice cores, which led to its synthesis and rigorous characterisation (Belt *et al.*, 2007). IP_{25} has also been routinely isolated and monitored in a variety of Arctic sediments (e.g. Belt *et al.*, 2010; Vare *et al.*, 2010) facilitating palaeo-sea ice extent reconstructions. However, the impacts of different environmental conditions on the production of IP_{25} in sea ice algae are unknown. Therefore, the main aims of this study were to:

i. Establish the temporal and spatial constraints on the production of IP_{25} and other HBIs in diatoms within Arctic sea ice.
ii. Determine the extent of dispersion of diatoms containing IP_{25} and other HBIs in the water column upon melting of seasonal sea ice.
iii. Examine the potential diagenetic effects imposed on IP_{25} and other HBIs in recently deposited shallow Arctic marine sediments.

The outcomes of these key aims are the main focus of this study and are presented and discussed as such in the following chapters with reference to samples collected mainly from the Amundsen Gulf, with some additional pan-Arctic examples:

Chapter 2: *Environmental setting*; discusses the environmental setting of the study region in detail describing the geographical features that are relevant for interpreting the outcomes of the study.

Chapter 3: *Methodologies*; describes the detailed methods that were both adopted and developed that were necessary to obtain the data used to address the aims of the study.

Chapter 4: *Temporal distribution of highly branched isoprenoids in Arctic sea ice*; describes the temporal examination of IP_{25} and other HBI occurrences through time by

studying various types of Arctic sea ice from the Amundsen Gulf region of the Canadian Arctic Archipelago (CAA). Additional biomarker analysis was adopted to contextualise the findings in terms of established sea ice biomarkers and the Arctic sea ice algal bloom. As a result, the temporal constraints of IP_{25} production, along with other polyunsaturated HBIs and established biomarkers, were determined.

Chapter 5: *Vertical distribution of highly branched isoprenoids in Arctic sea ice*; describes the vertical examination of IP_{25} and other HBI concentrations within Arctic sea ice cores from the Amundsen Gulf region of the CAA. Additional biomarker analysis was again adopted to clarify the observations and provide distinctions between biomarker production sources. As a result, the spatial constraints of IP_{25} production within sea ice, along with other polyunsaturated HBIs and established biomarkers, were determined.

Chapter 6: *Highly branched isoprenoid transport from within Arctic sea ice to the sediment*; describes the occurrence of IP_{25} and other HBIs within the pelagic Arctic Ocean, from the Amundsen Gulf region of the CAA and high Arctic. The potential for dispersion of the biomarker, and the diatoms responsible for its biosynthesis, is established. Additionally, a range of pelagic and benthic macrofaunal species were found to contain varying quantities of IP_{25} and polyunsaturated HBIs such that $\delta^{13}C$ isotopic characterisation was possible for some.

Chapter 7: *Highly branched isoprenoid preservation in Arctic sediments*; describes the sedimentary analysis of IP_{25} and other HBIs carried out on six shallow box core sediment cores from the Amundsen Gulf region of the CAA. Cores were selected to represent both deep, offshore, reduced biological activity, and shallow, near shore, high biological activity sediments. A variety of approaches were adopted to investigate possible influences capable of assisting either preservation or decomposition of IP_{25} and polyunsaturated HBIs in each case.

Chapter 8: *Conclusions and future work*; summarises the research carried out in this study and considers the impact of the outcomes in relation to the useful future application of IP_{25} as a sedimentary indicator of palaeo sea ice extent in the Arctic as well as detailing some further necessary research.

CHAPTER TWO

2 Environmental setting

2.1 Amundsen Gulf

The Amundsen Gulf is a relatively shallow (ca. 50 – 500 m) coastal shelf region of the Beaufort Sea located at the westernmost point of the CAA (Figure 2.1-1). The Amundsen Gulf lies alongside the continental coast of the Canadian Northwest Territories (NWT) and is semi enclosed by Victoria Island to the east, Banks Island to the north and to the west. At its widest point at 170 km it joins the southeast Beaufort Sea.

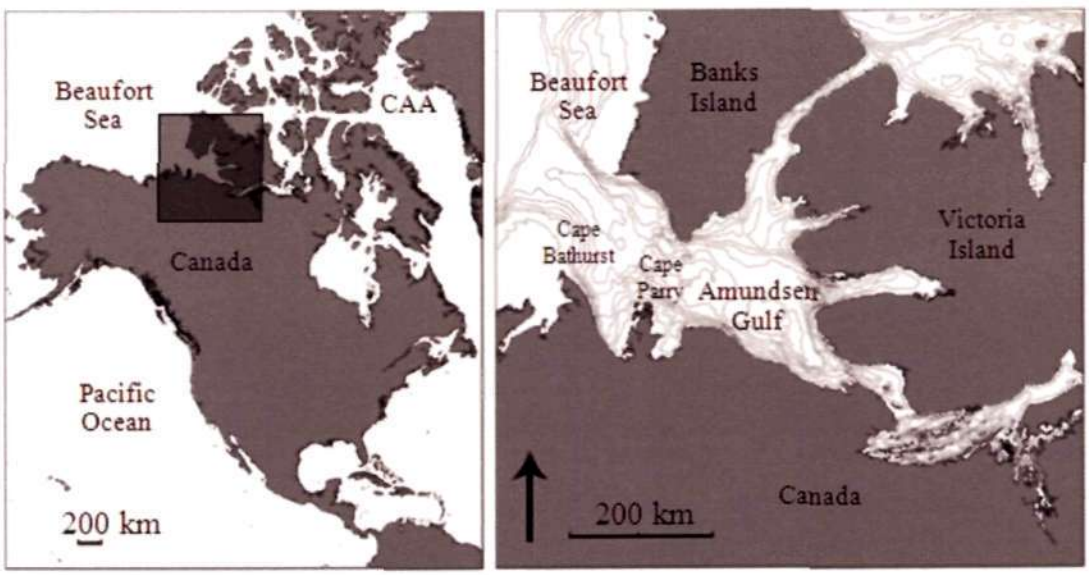

Figure 2.1-1. Map of the geographical setting and study location (Amundsen Gulf) with sea floor bathymetry of the Amundsen Gulf showing 50 m contours. (GEBCO digital atlas).

The entire gulf is in a region of Arctic tundra climate, characterised by low temperatures (typically < -20°C) through much of the year which maintains the terrestrial permafrost. The sea ice cover of the gulf varies greatly from year to year but, in general, begins to form in mid-October, persisting throughout the dark winter and begins to break up at the

end of May, where daylight extends to 24 h a day (Wang *et al.*, 2005; Richerol *et al.*, 2008). In the winter, landfast sea ice forms at the coast. Along the outer edge of this landfast ice is a zone where the ice breaks up and flaw leads (areas of open water) occur that permit the leeward transit of drift ice, often westerly into the Beaufort Sea (Hannah *et al.*, 2009) (Figure 2.1-2).

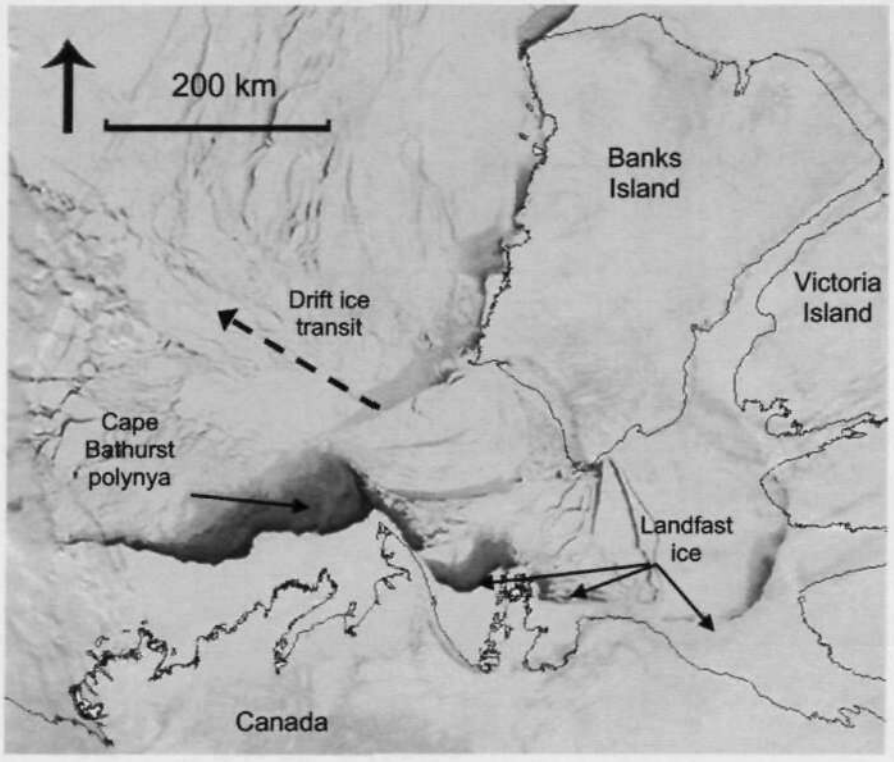

Figure 2.1-2. Moderate Resolution Imaging Spectroradiometer (MODIS) image of Amundsen Gulf sea ice cover, 6th April 2008, indicating land fast ice and the predominant westerly transit of unconsolidated drift ice.

Where winds, currents and upwellings converge, localised, permanently ice free conditions can occur in the gulf and is described as a polynya (Smith *et al.*, 2007).The Cape Bathurst polynya, at the western limit of the gulf, represents a region of cold water upwelling of nutrient rich water, supplying the shelf with a source of new nitrate and silicate (Williams *et al.*, 2008). To the southeast of the Cape Bathurst polynya lays Franklin Bay, a moderately shallow (ca. 200 m) region of coastal water receiving

riverine input from the 440 km long Horton River, originating from a lake ca. 80 km north of the Great Bear Lake (NWT). The reach of the sediment rich Horton River plume fluctuates in intensity and load in relation to local weather. The plume was observed as far north as Cape Bathurst during the field study (Figure 2.1-3).

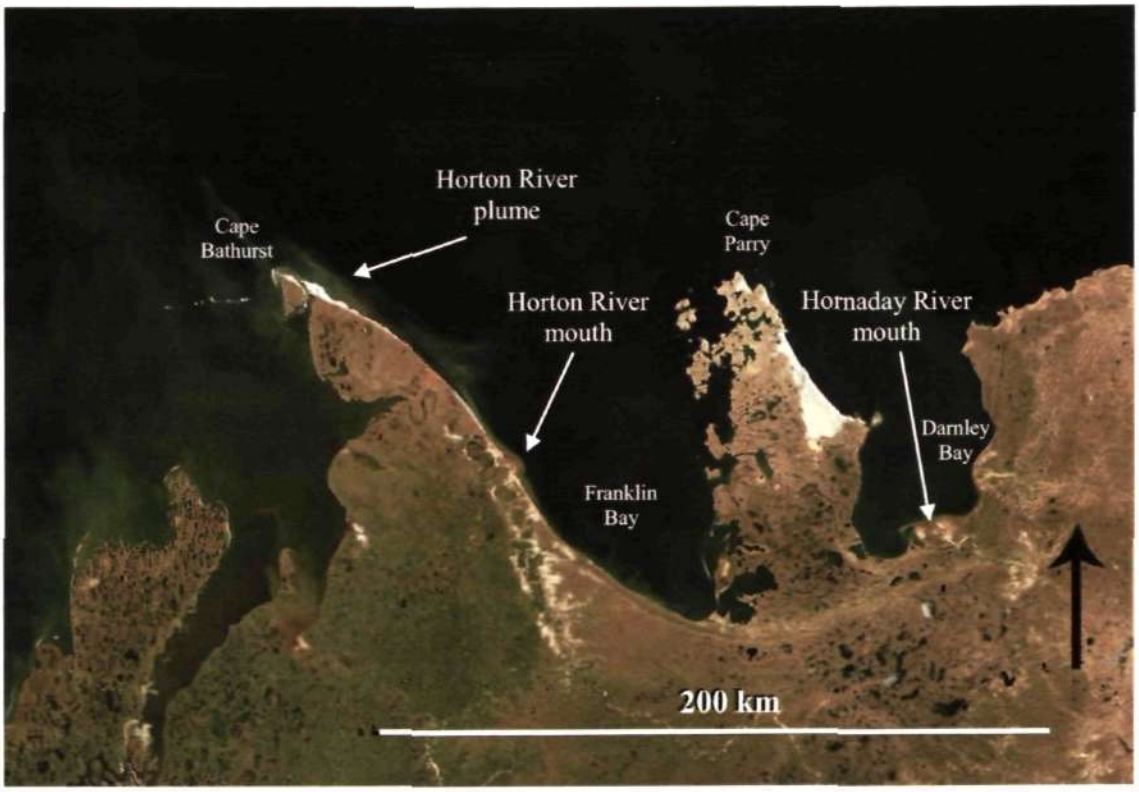

Figure 2.1-3. Moderate Resolution Imaging Spectroradiometer (MODIS) image of Horton River mouth, 3rd July 2008, showing the northward reach of Horton River discharge.

To the east of Franklin Bay (50 km), separated by the Parry peninsula, is Darnley Bay, another shallow (< 150 m) coastal bay. 110 km north of Darnley Bay, in the central Amundsen Gulf, is the deepest region of the gulf at ca. 510 m. The Amundsen Gulf region is believed to have been subjected to at least three major glaciations during the Quaternary: Banks (800 cal. kyr – 1.4 cal. Ma BP), Thomsen (ca. 130 – 780 cal. kyr BP) and the Amundsen (ca. 10 – 80 cal. kyr BP) glaciations, interluded by Morgan Bluffs and Cape Collinson interglacials respectively (Vincent, 1982; Vincent, 1990; Schell *et*

al., 2008; Blasco *et al.*, 2009; England *et al.*, 2009) and most recently the Holocene (ca. 12 cal. kyr BP - present). While glacial ice extent is reported to have never completely engulfed Banks Island (Vincent, 1982; Vincent, 1990), multibeam sonar investigations provide evidence for extensive glacial scouring throughout the Amundsen Gulf from the last glaciation (Stokes *et al.*, 2006) with a maximum westerly glacial extent evidenced by submarine drumlins encroaching on the Beaufort Sea shelf (Schell *et al.*, 2008).

2.2 Amundsen Gulf study locations

Collection of sea ice, plankton, sea floor macrobenthos and box core sediments was carried out as part of Team 3 ('Primary Production' led by Michel Gosselin (ISMER, Canada)) activities, between legs 5 and 9 (January – July 2008), during the Canadian Circumpolar Flaw Lead System Study as part of the International Polar Year (IPY-CFL). The cruise was carried out onboard the class 1200 Canadian Coast Guard Ship *Amundsen* (IPY-CFL, 2010).

Brief descriptions of the methods of sample collection, preservation and extraction procedures are detailed later in the relevant chapters relating to the objectives being investigated. For detailed descriptions of the methods used, each chapter refers to the relevant section of the methods chapter (Chapter 3).

CHAPTER THREE

3 Methodologies

3.1 Introduction

The following chapter contains the detailed analytical approaches adopted, adapted and developed to obtain the data required to address the aims of this research. The approaches described in this chapter describe laboratory procedures in addition to chemical identification and quantification. For descriptions of the sample management and specific chemical extraction techniques the reader is referred to the relevant chapter for the sample type, e.g. sea ice: **chapters 4** and **5**, plankton and macrobenthos: **chapter 6** and shallow marine sediments: **chapter 7**.

3.2 Freeze drying

Samples were frozen at -20°C for ca. 24 h. Once frozen, samples were arranged on trays and freeze dried using a Thermo Savant Modulyo D freeze dryer at -45°C; 0.2 mbar for ca. 24-48 h, depending on water content and number of samples.

3.3 Internal standards for lipid quantification

Addition of the following internal standards prior to extraction were used for the quantification of extracted compounds; 10 µL; 10 µg mL^{-1} of either 7-hexylnonadecane or 5α-androstan-3β-ol for hydrocarbons and sterols respectively, with nonadecanoic acid (10 µL; 0.1 mg mL^{-1}) added for fatty acid quantification.

3.4 Total organic extract

A sufficient volume of CH_2Cl_2/CH_3OH (2:1 v/v) was added to cover the sample in a glass vial where it was capped, sonicated (ca. 15 min) and centrifuged (2 min; 2500 rpm) before being transferred, by pipette, to a clean vial. This process was repeated a further two times yielding the total organic extract (TOE)

Typical sample quantities were; sea ice = 10 GF/F filters, seawater = 1 GF/F filter, sediment = 1 g with ca 6 mL solvent required for each extraction.

Where larger volumes of material required extracting, a soxhlet extractor was used to obtain the TOE using CH_2Cl_2/CH_3OH (2·1 v/v) and refluxed for ca 24 h.

Typical macrobenthos sample quantity = 1 organism (5 – 40g freeze dried mass),

3.5 Saponification of fatty acid triglyceride esters

Samples were saponified with sufficient methanolic potassium hydroxide (5% KOH; CH_3OH/H_2O (80/20 v/v)) to cover the sample which was capped and heated at 80°C for 60 min. The non saponifiable lipids (NSLs) were re-extracted into hexane (3 x 1 mL) and transferred to a clean vial. Saponifiable lipids, including free fatty acids were obtained by adding concentrated HCl (1 mL) to the saponified sample and re-extracting with hexane (3 x 1 mL) into an additional clean vial

3.6 Isolation and purification of lipids

Isolation and purification of highly branched isoprenoids and sterols from the TOE was achieved using a combination of open column chromatography (SiO_2; $AgNO_3$ with $C_6H_{14}/CH_2Cl_2/OC(CH_3)_2$) techniques and further preparative chromatography using high performance liquid chromatography (HPLC).

In the first instance extracted compounds were purified by open column silica chromatography (50:1 SiO_2:lipids) with hexane mobile phase (five column volumes) to yield apolar lipids. A further five column volumes CH_2Cl_2/CH_3OH (50:50 v/v) were used to elute more polar compounds such as sterols.

Where the purity of IP_{25} and other HBI compounds was insufficient following open column silica chromatography, (e.g. for $\delta^{13}C$ analysis), further purification was carried out with the addition of 5%, by weight, $AgNO_3$ to the silica before being fully activated in an oven (110°C; until white). Chromatography columns were prepared with 0.5 g $AgNO_3/SiO_2$ (5%/95%) in low light conditions and remained in darkness throughout with aluminium foil jackets. 5 column volumes of hexane were used to elute alkanes with a further 5 column volumes of CH_2Cl_2 yielding IP_{25}. Acetone was used to remove the remaining compounds such as polyunsaturated HBIs from the column.

In some cases Individual HBI isomers were further separated by silver ion chromatography using HPLC, where necessary (Varian Chromspher 5 lipid, 250 x 4.6 mm ID) under an apolar (100% hexane) to polar (100% acetone) solvent gradient at 1 mL min^{-1}. An Agilent HP1100 HPLC system coupled to an Agilent G1314A variable wavelength detector (λ 205 nm) was used. Fractions containing HBI isomers were collected manually based on HBI elution with the following solvents (Table 3-1).

Table 3-1. HBIs isolated by HPLC and the mobile phase composition required for elution on Ag^+

HBI	Mobile phase
I	100% CH_2Cl_2
IIa	100% CH_2Cl_2
IIb	100% CH_2Cl_2
IIc	100% CH_2Cl_2
IIIa, IIIb and **IIIc**	78:22 CH_2Cl_2:acetone
IIId and Tetra-unsaturated HBIs	75:25 CH_2Cl_2:acetone
Penta-unsaturated HBI	100% acetone

3.7 Hydrogenation

Where elucidation of the saturated parent structure of unidentifiable HBIs was required, a sample was transferred to a round bottomed flask (50 mL) in ca 15 mL hexane. Whilst being stirred magnetically, pre-saturated hydrogen was gently bubbled through the solution at atmospheric pressure and room temperature (6 h) in the presence of ca. 10 mg palladium on charcoal (10%). Once completely reacted, samples were re-purified using the SiO_2 chromatographic technique previously described.

3.8 Derivatisation

To increase the volatility of polar compounds on the apolar GC/MS column (HP-5ms) free fatty acids and sterols were derivatised (50 µL BSTFA, 30 min; 70°C) before being diluted with CH_2Cl_2 to the appropriate concentration. For analysis by GC/IR/MS, fatty acids were derivatised with isotopically consistent ($\delta^{13}C$ = - 44 04‰) BF_3MeOH. Fatty acid methyl esters (FAMEs) were prepared with 14% w/v; 100 µL BF_3MeOH; 70°C; 1h. FAMEs were then extracted with chloroform with solvent evaporated under N_2.

3.9 Gas chromatography – flame ionisation detection

To ensure instrument longevity and reproducibility of results obtained from GC/MS analysis, good practice dictates the importance of samples being prepared at appropriate concentrations (ca. 0.001 mg mL^{-1}). This avoids instrument overloading which can result in poor chromatography and increased downtime requirements for maintenance. The relatively low mass of the extract present in small mass (typically < 1 g) samples makes the determination of compound mass for serial dilution impractical. Therefore analysis on the more robust gas chromatography-flame ionisation detection (GC/FID) instrument was employed for preliminary analysis. The final sample extract was

transferred (hexane) to a 2 mL glass gas chromatography (GC) vial with plastic screw cap and rubber/PTFE septa (Chromacol Ltd., UK) using minimal solvent (2 x 50 µL hexane), dried under a gentle stream of nitrogen at no more than 40°C and diluted to precisely 1 mL (hexane) for analysis on GC/FID. Sample concentration was determined on an Agilent 6890 gas chromatogram with flame ionising detector (300°C) fitted with an Agilent HP-5 (30 m x 0.25 mm x 0.25 µm) column. 1 µL auto-splitless injection (300°C) with constant flow (2 mL min^{-1}) helium carrier gas was used. The elution of detectable compounds was determined by a ramped temperature profile of 10°C min^{-1} from 40 – 300°C with a 10 minute isothermal at 300°C. Data was collected and analysed with Agilent Chemstation software and an overall dilution for GC/MS was determined.

3.10 Gas chromatography-mass spectrometry

Once the appropriate dilution was established by GC/FID the samples were re-analysed by GC/MS. An Agilent 7890A GC coupled to a 5975 series mass selective detector fitted with an Agilent HP-5ms (30 m x 0.25 mm x 0.25 µm) column along with 1 µL auto-splitless injection (300°C) with helium carrier gas (1 mL min^{-1} constant flow) was used. The elution of detectable compounds was determined by both total ion current (TIC; *m/z* 50 – 500 daltons) and selective ion monitoring (SIM; –0.3 +0.7 *m/z* of interest) techniques, with an electron voltage of 70 eV, using a ramped temperature profile of 10°C min^{-1} from 40 – 300°C with a 10 minute isothermal at 300°C. Data was collected and analysed with Agilent Chemstation software. TIC chromatograms were used to identify the retention time and mass spectrum of selected compounds, while SIM chromatograms were used for compound quantification to take advantage of the high selectivity and increased sensitivity offered by this approach.

3.11 Gas chromatography x gas chromatography-time of flight mass spectrometry

An Agilent 7890A GC fitted with a Zoex GC x GC modulator, coupled to an Almsco bench time-of-flight (ToF) mass spectrometer fitted with VF-1ms (50 m x 0 25 mm x 0.4 μm, primary) and BPX50 (1.7 m x 0.1 mm x 0.1 μm; secondary) columns along with 1 μL auto-splitless injection (300°C) with helium carrier gas (0.7 mL min^{-1} constant flow) was used The elution of detectable compounds was determined with an electron voltage of 70 eV with a mass range of 50 – 600 daltons, using a ramped temperature profile of 5°C min^{-1} from 40 - 300°C with a 10 minute isothermal at 300°C, then 20°C min^{-1} to 320°C, with a 10 minute isothermal. Data processing was conducted using GC Image™ v 2 0

3.12 Highly branched isoprenoid quantification

Identification of HBIs isolated from sea ice, plankton, macrofauna and sediments was established by comparison of the respective mass spectra with those of authentic compounds isolated from culture Identification of molecular ions and fragmentation pathways, along with comparison of the respective retention indices (**I**; 2086: **IIa**, 2079 **IIb**; 2085: **IIIa**, 2045: **IIIb**; 2092 **IIIc**, 2103· **IIId**, 2107) (Figure 3.12-1, Figure 3.12-2 and Figure 3.12-3), calculated using the following formula, where *Ri* denotes retention index and *Rt* is retention time on GC/MS (HP-5ms), were used.

Equation 1

$$Ri = \frac{Rt^{HBI} - Rt^{nC_{20}}}{(Rt^{nC_{21}} - Rt^{nC_{20}})/100} + 2000$$

A quick reference foldout guide to the HBIs frequently referred to in this thesis is included at the back of this thesis.

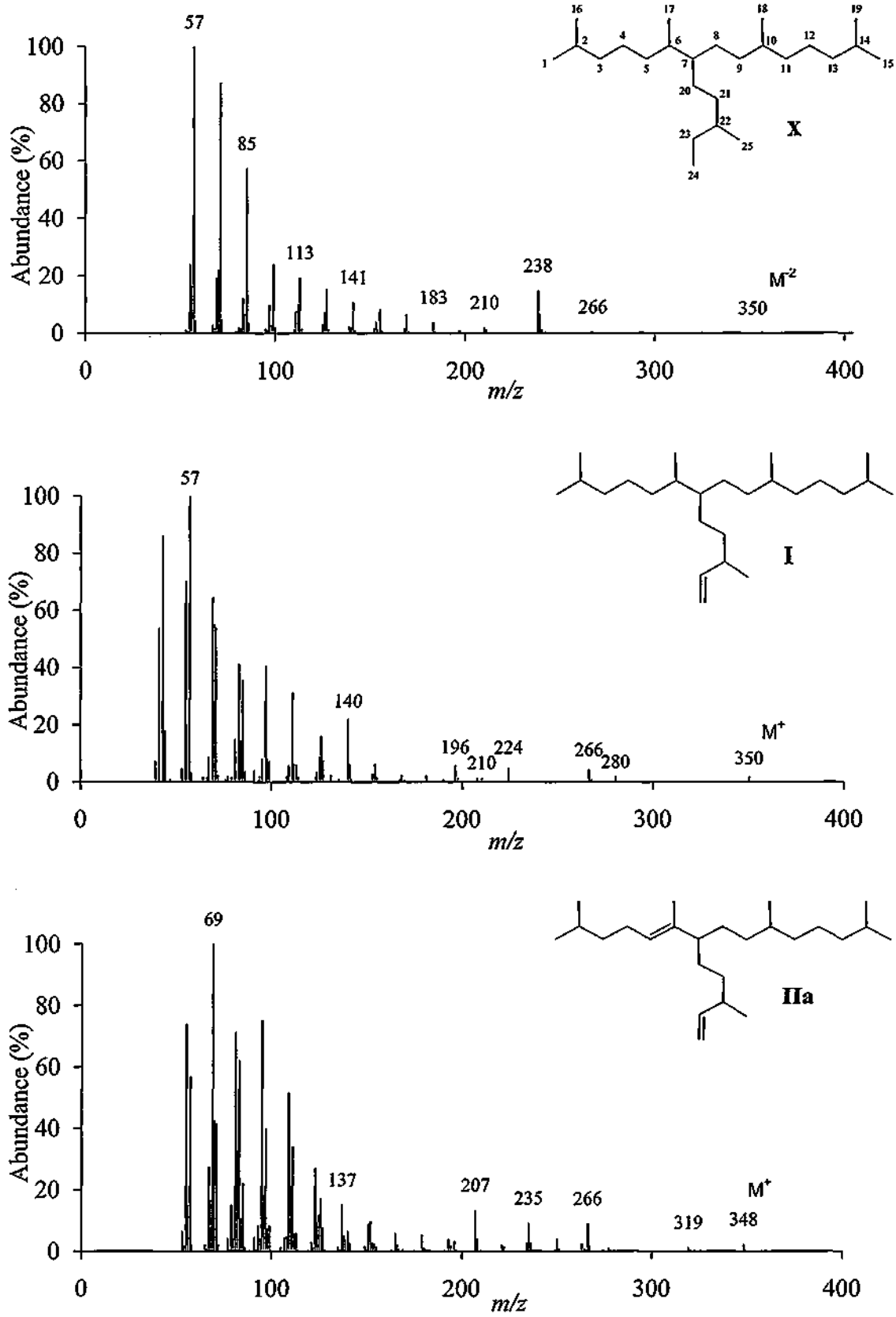

Figure 3.12-1. Background subtracted mass spectra and structures of highly branched isoprenoid alkane and alkenes described in the current study: (X): $C_{25:0}$ showing HBI numbering system. **I**: IP_{25} RI 2086. **IIa**, di-unsaturated HBI RI 2079 (HP 5ms).

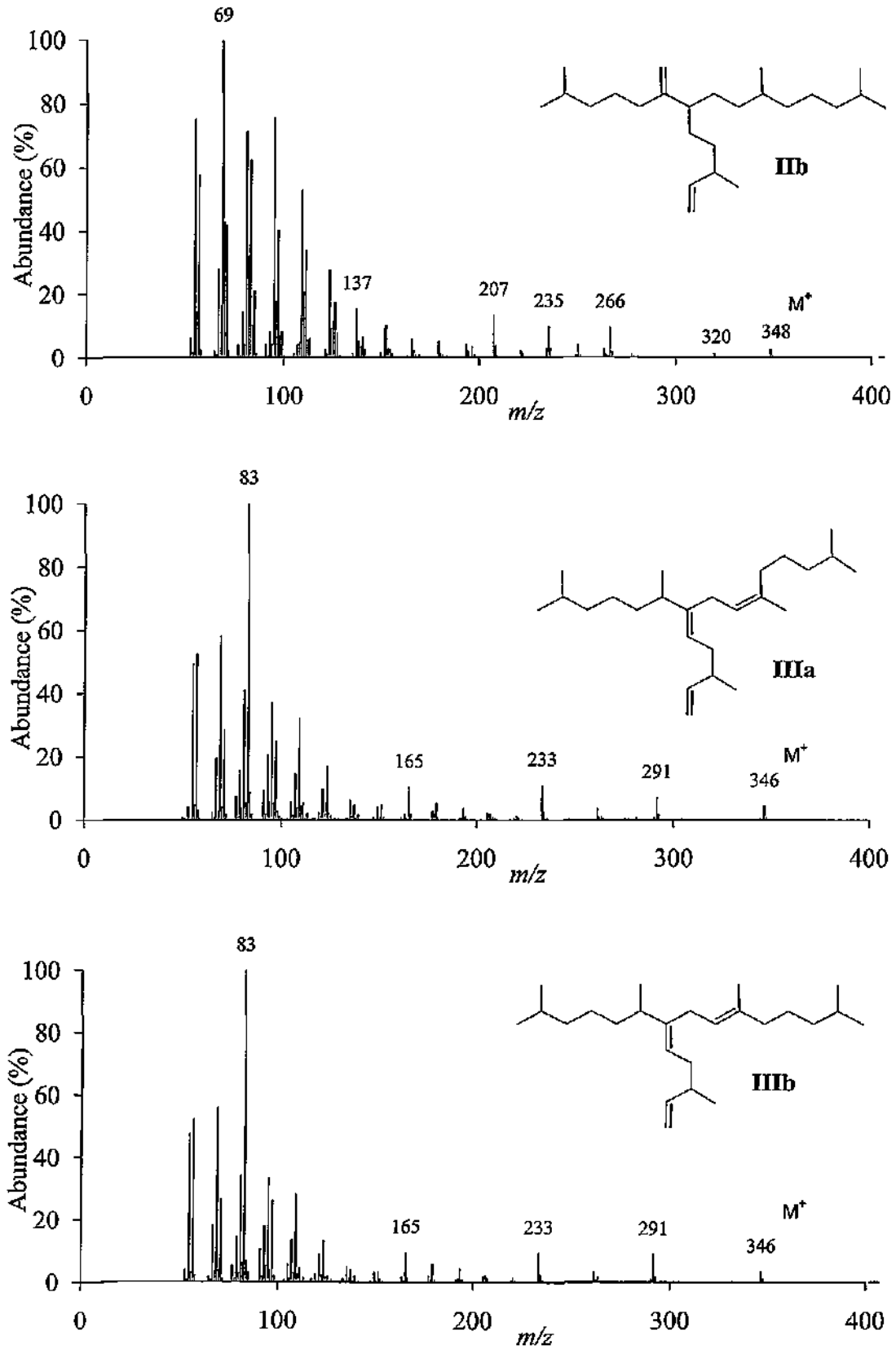

Figure 3 12-2 Background subtracted mass spectra and structures of highly branched isoprenoid alkenes described in the current study: **IIb**: di-unsaturated HBI RI 2085. **IIIa** and **IIIb**· tri-unsaturated HBIs RI 2045 and 2092 (HP 5ms).

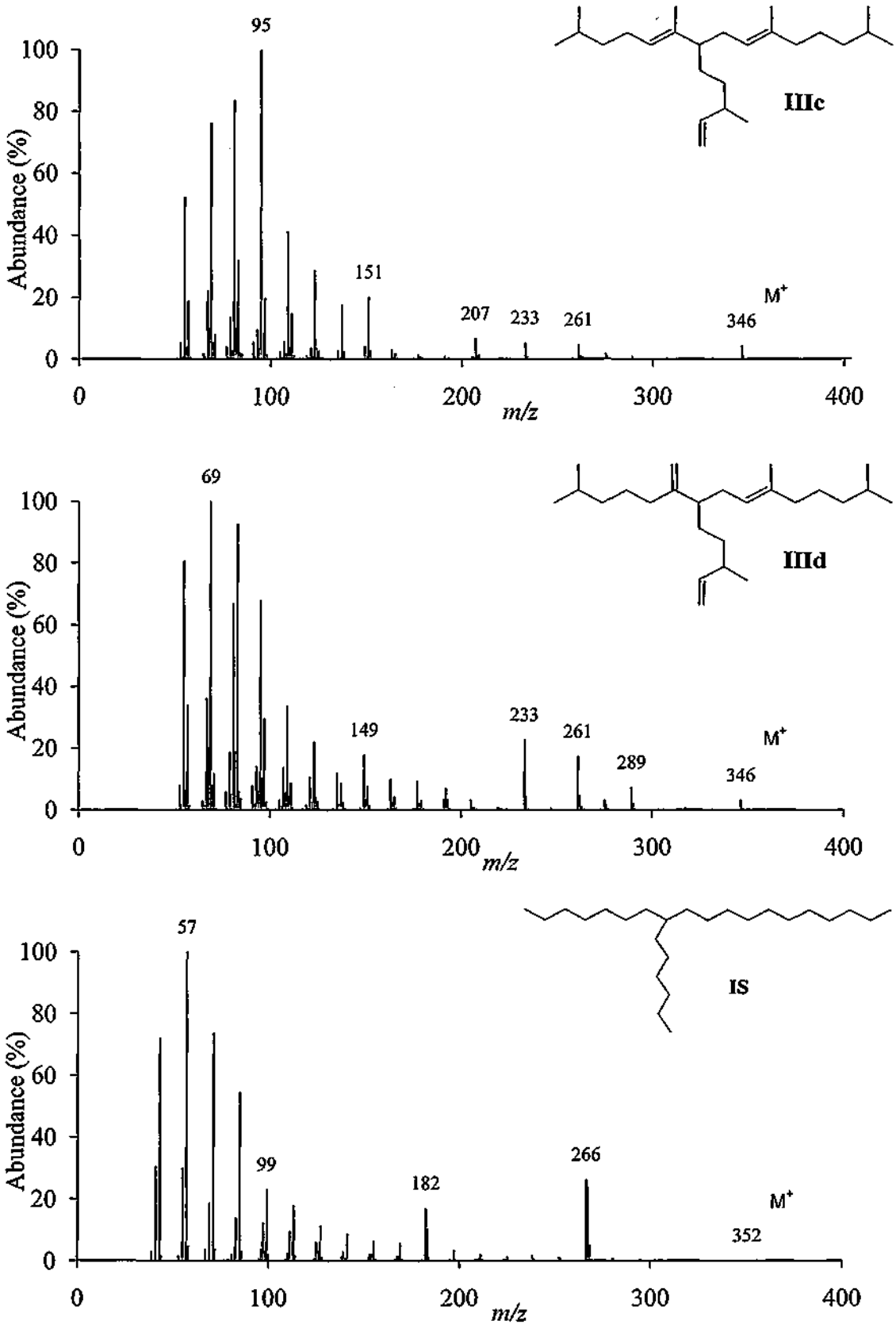

Figure 3.12-3. Background subtracted mass spectra and structures of highly branched isoprenoid alkane and alkenes described in the current study: **IIIc** and **IIId**: tri-unsaturated HBIs RI 2103 and 2107, and **IS**: internal standard; 7-hexylnonadecane RI 2357 (HP 5ms).

At 70 eV HBIs fragment readily in the mass selective detector (MSD) generating characteristic mass spectra (Figure 3.12-1, Figure 3 12-2 and Figure 3 12-3) with typically small molecular ions (ca 2-5% of base peak) and larger fragments. Reduction of the MSD ionisation energy to 60 eV in an attempt to increase molecular ion counts was unsuccessful (Figure 3.12-4).

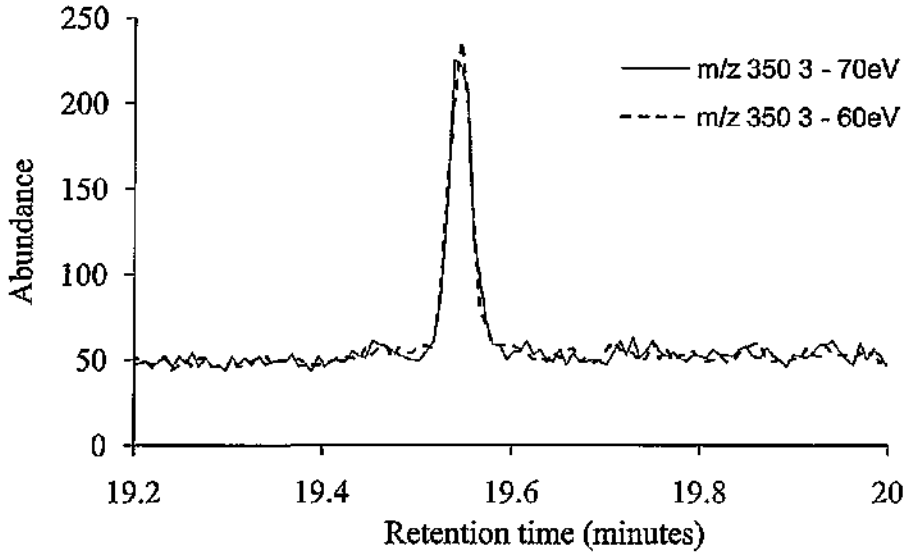

Figure 3.12-4. Partial GC/MS chromatogram (SIM *m/z* 350 3) comparison of electron voltage emission changes from the typical 70 eV to a lower 60 eV for the same sample.

Quantification of HBIs isolated from sea ice, plankton, macrofauna and shallow marine sediments was achieved by manual integration (Chemstation, version C 03.00 software) of each analyte's molecular ion signal as recorded by GC/MS SIM analysis (**I**: *m/z* 350.3. **IIa, IIb**: *m/z* 348 3. **IIIa, IIIb, IIIc** and **IIId**: *m/z* 346.3 (Figure 3.12-5).

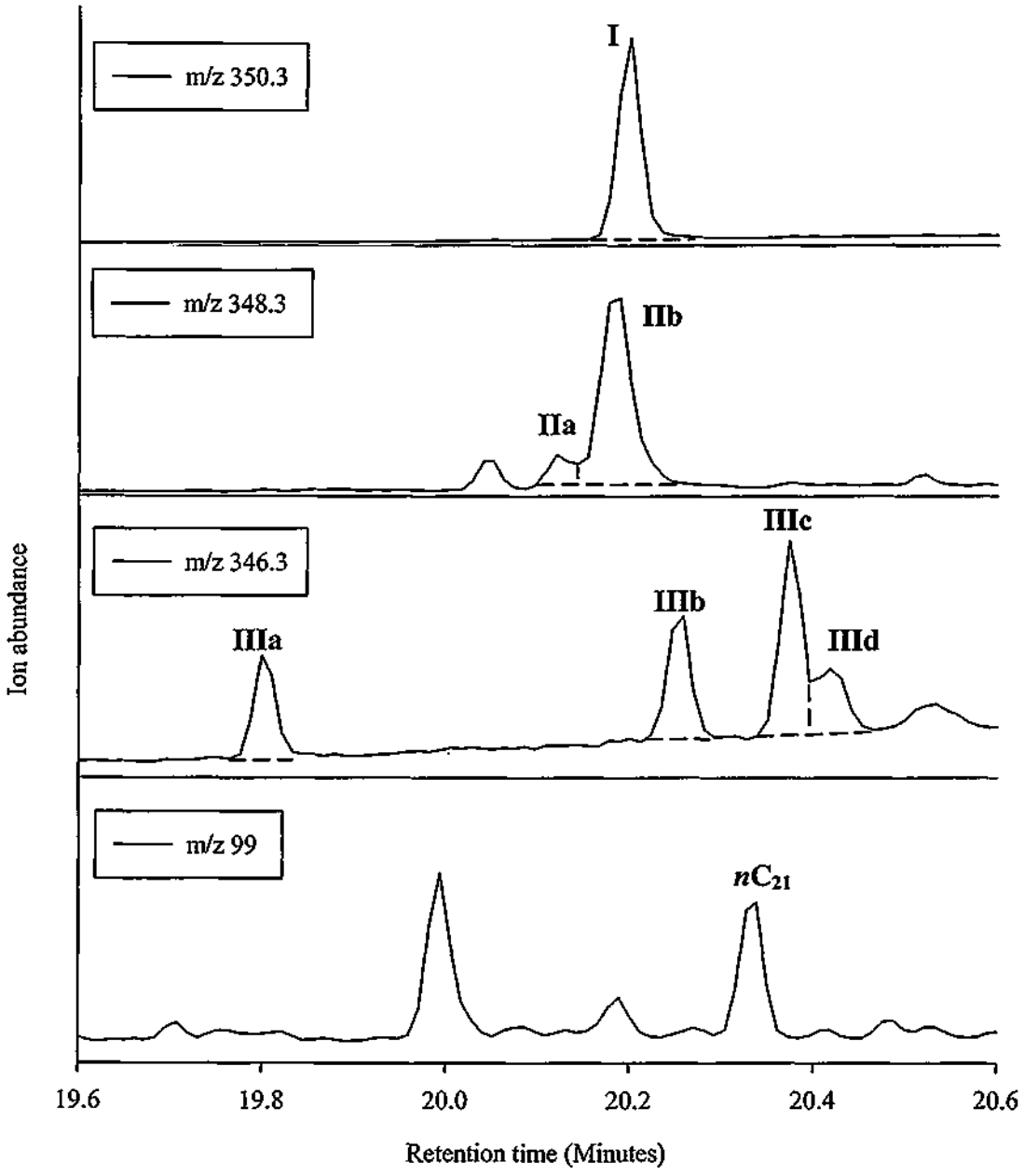

Figure 3.12-5. Partial GC/MS chromatograms (SIM *m/z* 350.3, 348.3, 346.3 and 99) of silica purified St.405b sediment extract showing relative position of HBIs to nC_{21} and the technique adopted for manual peak area integration for later quantification of HBIs (dashed lines).

Integration of the HBI response via SIM chromatogram alone was insufficient for accurate determination of abundance in samples. To arrive at a comparable value for the recorded analyte signal from GC/MS it was necessary to take into account a) internal

standards for varying extraction efficiencies b) sample mass or volume for variations in starting material mass and c) dry bulk density for exclusion of sediment density variation with d) GC/MS response factor to account for detector sensitivity. To perform the necessary quantification of HBI analytes, Equation 2 and Equation 3 were created where *Pa* denotes integrated peak area of HBIs, *Is* is integrated SIM (*m/z* 99) peak area of the internal standard 7-hexylnonadecane Sample mass or volume extracted is expressed as *Sm/Sv* respectively and GC/MS response factor as *Rf* with dry bulk density as DBD.

Equation 2

$$Analyte\ \mu g\ cm^{-3} = \left[\frac{\left(\frac{Pa}{Is}\right) xRf}{Sm} \times DBD\right] \times 0\,1$$

Equation 3

$$Analyte\ \mu g\ mL^{-1} = \left[\frac{\left(\frac{Pa}{Is}\right) xRf}{Sv}\right] \times 0.1$$

Table 3-2. Calculation steps necessary to quantify HBI concentration in sediment samples using Equation 2.

HBI	Pa	$\frac{Pa}{Is}$	$\left(\frac{Pa}{Is}\right) xRf$	$\frac{\left(\frac{Pa}{Is}\right) xRf}{Sm}$	$\frac{\left(\frac{Pa}{Is}\right) xRf}{Sm} \times DBD$	X 0 01 = µg cm^{-3}
I	301494	0 103	0 0036	0 0025	0 0011	1 2 x10^{-5}
IIa	47712	0 016	0 00068	0 00047	0 00022	2 2 x10^{-6}
IIb	202105	0.069	0 0049	0.0033	0 0016	1.6 x10^{-5}
IIIa	31837	0 011	0 0022	0 0015	0 00069	6 9 x10^{-6}
IIIb	45006	0 015	0 0015	0 0011	0 00049	4 9 x10^{-6}
IIIc	72588	0.025	0 0077	0.0052	0 0024	2 4 x10^{-5}
IIId	26499	0 009	0 0016	0 0011	0 00052	5 2 x10^{-6}

The response factor of the individual HBIs was calculated from calibration curves of HBI concentrations (0.0005 mg mL^{-1}, 0.001 mg mL^{-1}, 0.005 mg mL^{-1}, 0.025 mg mL^{-1}

and 0.01 mg mL^{-1}; r = 0.98) against the internal standard (7-hexylnonadecane) of equal concentration to obtain the following response values (Table 3-3) where sufficient quantities of pure compound was available.

Table 3-3. GC/MS response factors (Agilent 5975 series MS: HP-5ms: Gain autotune) calculated by calibration of pure standards (obtained from bulk diatom culture and chromatographic purification from bulk sediment extracts) against the internal standard; 7-hexylnonadecane.

HBI	Response factor (*Rf*)	Sample mass extracted (g) (*Sm*)	Dry bulk density (DBD)
I	0.035	1.46	0.47
IIa	0.042	1.46	0.47
IIb	0.071	1.46	0.47
IIIa	0.2	1.46	0.47
IIIb	0.1	1.46	0.47
IIIc	0.31	1.46	0.47
IIId	0.18	1.46	0.47

Where sediment was analysed it was necessary to account for the sediment density. The dry mass (*Dm*) and water content (*Wc*) of sediments were determined by carefully reweighing each horizon after freeze-drying before applying Equation 4 where *Wm* denotes wet mass (g).

Equation 4

$$Wc\ (g) = Wm - Dm$$

Once calculated for all horizons these data were used against standard densities for sediment (2.65 g cm^{-3}) and sea water (1.025 g cm^{-3}) to calculate the amount of sediment mass present in a specific volume of sediment, known as the dry bulk density by excluding water mass via the following equation (Vare *et al.*, 2009; Belt *et al.*, 2010):

Equation 5

$$DBD\ (g\ cm^{-3}) = \frac{Dm}{\left(Wc/_{1.025}\right) + \left(Dm/_{2.65}\right)}$$

3.13 Fatty acid (trimethylsilyl ester) quantification

Identification of fatty acids isolated from sea ice and plankton was established by comparison of the derivatised (trimethylsilyl (TMS) ester) mass spectra against authentic compounds to identify molecular ions and fragmentation pathways (**FI, FII, FIII, FIV, FV** and **FVI**) (Figure 3.13-1, Figure 3.13-2 and Figure 3 13-3). A quick reference foldout guide to the fatty acids frequently referred to is included in the back of this thesis

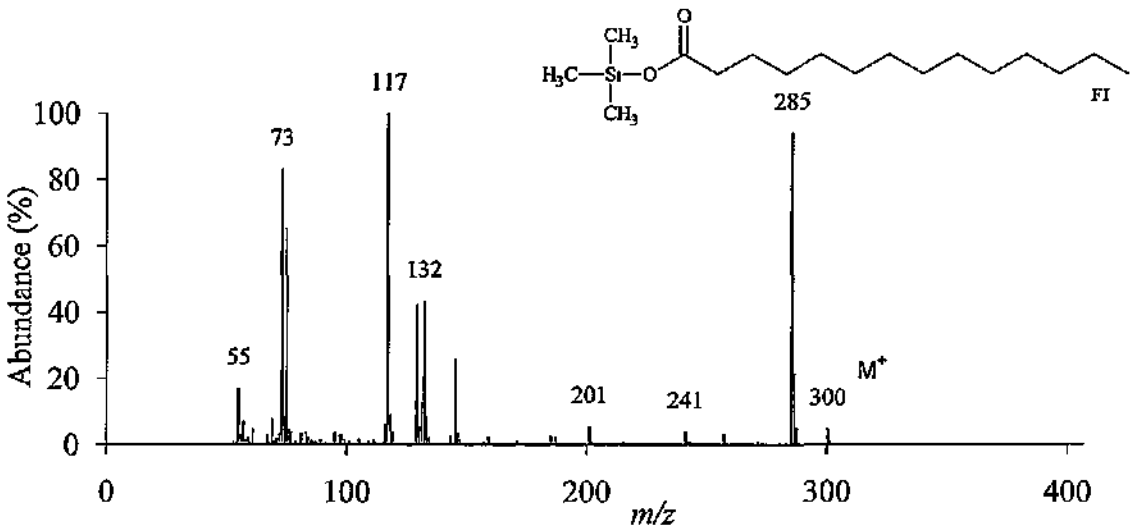

Figure 3 13-1. Background subtracted mass spectra and structure of fatty acid trimethylsilyl (TMS) esters described in the current study: Tetradecanoate - (**FI**).

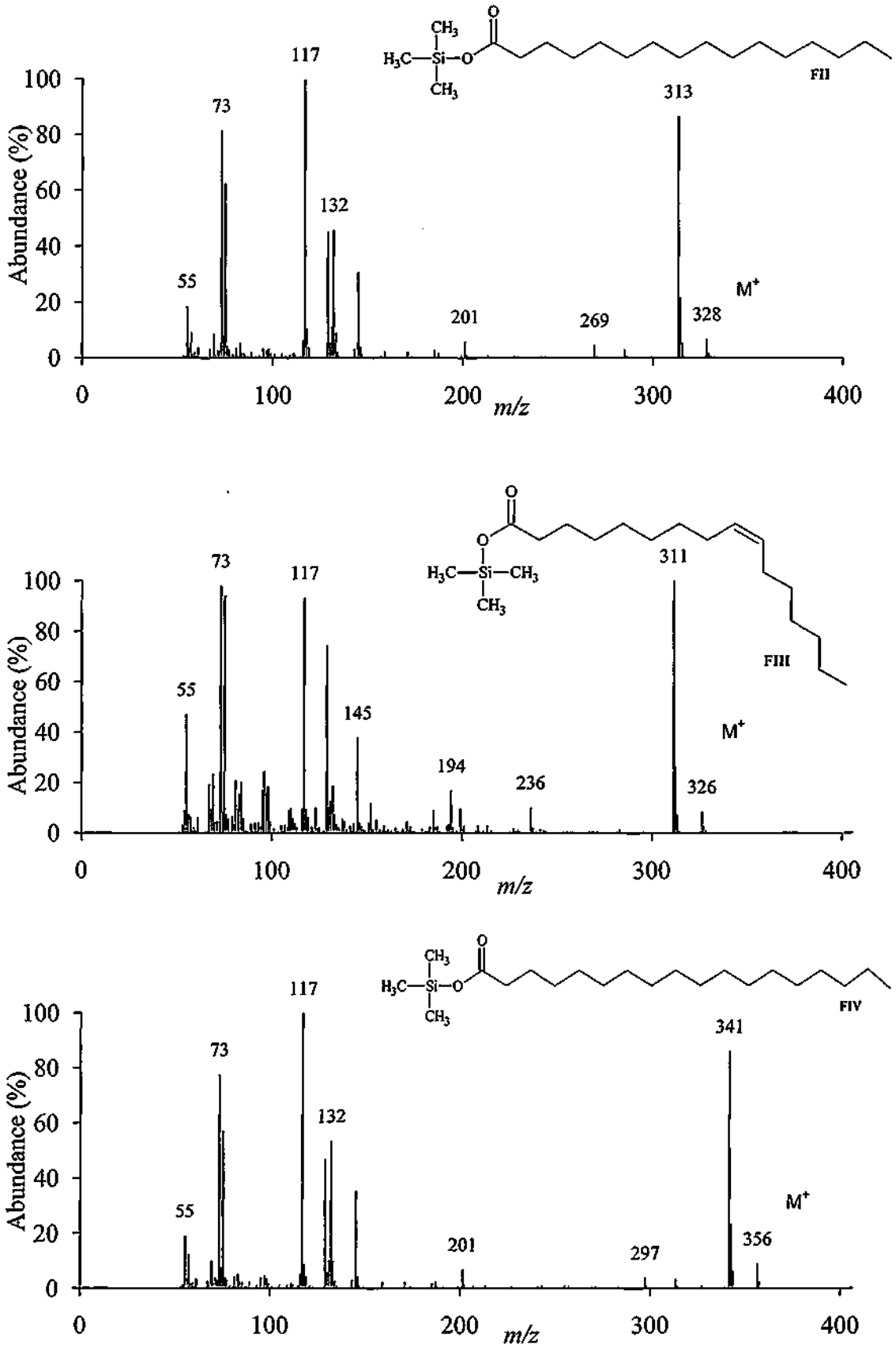

Figure 3.13-2. Background subtracted mass spectra and structures of fatty acid trimethylsilyl (TMS) esters described in the current study: Hexadecanoate - (**FII**): *cis* - 9-Hexadecanoate - (**FIII**): Octadecanoate – (**FIV**).

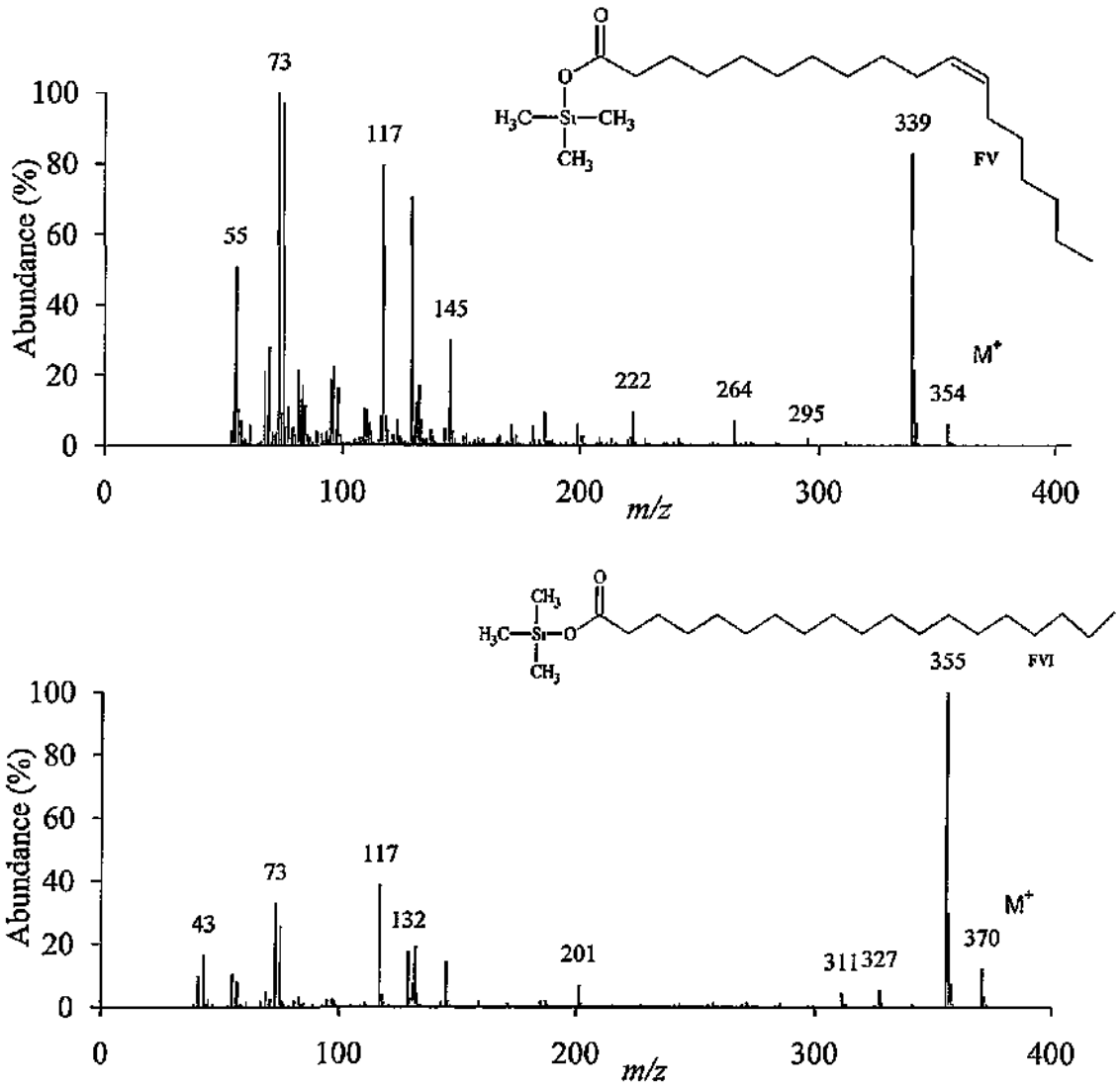

Figure 3.13-3. Background subtracted mass spectra and structures of fatty acid trimethylsilyl (TMS) esters described in the current study. *cis*-11-Octadecanoate - (**FV**): Nonadecanoate – (**FVI**)

Quantification of fatty acids isolated from sea ice and plankton was achieved by manual integration (Chemstation, version C.03.00 software) of the common TMS fragmentation ion (*m/z* 117) signal as recorded by GC/MS SIM (Figure 3.13-1, Figure 3.13-2 and Figure 3.13-3)

Integration of the *m/z* 117 response via SIM chromatogram alone was insufficient for accurate determination of lipid concentrations in samples. To arrive at a usable, comparable value for the recorded analyte signal from GC/MS it was necessary to take into account a) internal standards for varying extraction efficiencies b) sample volume for variations in starting material and c) GC/MS response factor to account for detector sensitivity. Equation 6 was created to perform the necessary quantification of analytes. Where *Pa* denotes integrated peak area of TMS fragment, *Is* is integrated peak area of the internal standard nonadecanoate. Sample volume extracted is expressed as *Sv* and GC/MS response factor as *Rf*.

Equation 6

$$Analyte\ \mu g\ mL^{-1} = \left[\frac{\left(\frac{Pa}{Is}\right) xRf}{Sv}\right]$$

The response factor of the individual fatty acids was calculated from calibration curves of fatty acid concentrations (0.005 mg mL^{-1}, 0.01 mg mL^{-1}, 0.02 mg ml^{-1}, 0.05 mg mL^{-1} and 0.08 mg mL^{-1}; r = > 0.98) against the internal standard of equal concentration to obtain the following response values.

Table 3-4. GC/MS fatty acid response factors calculated by calibration of the *m/z* 117 of pure standards against the *m/z* 117 of the internal standard; nonadecanoic acid (**FVI**).

Fatty acid	Response factor (*Rf*)
FI	1.18
FII	1.26
FIII	0.96
FIV	1.03
FV	0.48

3.14 Sterol (trimethylsilyl ether) quantification

Identification of sterols isolated from sea ice and plankton was established by comparison of the derivatised (TMS) mass spectra against authentic compounds to identify molecular ions and fragmentation pathways (**SI, SII, SIII, SIV, SV, SVI, SVII, SVIII** and **SIX**) (Figure 3.14-1, Figure 3.14-2 and Figure 3.14-3). A quick reference foldout guide to the sterols frequently referred to in this thesis is included in the back of this thesis.

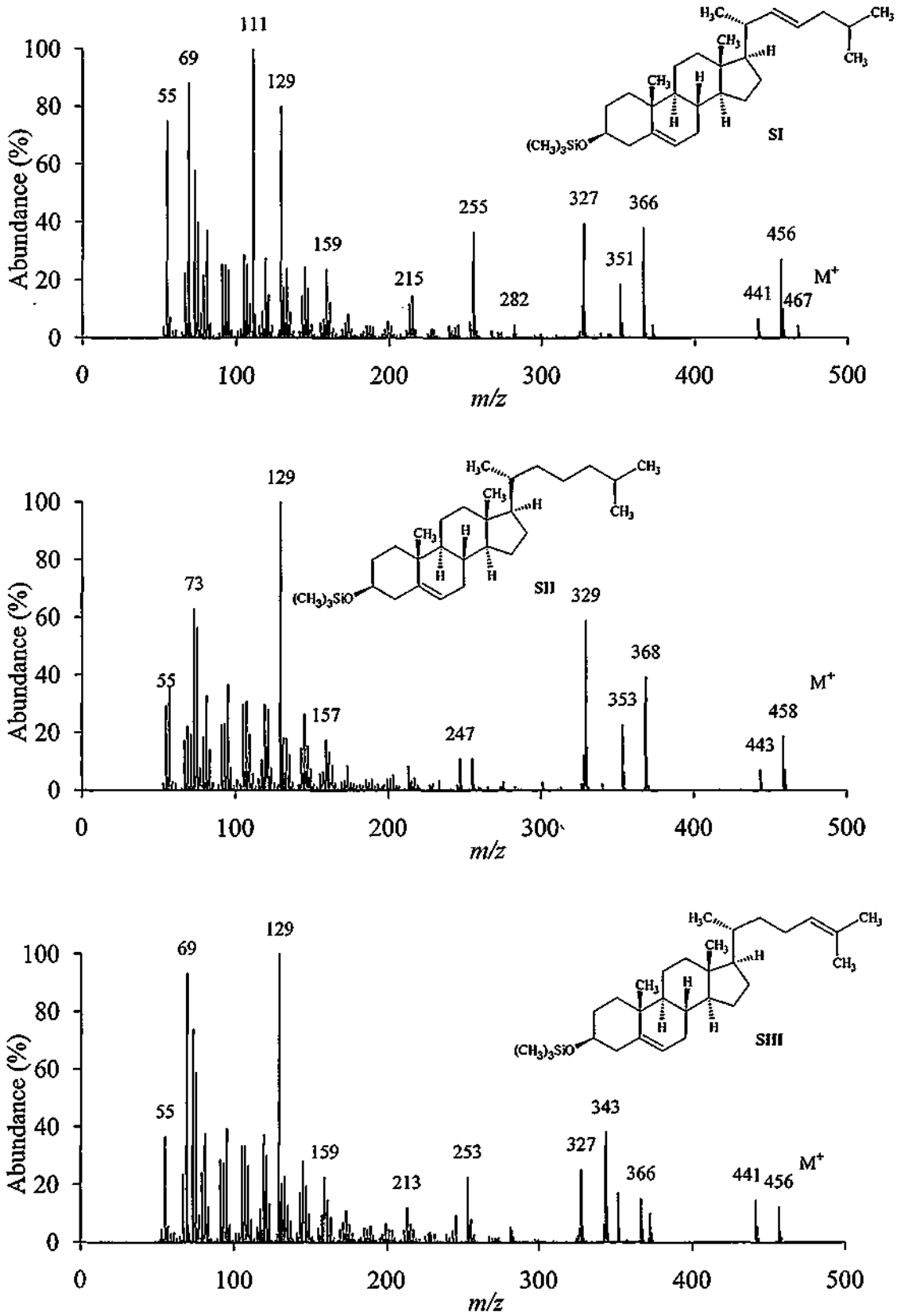

Figure 3.14-1. Background subtracted mass spectra and structures of C_{27} trimethylsilyl (TMS) sterol ethers described in the current study: (22E)-cholesta-5,22-dien-3β-ol - (**SI**): Cholest-5-en-3β-ol - (**SII**): Cholesta-5,24-dien-3β-ol - (**SIII**).

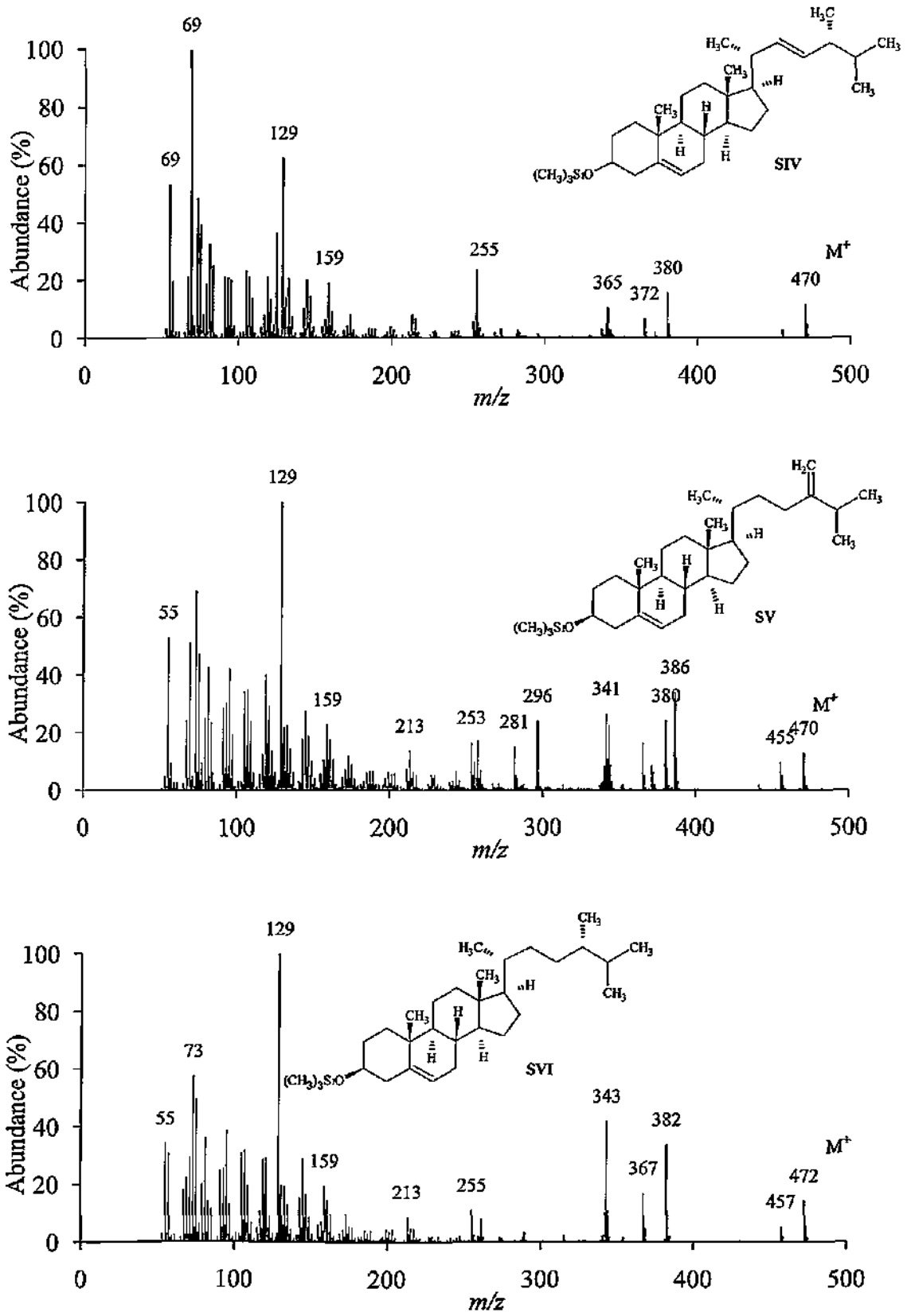

Figure 3 14-2. Background subtracted mass spectra and structures of C_{28} trimethylsilyl (TMS) sterol ethers described in the current study: (22E)-Ergosta-5,22-dien-3β-ol – (**SIV**): Ergosta-5,24(24^1)-dien-3β-ol - (**SV**): Campesta-5-en-3β-ol – (**SVI**).

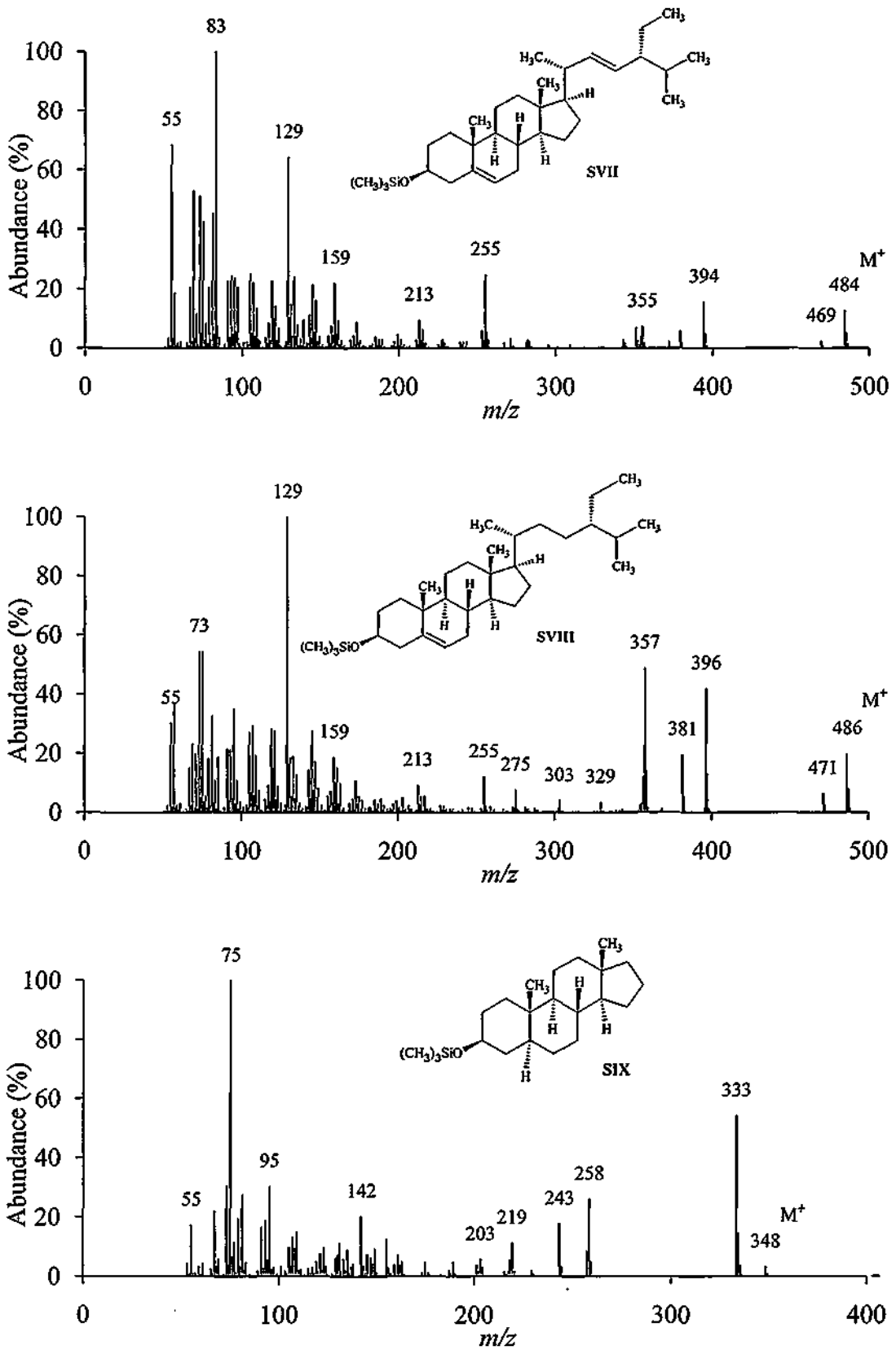

Figure 3.14-3. Background subtracted mass spectra and structures of C_{29} trimethylsilyl (TMS) sterol ethers described in the current study: (22E)-Stigmasta-5,22-dien-3β-ol – (**SVII**): Stigmast-5-en-3β-ol – (**SVIII**): and the internal standard 5α-Androstan-3β-ol – (**SIX**).

Quantification of sterols isolated from sea ice and plankton was achieved by extraction and manual integration (Chemstation, version C.03 00 software) of selected TIC ions Ions were chosen to be unique to each analyte whilst enabling the deconvolution of co-eluting sterols (Table 3-5).

Table 3-5. Identification system used in this study for sterol TMS ethers and the selected ions with relative abundance to the base peak that were selected for GC/MS (TIC) integration and quantification.

Identifier	IUPAC name	Trivial name	Integration ion	Relative ion abundance to base peak (%)
SI	Cholest-5,22*E*-dien-3β-ol	22-dehydrocholesterol	*m/z* 327	40
SII	Cholest-5-en-3β-ol	Cholesterol	*m/z* 458	18
SIII	Cholest-5,24-dien-3β-ol	Desmosterol	*m/z* 343	38
SIV	24-Methylcholesta-5,22*E*-dien-3β-ol	Brassicasterol	*m/z* 470	12
SV	24-Methylcholesta-5,24(28)-dien-3β-ol	Chalinasterol	*m/z* 470	13
SVI	24-Methylcholest-5-en-3β-ol	Campesterol	*m/z* 382	34
SVII	24-Ethylcholesta-5,22*E*-dien-3β-ol	Stigmasterol	*m/z* 255	25
SVIII	24-Ethylcholest-5-en-3β-ol	*β*-Sitosterol	*m/z* 396	42
SIX	5α-Androstan-3β-ol	Androstanol	*m/z* 333	54

Integration of the analyte response via selected ion chromatogram alone was insufficient for accurate determination of concentration in samples To arrive at a useable, comparable value for the recorded analyte signal from GC/MS it was necessary to take into account a) internal standard for varying extraction efficiencies b) sample volume for variations in starting material mass and c) GC/MS response factor to account for detector sensitivity. Equation 7 was created to perform the necessary quantification of analytes. Where *Pa* denotes integrated peak area of sterols, *Is* is integrated extracted ion peak area of the internal standard 5α-androstan-3β-ol. Sample volume extracted is expressed as *Sv* and GC/MS response factor as *Rf*.

Equation 7

$$Analyte\ \mu g\ mL^{-1} = \left[\frac{\left(\frac{Pa}{Is}\right) x Rf}{Sv}\right] \times 0\,1$$

The response factor of the individual sterols was calculated from calibration curves of sterol concentrations (0.0005 mg mL^{-1}, 0.001 mg mL^{-1}, 0.0025 mg ml^{-1}, 0.005 mg mL^{-1} and 0.01 mg mL^{-1}; r = > 0.98) against the internal standard (5α-androstan-3β-ol) of equal concentration to obtain the following response values Table 3-6.

Table 3-6. GC/MS response factors calculated by calibration of pure standards against the internal standard; 5α-Androstan-3β-ol.

Sterol	Response factor (*Rf*)
SI	-
SII	0.04
SIII	0.08
SIV	0.15
SV	-
SVI	0.52
SVII	0.16
SVIII	0.31

- Standards not available

3.15 Alkane quantification

Identification of alkanes isolated from sea ice and shallow Arctic marine sediments was established by comparison of the mass spectra against authentic compounds to identify molecular ions and fragmentation pathways (Figure 3.15-1).

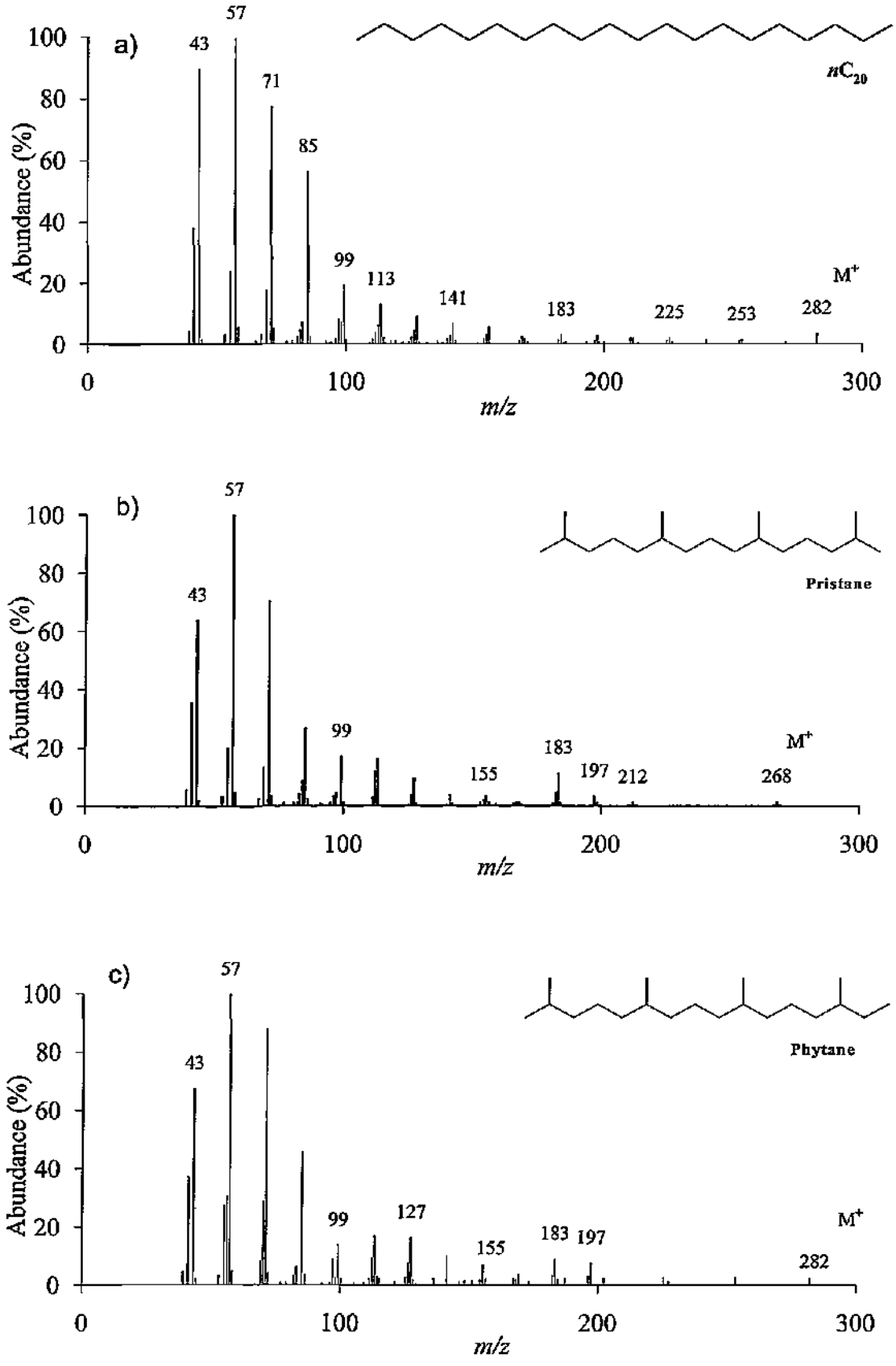

Figure 3.15-1. Background subtracted mass spectra and structures of alkanes described in the current study a) typical *n*-alkane (nC_{20}) b) Pristane c) Phytane .

Quantification of *n*-alkanes isolated from sea ice and shallow Arctic marine sediments was achieved by extraction and manual integration (Chemstation, version C.03.00 software) of each analyte's *m/z* 99 common fragment ion signal recorded by GC/MS, SIM signal (Figure 3.15-1).

Table 3-7. Chemical formulae, molecular weights and GC/MS response factor of saturated hydrocarbon compounds monitored by GC/MS SIM (*m/z* 99) for quantification in this study.

alkane	Chemical formula	Molecular mass (g mol^{-1})	Response factor
nC_{15}	$C_{16}H_{34}$	212	0.59
nC_{16}	$C_{17}H_{36}$	226	0.71
nC_{17}	$C_{18}H_{38}$	240	0.79
Pristane	$C_{19}H_{40}$	268.5	-
***n*C18**	$C_{18}H_{38}$	254	0.9
Phytane	$C_{20}H_{42}$	282.6	-
nC_{19}	$C_{19}H_{40}$	268	1.00
nC_{20}	$C_{20}H_{42}$	282	1.12
nC_{21}	$C_{21}H_{44}$	296	1.14
nC_{22}	$C_{22}H_{46}$	310	1.25
nC_{23}	$C_{23}H_{48}$	324	1.27
nC_{24}	$C_{24}H_{50}$	338	1.33
nC_{25}	$C_{25}H_{52}$	352	1.27
nC_{26}	$C_{26}H_{54}$	366	1.15
nC_{27}	$C_{27}H_{56}$	380	1.26
nC_{28}	$C_{28}H_{58}$	394	0.76
nC_{29}	$C_{29}H_{60}$	408	0.53
nC_{30}	$C_{30}H_{62}$	422	0.34
nC_{31}	$C_{31}H_{64}$	436	0.20
nC_{32}	$C_{32}H_{66}$	450	0.11
nC_{33}	$C_{33}H_{68}$	464	0.06

- Not calculated

Integration of the analyte response via SIM ion chromatogram alone was insufficient for accurate determination of concentration in samples. To arrive at a useable, comparable value for the recorded analyte signal from GC/MS it was necessary to take into account a) internal standard for varying extraction efficiencies b) sample mass or volume for variations in starting material mass c) GC/MS response factor to account for detector sensitivity and d) dry bulk density for exclusion of sediment density variation. Equation 8 and Equation 9 were created to perform the necessary quantification of *n*-alkanes.

Where *Pa* denotes integrated peak area of *n*-alkanes, *Is* is integrated SIM peak area of the internal standard 7-hexylnonadecane Sample mass or volume extracted is expressed as *Sm/Sv* respectively and GC/MS response factor as *Rf* with dry bulk density as DBD where necessary.

Equation 8

$$Analyte\ \mu g\ cm^{-3} = \left[\frac{\left(\frac{Pa}{Is}\right) xRf}{Sm} \times DBD\right] \times 0.1$$

Equation 9

$$Analyte\ \mu g\ mL^{-1} = \left[\frac{\left(\frac{Pa}{Is}\right) xRf}{Sv}\right] \times 0.1$$

The response factor of the individual *n*-alkanes was calculated from calibration curves of *n*-alkane concentrations (0 0005 mg mL^{-1}, 0 001 mg mL^{-1}, 0 002 mg ml^{-1}, 0 004 mg mL^{-1}, 0.006 mg mL^{-1} and 0.008 mg mL^{-1}, r = > 0 98) against the internal standard (7 - hexylnonadecane) of equal concentration to obtain the response values shown in Table 3-7.

3.16 Dry bulk density

Where sediment was analysed it was necessary to account for variations in the sediment density. The dry mass (*Dm*) and water content (*Wc*) of sediments were determined by carefully reweighing each horizon after freeze-drying before applying Equation 4, where *Wm* denotes wet mass (g). Once calculated for all horizons this data was used against standard densities for sediment (2.65 g cm^{-3}) and sea water (1.025 g cm^{-3}) to calculate the amount of sediment mass present in a specific volume of sediment, known

as the dry bulk density by excluding water mass via Equation 5 (Vare *et al.*, 2009; Belt *et al.*, 2010).

3.17 Isolation of diatoms from sample matrices

3.17.1 Internal standard preparation

A 50 µL aliquot of *Haslea crucigera* cells (10 mg mL^{-1} in deionised H_2O) was dried (110°C; 30 min) and 0.25 g ± 0.01 pre-acidified (HCl; 12.2M, 70°C; 30 min) and base treated (KOH; 2M, 70°C; 30 min) freeze dried sediment was added. Simultaneously 50 µL aliquots of *H. crucigera* cells (10 mg mL^{-1} in deionised H_2O) were prepared in replicates of six on glass cover slips (2.4 mm Ø) and mounted with naphrax for cell quantification. From herein the internal standard samples were treated as per sediment samples for diatom isolation.

3.17.2 Diatom isolation from sediment

Approximately 5 mL LST Fastfloat, of 2.21 ± 0.01 specific gravity (relative density with respect to water), was added to 0.25 g ± 0.01 freeze dried sediment and gently agitated (250 horizontal motions min^{-1}; 10 min) and left to settle for 12 h. The surface 0.2 mL LST was then transferred to a polycarbonate centrifuge tube, diluted (1:20 LST:deionised H_2O; v/v) and centrifuged (3500 rpm, 10 min) with the resulting supernatant being carefully transferred to another centrifuge tube which was further diluted (1:2 supernatant:deionised H_2O, v/v) and centrifuged (3500 rpm, 20 min). The supernatant was collected for later recovery of LST and the resulting diatom pellets transferred to the original centrifuge tube. This process was repeated eight times. Traces

of LST Fastfloat were removed from the diatom pellet and sediments with deionised H_2O prior to freeze drying and weighing Diatom cells were re-diluted (deionised H_2O) and 50 µl aliquots were transferred to glass cover slips (2.4 mm Ø), air dried and mounted with naphrax for quantification. Entire cover slips were counted, rather than transects The remaining sample-diatoms and sediments were dried prior to extraction of HBIs. Internal standard samples and slides were produced and separated alongside samples of interest as an alternative to the spiking of diatom cells.

3.17.3 Diatom isolation and identification from sea ice

For the identification and enumeration of protist cells, colleagues melted sea ice sub-samples (0 – 3 cm) and preserved them with acidic Lugol's solution (Parsons *et al*, 1984) Cells ≥ 4 µm were identified to the lowest possible taxonomic rank and enumerated under an inverted microscope (WILD Heerbrugg) equipped with phase contrast optics (Lund *et al.*, 1958). A minimum of 400 cells were counted in each settling chamber (except for two low abundance samples in March where 200–300 cells were counted). The following references were used for ice protist identification: Poulin and Cardinal (1982a, 1982b; 1983), Medlin and Hasle (1990a) Medlin and Priddle (1990b), Poulin (1990a; 1993), Thomsen (1992), Hasle and Syvertsen (1997) and von Quillfeldt (von Quillfeldt, 1997).

3.18 Determination of chlorophyll *a* concentrations in sea ice

Colleagues melted sea ice sub-samples (0 – 3 cm) for the determination of chlorophyll *a* and filtered them onto Whatman GF/F filters (0.7 µm). Concentrations of chlorophyll *a*

were measured using a Turner Designs 10-AU fluorometer after 18 h extraction in 10 mL of 90% acetone at 5 °C in the dark (Parsons *et al.*, 1984).

3.19 Microscopy

3.19.1 Light microscopy

Following isolation (Section 3.17) diatoms were air dried (24 h) onto glass cover slips before being mounted in high refractivity naphrax medium on glass slides, then counted using an Olympus CH2 transmitting light microscope (10x and 40x objective), and a Nikon Eclipse TS100 transmitting light microscope with phase contrast optics (10x and 40x objective).

3.19.2 Scanning electron microscopy

Diatoms were mounted either treated (HCl, 37%; 70°C; 30 min) or untreated on carbon adhered glass surface to metal stubs before being sputter coated (Au/Pd) and viewed on a JEOL 5600 low vacuum scanning electron microscope.

3.20 Total organic carbon

Total organic carbon (TOC %) and nitrogen (TON %) of the marine sediment core horizons were determined using 100 mg ± 5 mg freeze dried sediment which was digested with precisely 1 mL 10% HCl for 18 h at room temperature after which the HCl was removed and washed 3 times from the sample with milli-Q water. Samples were analysed by Andrew Tonkin (University of Plymouth) with a Carlo Erba EA 1110 elemental analyser for carbon, nitrogen and hydrogen.

3.21 Inorganic geochemical analysis

Approximately 0.75 g freeze dried sediment was ground and sieved (250 µm plastic sieve) of which 0 5 g ± 0.05 was transferred to acid clean glass tubes where 2 5 mL HNO_3 (70%) and 7 mL HCl (37%) were also added and subjected to a ramped heating profile (30 min, 85°C, 60 min; 105°C, 60 min, 120°C, 120 min, 140°C). Once cooled the contents were transferred to volumetric flasks and made up to 50 mL (milli-Q). From here samples were homogenised and transferred to polycarbonate centrifuge tubes and centrifuged (3000 rpm, 5 min) with the supernatant being decanted into clean nalgene tubes for later analyses against calibration standards via inductively coupled plasma - optical emission spectroscopy using a Varian 725-ES ICP-OES

3.22 Sediment dating using ^{210}Pb isotopes

Estimates of sediment accumulation rates for shallow Arctic marine box core sediment material were derived using measurement of the excess ^{210}Pb isotope Sub-samples (ca. 3 g) of sediment were selected from box core horizons. ^{210}Pb was measured by Dr. Sabine Schmidt (CNRS, University of Bordeaux) using a low background, high-efficiency, well-shaped λ detector exhibiting good reproducibility (Schmidt *et al.*, 2007; Schmidt *et al* , 2009). Calibration of the λ detector was achieved using IAEA standards (RGU-1, RGTh-1) ^{210}Pb excess was calculated by subtracting the measured activity supported by its parent isotope, ^{226}Ra, from the total ^{210}Pb activity in the sediment. Errors in ^{210}Pb excess were calculated by propagation of errors in the corresponding pair (^{210}Pb and ^{226}Ra) and represented graphically.

3.23 Carbon isotope analysis

Following initial purification, hydrocarbon fractions were further purified (5:95, $AgNO_3$:SiO_2) and isolated as *n*-alkanes, IP_{25} and remaining HBIs respectively. Samples were analysed for $^{13}C/^{12}C$ stable isotope ratios at the Natural Environmental Research Council (NERC, UK) Life Sciences Mass Spectrometry Facility at the University of Bristol on a Delta *plus* XP, ThermoFinnigan trace gas chromatograph coupled to a ThermoFinnigan combustion III stable isotope ratio mass spectrometer fitted with a Varian CP-Sil 5 CB (50 m x 0.32 mm x 0.12 μm) column. Compounds were eluted using a ramped temperature profile from 40 – 300°C, with a 10 min isothermal at 300°C. Data was collected using isodat v3.0 software. Individual compounds were identified by comparison of their gas chromatogram retention times and retention indices derived from previous GC/MS analysis. Isotope compositions reported here are referenced to the Vienna Pee Dee Belemnite (VPDB) standard and are calculated according to Equation 10. The isotopic composition of the derivatising reagent (BF_3MeOH; -44.04‰) was accounted for (where used) according to Riley (1994) using Equation 11 where *nC* is the number of carbons in the molecule of interest.

Equation 10

$$\delta^{13}C\ (‰)\ instrumental\ value = \left(\frac{\left(\frac{^{13}C}{^{12}C}\right) sample}{\left(\frac{^{13}C}{^{12}C}\right) VPDB} - 1\right) \times 1000$$

Equation 11

$$\delta^{13}C\ (‰) = \delta^{13}C\ instrumental\ value - \left(\frac{1}{nC}\right) \times \delta^{13}C\ BF_3MeOH$$

3.24 Sediment particle size analysis

Particle size analyses were undertaken by Richard Hartley (University of Plymouth) using a Malvern Mastersizer 2000 laser particle sizer. Freeze dried sediments (ca. 0.5 g) were taken at intervals throughout sediment cores. Individual distributions of particle size measurements (3 replicates) were made using a red and blue laser for 30 s, with a particle refractive index of 1.53 and a light absorption value of 0.005. Individual distributions of particle sizes were calculated using previously reported methods (Friedman *et al.*, 1978), according to the following classifications – clay: < 2 μm, silt: 2 – 63 μm; sand (coarse): 63 μm – 2 mm.

3.25 Principal components analysis

To better realise any potential covariance and to understand the underlying numerical structure in HBIs, fatty acids and sterols, a multivariate approach, such as principal components analysis (PCA) is invaluable (e.g Yunker *et al.*, 1995) PCA is considered an exploratory tool, essentially rotating and scaling the data, providing a simplified basis on which to discuss underlying trends. With this method, a large number of biomarker observations can be transformed (orthogonal linear transformation) into a smaller, more manageable, coordinate set of data These data are orientated to account for the majority of variation in as few dimensions as possible (components). The reliability of interpretations made from the data increases where greater proportions of variability are accounted for in the first, second and sometimes third components. PCA was performed using correlation matrix standardised values in Minitab 15 Zero-values were not present. Robustness of each test was determined by; a) consideration of the ratio of observations to variables, with the former being greater, b) variability in the projection following removal and incorporation of lipid classes, c) loading magnitude of

the first two or three principal components (PCs). It was concluded that all PCA model projections were stable and were an accurate reflection of the underlying geochemical relationships. The influence each variable has on the projection is known as the leverage, with variables farthest from the axis crossing having the greatest leverage on the PCA model (Jolliffe, 2002).

CHAPTER FOUR

4 Temporal distribution of HBIs in Arctic sea ice

4.1 Introduction

Chapter 4 describes the examination of the occurrence of IP_{25} and HBIs within Arctic sea ice from the Amundsen Gulf region of the CAA. Additional biomarker analysis was conducted to contextualise the findings in terms of established sea ice biomarkers. As a result, the temporal constraints of IP_{25} production, along with other polyunsaturated HBIs and established biomarkers, were determined.

4.1.1 Physical structure of Arctic sea ice

The growth and microstructure of Arctic sea ice (and therefore its ability to accommodate biological communities) can be considered a function of the environmental conditions in which the ice is formed (Eicken *et al.*, 1991; Mundy *et al.*, 2005). With additions from, for example, gas intrusions, brine channel formation and particulate matter, both the optical and mechanical properties of sea ice can be affected. Under-ice irradiance is a function of the optical properties of sea ice, which are highly significant in terms of providing available light for photosynthesis to sea ice bottom ecosystems (Gosselin *et al.*, 1990a). Unlike planktonic species, sea ice diatoms comprise ca. 89% benthic species (Melnikov, 1997) which are incapable of significant motility (Poulin, 1990b; Round *et al.*, 1990) and are thus more susceptible to considerable variations in irradiance. Inconsistencies in the crystalline sea ice structure that form following the inclusion of gas bubbles, particulate matter or structural

fractures can refract solar irradiance, reducing available light to the photosynthetic algae (Jiang *et al.*, 2005).

The inclusion of some biological adaptations are also capable of exerting micro structural changes within the ice matrix (Krembs *et al.*, 2002a) The production of exopolymeric substances (EPS) in aquatic systems has long been demonstrated as a means to form and maintain protective microhabitats for microbes (Decho, 1990) and more recently, sea ice diatoms (Krembs *et al* , 2002b). EPS can account for up to 4 g C m^{-2} sea ice and appears to play important cryoprotection roles for diatoms against winter conditions of high salinity and potential ice-crystal damage (Krembs *et al* , 2002b). The production of substances such as EPS in sea ice is therefore an important consideration in terms of the structural integrity and refractive capacity of sea ice.

4.1.2 Arctic sea ice and snow thickness

Sea ice thickness and snow cover both exert a degree of control over ice associated biomass, by controlling the amount of light that can reach bottom-ice habitats (e.g. Cota, 1985; Rolf *et al.*, 1991, Mundy *et al* , 2005; Różanska *et al.*, 2009; Nicolaus *et al.*, 2010). Solar radiation is affected by a number of constantly varying atmospheric factors such as the respective solar angle, clouds, aerosol and ozone in the atmosphere (Bischof *et al* , 2007) The photosynthetically active radiation (PAR) for diatom primary productivity (400 – 700 nm) is then further subjected to spectral narrowing as a function of ice thickness (Arrigo *et al* , 2010). Increased snow cover also accentuates this, further restricting available light for photosynthesis. For example, measurements of the PAR and near ultra violet spectrum with a portable spectroradiometer in the sea ice of Kongsfjorden, Svalbard, revealed that 5 cm of snow was capable of reducing the PAR by up to a factor of ten (Jan-Gunnar *et al* , 2004) It therefore stands that snow covered

ice is capable of generating a consistently greater albedo than snow free ice by reflecting more of the sun's radiation (Robock, 1980). The ability of snow to restrict PAR can therefore affect the physical structure of the ice by influencing the growth of microorganisms (Krembs *et al.*, 2002a; Krembs *et al.*, 2002b).

In addition to the biological controls on PAR, snow has also been shown to prevent effective heat release from freezing ice, due to its insulating properties (Eicken, 2003). An investigation involving over eighty point samples of Beaufort Sea snow-covered sea ice, revealed an average thermal conductivity difference of more than five times, between exposed sea ice and snow covered sea ice (Sturm *et al.*, 2002b). While there were some inter-sample variations, a bulk thermal conductivity value was confidently achieved (0.14 W $m^{-1} K^{-1}$). As a result of this restricted release of heat, sea water beneath the ice cannot effectively radiate its thermal energy required to reach the critical freezing point (approximately -1.8°C depending on the quantity of inorganic salts present). The restriction of heat release consequently obstructs the formation of new platelet ice, further influencing available habitat for biomass production. When considered in terms of thermodynamics, snow provides a much greater impact on the sea ice community than ice thickness. If just 50 cm of ice are considered, it requires only 3 - 5 cm of snow to effectively double the thermal capacity of the ice (Eicken, 2003). Such conditions are commonly found in Arctic regions. In contrast, some regions of the Arctic sea maintain heat exchanges with the atmosphere throughout winter in regions of open water termed polynyas.

4.1.3 Polynyas in the Arctic

The occurrence of large areas of open water and sometimes thin sea ice are important features in the Arctic during the winter. Polynyas occur where environmental conditions

are counter productive for sea ice formation (Smith *et al.*, 2007) either resulting from strong winds or ocean currents driving away newly forming sea ice, preventing its consolidation (latent heat), or effective thermal transfer from warmer water from regions of upwelling (sensible heat). The Cape Bathurst polynya in the Amundsen Gulf (Figure 4.1-1) is formed partly by strong easterly winds (Hoppema *et al.*, 2007) and is noted to provide a highly variable input of organic carbon to the region (90 – 170 g C m^{-2} yr^{-1}) (Arrigo *et al.*, 2004; Hoppema *et al.*, 2007).

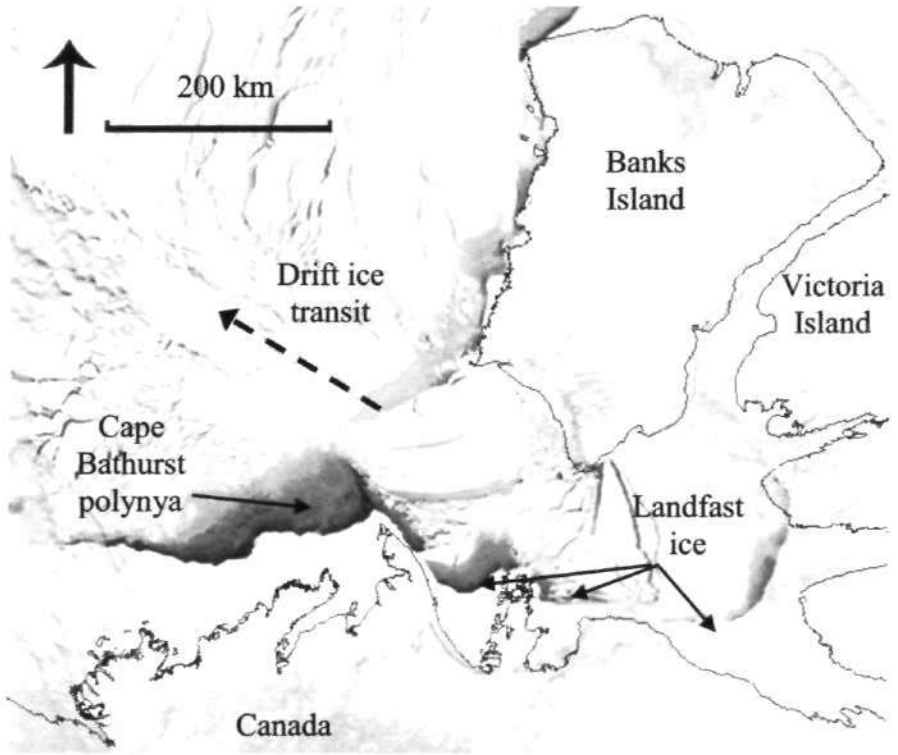

Figure 4.1-1. Moderate Resolution Imaging Spectroradiometer (MODIS) image of Amundsen Gulf sea ice cover, 6th April 2008, indicating land fast ice and the predominant westerly transit of unconsolidated drift ice.

Additionally, the sea floor topography rises relatively steeply (0 – 60 m) in just 8 km from the deeper water of the Amundsen Gulf to the Cape Bathurst region. The resulting significant isobath divergence provides the drive for topographically enhanced shelf-break upwelling (Williams *et al.*, 2008).

4.1.4 Microstructure of Arctic sea ice

Temperature and salinity are considered to be two of the most influential factors to affect sea ice microstructure (Golden *et al.*, 2007; Dieckmann *et al.*, 2010). A basic understanding of sea ice formation provides evidence for the significance of temperature changes on the formation of brine within sea ice (Assur, 1960; Eicken, 2003). Sea water, as a solution, contains many ions (e.g. Na^+, K^+, Ca^{2+}, Mg^{2+}, Cl^-, SO_4^{2-}, CO_3^{2-}). During freezing, many of these ions are excluded from the crystalline structure of ice, leading to brine production and the formation of micro and macroscopic channels into which algae and other microorganisms can adhere. The extent of exclusion (and salinity) is a function of temperature. Therefore, temperature is considered capable of altering the porosity and pore size of sea ice, effectively increasing, or otherwise, habitable area. Studies of permeability and the fluid volume fraction of sea ice have established that columnar sea ice becomes effectively impermeable to brine transport where the fluid volume fraction is less than 5% (Cox *et al.*, 1983; Golden *et al.*, 2007). Above 5%, the connectivity of brine channels becomes sufficient for organisms such as diatoms to successfully inhabit the ice (Figure 4.1-2).

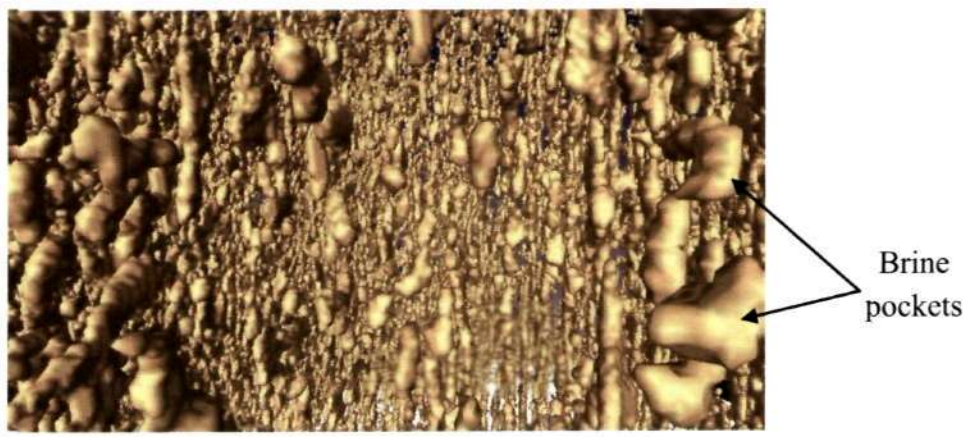

Figure 4.1-2. X-ray computed tomography of the internal brine inclusions of a single crystal of laboratory-grown sea ice at -8°C (Golden *et al.*, 2007). The porosity, or relative brine volume fraction, is 5.7%.

Further, as previously mentioned, the thermal capacity of the sea ice is greatly influenced by irradiance and therefore snow cover, a factor which is observed as being highly variable (ca. 40 cm variation in snow thickness within 10 m was observed for example during the CFL cruise 2008). Inconsistencies in snow cover could therefore be expected to produce irregular patterns of growth in the sea ice community. Arctic sub-ice communities are known to exhibit sporadic habitation of the ice (Figure 4.1-3). This is possibly attributable not only to snow cover (Gosselin *et al.*, 1986; Mundy *et al.*, 2005), but to the macro relief of the ice affording protection from currents (Melnikov *et al.*, 1987).

Figure 4.1-3. Uneven distribution of algae on the underside (ice/water interface) of Arctic drift ice (ca. 1.5 m thick) in the Amundsen Gulf (71°17.7 N, 124°31.3 W), 08/04/2008.

4.1.5 The inclusion of algae within Arctic sea ice

The precise mechanisms for the inclusion of algae into sea ice are not fully understood. In determining sea ice algal contributions to marginal ice zone blooms, Lixotte (2001) suggests seeding from sea ice diatoms, yet he is unable to account, with confidence, for the mechanism that diatoms adopt to become included in the sea ice in the first place. Various hypotheses exist (Bunt, 1970; Andersen, 1977; Garrison *et al.*, 1983; Riebesell *et al.*, 1991; Lizotte, 2001), where the incorporation of protists into sea ice has been observed in the Arctic and Antarctic. Two recurring theories are evident; harvesting/scavenging and nucleation. The most common view involves the incorporation of algae into frazil ice from within the water column (Bunt, 1970; Garrison *et al.*, 1983; Reimnitz *et al.*, 1990). The formation of small frazil ice crystals, in the upper 100 m of the water column (Dieckmann *et al.*, 1986; Dieckmann *et al.*, 2003), is followed by the subsequent flocculation of the newly forming ice crystals around microscopic particles of various origins which act as nuclei. As the crystals flocculate, algae can act as nuclei and become incorporated into the matrix of the newly forming ice (Reimnitz *et al.*, 1990). As a popular hypothesis of sea ice algal seeding, algal sequestration within forming frazil sea ice implies that diatoms are present in the upper water column of ice free seas. An indirect contradiction to this proposed seeding mechanism exists for the *Haslea* genus following a broad investigation into the distribution of this and other species in Arctic ice habitats (Booth *et al.*, 1997). Booth and Horner (1997) noted that while *Haslea* spp. diatoms were relatively abundant within sea ice, the water column appeared void of the ice endemic *Haslea* spp. An alternative theory for the incorporation of *Haslea* spp. into sea ice was instead proposed on the basis of diatom cellular structure and its association with habitat. For example *Haslea crucigeroides*, being a pennate variety of diatom, is highly typical of epipelic

species associated with fine sediments (Round *et al*, 1990). This benthic origin, combined with deep (250 m) water frazil flocculation (Dieckmann *et al.*, 1986) within relatively shallow (ca. 300 m) Arctic shelf seas (Dieckmann *et al*, 2003), provides a more feasible mechanism for incorporation of such species into sea ice Both mechanisms seem reasonable and therefore likely, given the environmental circumstances present in the Amundsen Gulf, yet neither has been conclusively proven.

4.1.6 Ice types in the Arctic

Arctic sea ice is not homogenous in type or distribution. Each specific type of sea ice is representative of the conditions in which it was formed, with two distinct categories evident. Perennial multiyear ice is characteristically thick (ca. 2 - 4 m) owing to its longer residence in the Arctic (up to 7 yrs, Hop *et al.*, 2006) and contains much less brine and more gas inclusions than first year sea ice (Aleksandrov, 1994; Walker *et al.*, 2006). In contrast, annual first year ice reaches a maximum of ca. 2 m thickness in a short period of time from the onset of freezing (ca. 4 months) before melting in the spring. First year ice generally contains more brine than multiyear ice and is structurally weaker (Aleksandrov, 1994; Walker *et al.*, 2006).

A further subdivision of the annual first year ice into drift ice and landfast ice, is also necessary. Both drift ice and landfast ice are formed primarily by the flocculation of frazil ice crystals within the water column, theoretically exposing both varieties to the biological seeding mechanisms discussed previously However, landfast ice is measurably denser than drift ice as a consequence of calmer surface waters permitting the formation of stable ice types with the subsequent formation of congelation ice In contrast, drift ice is commonly formed in regions of greater turbulence, such as open water, marginal ice zones and polynyas, where dynamic currents and/or wind mixing

lead to rough pancake ice production. The resulting density variation between landfast and drift ice can result in disproportionate grazing of sea ice algae by predators. This reduced grazing of lower porosity landfast ice (Arrigo *et al.*, 2010) can result in a greater quantity of algal biomass compared to drift ice.

4.1.7 Presence and formation of melt ponds in Arctic sea ice

An important control on sea ice permeability is the influence of temperature and sea ice melt. During winter, the net heat flux is usually from the water to the ice (Petrich *et al.*, 2010), yet, due to the much lower atmospheric air temperature, the ice does not melt. Instead, the ice is, initially, warmed, leading to the melting of it's microstructure, potentially further increasing bottom-ice porosity. As air temperature increases, along with the affect of solar radiation, snow that has settled on the ice over winter generally begins to melt. Eventually, the surface of the ice will also begin to melt resulting in considerable reduction of salinity in the surface layers of ice (Untersteiner, 1968). The mechanisms involved in the distribution of this low salinity melt water, throughout the period of sea ice melt, are complicated in terms of Arctic sea ice energy budgets. A tracer study (^{2}H, ^{18}O and ^{7}Be) carried out in the Arctic in 1998, estimated that 50% of this water will percolate into the ice, flushing it in the process, while 25% of the water will remain as melt ponds, with the rest draining into ocean surface waters (Eicken *et al.*, 2002). Eventually, through ablation and bottom-ice melt (Perovich *et al.*, 2003), the melt ponds will extend through to the ocean beneath.

4.1.8 Primary production in Arctic sea ice

Sea ice provides adapted micro-organisms with a unique habitat. While planktonic algae are generally more biologically productive than ice-associated algae, the latter are often considered wholly responsible for the carbon fixation that occurs within ice covered waters (Arrigo *et al*, 2010). By adapting to the unique microstructure of sea ice, ice algae ensure, to a degree, the availability of PAR. In contrast, planktonic algae achieve this through the development of pores and cellular protrusions that promote a degree of buoyancy control (Round *et al*, 1990). Habitation of sea ice is therefore dominated by benthic rather than planktonic diatoms (Poulin, 1990b). By occupying sea ice, diatoms greatly restrict their ability to respond rapidly to physical or chemical changes Unlike their planktonic counterparts, the inability of ice algae to physically migrate with changes in light intensity is overcome by certain specific adaptations Variation in light attenuation, for instance, is combated by control of photosynthetic accessory and photoprotective pigments such as chlorophyll-*c* and β-carotene, respectively (Arrigo *et al*, 2010) The high dependence of ice algae on their physical environment results in variation in both abundance and primary production in relation to the highly variable chemical and physical nature of sea ice.

It is therefore considered that both the abundance and diversity of sea ice algal communities are controlled by the specific environmental conditions of a region (Arrigo *et al*, 2010)

4.1.9 Environmental variables that affect sea ice algal primary production

While there are numerous influences on algal growth, some are considered more significant than others and as such, are routinely recorded and observed These factors

generally include, but are not limited to, salinity (e.g. Grant *et al.*, 1976; Arrigo *et al.*, 1992; Andreas *et al.*, 2007), temperature (e.g. Arrigo *et al.*, 1992; Peter *et al.*, 2005; Eddie *et al.*, 2008) and nutrients (e.g. Lizotte *et al.*, 1992; Smith *et al.*, 1993; Estrada *et al.*, 2009). Of the nutrients, silica is perhaps the most restrictive for diatoms (Gosselin *et al.*, 1990b). Further, light limitation as a response to ice and snow cover (e.g. Anna *et al.*, 1985; Irwin, 1990; Rolf *et al.*, 1991), as well as seasonal variations in daylight hours (Lee *et al.*, 2008; Różanska *et al.*, 2009) are also significant. Through observation, many of the significant factors affecting algal growth are localised restrictions, such as nutrient supply and temperature, thereby potentially reducing their significance on a pan-Arctic scale. The seasonal availability of daylight, in contrast, influences the entire Arctic Ocean. The return to a diurnal light regime from the Arctic polar night therefore effectively enables the onset of diatom photosynthesis (Werner *et al.*, 2007) which, where other conditions are appropriate, initiates what is commonly referred to as a bloom (Smith *et al.*, 1993; Różanska *et al.*, 2009). The Arctic spring ice algal bloom is characterised by the rapid growth of sea ice algae, usually toward the bottom of the ice, near the ice-water interface, which typically coincides with the onset of ice melt (Różanska *et al.*, 2009).

In an investigation into ice organism distributions in Kobbeijord, West Greenland, Mikkelsen, Rysgaard and co-workers (2008) noted that there was a significant succession in the observed species within the sea ice throughout an entire sea ice season. They found the sea ice from December to February was dominated by flagellates (dinoflagellates and cryptophytes), followed by a dominance of the small centric diatom *Chaetoceros simplex* in March, finally culminating in increased pennate diatom abundance through May until the ice melted. The growth rates of microorganisms during algal blooms are generally observed in the chlorophyll *a*, fatty

acid and/or sterol composition of sea ice and the water column (e.g. Nichols *et al*, 1993; Yunker *et al.*, 1995, Gosselin *et al*, 1997; Heide-Jørgensen *et al.*, 2007).

Smith, Cavaletto and co-workers (1993) established the sensitivity of the lipid content of sea ice algae to environmental conditions at Resolute, CAA. By observing the lipid content of sea ice algal organisms, in addition to the distribution of organisms, they established a shift in lipid composition from early to late bloom An early, pre-bloom predominance of polar lipids (glycolipids and phospholipids) and pigments switched to an increased production of neutral lipids, such as triacylglycerols and free fatty acids both through and towards the end of the bloom

4.1.10 Fatty acids in Arctic sea ice diatoms

Saturated and unsaturated fatty acids are important chemicals in diatoms as storage for energy as well as regulation of cell fluidity at low temperatures (Gillan *et al*, 1981; Linda *et al*, 1988) In marine diatoms, saturated fatty acids are generally observed as more abundant than polyunsaturated fatty acids (PUFAs) (Round *et al.*, 1990). The general fatty acid composition of microalgae is also usually distinctive, with diatoms exhibiting high concentrations relative to other classes of cellular lipids (Volkman *et al*, 1989). Various studies of single species cultures show that the C_{14}, $C_{16\,1\omega7}$, C_{16} and $C_{20\,5\omega3}$ fatty acids are representative of marine diatoms (e.g. Opute, 1974; Volkman *et al.*, 1989, Dunstan *et al*, 1994, Zhukova *et al.*, 1995; Ying *et al.*, 2000), providing an abundant, readily detectable biomarker suite for general marine diatom presence and abundance Discrimination between the sea ice and planktonic origin of these compounds, however, is not possible, yet changes in distribution can be used to infer events such as algal blooms. For example, off the West Greenland coast the total diatom specific fatty acid concentrations ranged from 55 $\mu g\ L^{-1}$ to 132 $\mu g\ L^{-1}$ during an algal

bloom, before declining to ca. 3 μg L^{-1} post-bloom, in correlation (r = 0.7) with diatom mass (Reuss *et al.*, 2002). Additionally, Arae *et al.*, (1987) and Yi-Sun *et al.*, (2009) identified the presence of C_{18} fatty acids in varying abundance in both ice algae and phytoplankton. In contrast, *cis*-vaccenic acid ($C_{18:1\omega7}$) has been associated with a bacterial origin in some regions (Theberge *et al.*, 1996; Rontani *et al.*, 2002; Yi-Sun *et al.*, 2009).

4.1.11 Sterols in Arctic sea ice diatoms

Sterols are also useful biochemicals for recording primary productivity in the ocean and sea ice (Volkman *et al.*, 1998). A variety of phytosterols are abundant as important structural constituents of the cell membranes of terrestrial and marine plants (Barenholz, 2002; Bechtel *et al.*, 2009), including microalgae such as diatoms, which primarily contain sterols with between 27 and 29 carbon atoms (C_{27} – C_{29} sterols). Phytosterols are biosynthesised, typically, from a common precursor chemical, squalene, via the MVA/MEP isoprenoid pathways (Vieno *et al.*, 2000; Massé, 2003). However, no individual sterol appears to be unique or indeed diagnostic of any one species of diatom (Volkman *et al.*, 1998; Rampen *et al.*, 2010). In analyses of numerous species of marine diatoms (up to more than 100) a range of sterol distributions was observed, with none being considered wholly representative of diatoms (Barrett *et al.*, 1995; Rampen *et al.*, 2010). Further, it has also been found that environmental stress can trigger a change in common sterol production in individual flagellates, adding additional complications to deciphering the origins of marine sterols (Marco Vincenzo *et al.*, 1997). While their non-specific nature hinders detailed determination of source organisms, the analysis of sterols can still be useful with respect to measuring primary productivity. Additionally, tentative assumptions based on terrestrial or marine origins may be possible where some

sterols (e g β-sitosterol) are considered to be largely indicative of higher order plant production, while cholesterol, for example, is a major animal sterol (Volkman *et al*, 1998). As suggested however, studies are making it increasingly apparent that some sterols can be widely distributed and that care must be taken when making inferences regarding their source

While a range of fatty acids and sterols are produced by sea ice algae, neither are considered representative due to the array of further sources such as planktonic algae, animals and terrestrial plants These lipids therefore provide limited specific information on the affects of environmental variables on sea ice primary production In contrast, the recently discovered lipid, IP_{25}, is believed to be produced only by sea ice diatoms and as such provides an opportunity to investigate sea ice specific productivity.

4.2 Aims and objectives of sea ice lipid investigations

IP_{25} has been routinely isolated and monitored in a variety of Arctic sediments facilitating palaeo-sea ice reconstructions (e.g. Belt *et al.*, 2007; Andrews *et al.*, 2009; Müller *et al.*, 2009; Vare *et al.*, 2009; Belt *et al.*, 2010). Despite this, little is known about the environmental influences affecting sea ice diatom production of IP_{25}. For example, little is understood of the temporal and spatial production of the biomarker in sea ice, or the impact of localised environmental stresses and variations in sea ice type. Therefore, the main aims of this study relating to sea ice were to:

i. Establish the temporal constraints in the production of IP_{25} and other HBIs in diatoms within Arctic sea ice
ii. Investigate the co-variance of IP_{25} and other HBIs and lipids throughout the period of study
iii. Resolve the potential for localised discrepancies in the production of IP_{25} and other HBIs as a function of snow cover

4.3 Method

4.3.1 Selection of sea ice samples and fieldwork

Collection of sea ice samples was carried out as part of Team 3 ('Primary Production', led by Michel Gosselin (ISMER, Canada)) activities, between legs 5 and 9 (January – July 2008), during the Canadian Circumpolar Flaw Lead System Study, as part of the International Polar Year (IPY-CFL). The cruise was carried out onboard the class 1200 Canadian Coast Guard Ship, Amundsen (IPY-CFL, 2010). Of the 81 sea ice cores collected, 69 (85%) of these represented the collection of triplicate cores, with 10 (12%) in duplicate cores. The remaining 2 (3%) cores were without replicates (Table 4-1).

Table 4-1 Sea ice core collection data from legs 5 to 9 of the IPY-CFL cruise, 2008

Date	Ice type	Ice thickness (cm)	Snow thickness (cm)	Station ID	Location				Ice sampled (cm)
16-Jan	Drift	69	2	D17	71°30'	N	124°55'	W	10 x 1
19-Jan	Drift	51	3	D17	71°32'	N	124°59'	W	10 x 1
26-Jan	Drift	94	10	D19	71°07'	N	124°57'	W	10 x 1
08-Feb	Drift	105	4-18	D19	71°04'	N	124°49'	W	10 x 3
27-Feb	Drift	110	3-5	D26	70°55'	N	123°58'	W	10 x 1
07-Mar	Drift	120	-	D29	71°01'	N	123°28'	W	10 x 2
17-Mar	Drift	130	4	D29	70°54'	N	123°28'	W	10 x 2
19-Mar	Drift	30	3	D31	70°54'	N	123°01'	W	10 x 2
22-Mar	Drift	135	3	D32	71°03'	N	121°47'	W	10 x 3
25-Mar	Drift	145	2	D33	71°03'	N	121°47'	W	10 x 3
28-Mar	Drift	150	3	D33	71°03'	N	121°47'	W	10 x 3
31-Mar	Drift	157	3	D33	71°03'	N	121°47'	W	10 x 3
03-Apr	Drift	151	3	D33	71°03'	N	121°47'	W	10 x 2
06-Apr	Drift	158	3	D36	71°12'	N	124°08'	W	10 x 3
08-Apr	Drift	158	2	D36	71°17'	N	124°31'	W	10 x 3
11-Apr	Drift	124	2	D38	71°15'	N	134°37'	W	10 x 1
01-May	Drift	144	4	D43	70°50'	N	124°46'	W	10 x 3
05-May	Drift	146	4	D43	71°10'	N	126°18'	W	10 x 3
08-May	Fast	131	4	F1	70°10'	N	124°49'	W	10 x 3
12-May	Fast	173	0	F2	69°56'	N	126°10'	W	10 x 3
16-May	Fast	170	0	F2	69°56'	N	126°10'	W	10 x 3
20-May	Fast	125	10	F3	71°34'	N	119°36'	W	10 x 3
21-May	Drift	132	7	D45	70°43'	N	124°03'	W	10 x 3
24-May	Fast	125	8	F4	72°36'	N	126°02'	W	10 x 3
28-May	Fast	183	5	F5	74°30'	N	124°05'	W	10 x 2
30-May	Drift	84	9	D46	71°34'	N	125°17'	W	10 x 3
02-Jun	Fast	148	8	F6	69°51'	N	123°45'	W	10 x 3
07-Jun	Fast	143	0	F7	69°49'	N	123°37'	W	10 x 3
09-Jun	Fast	135	0	F7	69°49'	N	123°37'	W	10 x 3
11-Jun	Fast	130	0	F7	69°49'	N	123°37'	W	10 x 3
13-Jun	Fast	126	0	F7	69°49'	N	123°37'	W	10 x 3
15-Jun	Fast	111	0	FB04	69°57'	N	125°52'	W	10 x 3
18-Jun	Fast	165	8	F7	69°48'	N	123°39'	W	10 x 3

- Data not available

The spatial and temporal distribution of sea ice cores is shown in Figure 4.3-1 and Figure 4.3-2. In terms of temporal distribution, sea ice cores were collected over a time window chosen to encompass the previously documented Arctic sea ice algal bloom (e.g. Lee *et al.*, 2008; Różanska *et al.*, 2009).

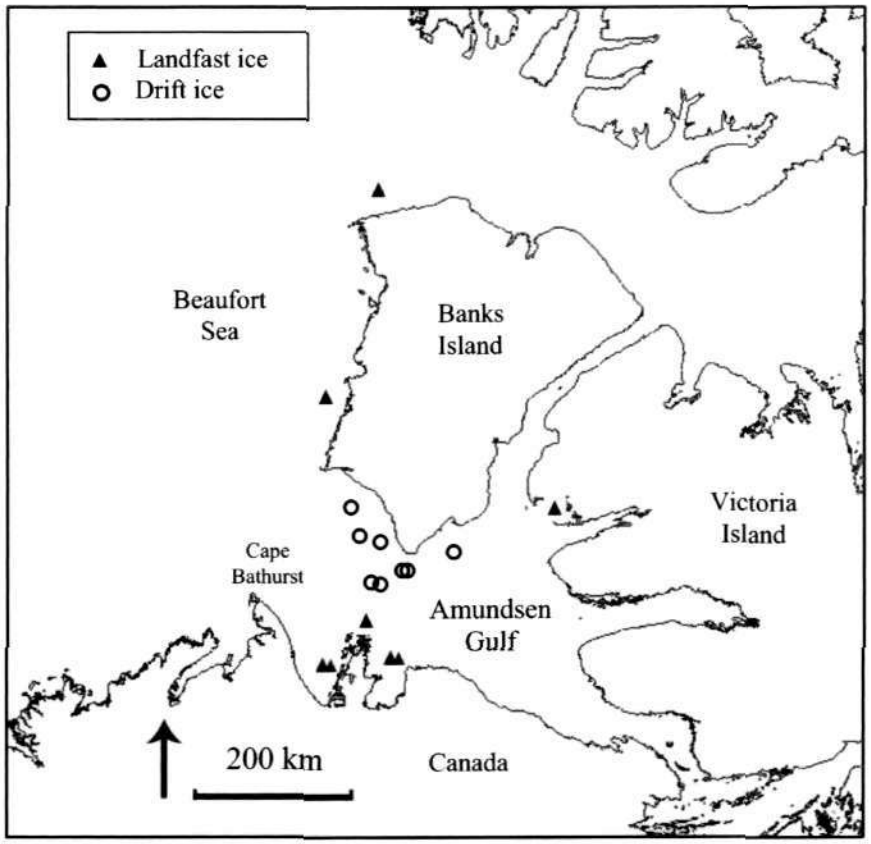

Figure 4.3-1. Spatial distribution of sea ice core collection sites from drift ice (circles) and landfast ice (triangles) both within and adjacent to the Amundsen Gulf region of the CAA during the IPY-CFL cruise, 2008.

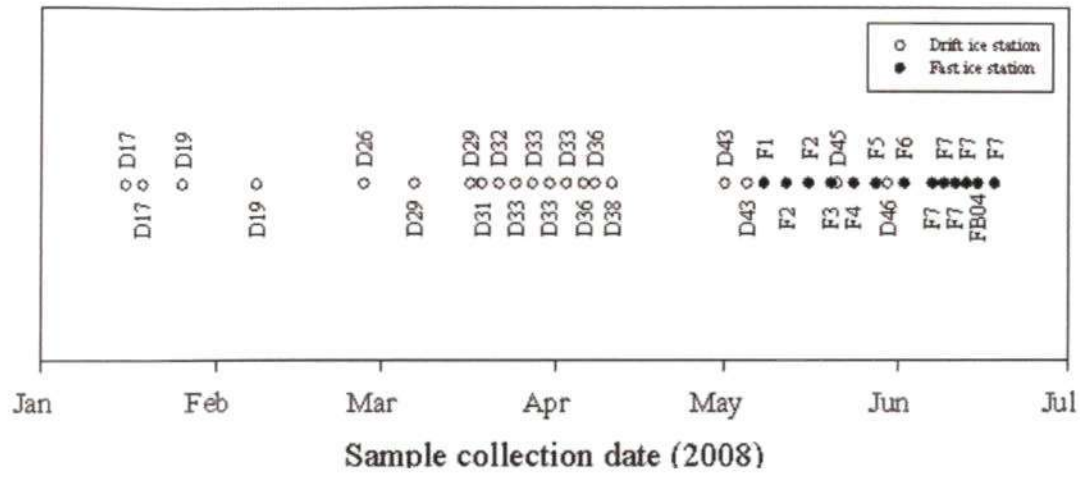

Figure 4.3-2. Temporal distribution of sea ice core samples collected from within and adjacent to the Amundsen Gulf region of the CAA during the IPY-CFL cruise; 01/01/08 – 01/07/08.

Samples of drift ice and landfast ice were collected during this study using a Kovacs Enterprises© Mark II, 90 mm Ø core barrel (Figure 4.3-3) (Kovacs, 2010).

Figure 4.3-3. Kovacs Enterprises © Mark II sea ice corer and accessories used to collect sea ice samples during the IPY-CFL cruise, 2008 (Kovacs, 2010).

Sea ice cores were retrieved and sectioned, *in situ*, by hand to ca. 15 – 20 cm (Figure 4.3-4). Cores were then stored, temporarily, in pre-labelled plastic bags. Onboard the Amundsen, the sea ice cores were further sectioned in a temperature-controlled laboratory (-20°C), using an Omcan food preparation band saw at 5 and 10 cm, yielding

sea ice sections spanning 0 – 5 cm and 5 – 10 cm from the ice-water interface (Figure 4.3-4).

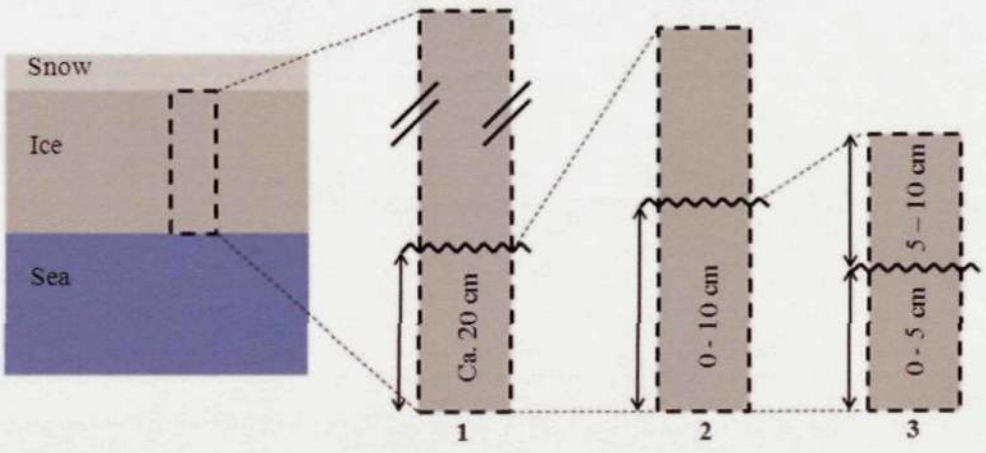

Figure 4.3-4. Schematic of sea ice core sectioning: 1, *in situ* handsaw cut (zig-zag line): 2, Temperature controlled room (-20°C), 10 cm band saw cut (zig-zag line): 3, Temperature controlled room (-20°C) 5 cm band saw cut (zig-zag line) to obtain two 5 cm sub-samples

Bottom-ice sections (0 – 5, 5 – 10 cm) were melted (24 h in the dark) in pre-filtered sea water (0.2 μm; 500 mL each at room temperature), to reduce osmotic shock to the diatom cells that can occur when using freshwater (Garrison *et al.*, 1986). Volume, salinity and conductivity of the resulting solutions were recorded before samples were filtered under vacuum onto GF/F filters (0.7 μm) and stored (Whirl-Pak, -20°C).

Additional samples were collected in close proximity (< 10 m) by colleagues (B. Philippe and C. J. Mundy) to determine chlorophyll *a* and eukaryote cell abundance in sea ice.

4.4 Experimental

Each of the biomarkers of interest (sterols, fatty acids and hydrocarbons, including IP_{25}) required initial extraction from the filtered sea ice samples, with subsequent separation into respective fractions to enable analysis based on polarity and volatility.

4.4.1 Extraction, purification and analysis of sea ice lipids

Detailed descriptions of the procedures shown in Figure 4.4-1, are given (Chapter 3). Briefly, following the addition of individual internal standards to the GF/F filters, filtered sea ice samples were saponified (KOH 5%; 70°C; 30 min), after which the non saponifiable lipids (NSLs) were extracted into hexane (3 x 1 mL) and purified by open column chromatography (SiO_2) to yield apolar lipids (hexane: 3 column volumes). Dichloromethane/methanol (3 column volumes) was used to elute sterols. Where $\delta^{13}C$ analysis of individual lipids was required, samples were further chromatographically purified (open column; 5% $AgNO_3$). Fatty acids were obtained by the addition of concentrated HCl (1 mL) to the saponified solution (after extraction of NSLs) and re-extracted with hexane (3 x 1 mL). Prior to analysis by GC/FID, GC/MS or GC/IRM/MS fatty acids and sterols were derivatised (BSFTA: 50 µl: 30 mins: 70°C).

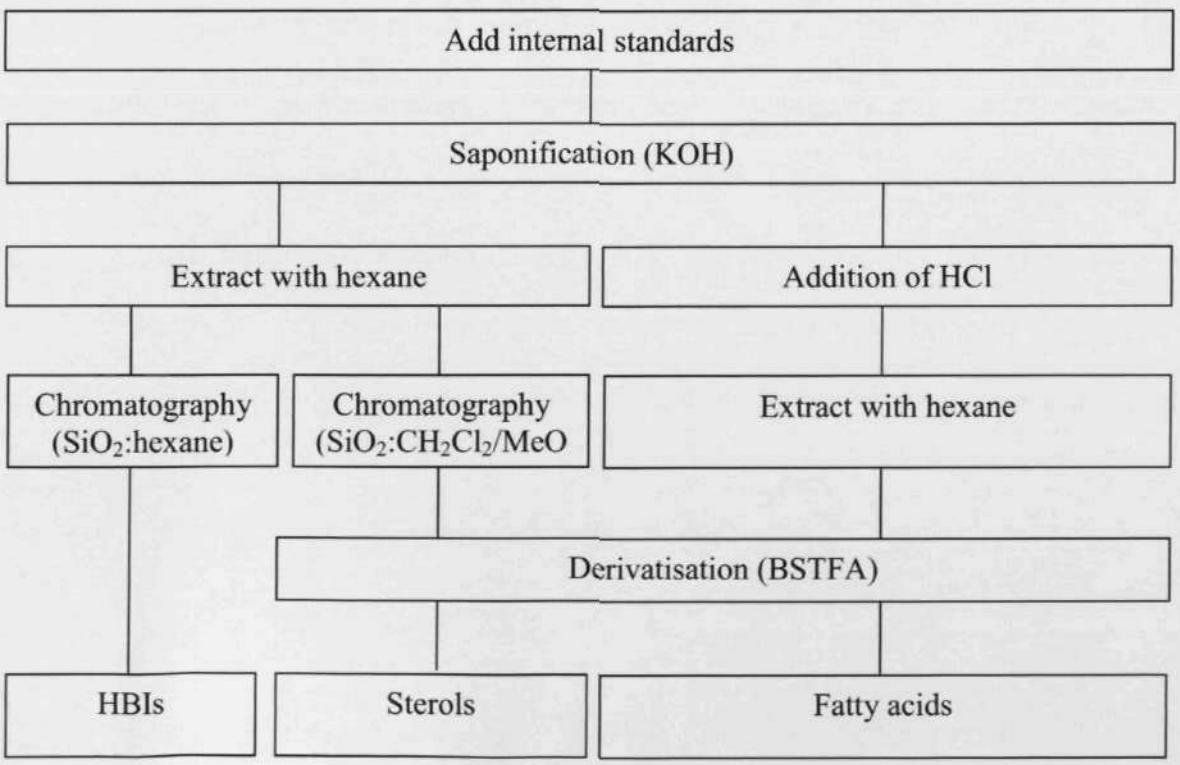

Figure 4.4-1. Sample extraction flow diagram for lipid biomarkers.

4.5 Results

4.5.1 Highly branched isoprenoid biomarkers in sea ice

Analysis (GC/MS) of the bottom 10 cm (0 – 5, 5 – 10 cm) of sea ice cores, enabled observation of HBI content through the Arctic spring period (Figure 4.5-1 and Figure 4.5-2).

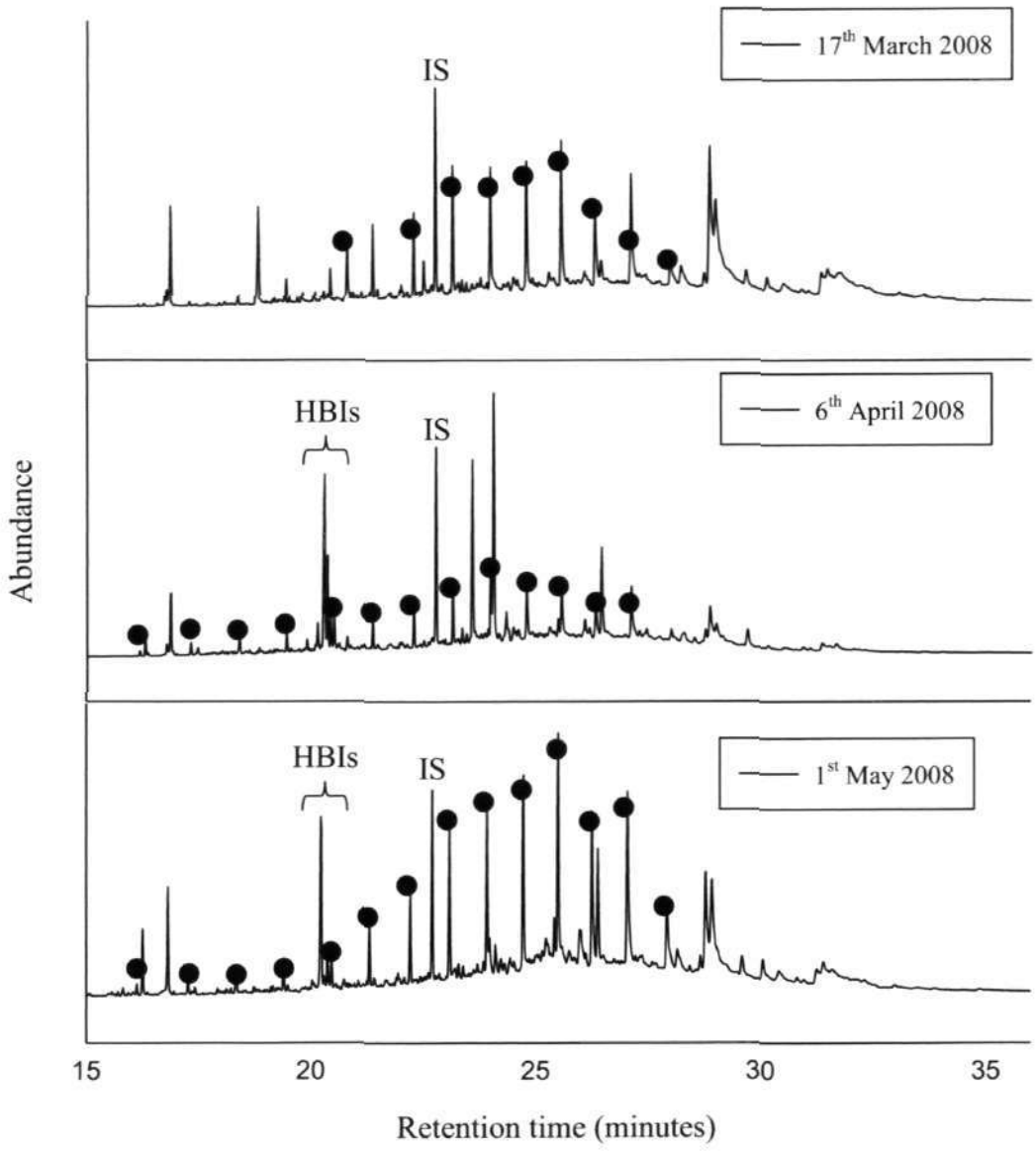

Figure 4.5-1. Partial GC/MS SIM (*m/z* 350.3, 348.3, 346.3 and 99) chromatograms of fractions containing HBIs and *n*-alkanes (black dots) isolated from sea ice cores collected during the IPY-CFL cruise 2008.

While sea ice cores were collected in 0 – 5 cm and 5 – 10 cm sections, substantial, non-consecutive, inter-core variability complicated interpretation of the data. As such, the data reported in this chapter correspond to combined bottom-sea ice sections (0 - 5 + 5 – 10 cm; Figure 4.5-2), with individual sections being discussed further in Chapter 5.

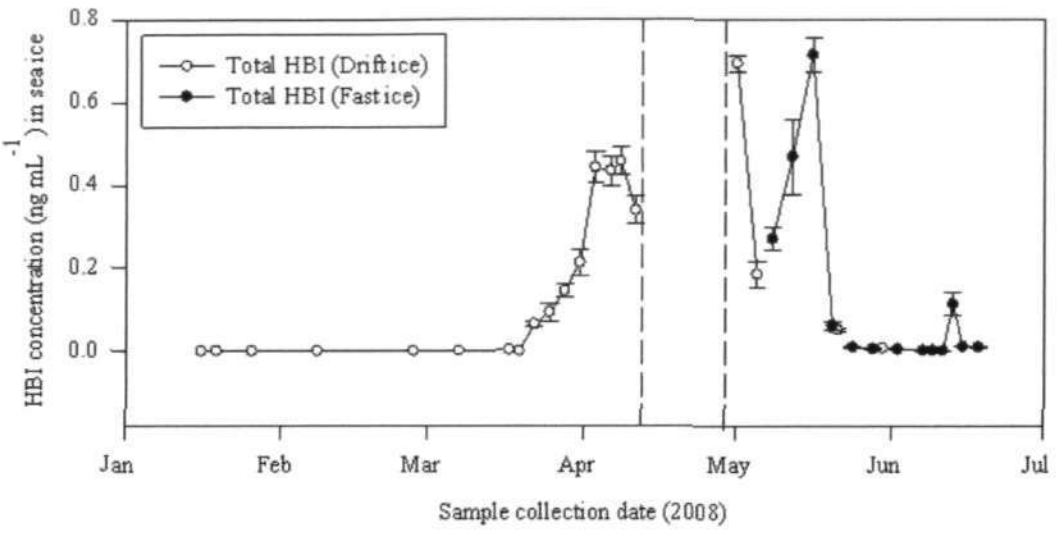

Figure 4.5-2. Temporal concentration of combined individual HBIs (**I**, **IIa**, **IIb**, **IIIa**, **IIIb**, **IIIc** and **IIId**) observed in the lower 10 cm of sea ice during the IPY-CFL cruise (1/1/08 to 1/7/08); ±1 s.d. n = 3. Dashed lines represent a temporary break in sampling.

The combined concentrations of individual HBIs (**I**, **IIa**, **IIb**, **IIIa**, **IIIb**, **IIIc** and **IIId**) in concentrated samples from January to mid-March remained undetectable by GC/MS SIM analysis, before increasing to 0.45 ng mL^{-1} during early April. The absence of HBI concentration data for a period of 20 days (11/4/08 to 1/5/08) resulted from inappropriate sample handling by a third party. Successful sample collection and analysis was reinstated from 1/5/08 and continued until 18/6/08, where a gradual change in the sample ice type, from drift ice to fast ice, occurred as a response to necessary ship mobility. Sea ice collection terminated on the 18/6/08 following the melting of suitable sea ice for safe collection. Throughout the observed period, the highest, combined individual HBI concentration was recorded in fast ice (1/5/08; 0.72 ng mL^{-1}), while a similar concentration was also observed in drift ice (16/5/08; 0.69 ng mL^{-1}).

Determination of the relative contributions of individual HBI isomers over the same time period (Figure 4.5-3), revealed **IIb** to be the most abundant isomer, contributing (on average) ca. 31% (0.046 ng mL^{-1}) of the total, mean HBI concentration in sea ice, with **IIIb** and **I**, contributing 28.1% and 27.2% (0.041 ng mL^{-1} and 0.040 ng mL^{-1}), respectively. Contributions from the remaining HBI isomers are summarised in Table 4-2.

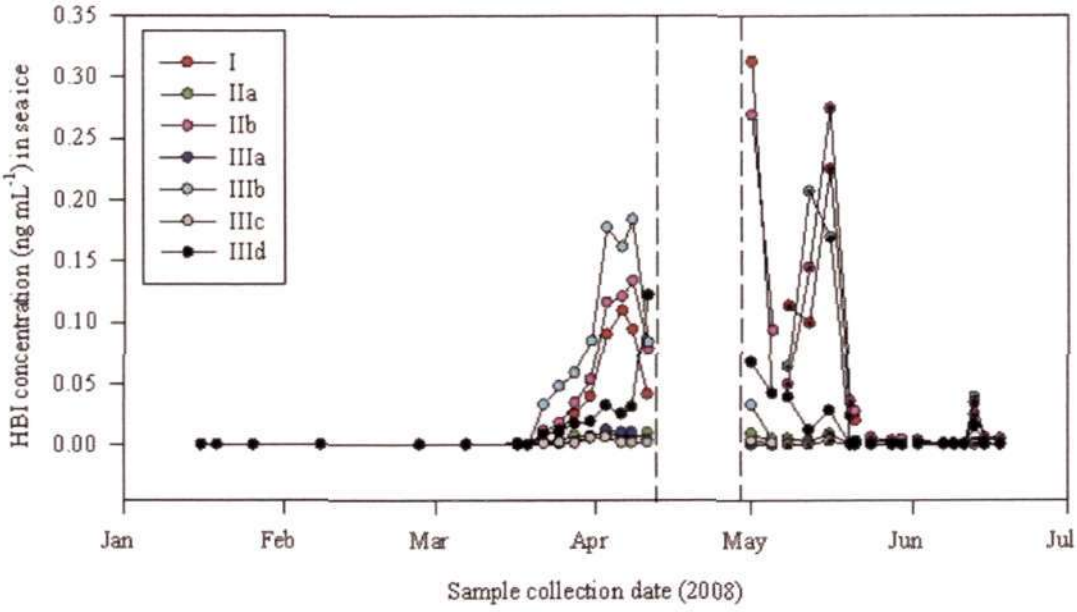

Figure 4.5-3. Temporal concentration of individual HBIs (**I**, **IIa**, **IIb**, **IIIa**, **IIIb**, **IIIc** and **IIId**) observed in the lower 10 cm of drift ice (circles) and fast ice (spotted circles) during the IPY-CFL cruise (1/1/08 to 1/7/08). Dashed lines represent a temporary break in sampling.

Table 4-2. Mean concentration (ng mL^{-1} and %) of HBI isomers observed in the lower 10 cm of sea ice cores during the IPY-CFL cruise (1/1/08 to 1/7/08) ± 1 s.d. n = 33.

	I	**IIa**	**IIb**	**IIIa**	**IIIb**	**IIIc**	**IIId**
Mean concentration (ng mL^{-1})	0.040 ± 0.070	0.0025 ± 0.003	0.046 ± 0.073	0.0015 ± 0.003	0.041 ± 0.065	0.0012 ± 0.002	0.014 ± 0.025
% of total mean HBI concentration	27.2	1.7	31.4	1.0	28.1	0.8	9.8

Inspection of peak production of **I**, in the bottom 10 cm of Arctic sea ice (2008), was compared to sediment trap collection data from three years earlier (Brown, 2007), revealing similarities in timing (Figure 4.5-4). The presence of **I** and *Haslea* spp.

diatoms in the water column was established from station CA20 near Franklin Bay in the CAA using automatic rotating sample collection cups on a Nichiyu 26 sediment trap. The trap was set at a depth of 211 m to collect sedimenting material. Supplementary diatom cell counts carried out on the sediment trap particles also demonstrated the reduced presence of *Haslea* spp. diatoms in the water column prior to the increase in sea ice concentrations of **I**.

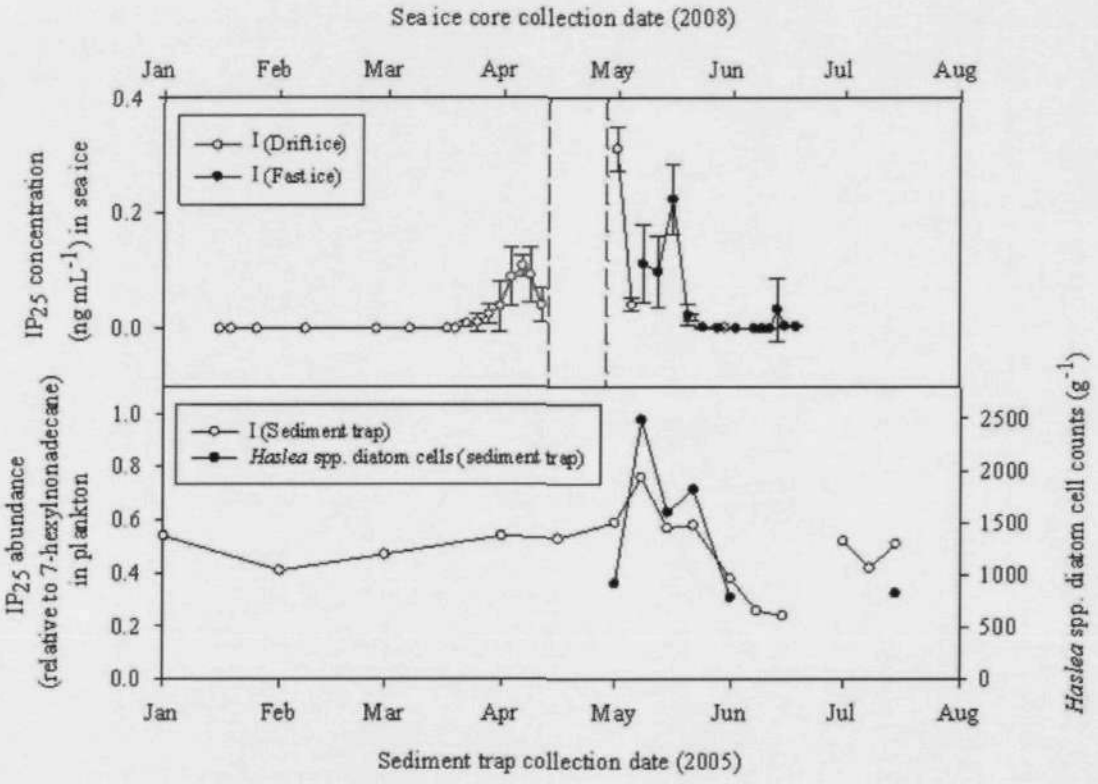

Figure 4.5-4. Top: Temporal concentration of **I**, observed in the lower 10 cm of sea ice during the IPY-CFL cruise (1/1/08 to 1/8/08); ±1 s.d. n = 3. Dashed lines represent a temporary break in sampling. Bottom: Temporal concentration of **I** and *Haslea* spp. diatom cells observed in sediment trap CA20 during the ArcticNet cruise (1/1/05 to 1/8/05) (Brown, 2007).

Multivariate analysis of HBIs was carried out using principal components analysis (PCA) to classify isomers according to their primary source e.g. sea ice diatoms; plankton (Figure 4.5-5). The PCA model was robust, using 8 variables and 27 observations. The first two PCs accounted for 84% of the variance in the data, enabling

reliable representation on two axes. Visual interpretation of the PCA model suggested the following grouping mechanism: Sea ice diatom - **I, IIa** and **IIb** (circled); mixed, plankton, and sea ice diatom (epontic) – **IIIa, IIIb, IIIc** and **IIId**.

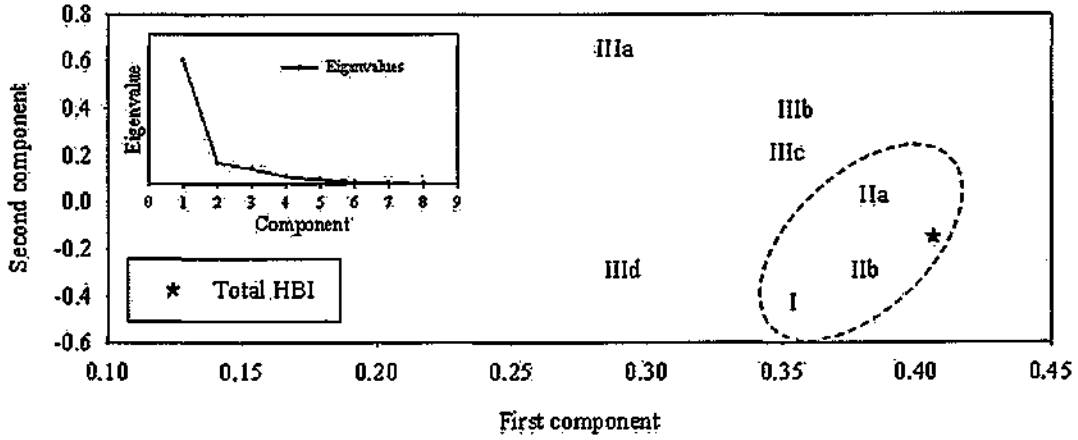

Figure 4.5-5. First and second component variable (loadings) plot of the principal components analysis for HBIs recorded in the lower 10 cm of sea ice during the IPY-CFL cruise 2008. I:IIa: r = 0.72; p = < 0.001. I:IIb: r = 0.95; p = < 0.001 (circled). I:IIIa: r = 0.33; p = 0.06. I:IIIb: r = 0.58; p = < 0.001. I:IIIc: r = 0.62; p = < 0.001. I:IIId: r = 0.56; p = 0.001. Inset: Eigenvalue plot showing the proportion of variability accounted for by the first two components (84%).

4.5.2 Fatty acid biomarkers in sea ice

Analysis (GC/MS) of lipids in the lower 10 cm of sea ice cores enabled measurement of the fatty acid content of sea ice. A wide variety of saturated, mono- and polyunsaturated fatty acids were present (e.g. Figure 4.5-6).

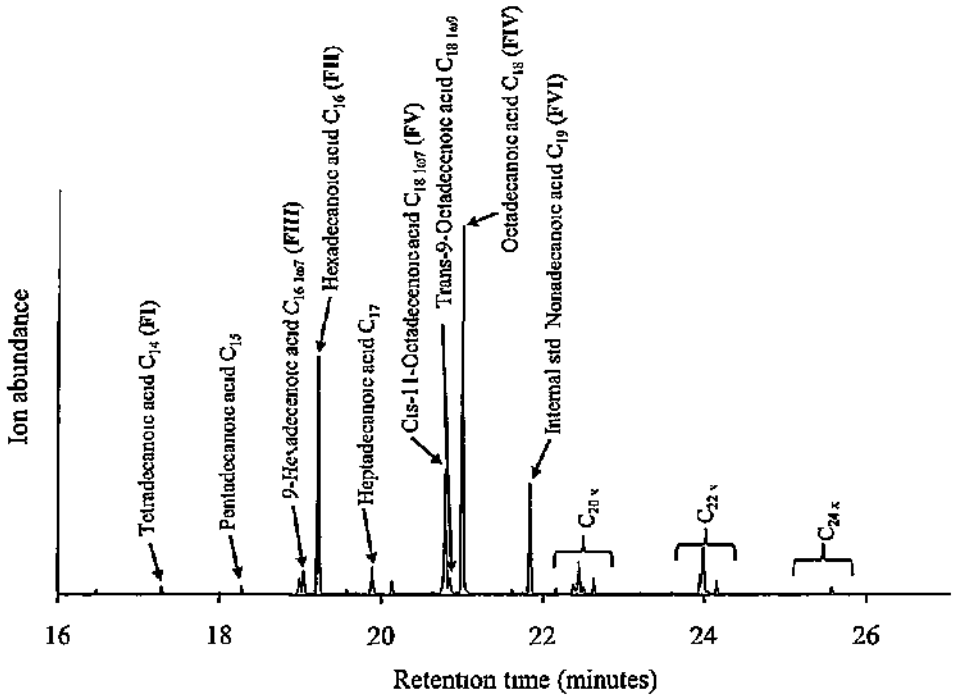

Figure 4.5-6 **Partial selective ion monitoring (*m/z* 117) chromatogram of the hexane extractable lipids obtained from the hydrolysed, saponified fraction, of a typical sea ice core collected (lower 10 cm of sea ice) during the IPY-CFL cruise 2008. Abundant fatty acid TMS esters are identified, with those used in the current study suffixed with FI, FII, FIII, FIV, FV and FVI.**

As a result of the considerable variation in concentration of individual fatty acids between ice cores, a refined suite of useful, proxy, fatty acid compounds was instead identified following the extraction and analysis of fatty acids from cultures of *Haslea crucigeroides* and *Pleurosigma intermedium* (Figure 4.5-7) and those reported in diatoms previously (Opute, 1974, Linda *et al* , 1988; Volkman *et al.*, 1989, Dunstan *et al* , 1994; Ying *et al.*, 2000; Budge *et al.*, 2008).

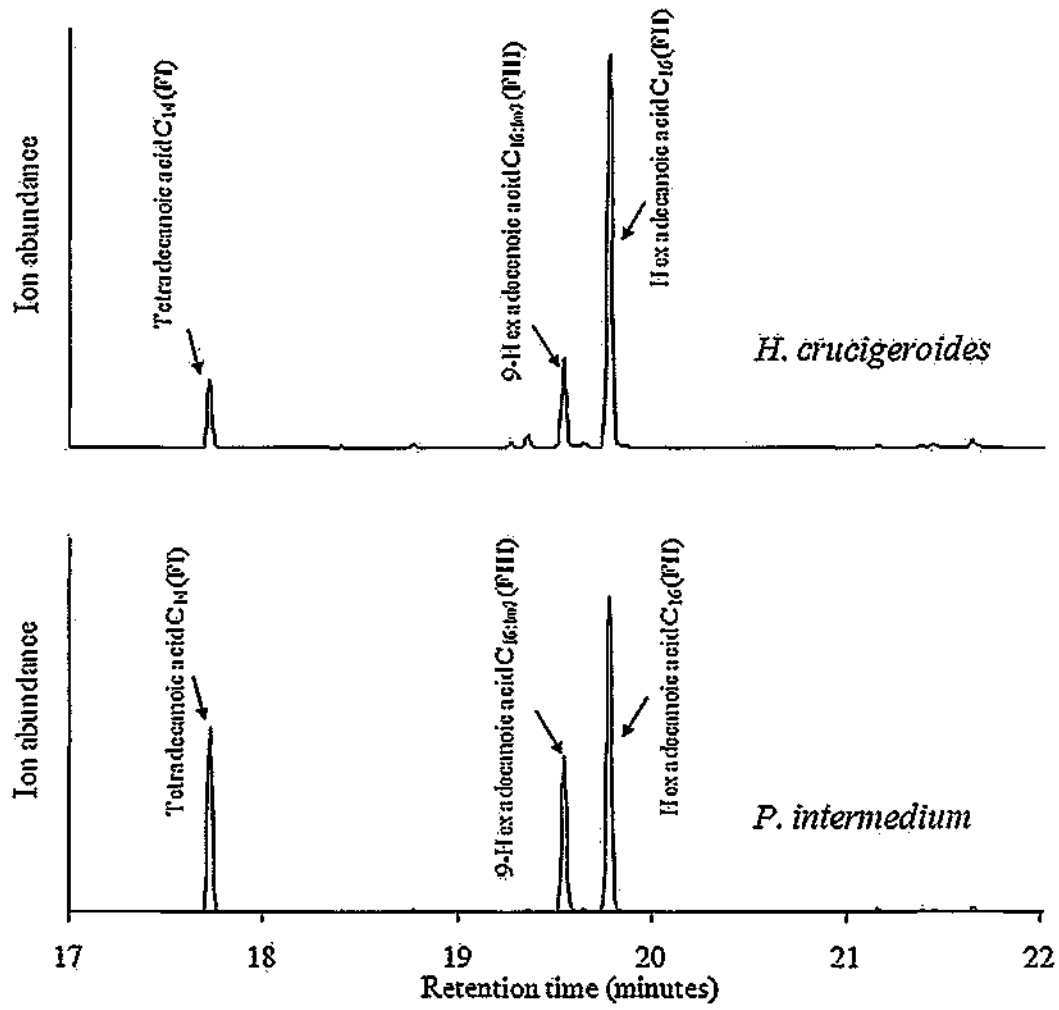

Figure 4.5-7. Partial selective ion monitoring (*m/z* 117) chromatogram of the hexane extractable lipids obtained from the hydrolysed saponified fraction of *Haslea crucigeroides* (top) and *Pleurosigma intermedium* (bottom) cultures. Abundant fatty acid TMS esters are identified; those used in the current study are suffixed with **FI**, **FII**, and **FIII**.

The suitability of the selected fatty acids to represent, for example, primary productivity, was further established following $\delta^{13}C$ analyses of some samples (n = 5) (Figure 4.5-8). Fatty acids **FI**, **FII**, **FIII**, **FIV** and **FV** comprised distinctively heavy ^{13}C enriched (with respect to ^{12}C), values (ca. $\delta^{13}C$ = -14 to -17 ‰) which are indicative of sea ice origin (Belt *et al.*, 2008). In contrast, the non-biogenic C_{17} acid and C_{19} internal standard, **FVI**, were significantly lighter with $\delta^{13}C$ = > -22 ± 2 ‰.

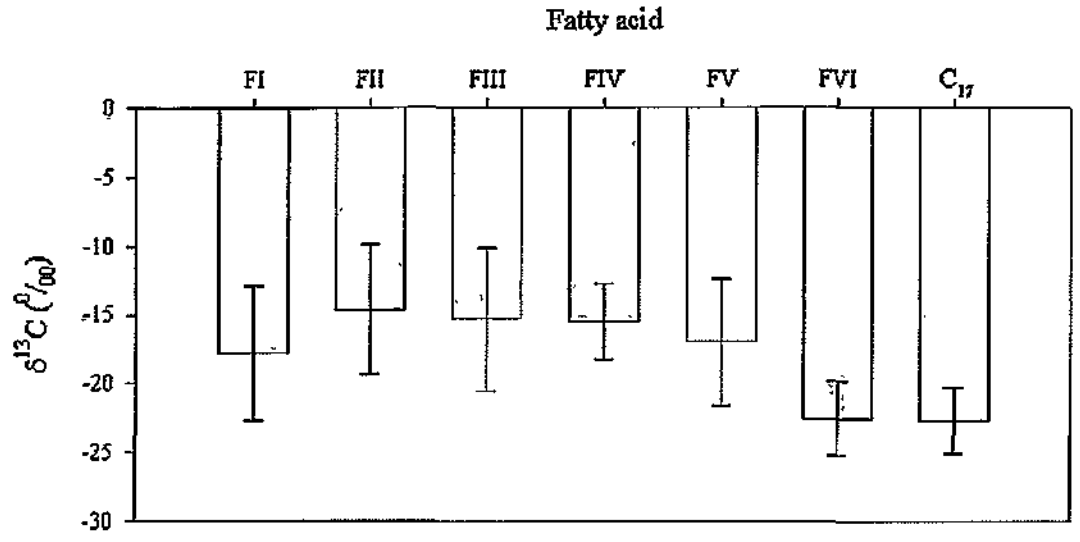

Figure 4 5-8 Average $\delta^{13}C$ ‰ (VPDB) of fatty acids collected in the lower 0 - 10 cm of sea ice cores during the IPY-CFL cruise 2008; ±1 s.d n = 5 (25th Mar, 6th Apr; 1st, 5th and 16th May 2008). Inclusion of the internal standard (**FVI**) and the largely non-biogenic fatty acid C_{17}, also found in sea ice, is included to contextualise variability.

Observation of the combined individual, selected, fatty acid concentrations for the period 16/1/08 to 1/6/08 (Figure 4.5-9), revealed a similar trend to that of combined individual HBI concentrations ($r = 0.67$; $p = < 0.001$). The combined individual fatty acid (**FI, FII, FIII, FIV** and **FV**) concentration, for the period January to mid-March, remained low at < 28 ng mL^{-1} The 20 day gap in sampling, observed in the HBI time series (11/4/08 to 1/5/08), was partially compensated for, the greater concentration of fatty acids compared to HBIs by a factor of ca. 1000, permitted detection in additional, low volume samples that were supplied by a co-worker (Jean Eric Tremblay). A delay in the increase in fatty acid concentration is apparent, when compared to HBIs, with concentrations not increasing significantly until early to mid April, where a maximum concentration occurs in drift ice (16/5/08; 1270 ng mL^{-1}). Some variation in fatty acid concentration, similar to values observed in HBIs, is then evident for the period 1/5/08 to 20/5/08, before returning to early season (January to April) concentrations. Sea ice collection ended on 18/6/08 following the melting of suitable sea ice for safe collection.

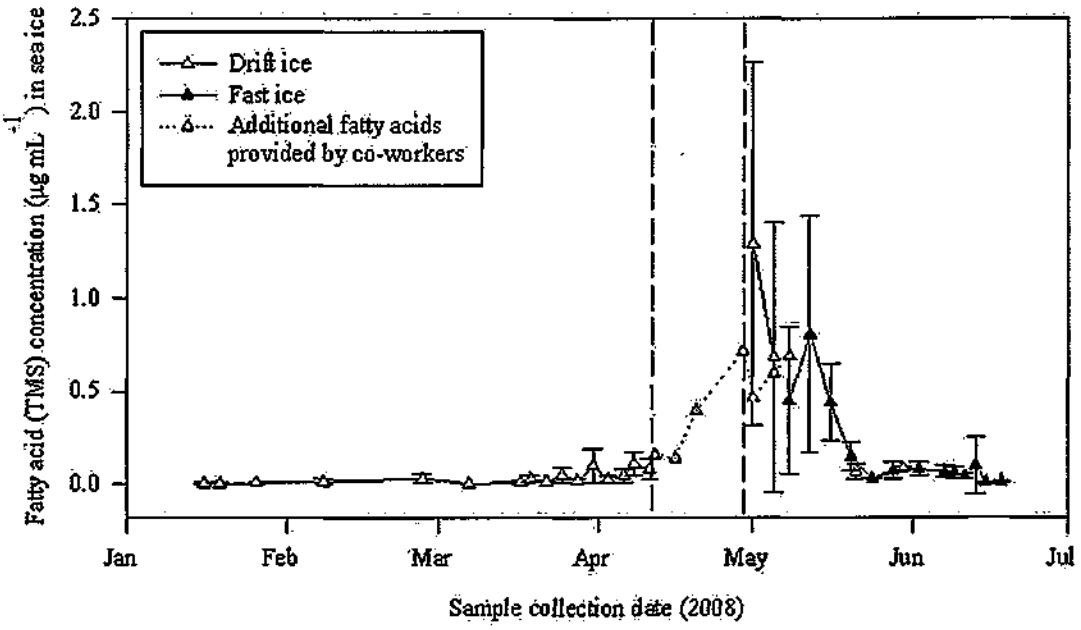

Figure 4.5-9. Temporal concentration of combined individual fatty acids (**FI, FII, FIII, FIV** and **FV**) observed in the lower 0 - 10 cm of sea ice cores during the IPY-CFL cruise (1/1/08 to 1/7/08); ±1 s.d. n = 3. Dashed line represents a temporary gap in the original samples.

Determination of the relative contributions of individual fatty acids over the same period (Figure 4.5-10), revealed that **FII** was the most abundant fatty acid, contributing ca. 39% (78 ng mL^{-1}) of the mean combined individual fatty acid concentration (210 ng mL^{-1}). **FIII** contributed ca. 33% (66 ng mL^{-1}) of the total fatty acids, while **FI** was responsible for ca. 17% (34 ng mL^{-1}). Contributions from the remaining fatty acids are summarised in Table 4-3. The frequently reported diatom fatty acid ($C_{20:5}$) represented only a minor and highly variable contribution in sea ice samples (1.4 ± 2.1%) and, alongside other minor components, was not included in the calculations of total fatty acid concentrations (**FI, FII, FIII, FIV** and **FV**).

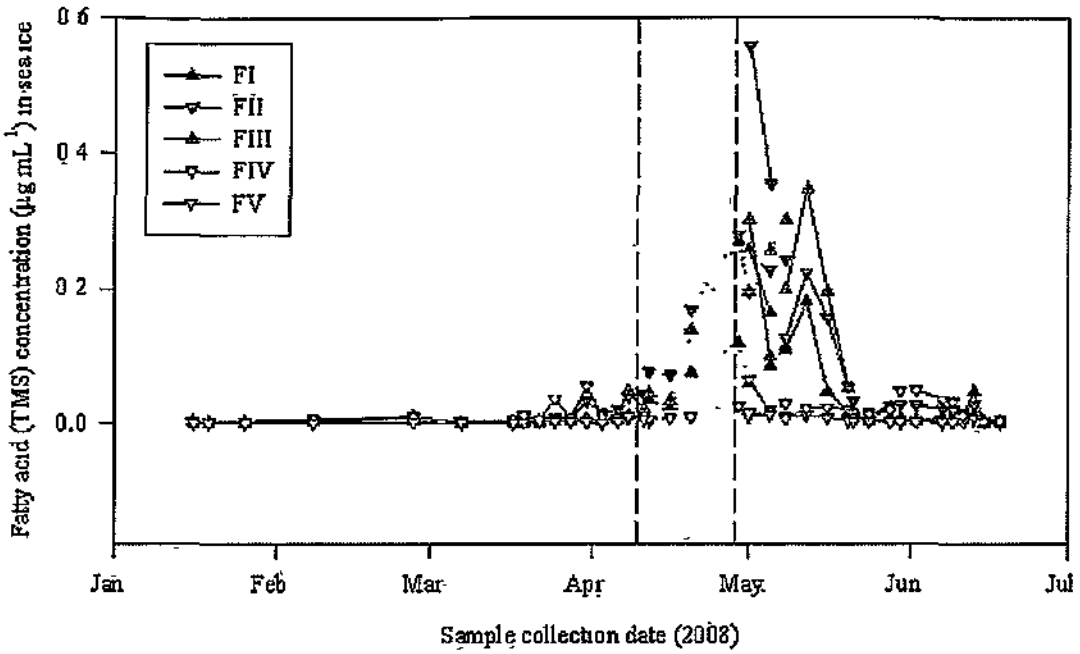

Figure 4.5-10. Temporal concentration of individual fatty acids (**FI, FII, FIII, FIV** and **FV**) observed in the lower 0 - 10 cm of sea ice cores during the IPY-CFL cruise (1/1/08 to 1/7/08) Dashed line represents a temporary gap in the original samples.

Table 4-3 Mean concentration (µg mL^{-1} and %) of fatty acids observed in the lower 10 cm of sea ice cores during the IPY-CFL cruise (1/1/08 to 1/7/08) ± 1 s.d. n = 33.

	FI	**FII**	**FIII**	**FIV**	**FV**
Mean concentration (µg mL^{-1})	0.034 ± 0 002	0.078 ± 0 004	0 066 ± 0 003	0 016 ± 0 0005	0 0095 ± 0.009
% of total mean fatty acid concentration	16 6	38 5	32.6	7 6	4.7

The stable carbon isotope compositions of the most abundant fatty acids found in sea ice (**FI, FII, FIII**), were relatively enriched in ^{13}C (with the exception of 6/4/08, $\delta^{13}C$ = -23.8 ‰) consistent with biosynthetic production in sea ice (e.g. Budge *et al* , 2008) (Figure 4.5-11)

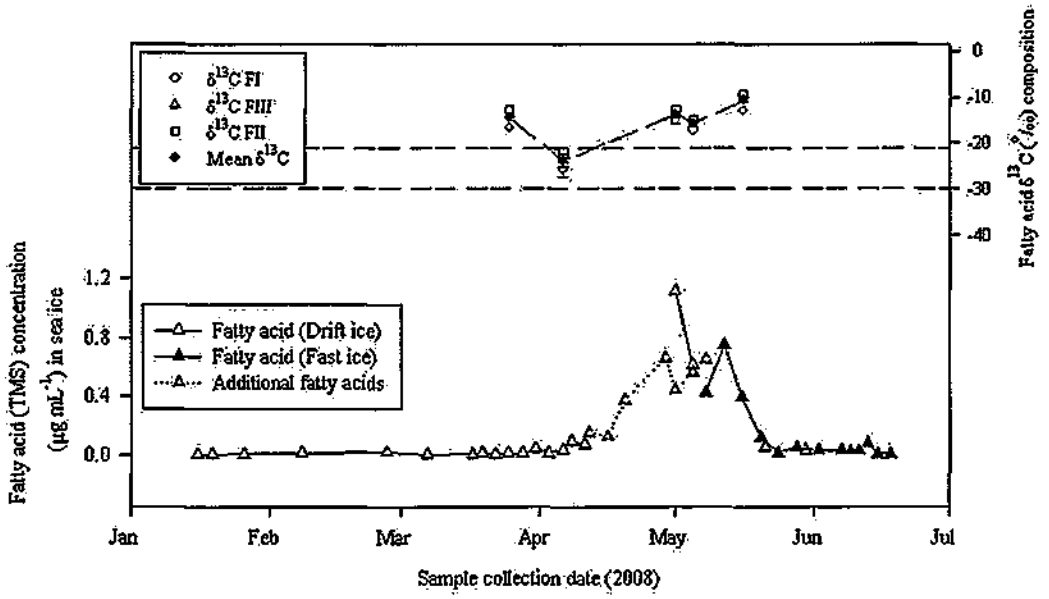

Figure 4.5-11. Top: Individual and mean $\delta^{13}C$ ‰ (VPDB) of fatty acids in sea ice cores (lower 10 cm) collected during the IPY-CFL cruise 2008 (1/1/08 to 1/7/08); ±1 s.d. n = 3. Medium dashed lines represent upper and lower literature $\delta^{13}C$ values for planktonic lipids (Kennedy *et al.*, 2002; Drenzek *et al.*, 2007; Belt *et al.*, 2008; Tamelander *et al.*, 2008). Bottom: Temporal mean concentration of combined individual fatty acids (**FI**, **FII**, and **FIII**) observed during the IPY-CFL cruise (1/1/08 to 1/7/08).

PCA was used to conduct the multivariate analysis of fatty acids to classify compounds according to their primary source, e.g. sea ice diatom, plankton (Figure 4.5-12). The PCA model was robust, using 7 variables and 27 observations. The first two PCs accounted for more than 90% of the variance in the data which enabled reliable representation on two axes. Visual interpretation of the PCA model suggested the following grouping mechanism: Sea ice diatom - **FI**, **FII**, **FIII** and **FV** (circled); other – **FIV**.

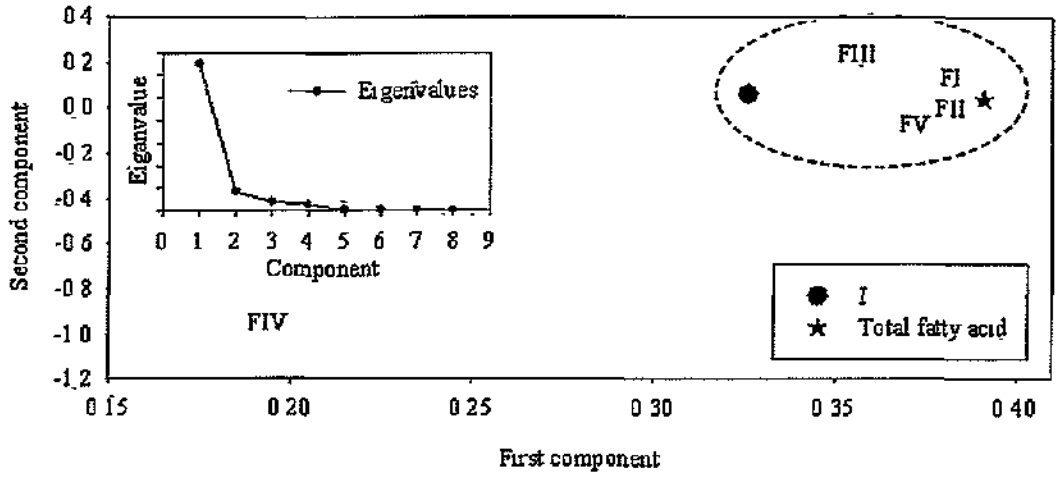

Figure 4.5-12. First and second component variable (loadings) plot of the principal components analysis for fatty acids recorded in the lower 10 cm of sea ice during the IPY-CFL cruise 2008. **I:FIII**: r = 0 78, p = < 0 001. **I:FV**: r = 0.76; p = < 0.001. **I:FII**: r = 0 77; p = < 0 001 **I:FI**. r = 0.72; p = < 0.001. (circled) **I-FIV**. r = 0 36; p = 0.04. Inset: Eigenvalue plot showing the proportion of variability accounted for by the first two components (91%).

4.5.3 Sterol biomarkers in sea ice

Analysis of the bottom 10 cm of sea ice cores also enabled observation of the sterol content of sea ice through the Arctic spring period (Figure 4.5-13). Combined individual calibrated sterol (**SII, SIII, SIV, SVI, SVII** and **SVIII**) concentrations, for the period January to early-March, like fatty acids, remained low (ca 1 - 2 ng mL^{-1}), before increasing to ca. 4 - 5 ng mL^{-1} during early to mid-April. The absence of sterol values for the 20 day period (11/4/08 to 1/5/08), resulted from inappropriate sample handling by a third party. Successful sample collection and analysis was reinstated from 1/5/08 and continued until 18/6/08, where a gradual change in the sample ice type from drift ice to fast ice occurred. Sea ice collection ended on 18/6/08 following the melting of suitable sea ice for safe collection. Throughout the observed period, maximum combined individual sterol concentration were recorded in fast ice (12/5/08; 8.32 ng mL^{-1})

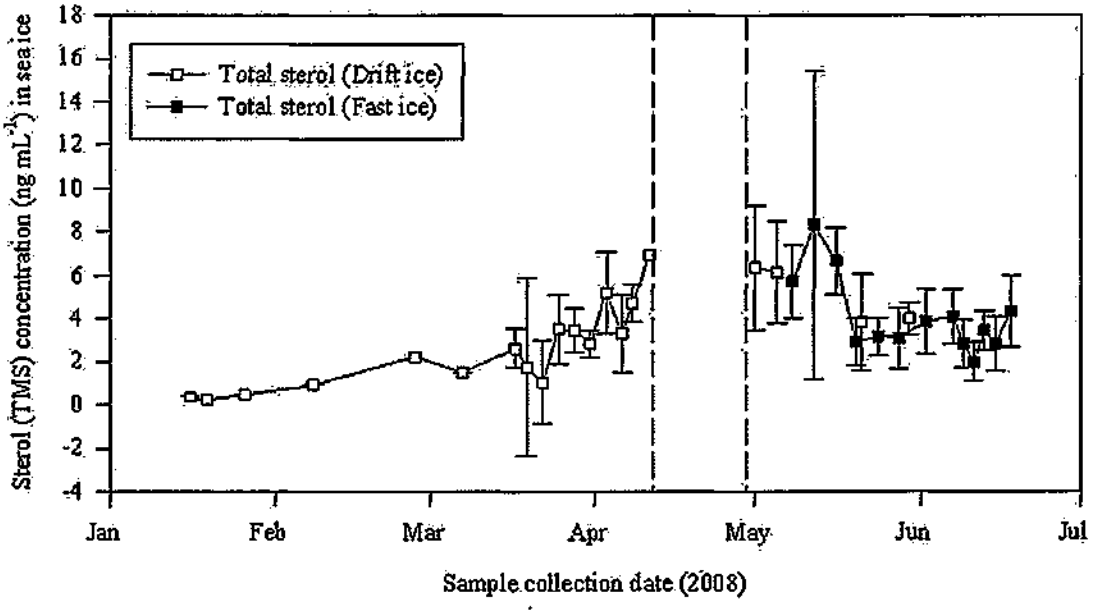

Figure 4.5-13. Temporal concentration of total sterols (**SII, SIII, SIV, SVI, SVII** and **SVIII**) observed in the lower 10 cm of sea ice during the IPY-CFL cruise (1/1/08 to 1/7/08); ±1 s.d. n = 3. Dashed lines represent a temporary break in sampling.

Determination of the relative contributions of individual sterols over the period (Figure 4.5-14) reveals that, of the mean combined individual sterol concentration (3.48 ng mL^{-1}), the animal-derived (Volkman, 1986) sterol, cholesterol (**SII**), was most abundant, contributing ca. 52% (1.79 ng mL^{-1}). The higher plant sterol (Volkman, 1986), β-sitosterol (**SVIII**), was also abundant, contributing 34% (1.18 ng mL^{-1}). Contributions (%) from the remaining sterols were significantly lower and are summarised in Table 4-4. Since authentic standards for all sterols were not available, analyses are divided to include the non-calibrated mass and volume compensated abundance of **SI** and **SV**, relative to the internal standard (**SIX**).

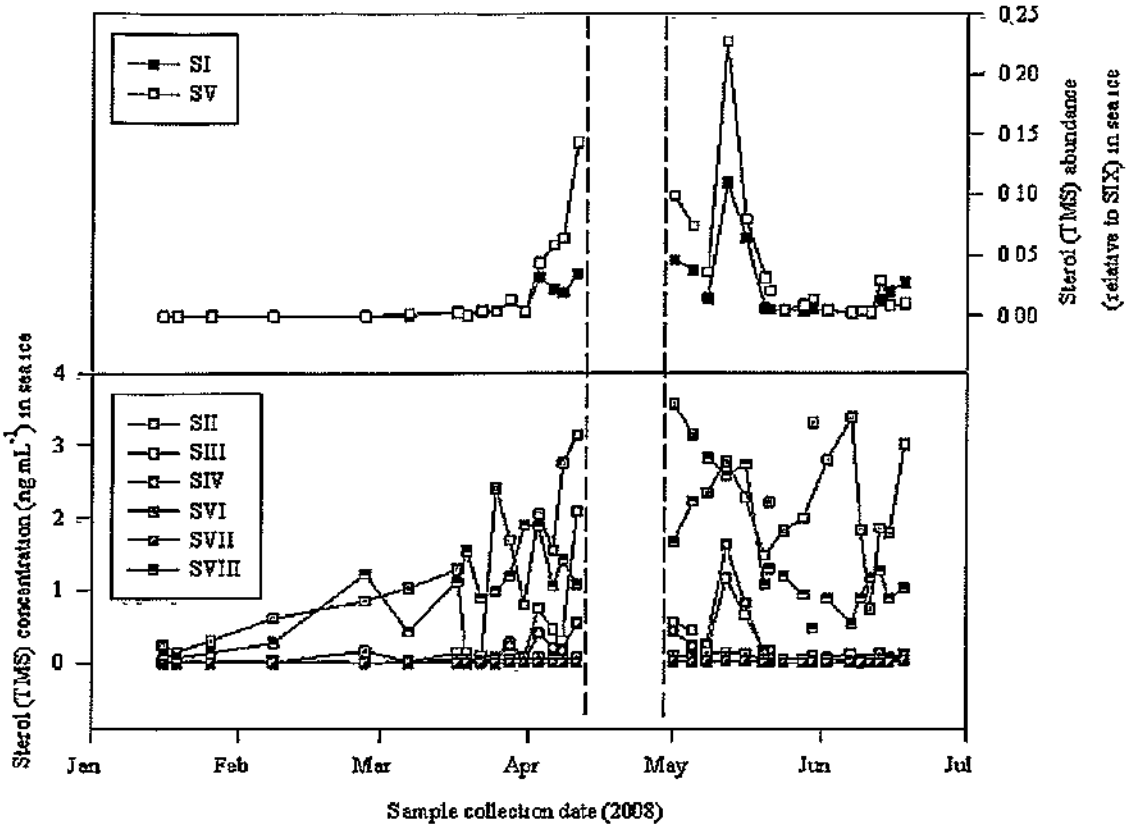

Figure 4 5-14. Top: Temporal concentration of individual sterols (**SI** and **SV**) observed in the lower 10 cm of sea ice cores during the IPY-CFL cruise (1/1/08 to 1/7/08). Dashed lines represent a temporary break in sampling. Bottom: Temporal concentration of individual sterols (**SII, SIII, SIV, SVI, SVII** and **SVIII**) observed during the IPY-CFL cruise (1/1/08 to 1/7/08). Dashed lines represent a temporary break in sampling.

Table 4-4. Mean concentration (ng mL^{-1} and %) of sterols observed in the lower 10 cm of sea ice cores during the IPY-CFL cruise (1/1/08 to 1/7/08) ± 1 s.d n = 33

	SII	**SIII**	**SIV**	**SVI**	**SVII**	**SVIII**
Mean concentration (ng mL^{-1})	1 79 ± 0 03	0.26 ± 0 01	0 18 ± 0 009	0.058 ± 0 001	0.0081 ± 0.0003	1 18 ± 0 02
% of total mean sterol concentration	51 5	7 4	5 2	1 7	0 23	34 0

Multivariate analysis, comprising of PCA, was carried out for the sterols to classify compounds according to their primary source, e.g. marine, terrestrial or animal (Figure 4.5-15). The PCA model was robust, using 10 variables and 27 observations. The first two PCs accounted for almost 80% of the variance in the data, which enabled reliable

representation on two axes. Visual interpretation of the PCA model suggested the following grouping mechanism for individual sterols: Marine - **SI, SIV, SV** (circled); Terrestrial – **SVI, SVII, SVIII**; Animal – **SII, SIII**. Of the sterols observed in sea ice, none were found to correlate substantially with the IP_{25} biomarker, **I** ($r = < 0.66$).

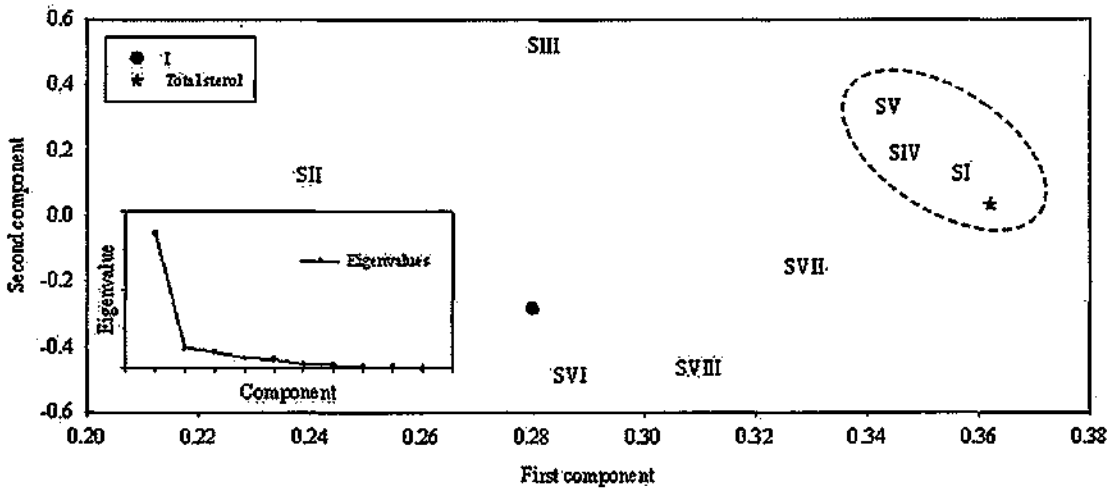

Figure 4.5-15. First and second component variable (loadings) plot of the principal components analysis for sterols recorded in the lower 10 cm of sea ice during the IPY-CFL cruise 2008. **I:SVI**: $r = 0.58$; $p = < 0.001$. **I:SVIII**: $r = 0.61$; $p = < 0.001$. **I:SVII**: $r = 0.66$; $p = < 0.001$. **I:SII**: $r = 0.41$; $p = 0.02$. **I-SIII**: $r = 0.42$; $p = 0.02$. **I:SIV**: $r = 0.57$; $p = 0.001$. **I:SV**: $r = 0.58$; $p = < 0.001$. **I:SI**: $r = 0.64$; $p = <0.001$. Inset: Eigenvalue plot showing the proportion of variability accounted for by the first two components (79%).

4.5.4 Comparison of lipid biomarkers extracted from sea ice

Having assessed individual co-variance within lipid classes, the co-variance between bulk lipid classes was also considered. Comparison of the biomarkers analysed in sea ice samples revealed similarities in the timing of peak concentration in each class of compound (Figure 4.5-16). Firstly, for the period January to mid-March, the low concentrations recorded in HBIs, fatty acids and sterols were reflected in the onset of low eukaryote cell and chlorophyll *a* observations. Secondly, rapid increases in HBI concentrations (with gradual increases in sterol and fatty acid concentrations) from mid-

March, continued to be reflected in both eukaryote cell and chlorophyll *a* observations (Figure 4.5-16). Thirdly, maximum concentrations observed for all biomarkers occurred on, or after, 1/5/08 and subsequently fluctuated, before again decreasing until the end of sampling (18/6/08). Finally, the rapid reduction of chlorophyll *a* from mid-May, further implicated an association between primary productivity in sea ice and some of the lipid biomarkers recorded in sea ice for the same time. More quantitative correlations between measurements obtained from different cores (lipids *vs.* chlorophyll *a* and eukaryote cell abundance) were not carried out due to potential variation in ice core microstructure and algal content

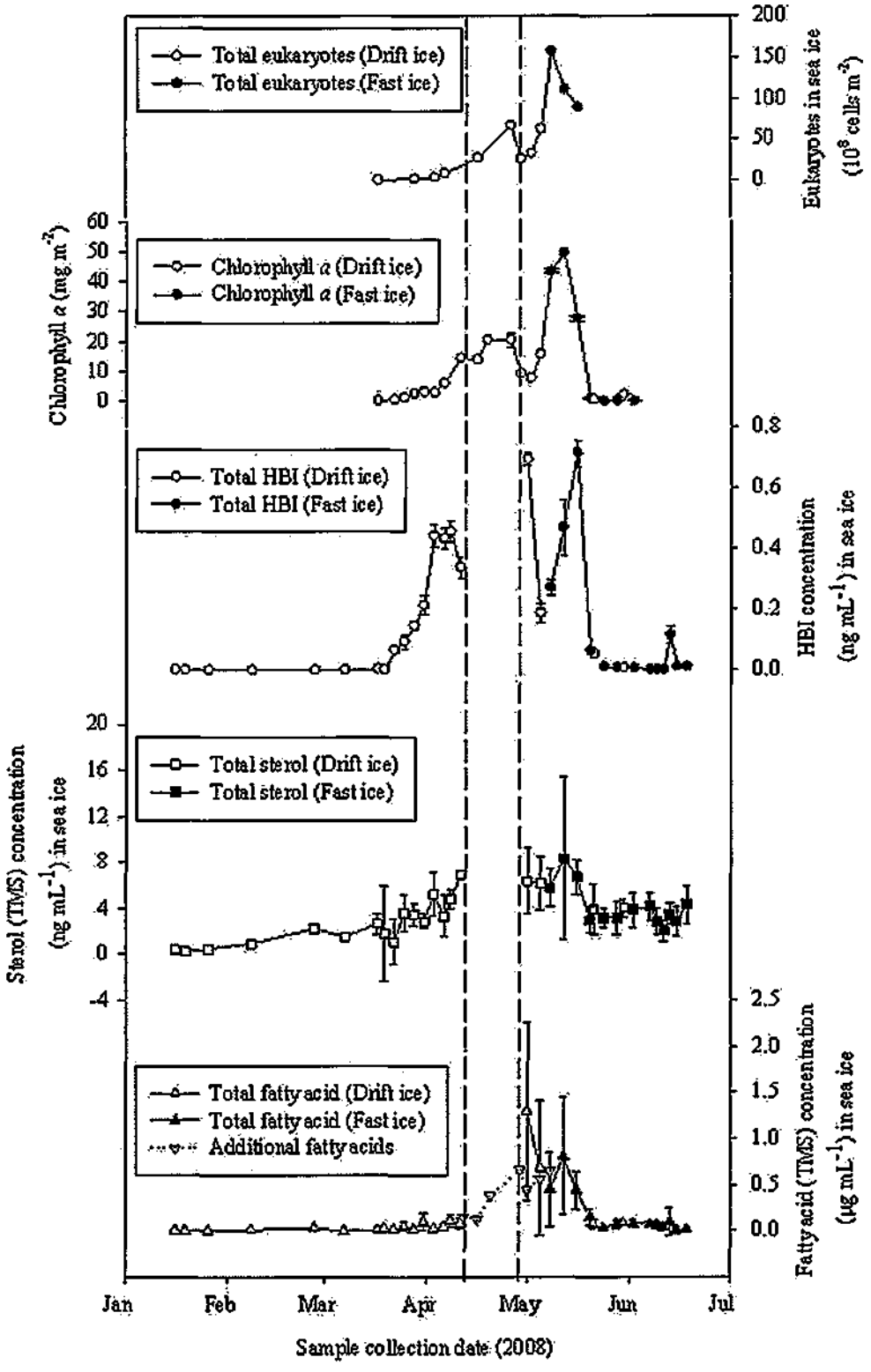

Figure 4.5-16. Comparison of the temporal abundance of eukaryote cells and chlorophyll *a* from within the lower 0 - 10 cm of Arctic sea ice and biomarker concentrations also from within the lower 0 - 10 cm of Arctic sea ice observed during the IPY-CFL cruise (1/1/08 to 1/7/08). From top to bottom; Total eukaryote cell abundance; Chlorophyll *a*; Total HBI (**I, IIa, IIb, IIIa, IIIb, IIIc** and **IIId**) concentration; Total sterol (**SII, SIII, SIV, SVI, SVII** and **SVIII**) concentration; Total fatty acid (**FI, FII, FIII, FIV** and **FV**) concentration. Dashed lines represent a temporary break in some sampling.

Additional PCA was carried out on HBIs, fatty acids and sterols, to characterise each class of lipid, relative to one another and to investigate the potential range of sources of the HBIs, **IIa, IIb, IIIa, IIIb, IIIc** and **IIId**. The PCA model was robust, although with 20 variables used for 27 observations, sufficient variation was not accounted for in the first two PCs. Given the number of variables, it was felt that representation on three axes (accounting for 80% of the variation) would provide better interpretation (Figure 4.5-17). Distinct grouping is evident in both the sterols and fatty acids, with vertical spread reflecting variation within each group A degree of variation is again observed in the sterols, with **SII** and **SIII** separated the most. Similarly, **FIV** is separated the most in the projection of fatty acids, while the remaining fatty acids display a degree of vertical separation. Interpretation of the three dimensional projection of HBIs however, is more complicated. While the distribution of HBIs reflects that seen previously in two dimensions, the lack of clear grouping as a class of compounds is suggestive of multiple source contributions, potentially from different species of both sea ice and planktonic diatoms

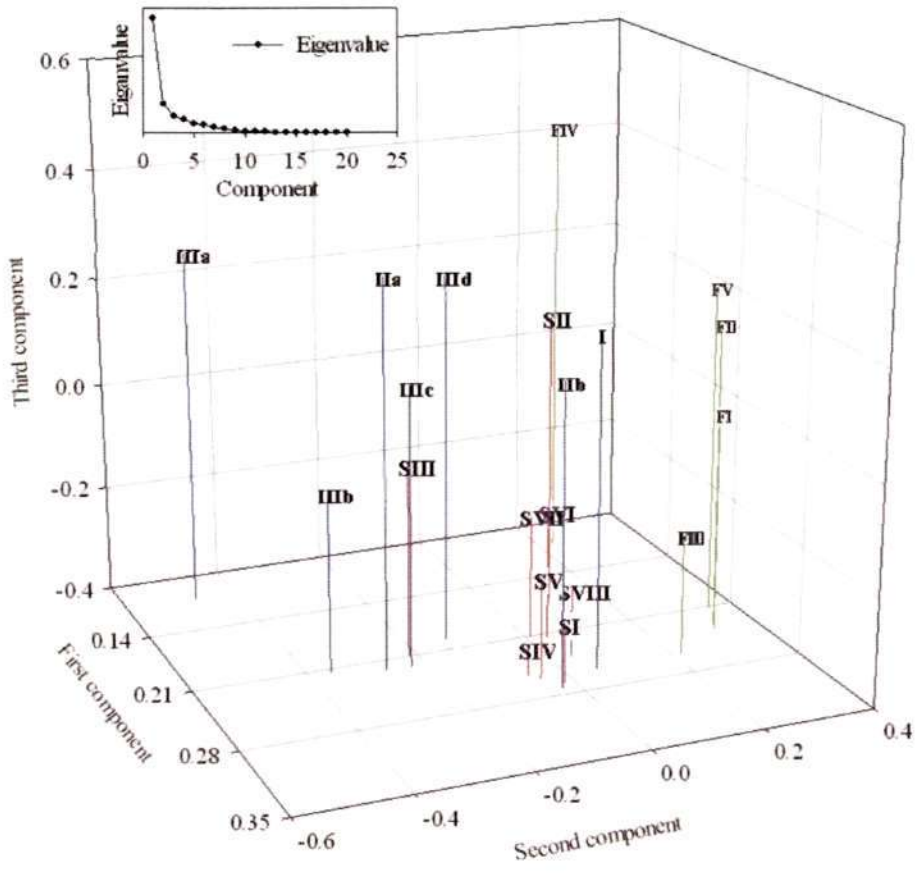

Figure 4.5-17. First, second and third component variable (loadings) plot of the principal components analysis for biomarkers recorded in the lower 10 cm of sea ice during the IPY-CFL cruise 2008. Proximity of compounds in three dimensions is a function of covariance. Red = sterols (**SI** to **SVIII**), green = Fatty acids (**FI** to **FV**), blue = HBIs (**I** to **IIId**). Inset: Eigenvalue plot showing the proportion of variability accounted for by the first three components (80%).

4.5.5 *n*-alkane distributions in sea ice

Additional analysis (GC/MS) of the bottom 10 cm of sea ice cores, enabled measurement of the *n*-alkane content of sea ice through the Arctic spring period (Figure 4.5-18). Combined individual, mean, *n*-alkane distributions revealed the dominance of long chain (C_{20} – C_{33}) homologues exhibiting an odd over even predominance. The presence of a similar odd to even distribution in the short (C_{15} – C_{20}) *n*-alkanes was absent. Partitioning of drift ice and fast ice *n*-alkanes revealed similar distribution patterns, albeit with slightly greater enhancement of the odd over even predominance in

drift ice. In addition, the enhanced mean concentration of nC_{21} is distinguished as being drift ice specific. Measurement of the stable carbon isotope composition ($\delta^{13}C$) of *n*-alkanes detected in sea ice (nC_{21} – nC_{34}) from 2/6/08 provided values -29.3 ‰ to -31.2 ‰ with a mean $\delta^{13}C$ = 29.9 ‰.

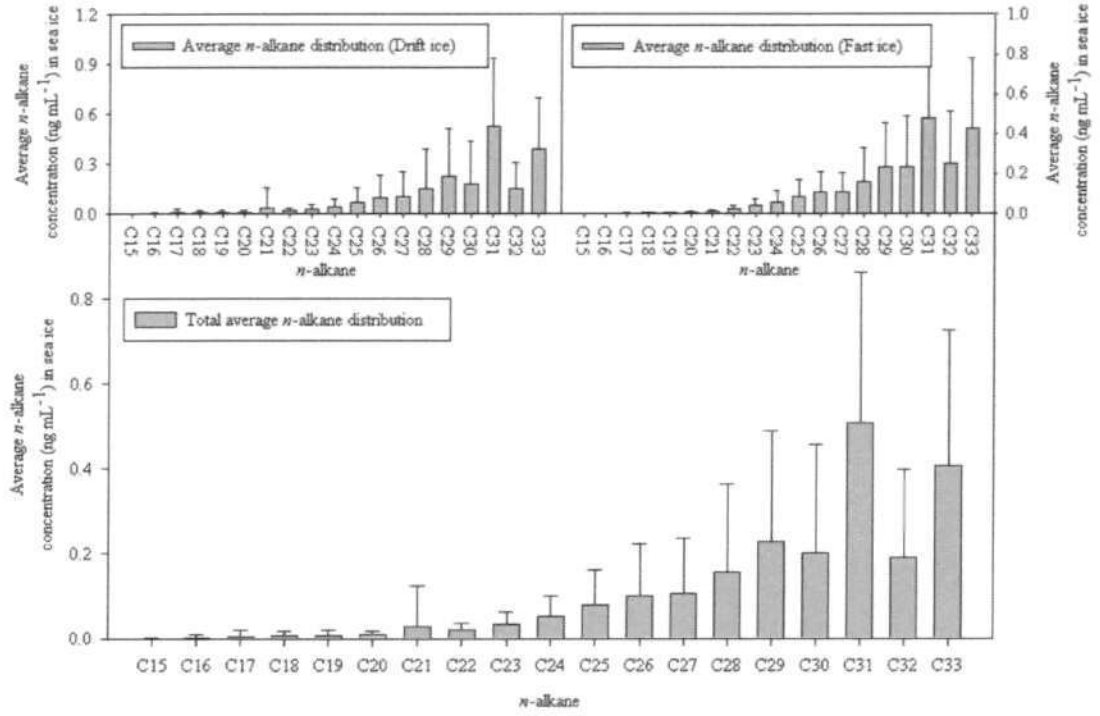

Figure 4.5-18. Mean distribution of *n*-alkanes observed in the lower 0 - 10 cm of sea ice cores during the IPY-CFL cruise (1/1/08 to 1/7/08). Top: Mean distribution in drift ice (left) and fast ice (right) (± 1 s.d. n = 3). Bottom: Mean combined drift ice and fast ice distribution (± 1 s.d. n = 3).

4.6 Environmental variables

A suite of abiotic observations was recorded for each sea ice core that was collected, in order to investigate whether observed trends in individual and groups of biomarkers could be explained by bulk environmental factors. Abiotic measurements included; air temperature, water temperature, sea ice salinity and ice and snow thickness (Figure 4.6-1). Abiotic data was absent for the period 1/1/08 to 17/3/08.

While both air and water temperature increased over the period of observations, no significant correlation with any of the biomarkers was observed ($r = < 0.43$ and < 0.15 respectively). The salinity of the bottom 10 cm of sea ice cores was calculated using Equation 12 where V denotes volume and FSW is filtered seawater.

Equation 12

$$Salinity\ of\ sea\ ice\ (‰) = \left[\frac{V_{FSW}}{V_{FSW} + V_{ice}}\right] X\ Salinity_{FSW} + \left[\frac{V_{ice}}{V_{FSW} + V_{ice}}\right]$$

Variation in salinity was also observed as having no significant correlation with the suite of biomarkers ($r = < 0.52$). Freeboard (distance from the water surface to the top of the sea ice) and ice and snow thickness measurements also did not yield significant correlations ($r = < 0.45, < 0.27$ and < 0.44 respectively).

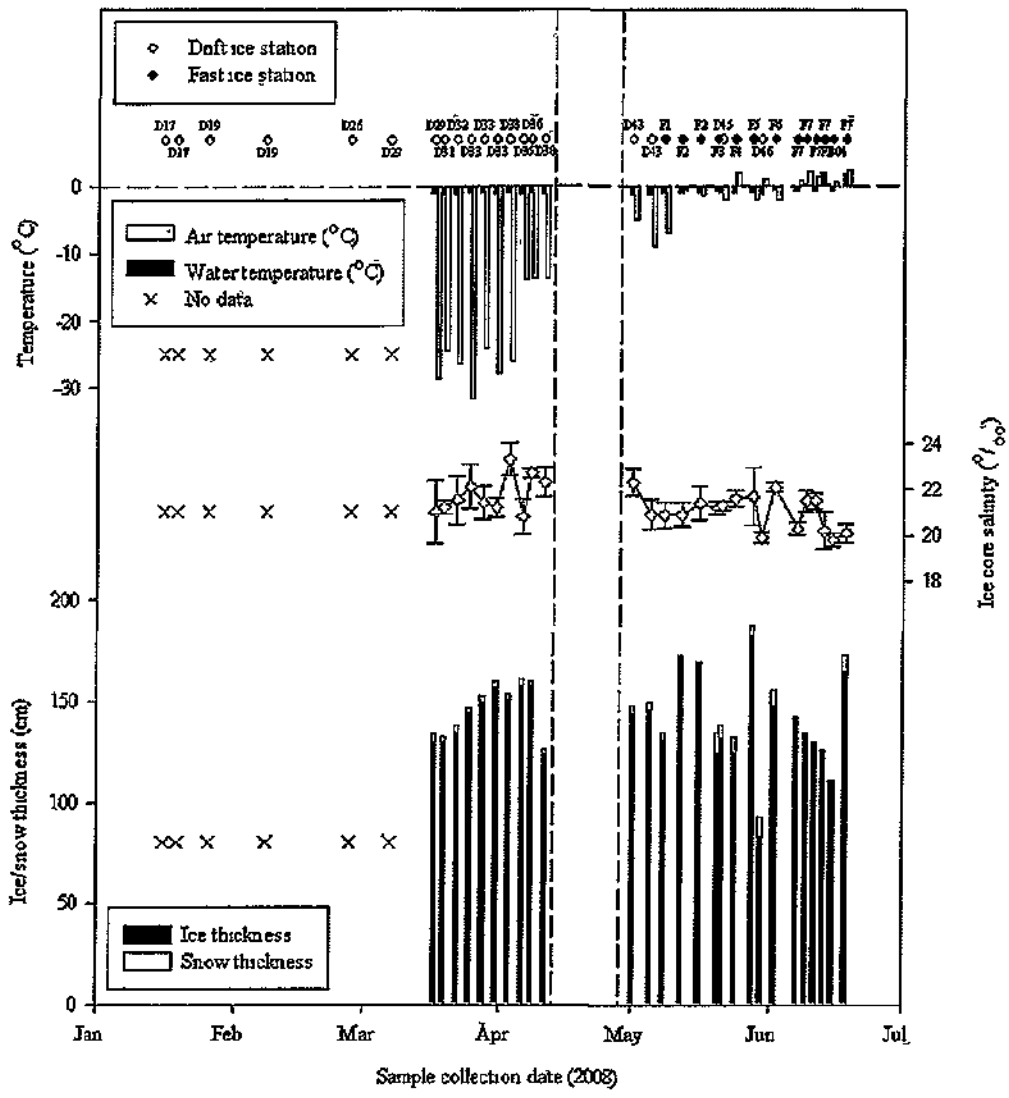

Figure 4 6-1. Temporal variation of abiotic variables observed during the IPY-CFL cruise (1/1/08 to 1/7/08) Annotated circles represent the station identity of sample sites from drift (white) and fast ice (black) locations. Air and water temperatures were derived from the ships log. Ice core salinity was calculated from filtered sea water and melted sea ice (lower 10 cm) and normalised for volume, ± 1 s.d. n = 3. Ice and snow thickness were measured through sample collection holes in the ice Dashed lines represent a temporary break in sampling.

4.7 Discussion

The results presented in this chapter have established the temporal constraints of IP_{25} and other HBIs produced within Arctic sea ice. The Arctic spring sea ice algal bloom is a well documented occurrence (Lee *et al.*, 2008; Różanska *et al.*, 2009), with previous reports providing the basis for the selected period of observation for this current investigation. Briefly, maximal concentrations and variation in concentrations of IP_{25} and some other HBIs were observed to coincide with the increase in concentration of some fatty acids and sterols, all of which coincide with the spring sea ice algal bloom. The distribution of IP_{25} in sea ice also exhibited similarities to chlorophyll *a* and the eukaryotic cell contents of sea ice.

4.7.1 Abiotic variable observations

Prior to the interpretation of lipid biomarkers, selected abiotic variables (ice and snow thickness, air and water temperature and sea ice salinity) were examined to determine any potential influence on the biomarker observations. Heat exchange between the ocean and atmosphere plays a significant role in controlling biological inhabitation of sea ice, being largely responsible for changes in the thickness, salinity, permeability and integrity of Arctic sea ice (e.g. Nihashi *et al.*, 2001; McPhee *et al.*, 2008; Petrich *et al.*, 2010).

Observed variability in air and water temperature, sea ice salinity and ice and snow thickness, is partly attributable to spatial variation. The *CCGS* Amundsen was particularly vulnerable to changes in wind direction that required constant repositioning to prevent entrapment by drifting sea ice. The resulting inconsistency in abiotic variables is most significant in ice thickness measurements. Statistical analysis of this

variation however, suggests that ice thickness has no significant impact on biomarker distributions ($r = < 0.27$).

While atmospheric air temperature in the Arctic varied greatly from March to June with ambient weather conditions (-32 to +2°C), sea water temperature remained more stable at typically < -1°C, before later warming in some coastal regions (+2°C). With a typical freezing point for sea water of ca. -1.8°C, the observed temperatures, recorded by ship-board equipment, suggest that sea ice was at its maximum thickness at the commencement of observations. Complementary sea ice salinity measurements further indicate toward the static nature of sea ice growth, due to the absence of hypersaline conditions, found from brine rejection during sea ice growth (e.g Cox *et al*, 1975; Petrich *et al*, 2010) The conditions observed, therefore, suggest sufficient pore-permeability to support inhabitation by sea ice organisms, including algae, prior to the observed occurrence of HBIs and the algal bloom.

In summary, despite the important influence these parameters impose on sea ice micro-structure, none of the observed variables was found to correlate notably with lipid biomarker production throughout the period of observation ($r = < 0\ 44$).

N.B Leading up to March 17th, abiotic data are absent as these were not recorded by colleagues who collected the early sea ice cores. Additionally, both abiotic and lipid biomarker data for the period April 11th to May 1st were also absent due to onboard handling errors.

4.7.2 Lipid concentrations in sea ice leading up to the spring sea ice algal bloom

For the period January 16th to March 17th, a baseline HBI signal was established from Arctic sea ice cores collected in the late winter (January to February), with HBI

concentrations below the GC/MS limit of detection (ca. 10 ng mL^{-1}; *s/n* = > 3 (Dyson, 1998)) in all sea ice cores (n = 8). The low HBI concentration in sea ice for this time is probably typical of the winter period, where the Arctic receives virtually no PAR, effectively preventing photosynthesis (e.g. Werner *et al.*, 2007). The observed connection between low PAR and HBI absence in the late winter/early spring is suggesting that algal production of HBIs is autotrophic, emphasising the specificity of these compounds to photosynthetic sea ice diatoms. In contrast, the presence of some fatty acids and sterols during this period, not only supports the contention that ice-core pore permeability was sufficiently established to be capable of supporting organisms, but also reflects the more diverse range of sources of these chemicals (e.g. Volkman, 1986; Volkman *et al.*, 1989; Barrett *et al.*, 1995; Volkman *et al.*, 1998).

While at least 20 different fatty acids were typically observed in many sea ice cores (Figure 4.5-6), extraction and analysis of the fatty acid content of cultures of *Haslea crucigeroides* (Figure 4.5-6) and *Pleurosigma intermedium* (Figure 4.5-7) revealed only three of these to be present (**FI**, **FII** and **FIII**). These relatively short chain (C_{14-16}) fatty acids are regularly considered to represent the presence of marine diatoms (e.g. Opute, 1974; Dunstan *et al.*, 1994; Reuss *et al.*, 2002). The significant concentration of these so-called diatom fatty acids in sea ice (up to 28 ng mL^{-1}) during a period where IP_{25} and other HBIs were absent is an indication of the reduced specificity of these and other fatty acids. The abundant, saturated fatty acid **FIV**, common to some flagellates (Reuss *et al.*, 2002), was also present. In addition, *cis*-vaccenic acid (**FV**), present in heterotrophic bacteria, as well as occurring from stereomutation resulting from photodegradation of *trans*-vaccenic acid (Rontani *et al.*, 2003; Christodoulou *et al.*, 2010), was also recorded. Neither revealed any appreciable deviation from the distributions from other fatty acids. Stable carbon isotope analysis of each of the fatty

acids (**FI**, **FII**, **FIII**, **FIV** and **FV**) revealed a relative enrichment of ^{13}C (typical $\delta^{13}C$ of -14 to -17 ± < 1.9 ‰), compared to phytoplankton lipids, an observation that is characteristic of biosynthesis within sea ice (Belt *et al.*, 2008), verifying the capacity of these ^{13}C-depleted lipids to represent general sea ice production.

Some sterols were also present, in low concentrations (ca. 1 – 2 ng mL^{-1}), for the period prior to the bloom (January 16th to March 17th). In contrast to the fatty acids, only some of the sterols monitored during this early period were present in sufficient concentrations for quantification (**SII** and **SVIII**). The mainly animal sterol, cholesterol (C_{27}, **SII**), was most abundant, representing more than half of the total concentration of the sterols detected throughout this early sampling. Increases in the concentration of cholesterol throughout the period leading up to the bloom (January 16th; 0.25 ng mL^{-1} to March 17th, 1.3 ng mL^{-1}), indicates a potential increase in the presence of heterotrophic animals. It is estimated that ca. 90%, by mass, of the zooplankton is comprised of copepods, making these algal grazing crustaceans (e.g. Arndt *et al*, 2006, Olli *et al*, 2007) a significant source of C_{27} sterols, such as cholesterol (Killops *et al.*, 1993).
The plant sterol, β-sitosterol (C_{29}; **SVIII**), was responsible for the bulk of the remaining sterol contribution (ca. 40%) throughout this early sampling The concentration of this, largely terrigenous plant sterol, was also highly variable throughout the observation period prior to the bloom and is indicative of diffuse source inputs Indeed, it is noted that a variety of hydrological and aeolian processes relating to the coastal proximity of some sample locations within the Amundsen Gulf, can lead to the incorporation of terrestrial lipids within sea ice (Thomas *et al.*, 2010). The ubiquitous presence of low concentration (ca. 0.2 ng mL^{-1}) *n*-alkanes exhibiting odd over even predominance in long chain (nC_{21} – nC_{33}) homologues, was also indicative of terrestrial (Schubert *et al*, 1996) and aeolian inputs (Kim *et al*, 2009), with distinctive terrestrial $\delta^{13}C$ composition

(-29.9 ± 0.9 ‰). Decarboxylation of fatty acids produced in terrestrial higher plant leaf cuticles, for example, results in enhancement of odd *n*-alkanes, upon transportation to the marine environment. In contrast, the observed low concentration of short chain ($nC_{14} - nC_{20}$) algal fatty acids for the period leading up to the bloom, is reflected in the absence of similar (odd over even) enhancement in the short ($nC_{13} - nC_{19}$) *n*-alkanes. Absence of C_{28} phytosterols, such as chalinasterol (**SV**) and brassicasterol (**SIV**), further support the lack of significant algal presence for this period. However, determination of the specific sources of sterols is particularly ambiguous (Volkman, 1986). For example, diatoms also contain some cholesterol, in addition to large quantities of brassicasterol, a distribution similar to that of other phyla of algae such as the haptophytes. Additionally, both marine and terrestrial invertebrates, along with some fungi, are just some of the organisms that can produce a range of C_{27} to C_{29} sterols, further complicating source assignment (Killops *et al.*, 1993).

4.7.3 Lipid concentrations in sea ice during the spring sea ice algal bloom

Of the combined individual HBI (**I, IIa, IIb, IIIa, IIIb, IIIc** and **IIId**) production within the lower 10 cm of sea ice cores, 97% was observed to occur in the period March 17th to May 24th. The sea ice biomarker **I**, accounted for a considerable proportion of the total HBI content (ca. 27%), with **IIb** and **IIIb** accounting for ca. 31% and 28%, respectively. Remaining HBI contributions were below 10%, suggesting both **I** and the di- and tri-unsaturated homologues **IIb** and **IIIb** could be most representative of the sea ice algal bloom. The onset of the production of **I** in drift ice was both rapid and steady for a period of almost 3 weeks, with concentrations increasing from ca. 0.5 pg mL^{-1} (17/3/08) to over 100 pg mL^{-1} (6/4/08), representative of diatom growth trends (e.g. Aletsee *et al.*, 1992; Tiselius *et al.*, 1996). The increase of less oblique sunlight

compared to early spring, has a greater potential of penetrating the ice, increasing the amount of PAR for diatom photosynthesis during this time. In fact, the return of significant daylight to the Arctic, with 77°N receiving ca. 12 h d^{-1} of sunlight on March 17th, increased to almost 15 h d^{-1} by April 6th, further implying an association between HBI concentration and PAR. After April 6th, an anomalous decrease in total HBI concentration to ca 0 34 ng mL^{-1} (11/4/08) occurred, prior to a gap in sampling, with large fluctuations in HBI values continuing throughout until May 24th. Significant fluctuations in all lipids, likely as a result of a range of factors such as the irregular underside of sea ice (Krembs *et al.*, 2002c) and difficulty in collecting samples in the extreme climate, were also seen in replicates collected within a 2 m radius of each other. The characteristic sea ice bloom distribution of **I** is, however, further confirmed with accurate determination of the timing of the Arctic sea ice algal bloom being achieved by measurement of chlorophyll *a* and eukaryote cell abundance in sea ice (Figure 4.5-16) Statistical determination of the extent of correlation was not carried out because the data for chlorophyll *a* and eukaryotes were obtained from different ice cores to those analysed for lipids However, these individual data sets do indicate the similar timing of both the initiation and termination of biological activity associated with the sea ice algae bloom. Further, the potential for significantly increased lipid concentrations during the break in sampling (11/4/08 to 1/5/08) was addressed with the addition of these data, with no indication of major changes to biological activity suggested from the fatty acids, chlorophyll *a* or eukaryote cell concentration profiles during this time

The timing of peak concentration in the sea ice biomarker **I** in both sea ice and sediment trap collections from a previous cruise (Figure 4.5-4, ArcticNet; 2005), provides evidence that the recorded observations occur annually, where maximum occurrence of both **I** and *Haslea* spp. cells appeared in sediment traps (Brown, 2007) a few weeks after they were first recorded appearing in sea ice in the CAA in January, 2008.

Of further importance, was the presence in sea ice of a hitherto tentatively identified di-unsaturated HBI (**IIc**; Figure 4.7-1). Previously, a di-unsaturated HBI exhibiting similar GC retention index ($2071_{HP\text{-}5}$) and mass spectral characteristics was reported in suspended particulates from Alfacs Bay (Spain), by Albaiges *et al.*, (1984). Since then, it has been observed in samples of the marine macroalga *Enteromorpha* (since reclassified as *Ulva*) by Hird (1992), before Massé *et al.*, (2004a) detected it in particulate matter and sediments from the Arabian Sea, Cariaco Trench and Peru Upwelling. Based on comparisons between mass spectral and chromatographic features described here with those reported previously, this di-unsaturated HBI has now been observed for the first time in sea ice. The concentrations of this HBI, proposed to originate from *Pleurosigma* spp. and containing $\Delta^{7(20)}$ unsaturation (Belt *et al.*, 2001a; Massé *et al.*, 2004a), also correlated well with those of **I** – r = 0.82; p = < 0.001, **IIa**: r 0.74; p = < 0.001, **IIb**: r = 0.70; p = <0.0001, **IIIb**: r = 0.74, p = < 0.001 and **IIId**: r = 0.91; p = < 0.001 in sea ice and will, from herein, be referred to as **IIc**.

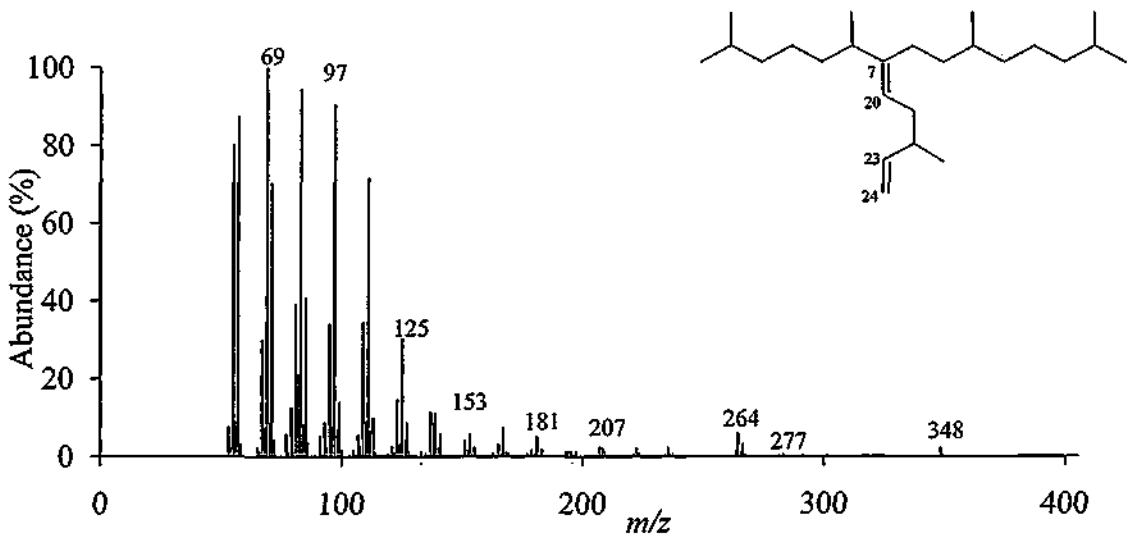

Figure 4.7-1. Background subtracted mass spectrum of a highly branched isoprenoid recorded in sea ice, with the tentatively assigned structure of a $\Delta^{7(20),\,23(24)}$ di-unsaturated HBI, RI_{2071}, HP-5 by Massé and Belt *et al.*, (2004a).

The greater concentrations measured in fatty acids (from ca. 5 to 2000 times greater) compared to those of HBIs in sea ice, enabled reconstruction of the likely lipid distribution for the gap in sampling (April 11th to May 1st; Figure 4.5-16). Fatty acid (**FI, FII, FIII, FIV** and **FV**) concentrations derived from GF/F filters previously analysed by colleagues for chlorophyll *a*, extended beyond the missing samples, complementing existing data. These additional sea ice cores, along with chlorophyll *a* and eukaryote cell abundance, provided strong evidence suggesting the continued increase in lipid production throughout the period April 11th to May 1st, with the diatom fatty acids, **FI, FII** and **FIII** being most abundant (16%, 38% and 32% respectively) Irrespective of the apparent diatomaceous origin of these three fatty acids, the increases observed in their concentrations occur about three weeks later than these of the HBIs. However, the isotopic composition of fatty acids throughout (except on 6/4/08; $\delta^{13}C$ = -24 ±1 2‰), is indicative of biosynthesis within a closed or semi-closed environment, such as sea ice (typical $\delta^{13}C$ = -14 to -17 ± < 1.9 ‰). However it is possible that where sufficient epontic (algae associated with the lower interface of sea ice and the upper water column) algal production occurs at the ice-water interface (Mock *et al* , 2003), it may also become possible for this region to become depleted in ^{12}C as well (McMinn *et al* , 1999).

The sea ice biomarker **I** and the related HBIs, **IIb** and **IIIb** collectively accounted for ca. 86% of the HBIs observed in sea ice, suggesting these compounds were representative of sea ice diatom growth. While **I** is believed to be biosynthesised exclusively by sea ice diatoms, the less specific fatty acids are produced by many varieties of abundant epontic diatoms such as *Fragilariopsis cylindrus*, as well as a range of other organisms. Additionally, where heterotrophs are present, they may also graze upon sea ice algae (e.g Gradinger *et al.*, 1992), potentially resulting in an apparent delay in the occurrence of fatty acids in sea ice. The presence of high

concentrations of cholesterol (**SII**) throughout the post bloom period is further support for the presence of grazers.

The complexity of source assignment is clear when sterol distributions for the period March 17th to June 2ndare considered. The C_{27} zoosterols, **SI** and **SIII** and the C_{28} phytosterols **SIV** and **SV**, appear to exhibit characteristic bloom distributions synonymous with algal growth for this period. However, this is not necessarily a result of diatom growth, with brassicasterol (**SIV**), for example, being a major sterol of the planktonic alga, *Emiliania huxleyi* (Christodoulou *et al.*, 2010). Conversely, the presence of cholesterol cannot be considered conclusive evidence of animal presence, due to its occurrence in many diatoms (e.g. Gillan *et al.*, 1981; Barrett *et al.*, 1995). However, the degree of variation in sterols is far greater than that seen in the HBIs or fatty acids, further suggesting diverse and varied inputs. This is further illustrated by the presence of terrestrially derived *β*-sitosterol throughout.

4.7.4 Lipid concentrations in sea ice following the spring sea ice algal bloom

From May 24th onwards, the presence of all HBIs remained dominated by **I**, **IIb** and **IIIb** (32%, 31% and 24% respectively), yet decreased in absolute concentrations, to values similar to early-bloom conditions (typically < 10 pg mL^{-1}). Similarly, a decline in total fatty acids (to < 0.8 μg mL^{-1}) and sterols (except **SII** and **SVIII**), reflected decreases in chlorophyll *a* indicating the end of the sea ice algal bloom in this region of the Arctic. The sterols **SII** and **SVIII** retained concentrations consistent with those recorded during the bloom, providing further indications of animal and terrestrial inputs.

While the sea ice does not appear to reduce significantly in thickness for this period, increases in both air and water temperatures indicated the initiation of ice decay. Summer ice decay in the Arctic begins with meltpond formation from melting snow and surface ice, resulting in a considerable presence of freshwater during this time. Approximately 50% of the freshwater from meltponds can percolate through the ice matrix (Eicken *et al*, 2002), reducing available nutrients and salinity in the lower ice column, restricting algal habitat Continued decay of the ice results in larger interstitial pore capacity and a greater volume of freshwater, effectively flushing nutrients and in some cases algae, from the ice (Petrich *et al*, 2010).

4.7.5 Lipid biomarker covariance in sea ice

In order to investigate any potential covariance between HBIs, fatty acids and sterols and to better understand the underlying numerical structure in these lipids, PCA was used to transform the data into a smaller, more manageable coordinate set.

The least unsaturated of the HBIs (**I**, **IIa** and **IIb**) recorded in Arctic sea ice provided the greatest leverage on the projection (Figure 4.5-5). With **I** and **IIb** accounting for ca. 58% of the HBIs observed in sea ice this is perhaps not surprising. However, structural similarities between **IIa** and **IIb** are manifested, by proximity, in the PCA model, despite the low concentration of **IIa** (ca. 2%) Given that both of these isomers are biosynthesised by some *Haslea* spp. (Johns *et al.*, 1999; Rowland *et al*, 2001b; Grossi *et al.*, 2004), configuration of the double bonds in **IIa** and **IIb** ($\Delta^{5(6)}$ and $\Delta^{6(17)}$ positions respectively), in addition to the relative abundance of the two isomers, suggests a potential biosynthetic preference for **IIb** However, the strong association of **IIa** to tri-unsaturated HBIs implies potential for additional planktonic production as well (**IIa**:**IIIc** and **IIa**:**IIId**; r = 0 79; $p = < 0.001$ and r = 0.78; $p = < 0.001$ respectively).

Additionally, the tri-unsaturated HBIs (**IIIa, IIIb, IIIc** and **IIId**) exhibit less leverage on the PCA model, reflecting their reduced abundance and association with sea ice production (Figure 4.5-5). While these tri-unsaturated HBIs are known to be synthesised by some *Pleurosigma* spp. (**IIIa** and **IIIb** (e.g. Johns *et al.*, 1999; Belt *et al.*, 2001c)) and *Haslea* spp. (**IIIc** and **IIId** (e.g. Rowland *et al.*, 2001b)) unambiguous assignment to either sea ice or planktonic production is not possible, most likely due to mixed source biosynthesis and the intrusion of plankton into sea ice.

For fatty acids, the diatom (**FI, FII** and **FIII**) and bacterial (**FV**) acids have the greatest leverage on the PCA model. The proximity of the grouped fatty acids to the sea ice biomarker **I**, is an indication of similarities in source organisms and is suggestive of the sea ice diatom origin of at least some of the fatty acids, consistent with the measured carbon isotope compositions ($\delta^{13}C$ = -14 to -17 ± < 1.9 ‰) and **I** ($\delta^{13}C$ = -16.9 ± 2‰). In contrast, the non-diatom source of the saturated fatty acid (**FIV**) is supported by its separation in the PCA model.

While previous source assignment of the observed sterols in sea ice was difficult, the PCA projection is a little more informative (Figure 4.5-15). The absence of significant grouping in many of the sterols is again indicative of the varied sources of these compounds (e.g. animal, marine and terrestrial). However, some grouping is apparent in the phytosterols (**SI, SIV** and **SV**). These sterols are generally synonymous with planktonic, rather than sea ice production, given their distal proximity to **I**, a property of **SIV** that was adopted in determining historical planktonic production for the Fram Strait (Müller *et al.*, 2009). Additionally, further tentative grouping is evident in the largely terrestrial sterols, **SVI, SVII** and **SVIII**, while the biosynthetic precursor of **SII** (**SIII**) is located nearest to **SII**. In opposition to these broad classifications, numerous studies of the lipid content of various diatoms reveal the presence of many of these sterols in significant abundance (Gillan *et al.*, 1981; Barrett *et al.*, 1995).

PCA characterisation of each lipid class, relative to each other, further indicated the mixed diatom source input of HBIs (Figure 4.5-17). Fatty acids carry the greatest leverage on the projection, most likely due to their abundance. Grouping of fatty acids and sterols reflect differences in production between these classes of lipids, with vertical separation within each class representing varying sources. For example, the largely 'planktonic' phytosterols **SI, SIV** and **SV** are furthest vertically, from the 'animal' sterols **SII** and **SIII,** with the terrestrial plant sterols **SVI, SVII** and **SVIII** positioned in-between. Similarly, the diatom fatty acids, **FI, FII** and **FIII** are also furthest, vertically, from the bacterial fatty acid (**FV**), while the flagellate acid **FIV**, is positioned on its own. Positioning of these lipids in three dimensions was intended to provide the basis for source assignment of the HBIs. The apparent absence of distinct grouping in the HBIs instead makes source assignment more complicated Conversely, the biosynthesis of both isoprenoids and sterols, in diatoms, higher plants and animals, from the C_5 precursors; isopentenyl diphosphate (IPP) and dimethylallyl diphosphate (DMAPP), (e.g. Massé, 2003; Suzuki *et al*, 2007; Okada *et al*, 2008) supports the proximity of some HBIs to sterols, rather than fatty acids. While the projection of the abundant **I** and **IIb** reflect this biosynthetic similarity to sterols, the spatial distribution of the remaining HBIs (**IIa, IIIa, IIIb, IIIc** and **IIId**) is potentially due to the sometimes low concentrations of these homologues.

4.7.6 Impact of snow cover on HBI concentrations

A short series of sea ice cores (3 replicates at four sites) from regions of high snow (ca 20 – 40 cm) were also collected during the onset of the sea ice algal boom (17/3/08 – 2/4/08). The associated reduction in solar irradiance caused by increased snow cover,

was reflected in the absence of even the most abundant HBIs (**I, IIb** and **IIIb**) in the bottom 10 cm of these sea ice cores. It is worth noting that regions of 'high' snow cover were sparse in expanses of flat sea ice, presumably a result of drifting caused by strong winds (Sturm *et al.*, 2002a; Mundy *et al.*, 2005; Qiang *et al.*, 2008). The longevity of the impact of snow-induced reduction in irradiance and the associated reduction in HBI abundance is unclear due to the absence of sea ice samples representative of high snow cover conditions beyond April 2nd. However, investigations of photoadaptation in the Canadian Arctic indicate that sympagic algae productivity under snow will normalise, over time, to achieve similar productivity to that of algae living in snow free sea ice (Cota, 1985).

4.8 Conclusion

This study has demonstrated that temporal HBI production in sea ice was dominated by **I** and the di- and tri-unsaturated homologues, **IIb** and **IIIb**, while the HBIs **IIa**, **IIIa**, **IIIc** and **IIId** had typical epontic characteristics. In addition, it was established that more than 90% of the production of **I** recorded in sea ice, occurred during the Arctic spring sea ice diatom bloom (March 17th to May 24th in 2008), correlating well with chlorophyll *a*, eukaryote cell abundance and some fatty acids, notably those associated with production by diatoms. Evidence of habitable sea ice, through the presence of some fatty acids and sterols during a pre-bloom period where no HBIs were detected, coincided with insufficient PAR for photosynthesis. Following the bloom, melting snow and sea ice probably percolated through the remaining sea ice matrix, reducing nutrients and salinity, ultimately terminating the bloom. Variation in lipid abundance between sample replicates was attributed to micro-structural variations in sea ice and the associated difficulties of working in an extreme climate.

In contrast, the poor correlation between **I** and most (if not all) sterols found in sea ice, suggest the latter are not useful sea ice diatom markers and are therefore indicative of mixed source inputs (sea ice, planktonic and terrigenous).

Finally, inspection, through time, of lipid concentrations in sea ice reveals a biomarker selectivity where the following association to sea ice was observed; **I, IIb** and **IIIb** > **IIa, IIIa, IIIc** and **IIId** > fatty acids > sterols.

CHAPTER FIVE

5 Vertical distribution of HBIs in Arctic sea ice

5.1 Introduction

Chapter 5 describes the examination of the occurrence of IP_{25} and other HBIs within Arctic sea ice cores from the Amundsen Gulf region of the CAA. Additional biomarker analysis was adopted to clarify the observations and provide distinctions between biomarker production sources. As a result, the spatial limitation of IP_{25} production within sea ice, along with other polyunsaturated HBIs and established biomarkers, were determined.

To contextualise the vertical distribution of IP_{25} and lipid biomarkers in sea ice, an understanding of the key physical aspects of sea ice are discussed in the previous chapter (Chapter 4).

5.2 Aims and objectives of sea ice HBI investigations

In Chapter 4, the temporal evolution of IP_{25} and other biomarkers was established for Arctic sea ice. In the present chapter, a more detailed down core assessment of the distribution of each individual lipid biomarker is carried out to further identify the content of IP_{25} in sea ice and in particular, distinguish between internal sea ice and epontic lipid sources. Therefore, the main aims of this study relating to sea ice were to

i. Determine the internal, vertical, distribution of IP_{25} and other HBIs within sea ice
ii Elucidate the variation, if any, in the vertical production of IP_{25} and other HBIs between two intervals broadly corresponding to pre-bloom and early-bloom conditions in sea ice
iii. Investigate the internal, vertical, distribution of IP_{25} and other biomarkers in sea ice and identify the potential for spatial classification of lipids into production zones relating to their biosynthetic origin

5.3 Selection of sea ice samples and fieldwork

Collection of sea ice was carried out as described previously (Chapter 4). Two stations were chosen, where sea ice cores were previously collected, for additional high resolution (1 cm) sectioning of sea ice (Station D32; 22/3/08 and station D38; 12/4/08). Figure 5.3-1 and Figure 5 3-2 illustrate the temporal and spatial distribution of sites chosen to investigate IP_{25} production within sea ice. Sea ice cores were collected over a time window chosen to represent the early and mid points of the documented Arctic sea ice algal bloom (e.g. Lee *et al.*, 2008; Rózanska *et al.*, 2009)

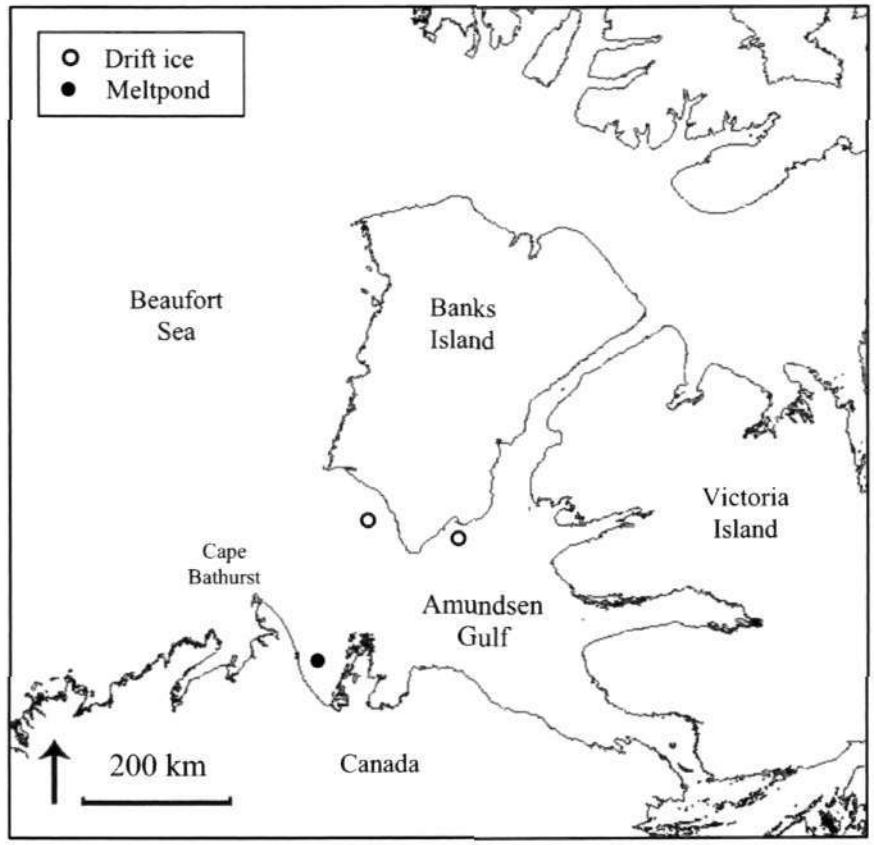

Figure 5.3-1. Spatial distributions of sea ice core collection sites, from drift ice (open circles), for high resolution sectioning (1 cm) and meltponds (black circle) from within the Amundsen Gulf region of the CAA during the IPY-CFL cruise, 2008.

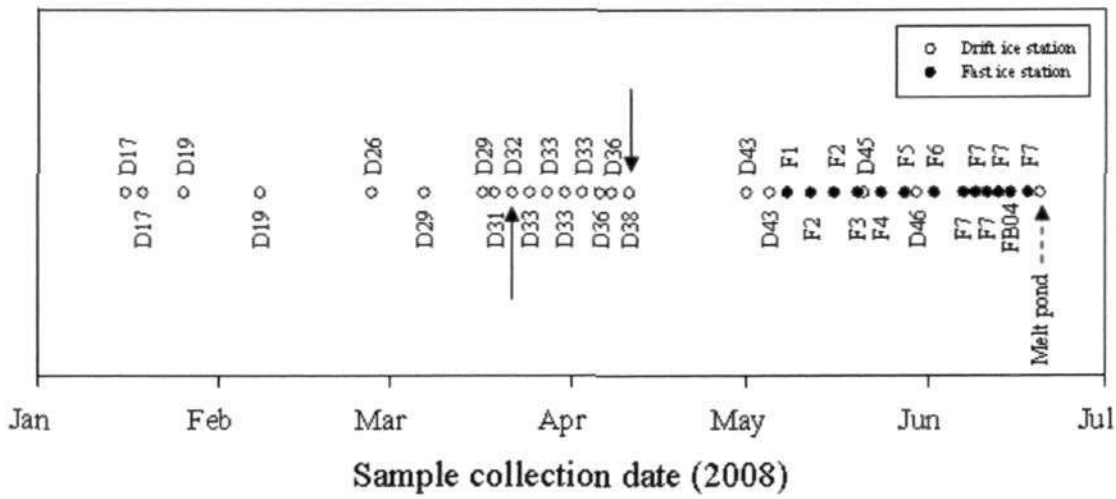

Figure 5.3-2. Temporal distribution of sea ice core samples collected for high resolution sectioning (1 cm; black arrows), dashed arrow represents meltpond sample collection, from within the Amundsen Gulf region of the CAA during the IPY-CFL cruise; 01/01/08 – 01/07/08.

Sea ice was collected as described previously (Chapter 4). Complete sea ice cores were retrieved and sectioned, *in situ*, by hand to ca. 15 – 20 cm (Figure 5.3-3). Cores were then stored temporarily in pre-labelled plastic bags. Onboard the Amundsen, the sea ice cores were further sectioned in a temperature-controlled laboratory (-20°C), using an Omcan food preparation band saw, at 10 cm. Additional cuts every centimetre, yielded sea ice sections spanning 0 – 1, 1 - 2, 2 - 3 cm, up to 9 – 10 cm, from the ice-water interface (Figure 5.3-3).

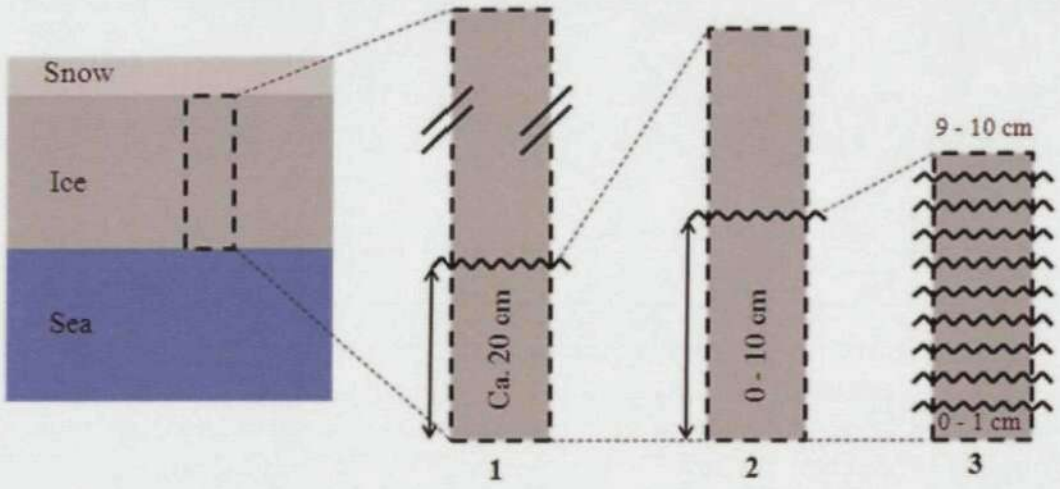

Figure 5.3-3. Schematic of sea ice core sectioning: 1, *in situ* handsaw cut (zigzag line): 2, Temperature controlled room (-20°C), 10 cm band saw cut (zigzag line): 3, Temperature controlled room (-20°C) 1 cm band saw cuts (zigzag lines) to obtain ten 1 cm sub-samples.

Bottom-ice sections (0 – 1 cm to 9 – 10 cm) were also melted and filtered as described previously (Chapter 4). Additionally, meltpond samples were collected in early summer (Figure 5.3-4) using a 'slurp-gun', similar to a large (60 x 5 cm) syringe, to extract the internal pore water of sea ice from meltponds. Water (4 L) was collected on each occasion and filtered under vacuum onto GF/F (0.7 μm) filters.

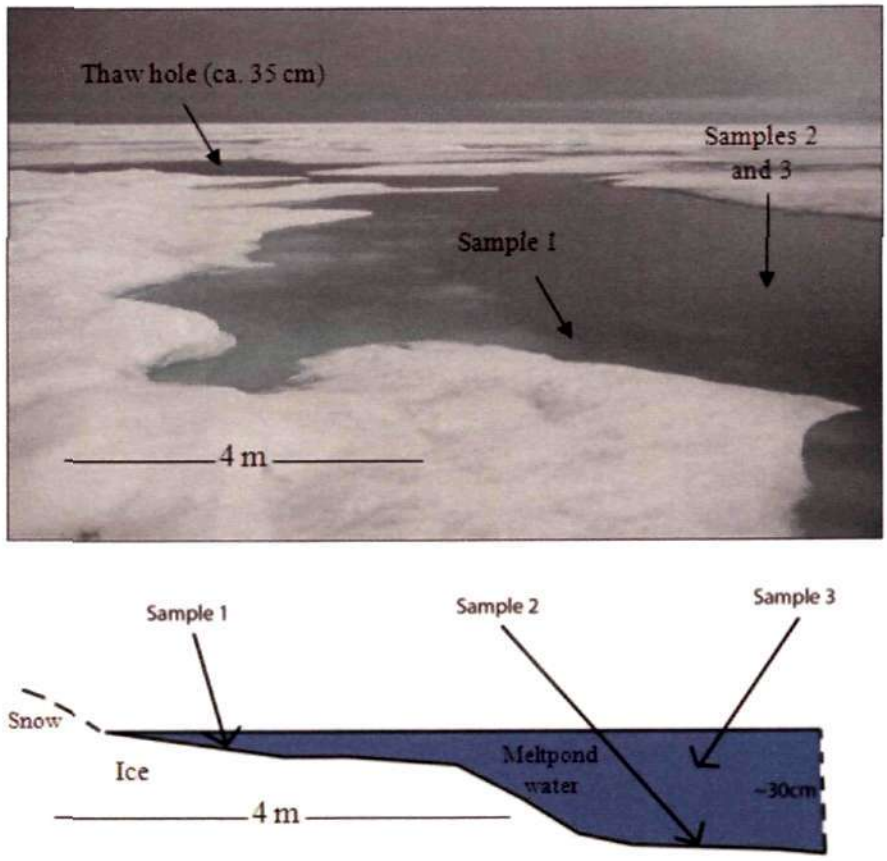

Figure 5.3-4. Meltpond sample sites, collected in early summer (FB06: 20/6/08) during the IPY-CFL cruise. Top: Photograph showing the extent of snow and ice melt and vicinity of nearest thaw-hole (complete melt of ice) to the sample locations. Bottom: Schematic representation of the sample locations showing meltpond water depth.

5.4 Experimental

Each of the biomarkers of interest (hydrocarbons, sterols and fatty acids) required extraction from the sample matrix, with further isolation into separate fractions, necessary to enable later analysis, based on their polarity and volatility. This was achieved as previously described (Chapter 4).

5.5 Results

5.5.1 Environmental variables

Salinity data for some sea ice cores, that corresponded to those where colleagues measured temperature, were used to assess the theoretical 5% brine volume permeability threshold model (Golden *et al.*, 2007). Corresponding data were collected on four occasions (17th and 25th March; 6th and 11th April 2008) over the early sea ice algal bloom period (Figure 5.5-1).

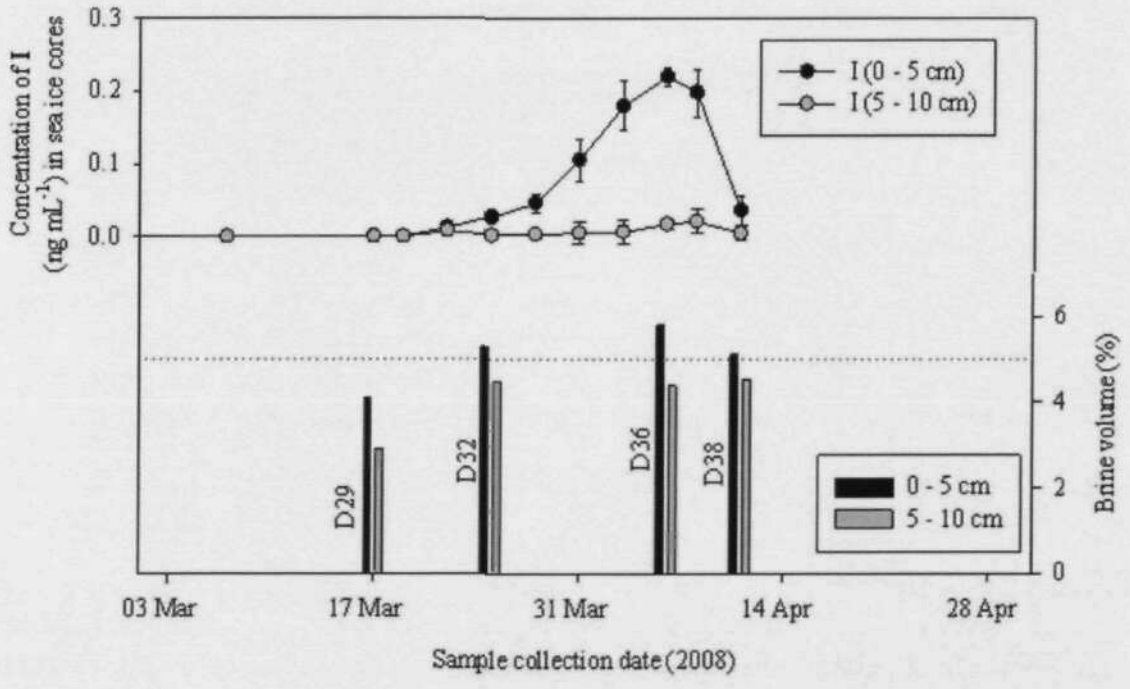

Figure 5.5-1. Partial time series comparison of **I** in the bottom 0 - 5 and 5 – 10 cm of sea ice against brine volume (%) in the bottom 0 – 5 and 5 – 10 cm of sea ice cores collected during the IPY-CFL cruise (1/3/2008 to 1/5/2008) ± 1 s.d. Dotted line represents the 5% permeability threshold.

Brine volume (%) was calculated using the following equation:

Equation 13

$$Brine\ volume\ (\%) = \left[\frac{P \times S_i}{f_1(t_i)}\right] \times 100$$

Formula used to calculate brine volume (%) of sea ice taking into account brine density, salinity and temperature (P, S_i, $f_1(t_i)$ respectively) of sea ice using Equation 14, 15 and 16.

Equation 14

$$P(mg\ m^{-3}) = 0.917 - 1.403 \times 10^{-4} \times t_i$$

Formula used to calculate the density of sea ice brine (mg m^{-3}) approximated from Cox and Weeks (1975), adjusted for measured sea ice temperature (t_i).

Equation 15

$$S_i = \left[\frac{V_{FSW}}{V_{FSW} + V_{ice}}\right] X\ Salinity_{FSW} + \left[\frac{V_{ice}}{V_{FSW} + V_{ice}}\right]$$

Formula used to calculate salinity (‰) of sea ice taking into account a known volume of filtered sea water (FSW) of known salinity, where V denotes volume (mL).

Equation 16

$$f_1(t_i) = \alpha_0 + \alpha_1 t_i + \alpha_2 t_i^2 + \alpha_3 t_i^3$$

Formula incorporating phase equilibrium coefficients for the least squared curves as a function of temperature (Assur, 1960).

Visual comparison of brine volume and concentrations of **I** in the lower 0 - 5 cm of sea ice cores, revealed that where the brine volume of these sea ice sections was greater than 5%, the concentration of **I** was easily measurable, suggesting a permeability threshold suitable for biological inhabitation (> 5%) within this region (Figure 5.5-1). Additionally, equivalent calculations carried out on the 5 – 10 cm (from the ice-water interface) region of sea ice cores, revealed considerably lower concentrations of **I**,

nearer the limit of detection, reflected by brine volumes consistently below 5%, which presumably restricted the ability of organisms to inhabit this region of ice. This distinct difference in the physical and chemical properties of the two horizons (0 – 5 and 5 – 10 cm) was therefore further investigated in higher resolution.

5.5.2 Brine volume (%) of D32 and D38

Brine volumes (%) were calculated from sea ice temperature and salinity data for two high resolution sea ice cores (D32 and D38) according to Equation 13 in order to determine, more accurately, the region of sea ice that can be inhabited by sea ice organisms. Once brine volume was determined for each 1 cm horizon, intersecting lines, corresponding to 5% brine volume, were used to establish the region of sea ice containing more than a 5% volume of brine (Figure 5.5-2). Above this horizon (ca. 3 cm and 6 cm in D32 and D38 respectively), termed the ice core permeability threshold, the connectivity of brine pores is insufficient to enable the growth of organisms owing to, among other things, a lack of accessibility and reduced possibility of nutrient replenishment

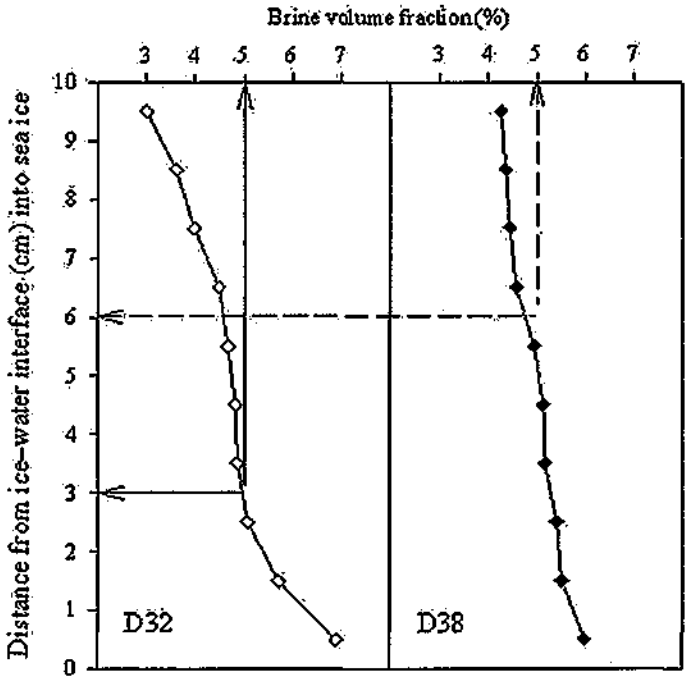

Figure 5.5-2. Vertical distribution of brine volume (%) observed in the bottom 0 - 10 cm of high resolution sea ice cores during the IPY-CFL cruise (D32; 22/3/08: D38; 11/4/08). Vertical solid and dashed lines represent 5% brine volumes of D32 and D38 respectively. Intersecting horizontal solid and dashed lines represent the vertical 5% permeability thresholds of D32 and D38 respectively.

5.5.3 Lipid biomarkers in sea ice: D32; 22/3/08

5.5.3.1 HBIs in high resolution sea ice cores

Analysis (GC/MS) of lipids obtained from 1 cm sections of sea ice cores, facilitated examination of the HBI content in Arctic sea ice (Figure 5.5-3). The combined concentration of individual HBIs (**I, IIa, IIb, IIIa, IIIb, IIIc** and **IIId**) in the bottom 0 - 1 cm of sea ice was very low (6.4 pg mL^{-1}), yet accounted for 21% of the total HBI concentrations in the core. Maximum combined individual HBI concentration (42 pg mL^{-1}) was restricted to the 1- 2 cm horizon and accounted for > 57% of the total HBI distribution in the bottom 0 - 10 cm. Above 2 - 3 cm from the ice-water interface, HBI concentration rapidly decreased, with no horizon contributing more than 2.5% to the

total distribution. The decrease above 2 - 3 cm, is in further agreement with the 5% permeability threshold restricting biological inhabitation (Zhu *et al*, 2006; Golden *et al*, 2007).

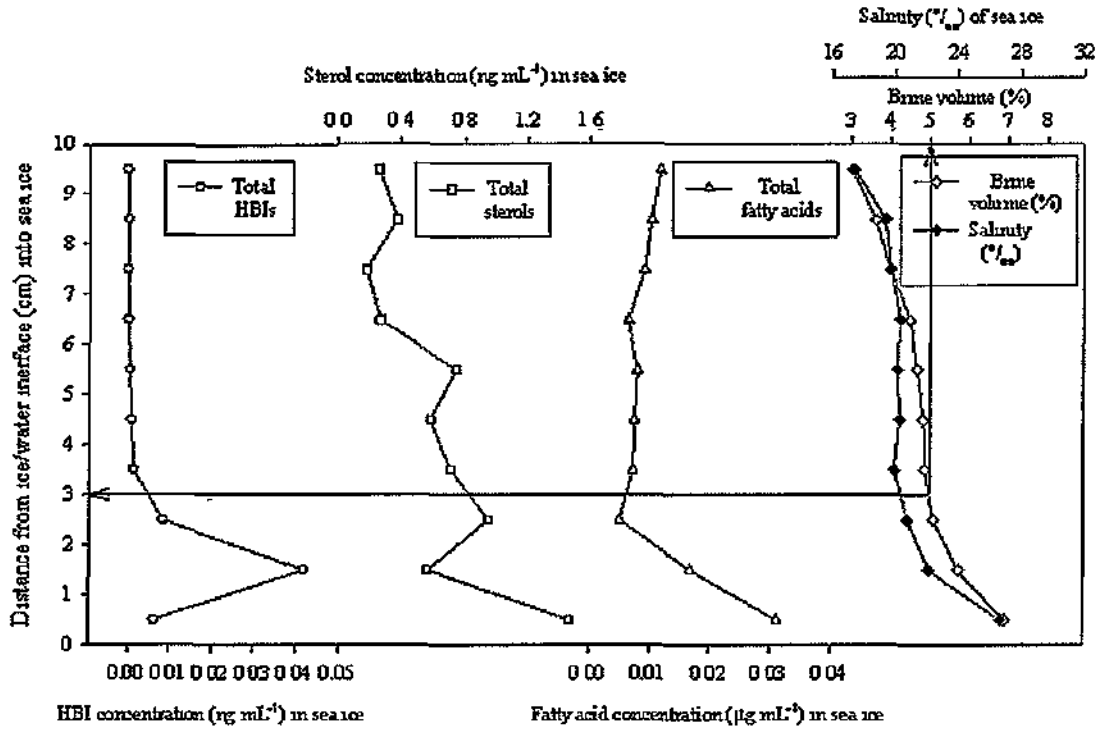

Figure 5.5-3. Vertical distribution of lipid biomarkers, salinity and brine volume observed in the bottom 0 - 10 cm of high resolution sea ice cores during the IPY-CFL cruise (D32; 22/3/08). From left to right: Total HBI (**I**, **IIa**, **IIb**, **IIIa**, **IIIb**, **IIIc** and **IIId**) concentration. Total sterol (**SII**, **SIII**, **SIV**, **SVI**, **SVII** and **SVIII**) concentration: Total fatty acid (**FI**, **FII**, **FIII**, **FIV** and **FV**) concentration Salinity and brine volume. Vertical solid line represents 5% brine volume. Intersecting horizontal line represents the *5% permeability threshold*

5.5.3.2 Sterols in high resolution sea ice cores

Examination (GC/MS) of the bottom 0 – 10 cm of sea ice cores enabled observation of the sterol content of Arctic sea ice (Figure 5 5-3). The combined individual sterol (**SII**, **SIII**, **SIV**, **SVI**, **SVII** and **SVIII**) concentration, in the bottom 0 - 1 cm of sea ice represented the greatest concentration and distribution within the core (1 48 ng mL^{-1}; 24%). Above this, total sterol concentration fluctuated, whilst steadily declining, with

the lowest concentration (0.18 ng mL^{-1}) occurring in the upper sections of the core (7 – 8 cm). The concentration profile of the sterols was in poorer agreement with the 5% permeability threshold required for algal growth and is consistent with varied input source mechanisms.

5.5.3.3 Fatty acids in high resolution sea ice cores

Analysis (GC/MS) of the bottom 0 - 10 cm of sea ice cores enabled observation of the fatty acid content of Arctic sea ice (Figure 5.5-3). The combined individual fatty acid (**FI, FII, FIII, FIV** and **FV**) concentration was highest in the bottom 0 - 1 cm of sea ice (31 ng mL^{-1}; 29%). The concentration of fatty acids declined over the subsequent horizons (1 – 2 cm; 11%), reaching a minimum (7.3 pg mL^{-1}; 5%) at 2 – 3 cm, in agreement with the 5% permeability threshold restricting biological inhabitation.

5.5.3.4 Vertical distribution of individual HBIs

Determination of the relative contributions of individual HBI isomers (Figure 5.5-4), showed that of the combined individual HBI concentrations (6.4 pg mL^{-1}), **IIIb, IIb** and **IIId** were the most abundant isomers, contributing on average, ca. 49%, 15% and 15%, respectively, of the total cumulative HBI abundance in sea ice. Compound **I** contributed 12% (0.74 pg mL^{-1}). Of the remaining HBIs, none contributed more than 10% of the total concentration. The total cumulative concentration of individual HBIs from all horizons (0 – 10 cm) was consistent with that of the 0 – 10 cm section of the time series core collected on 22nd March (6.5 pg mL^{-1}: Chapter 4).

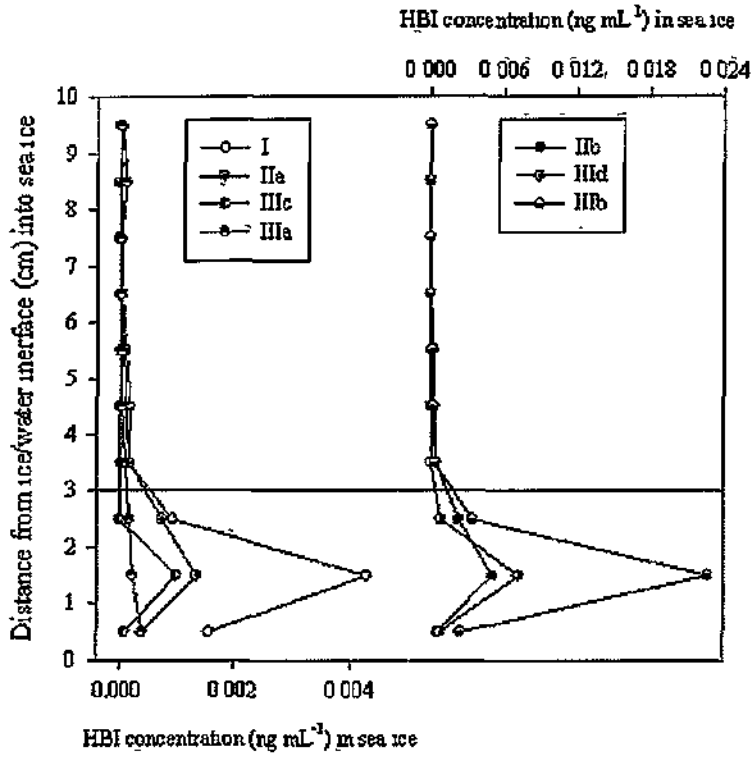

Figure 5 5-4 Vertical distribution of individual HBIs (**I, IIa, IIb, IIIa, IIIb, IIIc** and **IIId**) observed in the bottom 0 - 10 cm of high resolution sea ice cores during the IPY-CFL cruise (D32, 22/3/08). Note change of x-axis scale. Horizontal line represents the 5% permeability threshold.

Multivariate analysis of HBIs was carried out using PCA to classify isomers according to their primary source (e g. sea ice diatom or plankton; Figure 5.5-5). The PCA model is robust, using 8 variables and 10 observations, with the first two PCs accounting for 98% of the variance in the data, enabling reliable representation on two axes. Interpretation of the PCA model suggested that all HBIs were related, in terms of production, with **IIIa** exhibiting the greatest variation Additionally, the proposed $\Delta^{7(20)}$ di-unsaturated HBI, **IIc**, is also present and correlated extremely well to concentrations of all HBIs in this study ($r = > 0.92$; $p = < 0.001$), with the exception of **IIIa** ($r = 0.51$, $p = 0\ 13$). The poor correlation of **IIc** to **IIIa** is evident upon observation of the down core distribution of HBIs where the concentration of **IIIa** is distinctly different (Figure 5 5-4).

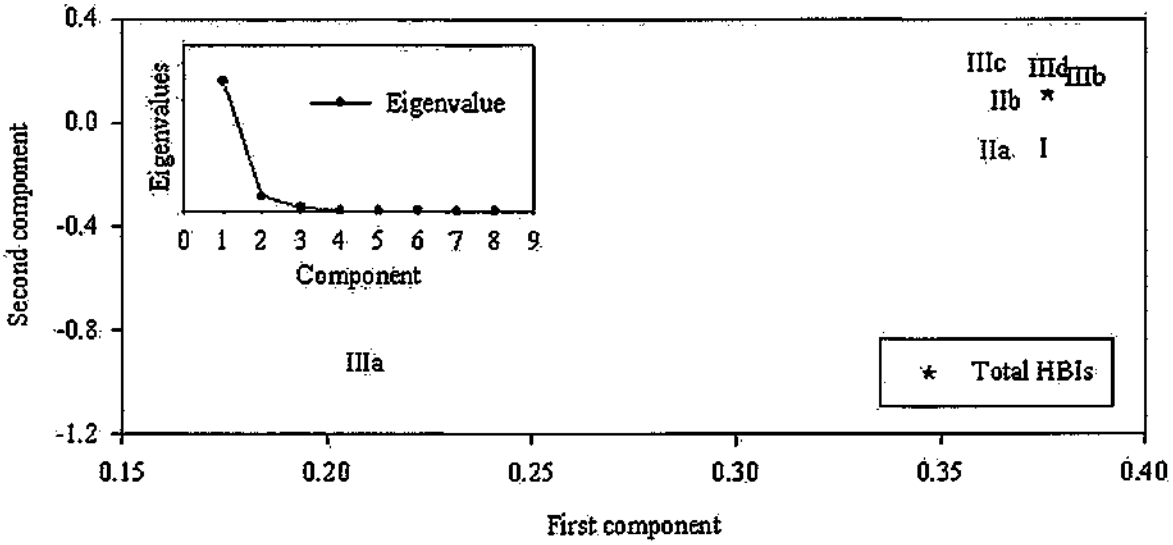

Figure 5.5-5. First and second component variable (loadings) plot of the principal components analysis for HBIs observed in the bottom 0 - 10 cm of high resolution sea ice cores during the IPY-CFL cruise (D32; 22/3/08). **I:IIa**: r = 0.94; p = < 0.001. **I:IIb**: r = 0.93; p = < 0.001. **I:IIIa**: r = 0.63; p = 0.05. **I:IIIb**: r = 0.97; p = < 0.001. **I:IIIc**: r = 0.94; p = < 0.001. **I:IIId**: r = 0.97; p = <0.0001. Inset: Eigenvalue plot showing the proportion of variability accounted for by the first two components (98%).

5.5.3.5 Vertical distribution of individual sterols

Determination of the relative contributions of individual sterols (Figure 5.5-6), showed that of the combined individual sterol concentration (0.61 ng mL^{-1}), the 'animal' sterol, cholesterol (**SII**), was the most abundant, contributing ca. 76%, of the total cumulative sterol concentration in sea ice. Cholesterol (**SII**) was therefore responsible for most of the total sterol profile and was noted as being non-representative in terms of the distribution of the remaining sterols. Sterols **SIV**, **SVI**, **SVII** and **SVIII**, like **SII**, were found in greatest concentration at the ice-water interface, but unlike **SII**, they rapidly decreased within the adjacent horizon (1 – 2 cm), before remaining low throughout the rest of the core. **SI**, **SIII** and **SV** were below the limit of detection for GC/MS TIC.

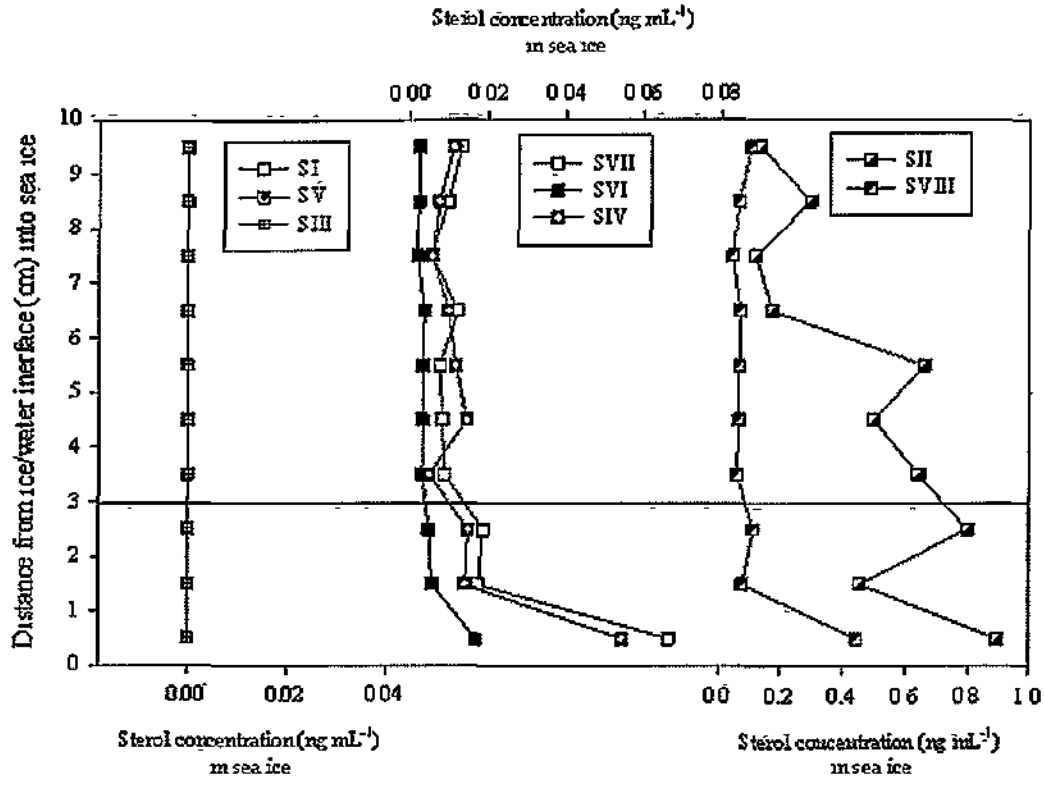

Figure 5 5-6. Vertical distribution of individual sterols (**SII, SIII, SIV, SVI, SVII** and **SVIII**) observed in the bottom 0 - 10 cm of high resolution sea ice cores during the IPY-CFL cruise (D32; 22/3/08). Horizontal line represents the 5% permeability threshold

Multivariate analysis of sterols was carried out using PCA to classify compounds according to their primary source, e.g. marine, terrestrial or animal (Figure 5.5-7). The PCA model was robust, using 7 variables and 10 observations, with the first two PCs accounting for almost 90% of the variance in the data, enabling reliable representation on two axes. Interpretation of the PCA model further exemplified the differences between **SII** and the remaining sterols and the poor correlation of all sterols to the HBI, **I** ($r = < 0.41$)

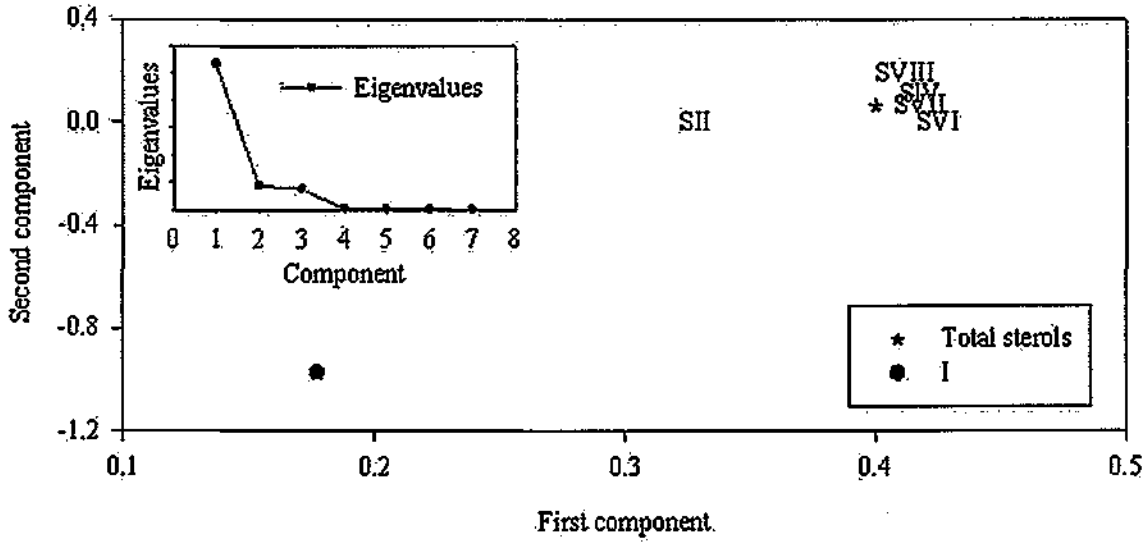

Figure 5.5-7. First and second component variable (loadings) plot of the principal components analysis for sterols observed in the bottom 0 - 10 cm of high resolution sea ice cores during the IPY-CFL cruise (D32; 22/3/08). **I:SII**: r = 0.27; p = 0.45. **I:SVII**: r = 0.36; p = 0.31. **I:SVIII**: r = 0.24; p = 0.50. **I:SIV**: r = 0.32; p = 0.37. **I:SVI**: r = 0.41; p = 0.24. Inset: Eigenvalue plot showing the proportion of variability accounted for by the first two components (89%).

5.5.3.6 Vertical distribution of individual fatty acids

Determination of the relative contributions of individual fatty acids (Figure 5.5-8), showed that of the combined individual fatty acid concentrations (0.011 μg mL^{-1}), the saturated compounds **FIV** and **FII,** were the most abundant, contributing ca. 41% and 38% respectively, of the total cumulative fatty acid concentration in sea ice. The bacterial fatty acid, **FV**, was also abundant (ca. 12%), while that of **FI** and **FIII** were comparably low (< 4%). All fatty acids observed followed the same relative distributions across horizons (r = > 0.79; p = < 0.006). Maximum concentration occurred at the ice-water interface and was followed by a decline, reaching in some cases, minimum concentration at the 5% permeability threshold. Above 3 cm, fatty acid profiles were considered relatively refractory.

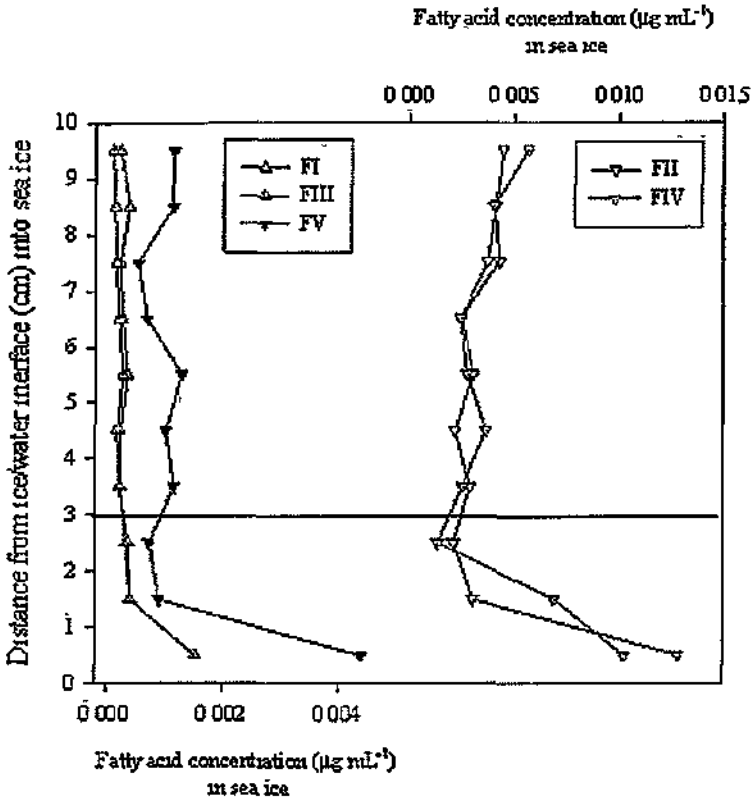

Figure 5.5-8. Vertical distribution of individual fatty acids (**FI, FII, FIII, FIV** and **FV**) observed in the bottom 0 - 10 cm of high resolution sea ice cores during the IPY-CFL cruise (D32, 22/3/08) Horizontal line represents the 5% permeability threshold.

Multivariate analysis of fatty acids was carried out using PCA to classify compounds according to their primary source (e.g. sea ice or planktonic, Figure 5.5-9). The PCA model was robust, using 7 variables and 10 observations, with the first two PCs accounting for 95% of the variance in the data, enabling reliable representation on two axes. Interpretation of the PCA model further exemplified the differences between **FIV** and the remaining fatty acids, in addition to a poor correlation between all fatty acids and the HBI, I ($r = < 0.52$; $p = < 0.79$)

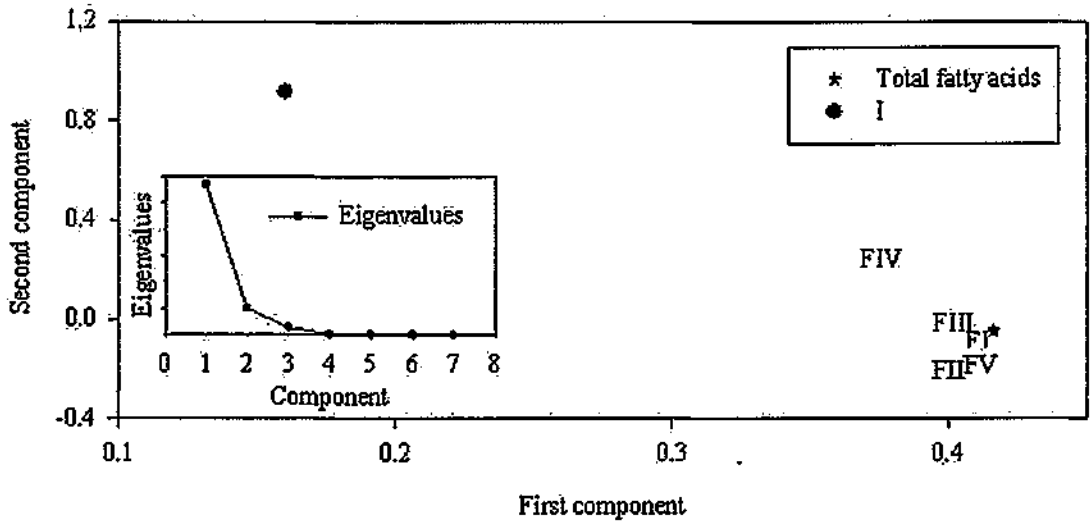

Figure 5.5-9. First and second component variable (loadings) plot of the principal components analysis for fatty acids observed in the bottom 0 - 10 cm of high resolution sea ice cores during the IPY-CFL cruise (D32; 22/3/08). **I:FIV**: r = 0.52; p = 0.12. **I:FIII**: r = 0.40; p = 0.29. **I:FI**: r = 0.31; p = 0.39. **I:FII**: r = 0.17; p = 0.64. **I-FV**: r = 0.18; p = 0.62. Inset: Eigenvalue plot showing the proportion of variability accounted for by the first two components (95%).

5.5.3.7 Comparison of sea ice lipid biomarkers

Additional PCA was carried out on HBIs, fatty acids and sterols to (a) characterise each class of lipid, relative to one another and (b) to investigate the potential range of sources of the HBIs **IIa, IIb, IIIa, IIIb, IIIc** and **IIId**. The PCA model was relatively robust, although with 17 variables used for only 10 observations, sufficient variation was not accounted for in the first two PCs. Given the number of variables, it was felt that representation on three axes (accounting for 98% of the variation) might enable better interpretation (Figure 5.5-10). Distinct grouping was evident in both the sterols and fatty acids, with vertical spread reflecting variation within each group. Significant variation was again observed with cholesterol (**SII**), which had the greatest separation from the other sterols. Similarly, **FIV** was separated the most in the projection of fatty acids, while the remaining fatty acids displayed a small degree of vertical separation. Interpretation of the three dimensional projection of HBIs, however, was more

complicated. While the distribution of HBIs reflected that seen previously, in two dimensions, the lack of clear grouping as a class of compounds was suggestive of different inputs to those of sterols and fatty acids. One distinction was, however, clear: HBI **IIIc** is significantly separated and tentatively grouped with **SII** and **FIV** (Figure 5.5-10).

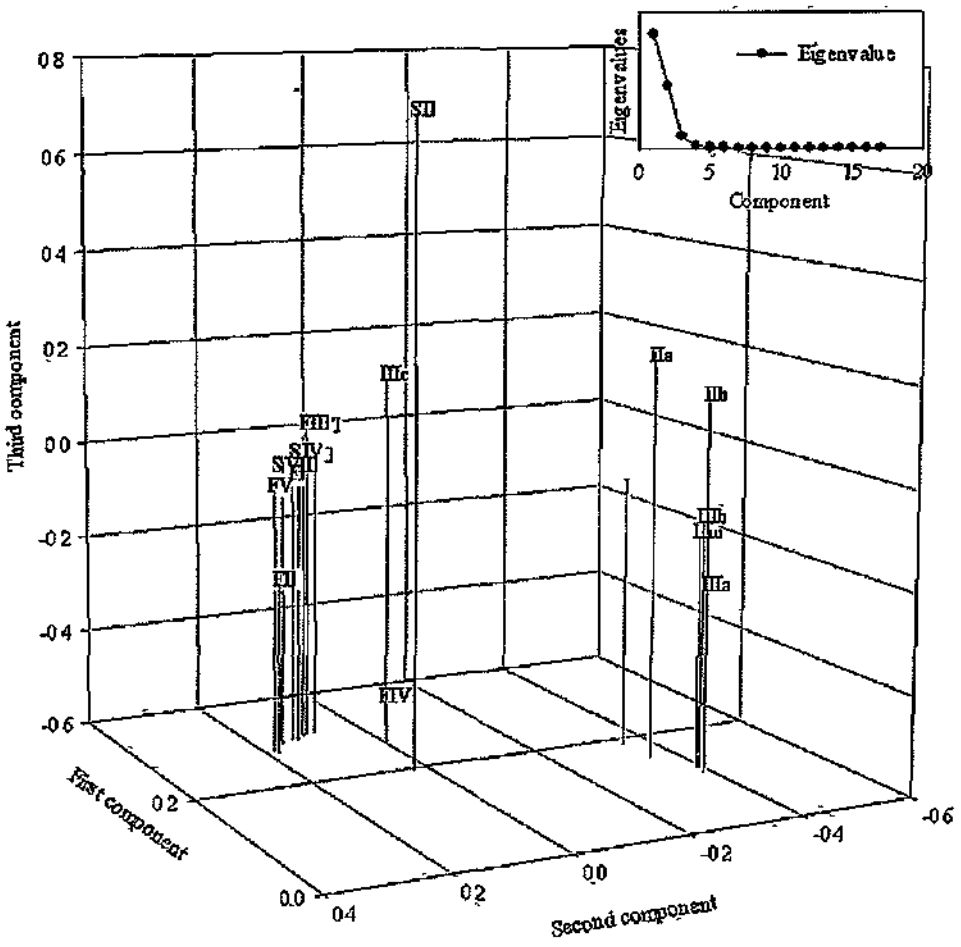

Figure 5.5-10. First, second and third component variable (loadings) plot of the principal components analysis for biomarkers observed in the bottom 0 - 10 cm of high resolution sea ice cores during the IPY-CFL cruise (D32; 22/3/08). Proximity of compounds in three dimensions is a function of covariance. Red = sterols (**SII, SIV, SVI, SVII** and **SVIII**), green = Fatty acids (**FI** to **FV**), blue = HBIs (**I** to **IIId**). Inset: Eigenvalue plot showing the proportion of variability accounted for by the first three components (98%).

5.5.4 Lipid biomarkers in sea ice: D38; 12/4/08

5.5.4.1 HBIs in high resolution sea ice cores

Analysis (GC/MS) of the bottom 0 - 10 cm of sea ice cores, enabled observation of the HBI content of Arctic sea ice (Figure 5.5-11). Combined individual HBI (**I, IIa, IIb, IIIa, IIIb, IIIc** and **IIId**) concentrations in the bottom 0 - 1 cm of sea ice in D38 (0.19 ng mL^{-1}) were > 30 x greater than in D32 (0.006 ng mL^{-1}), yet accounted for a similar distribution in total concentration (18.1% and 21% respectively). Maximum vertical HBI concentration (0.34 ng mL^{-1}) was still restricted to one horizon (1 – 2 cm), but only accounted for 33% of the total HBI distribution (ca. half as much as in D32; 57%). Above 1 - 2 cm, from the ice-water interface, HBI concentrations gradually decreased, with the combined contribution above the 5% permeability threshold (6 - 10 cm) being 5.5%, similar to that above the brine permeability threshold of D32 (3 – 10 cm; 6%).

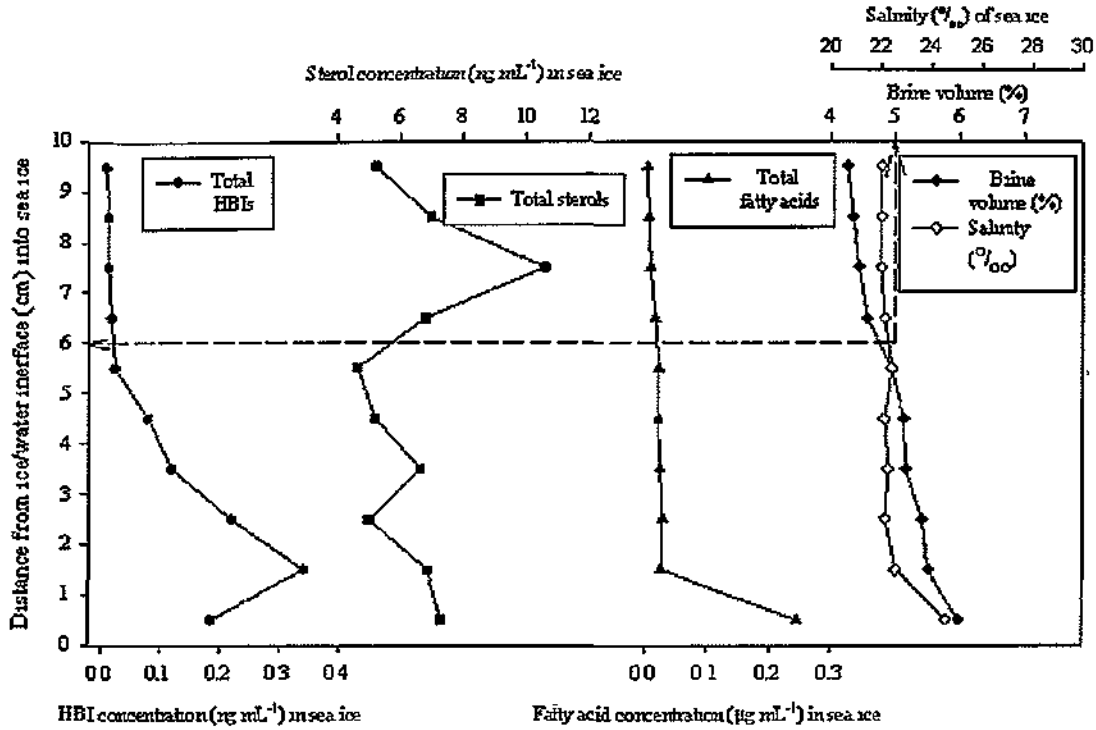

Figure 5.5-11. Vertical distribution of lipid biomarkers, salinity and brine volumes observed in the bottom 0 - 10 cm of high resolution sea ice cores during the IPY-CFL cruise (D38; 11/4/08). From left to right: Total HBI (**I, IIa, IIb, IIIa, IIIb, IIIc** and **IIId**) concentration Total sterol (**SII, SIII, SIV, SVI, SVII** and **SVIII**) concentration: Total fatty acid (**FI, FII, FIII, FIV** and **FV**) concentration: Salinity and brine volume. Vertical dashed line represents 5% brine volume Intersecting horizontal dashed line represents the 5% permeability threshold

5.5.4.2 Sterols in high resolution sea ice cores

Analysis (GC/MS) of the bottom 0 - 10 cm of sea ice cores, enabled observation of the sterol content of Arctic sea ice (Figure 5.5-11). Combined individual sterol (**SII, SIII, SIV, SVI, SVII** and **SVIII**) concentrations in the bottom 0 - 1 cm of sea ice, unlike D32, did not represent the greatest concentration within the core. At 0 – 1 cm, the total sterol concentration represented just 11% of the vertical distribution (10.6 ng mL^{-1}), while the average across all horizons was only 10% ± 6% Maximum sterol concentration, unlike other observed lipids, occurred at 7 – 8 cm (10.6 ng mL^{-1}; 16%). This observation was in contradiction of some biological habitation being restricted by

the permeability threshold, suggesting, like in D32, input of these particular lipids from varied alternative sources.

5.5.4.3 Fatty acids in high resolution sea ice cores

Determination of lipid concentrations (GC/MS) in the bottom 0 - 10 cm of sea ice cores also enabled observation of the fatty acid content within Arctic sea ice (Figure 5.5-11). The combined individual fatty acid (**FI, FII, FIII, FIV** and **FV**) concentration in the bottom 0 - 1 cm of sea ice, like D32, represented the greatest concentration and distribution within the core (24 $\mu g\ mL^{-1}$; 61%). Total fatty acids in the 0 – 1 cm horizon of D38 were over 750 times greater in concentration than in D32. Concentrations of fatty acids then rapidly declined in the next horizon (1 – 2 cm; 6.5%). Above this, the distribution was relatively constant (ca. 5% ± 1.7%) before further declining at 7 cm, reaching a minimum (3.4 $ng\ mL^{-1}$; < 1%) at 9 – 10 cm.

5.5.4.4 Vertical distribution of individual HBIs

Determination of the relative contributions of individual HBI isomers (Figure 5.5-12), showed **IIId, IIb** and **IIIb** to be most abundant, contributing ca. 28.6%, 27.5% and 25.8% respectively, of the cumulative combined HBIs in sea ice (1.03 $ng\ mL^{-1}$). While the mean concentrations of **IIId, IIb** and **IIIb** over 0 – 10 cm were consistent, exceptionally, the majority of **IIId** was actually distributed in only one horizon (1 – 2 cm; 59%). Consistent with observations for D32, the HBI, **I**, contributed 14% (14 pg mL^{-1}) to total HBI concentrations. Of the remaining HBIs, contributions were < 6% of the total concentration (**IIa**: 1.9%; **IIIa**: 1.4%; **IIIc**: 1.5%). In further agreement with D32, the presence of the proposed $\Delta^{7(20)}$ di-unsaturated HBI **IIc** was evident and

correlated exceptionally well to some HBIs (**IIIa, IIIb** and **IIId** r = > 0.79; p = < 0.001), and reasonably well with others (**I, IIa, IIb and IIIc** r = > 0.60; p = < 0.082).

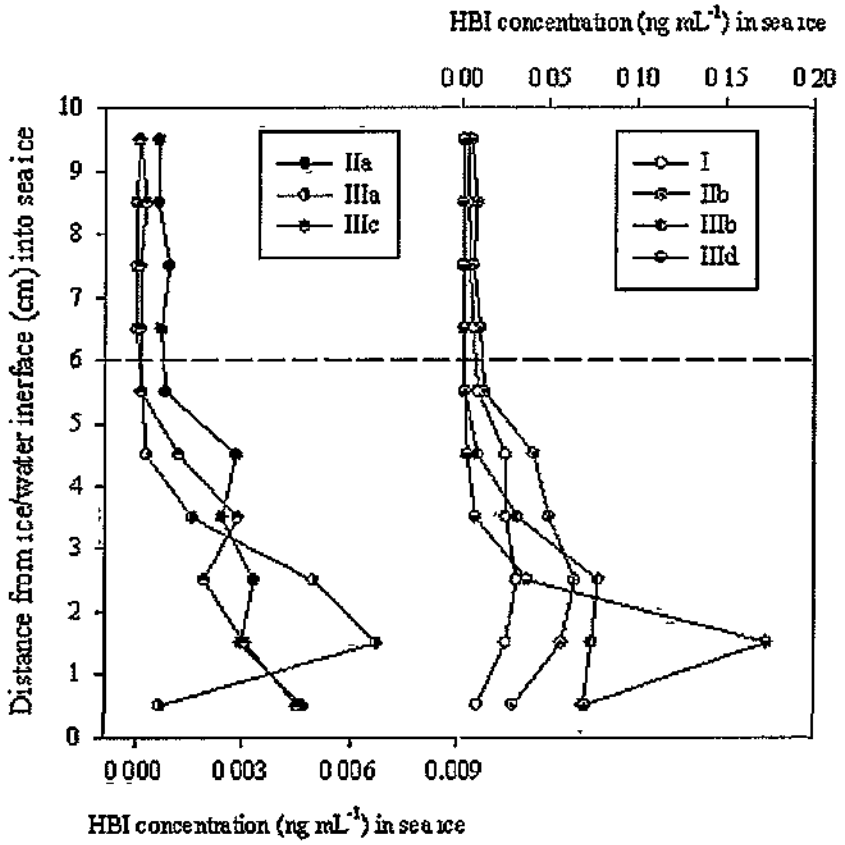

Figure 5.5-12. Vertical distribution of individual HBIs (**I, IIa, IIb, IIIa, IIIb, IIIc** and **IIId**) observed in the bottom 0 - 10 cm of high resolution sea ice cores during the IPY-CFL cruise (D38; 11/4/08). Dashed line represents the 5% permeability threshold.

Multivariate analysis of HBIs was carried out using PCA to classify isomers according to their primary source (e.g. sea ice diatom or plankton; Figure 5.5-13). The PCA model was robust, using 8 variables and 10 observations, with the first two PCs accounting for 88% of the variance in the data, enabling reliable representation on two axes. Interpretation of the PCA model suggested that all HBIs are related, in terms of production, with no clear distinction of grouping, unlike in D32.

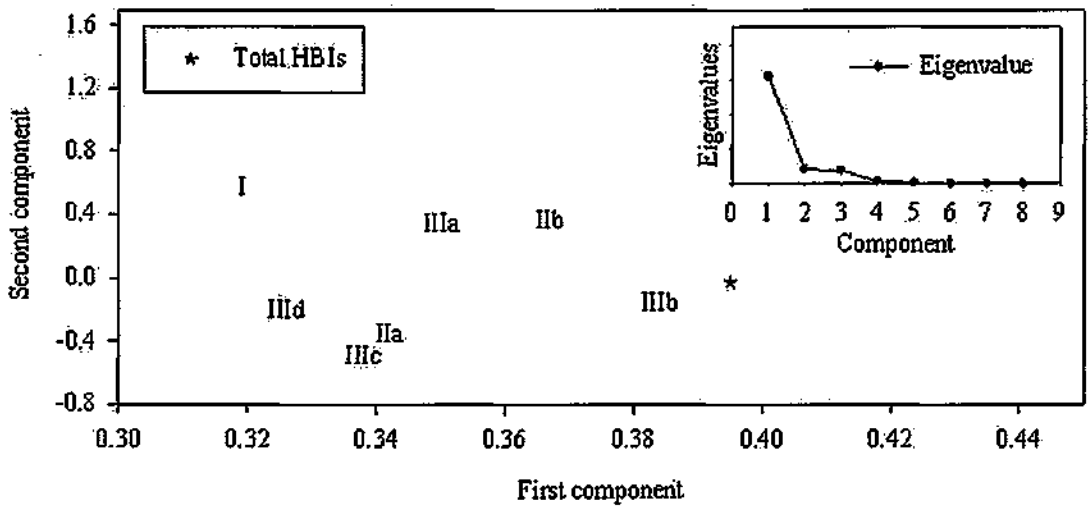

Figure 5.5-13. First and second component variable (loadings) plot of the principal components analysis for HBIs observed in the bottom 0 - 10 cm of high resolution sea ice cores during the IPY-CFL cruise (D38; 11/4/08). **I:IIa**: r = 0.62; p = < 0.057. **I:IIb**: r = 0.97; p = < 0.001. **I:IIIa**: r = 0.73; p = 0.017. **I:IIIb**: r = 0.65; p = < 0.044. **I:IIIc**: r = 0.50; p = < 0.14. **I:IIId**: r = 0.41; p = <0.24. Inset: Eigenvalue plot showing the proportion of variability accounted for by the first two components (88%).

5.5.5 Vertical distribution of individual sterols

Determination of the relative contributions of individual sterols (Figure 5.5-14) showed that the terrestrial sterol, β-sitosterol (**SVIII**), was most abundant, contributing ca. 63% of the total cumulative sterol concentration in sea ice (6.53 ng mL^{-1}). This was in contrast to D32 where the 'animal' sterol, cholesterol (**SII**) dominated. β-sitosterol (**SVIII**) was therefore responsible for most of the total sterol profile in D38, and was noted as being non-representative in terms of the distribution of all the sterols. The animal sterol **SII**, dominant in D32, instead represented 28% of the total concentration in D38. **SIII** (absent in D32) and **SIV** have comparably smaller contributions (4% and 1.4% respectively) and were, like the fatty acids, most abundant at the ice-water interface (0 – 1 cm).

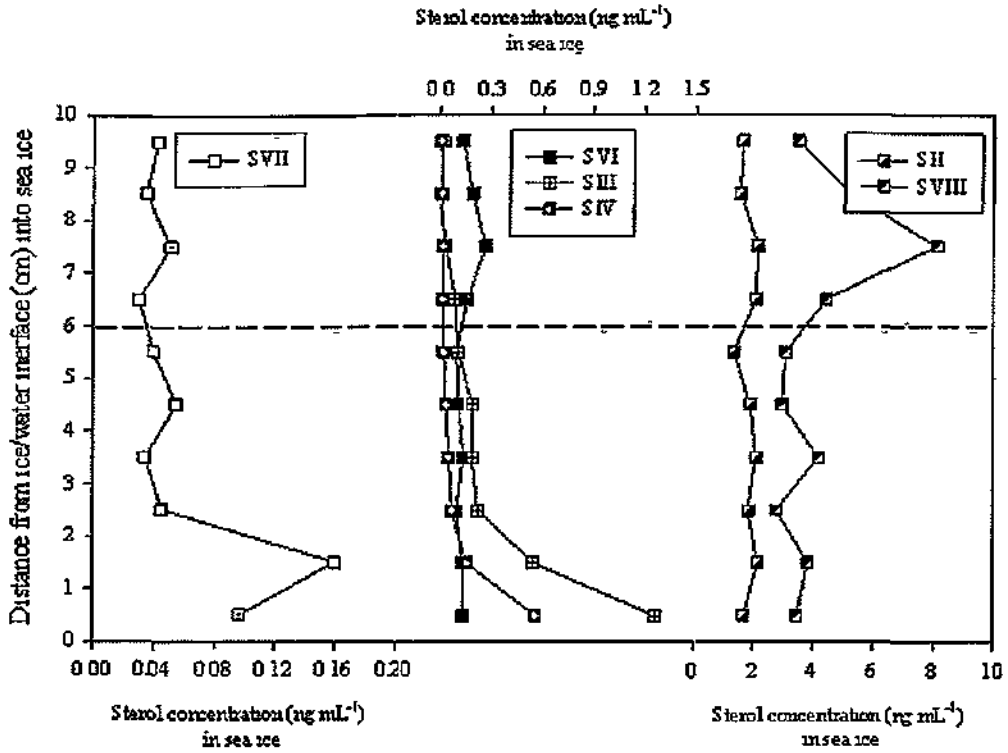

Figure 5.5-14. Vertical distribution of individual sterols (**SII, SIII, SIV, SVI, SVII** and **SVIII**) observed in the bottom 0 - 10 cm of high resolution sea ice cores during the IPY-CFL cruise (D38; 11/4/08). Dashed line represents the 5% permeability threshold

For multivariate analysis of sterols, PCA was used to classify compounds according to their primary source, e.g. marine, terrestrial or animal (Figure 5.5-15). The PCA model was relatively robust, using 10 variables and 10 observations, with the first two PCs accounting for 78% of the variance in the data, enabling reliable representation on two axes. Interpretation of the PCA model further exemplified the differences between sterols. **SI, SIII, SIV** and **SV** grouped tightly, representing marine algal sources. **SVI** and **SVIII** grouped together, representing terrestrial plant sources, while **SII** and **SVII** remained isolated in-between, representing combined sources. All sterols exhibited a poor correlation to HBI **I** ($r = < 0.52$).

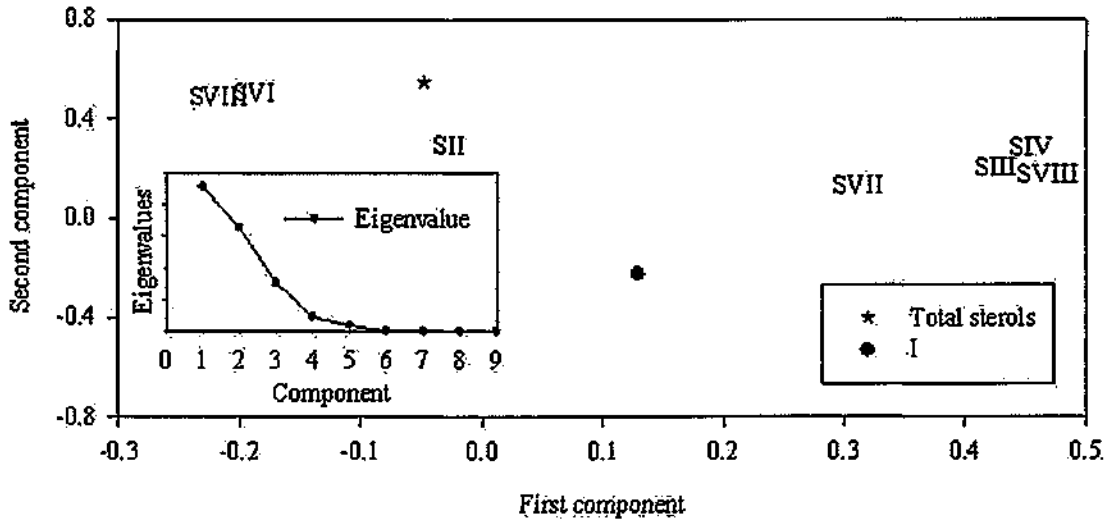

Figure 5.5-15. First and second component variable (loadings) plot of the principal components analysis for sterols observed in the bottom 0 - 10 cm of high resolution sea ice cores during the IPY-CFL cruise (D38; 11/4/08). **I:SII**: r = 0.37; p = 0.3. **I:SVII**: r = 0.30; p = 0.4. **I:SVIII**: r = -0.47; p = 0.2. **I:SVI**: r = -0.52; p = 0.1. **I:SI**: r = 0.21; p = 0.5. **I:SIII**: r = 0.14; p = 0.7. **I:SV**: r = -0.03; p = 0.9. **I:SIV**: r = 0.02; p = 0.9. Inset: Eigenvalue plot showing the proportion of variability accounted for by the first two components (78%).

5.5.5.1 Vertical distribution of individual fatty acids

Determination of the relative contributions of individual fatty acids (Figure 5.5-16), show the saturated compounds, **FI, FII** and the monounsaturated **FIII**, to be most abundant, contributing ca. 22%, 31% and 31% respectively, of the mean combined individual fatty acid concentrations in sea ice (40 ng mL^{-1}). The bacterial fatty acid, **FV**, and its saturated homologue, **FIV**, were less abundant (ca. 7% and 6% respectively). Overall, the combined fatty acids in D38 horizons were 4 times more concentrated than in D32. Like D32, the fatty acids observed in D38 followed the same distribution across horizons (r = > 0.91; p = < 0.001). Maximum concentration occurred at the ice-water interface and was followed by a steep decline, reaching minimum concentration at the upper 9 – 10 cm horizon in all cases. Additionally, the increased concentration of fatty acids in D38 permitted reliable determination of the carbon isotope composition ($\delta^{13}C$)

of **FI, FII** and **FIII.** At the outset it was expected that $\delta^{13}C$ values would be isotopically heavier where increased carbon fixation occurred as a result of preferential assimilation of ^{12}C over ^{13}C (Stein *et al.*, 2004). However, the measured $\delta^{13}C$ of fatty acids at the ice-water interface was surprisingly light ($\delta^{13}C$ = -20 6 ± 1.06 ‰) considering the greater concentration of fatty acids. This is potentially due to partial replenishment of the lighter ^{12}C from oceanic intrusion within the more porous bottom 0 – 1 cm of the ice. Further up within the ice, fatty acids became increasingly heavy (up to -18.2 ± 0.58 ‰), indicative of biosynthesis in a closed, or semi-closed environment, with limited ^{12}C replenishment (Stein *et al* , 2004). Above the 5% permeability threshold, at 6 – 7 cm in D38, the diatom fatty acids **FI, FII** and **FIII** were much lighter (up to -28.2 ‰) with regards to ^{13}C. This was probably due to the reduced biological demand in this region, resulting in less assimilation of carbon ^{12}C.

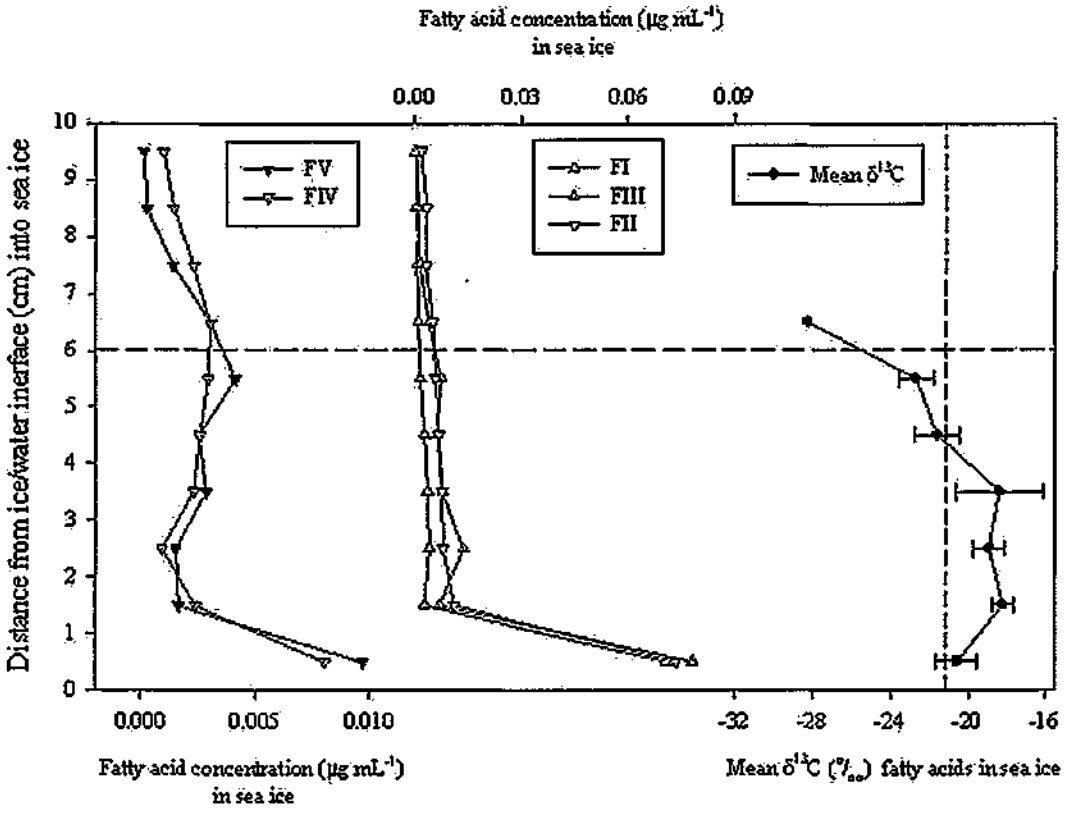

Figure 5.5-16. Vertical distribution of individual fatty acids (**FI, FII, FIII, FIV** and **FV**) and the mean $\delta^{13}C$ isotopic composition of **FI, FII** and **FIII** (± 1 s.d.; n =3) observed in the bottom 0 - 10 cm of high resolution sea ice cores during the IPY-CFL cruise (D38; 11/4/08). Vertical dashed line represents mean $\delta^{13}C$. Horizontal dashed line represents the 5% permeability threshold.

Multivariate classification of fatty acids was carried out using PCA to determine the primary source of these compounds (e.g. sea ice diatom or plankton; Figure 5.5-17). The PCA model was robust, using 7 variables and 10 observations, with the first two PCs accounting for 97% of the variance in the data, enabling reliable representation on two axes. Interpretation of the PCA model in comparison to that of D32 (Figure 5.5-9) showed a reduced difference between **FIV** and the remaining fatty acids, while confirming the poor correlation of all fatty acids to HBI **I** ($r = < -0.02$; $p = < 0.96$).

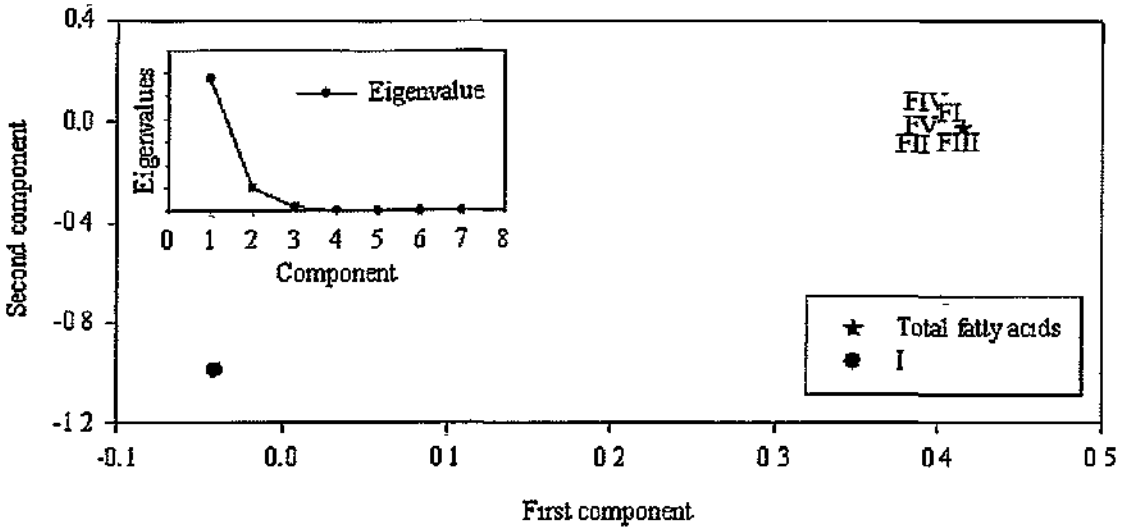

Figure 5.5-17 First and second component variable (loadings) plot of the principal components analysis for fatty acids observed in the bottom 0 - 10 cm of high resolution sea ice cores during the IPY-CFL cruise (D38; 11/4/08). **I:FIV**: r = -0.18; p = 0.63. **I:FIII**. r = -0.02; p = 0.96. **I:FI**· r = -0.11; p = 0.76. **I:FII**: r = -0.06; p = 0 96. **I-FV**· r = -0.04; p = 0.91. Inset: Eigenvalue plot showing the proportion of variability accounted for by the first two components (97%).

5.5.5.2 Comparison of sea ice lipid biomarkers

In a manner analogous to that performed on the data for core D32, additional PCA was carried out on HBIs, fatty acids and sterols in D38 to characterise each class of lipid, relative to one another, in addition to investigating the potential range of sources of HBIs **IIa, IIb, IIIa, IIIb, IIIc** and **IIId**. The PCA model was relatively robust, although, with 17 variables used for only 10 observations, sufficient variation was not accounted for in the first two PCs. Given the number of variables, it was felt that representation on three axes (accounting for 91% of the variation) would provide better interpretation (Figure 5.5-18). Distinct grouping was evident in both the sterols and fatty acids, with vertical spread reflecting variation within each group Distinct grouping was also evident within the short chain fatty acids and marine sterols (**SI, SIII, SIV** and **SV**), and was better resolved than in D32 due to the increased concentrations. Significant variation was again observed in the animal sterol, cholesterol (**SII**), in

addition to the terrestrial plant sterols, **SVI**, **SVII** and **SVIII**. Interpretation of the three dimensional projection of HBIs was complex, consistent with D32. While the distribution of HBIs reflected that seen previously in two dimensions, the lack of clear grouping as a class of compounds was still suggestive of slightly different inputs from one another. While stable isotope analysis ($\delta^{13}C$) is a valuable tool in differentiating between the potential sources of lipids, the relatively small sample volume in these high resolution samples rendered this approach impractical for the HBIs.

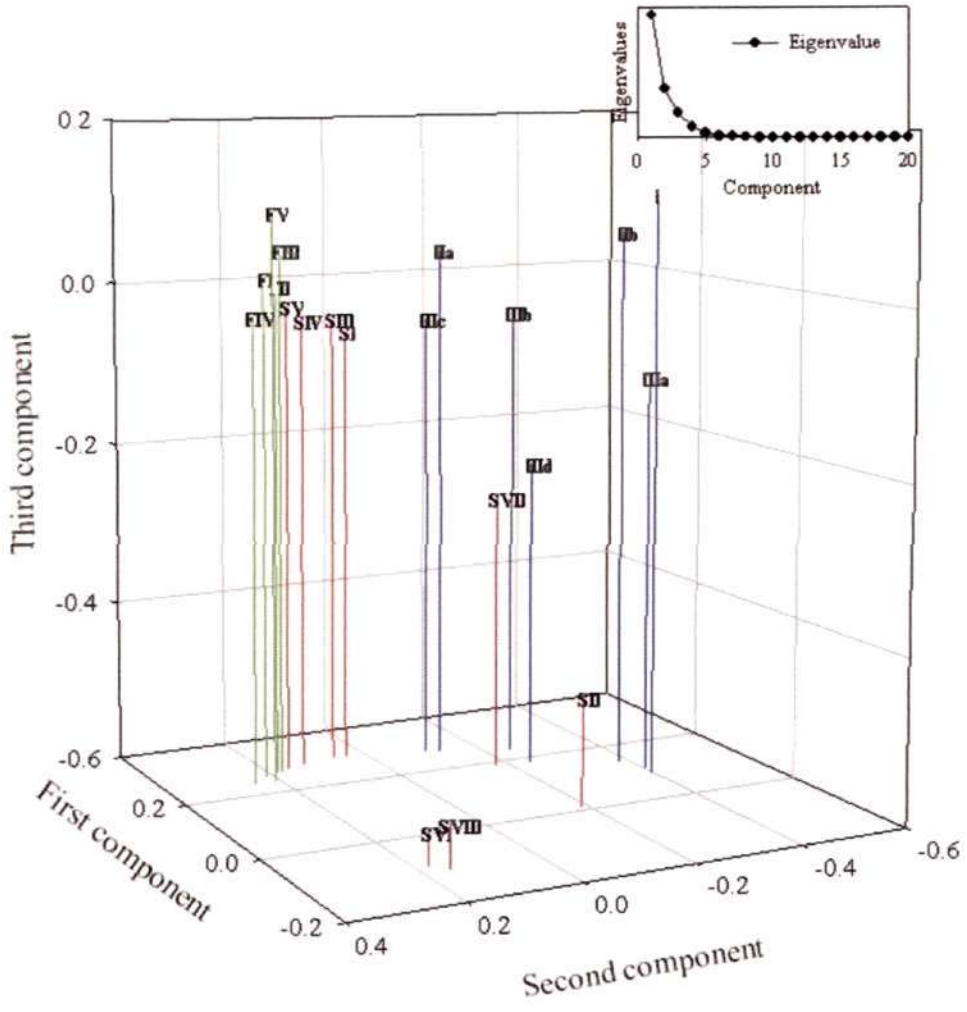

Figure 5.5-18. First, second and third component variable (loadings) plot of the principal components analysis for biomarkers observed in the bottom 0 - 10 cm of high resolution sea ice cores during the IPY-CFL cruise (D38; 11/4/08). Proximity of compounds in three dimensions is a function of covariance. Red = sterols (**SI** to **SVIII**), green = Fatty acids (**FI** to **FV**), blue = HBIs (**I** to **IIId**). Inset: Eigenvalue plot showing the proportion of variability accounted for by the first three components (91%).

5.5.6 Comparison of lipid biomarkers in D32 and D38 ice cores

5.5.6.1 Total lipid biomarker concentrations

Subtle variations in lipid distribution in high resolution sea ice cores, collected early in the Arctic sea ice algal bloom (D32; 22/3/08) and midway through the bloom (D38; 12/4/08), were evident (Figure 5.5-19). All lipid classes experienced significant enhancement through the sea ice algal bloom, with HBIs showing the largest (relative) increase. Total cumulative HBIs increased from 6.0 pg mL^{-1} in D32 to 103 pg mL^{-1} in D38, an increase of almost 2000%. Total cumulative sterols also increased from 0.61 ng mL^{-1} in D32 to 6.52 ng mL^{-1} in D38, an increase of over 1000%. Fatty acids showed the least increase, from 11 ng mL^{-1} in D32, to 40 ng mL^{-1} in D38, an increase of just under 400%.

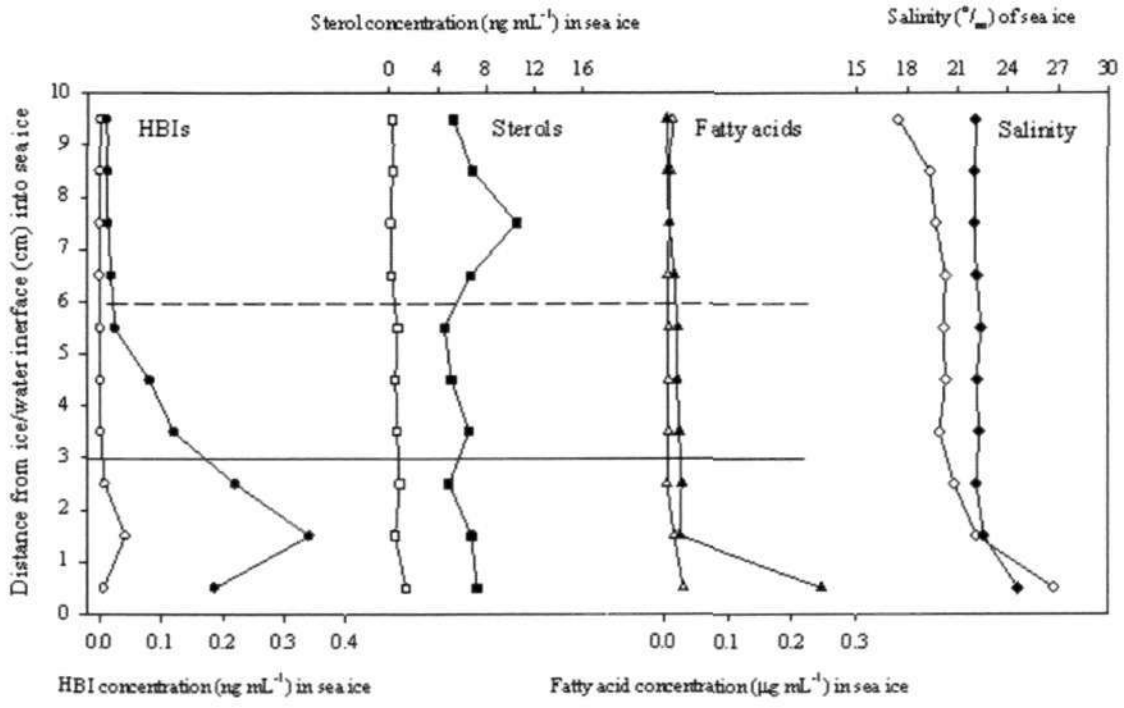

Figure 5.5-19. Comparison of the vertical distribution of lipid biomarkers and salinity observed in the bottom 0 - 10 cm of high resolution sea ice cores during the IPY-CFL cruise (D32; 22/3/08 (white) and D38; 11/4/08 (black)). From left to right: Total HBI (**I**, **IIa**, **IIb**, **IIIa**, **IIIb**, **IIIc** and **IIId**) concentration: Total sterol (**SII**, **SIII**, **SIV**, **SVI**, **SVII** and **SVIII**) concentration: Total fatty acid (**FI**, **FII**, **FIII**, **FIV** and **FV**) concentration: Salinity. Solid and dashed lines represent the 5% permeability threshold of D32 and D38 respectively.

5.5.6.2 Changes in the distribution of HBIs through time

In addition to general increases in concentration, HBIs, unlike fatty acids and sterols, experienced a significant spread of internal distribution between the two sea ice cores (Figure 5.5-20). In the earlier sea ice core (D32), maximum concentration of HBIs occurred in the 1 – 2 cm horizon in all isomers, except **IIIa**, which was most abundant at 0 – 1 cm, with a gradual decline in concentration further up the core. For all isomers, except **IIIa**, 90% of the concentration distribution was accounted for in the lower 3 cm, or within the 5% permeability threshold. In contrast, 90% of **IIIa** was distributed over the bottom 0 – 8 cm region.

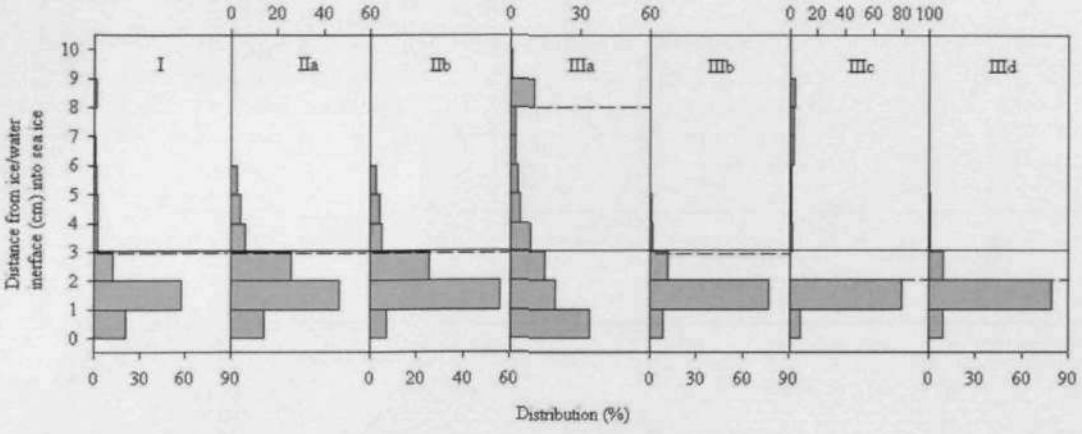

Figure 5.5-20. Comparison of % vertical distribution of individual HBIs (Left to right - **I**, **IIa**, **IIb**, **IIIa**, **IIIb**, **IIIc** and **IIId**) observed in the bottom 0 - 10 cm of high resolution sea ice cores from D32 (22/3/08) during the IPY-CFL cruise. Solid line represents the 5% permeability threshold. Dashed lines represent the upper limit of the region of ice that contains 90% HBI distribution.

In the later sea ice core (D38), the distribution of HBI concentrations within the core also varied greatly between each isomer (Figure 5.5-21). The distribution of each isomer, accounting for 90% of the concentration, either occurred in the region from the ice-water interface, up to the permeability threshold (**I**, **IIa** and **IIb**), or within a narrower range and below the permeability threshold (**IIIa**, **IIIb**, **IIIc** and **IIId**).

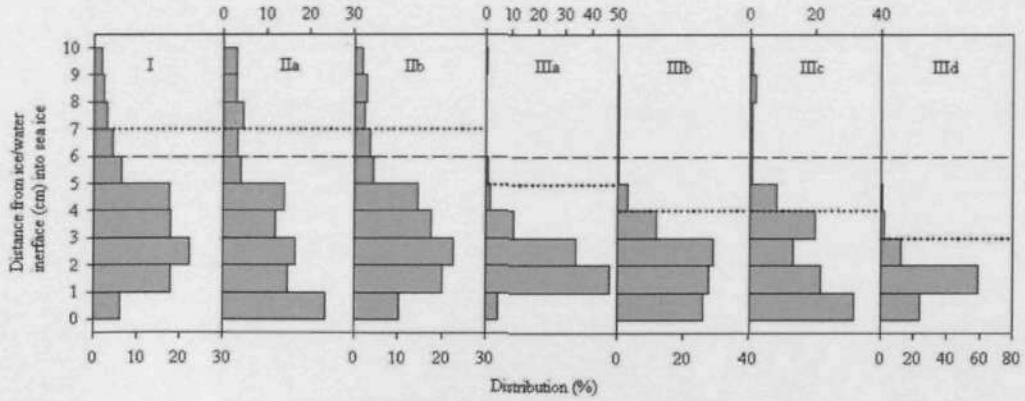

Figure 5.5-21. Comparison of % vertical distribution of individual HBIs (Left to right - **I**, **IIa**, **IIb**, **IIIa**, **IIIb**, **IIIc** and **IIId**) observed in the bottom 0 - 10 cm of high resolution sea ice cores from D38 (12/4/08) during the IPY-CFL cruise. Dashed line represents the 5% permeability threshold. Dotted lines represent the upper limit of the region of ice that contains 90% HBI distribution.

Following the melting of snow and early decay of sea ice, the downward percolation of melt-water can result in considerable widening of the brine channel network (Eicken *et al.*, 2002; Perovich *et al.*, 2003), resulting in considerable upward migration of the permeability threshold. Given the consistent correlation in both D32 and D38 between **I, IIa, IIb** and the permeability threshold, one might predict that the occurrence of these and other HBIs could extend vertically to any region, within sea ice, so long as the permeability of the ice, in addition to other chemical and physical parameters, were sufficient for biological inhabitation.

5.5.7 HBI concentrations in Arctic sea ice melt ponds

Determination of the combined individual HBI concentrations in melt ponds revealed very low concentrations (< 2.2 pg mL^{-1}) compared to those observed in D32 and D38 (ca. 300% and 4500% less, respectively). Samples 1 and 2 yielded similar relative distributions of HBIs **I** and **IIb**, with sample 1 containing an equal proportion of **IIId** to **I** and **IIb** (Figure 5.5-22). In contrast, melt pond sample 3 was dominated by HBI **I** (76%).

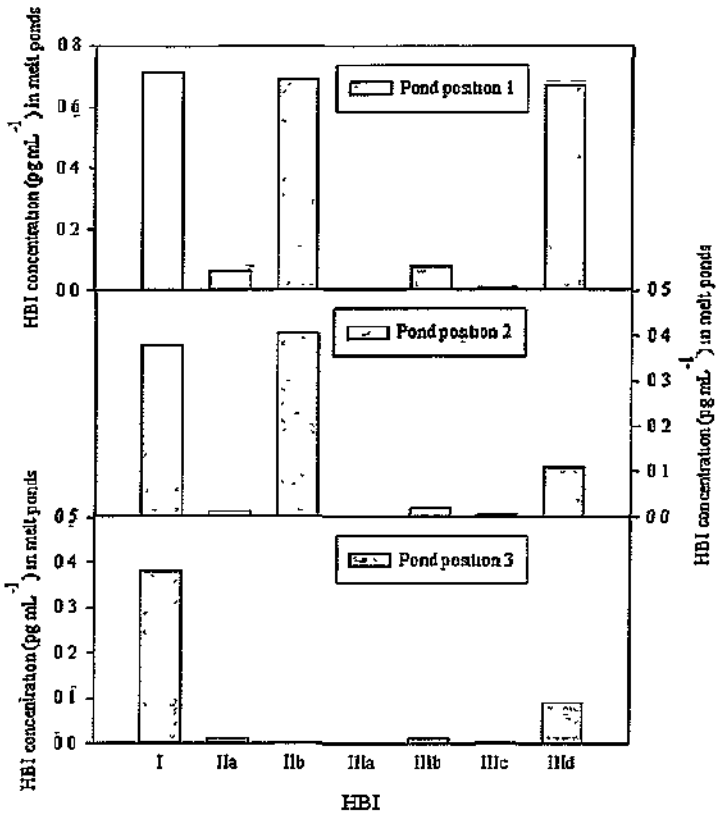

Figure 5.5-22. HBI concentration of meltpond samples, collected early in the Arctic summer (FB06· 20/6/08), during the IPY-CFL cruise.

In summary, analysis of HBIs, fatty acids and sterols over two high resolution sea ice cores established a significant dependence of lipid distribution on sea ice salinity and temperature. In addition, this derived, upper permeability limit of sea ice algae habitation was observed to extend upwards in correlation to the advancing spring bloom Interpretation of fatty acid and sterol biomarkers provided the basis of a proposed tiered sea ice habitat model (Figure 5.6-1)

5.6 Discussion

5.6.1 Vertical distribution of lipids in sea ice cores

In order to investigate the sources of IP_{25} and other HBIs in sea ice, a multiproxy biomarker approach was adopted using the established fatty acid and sterol biomarkers in two high resolution sea ice cores. Evidence for variation in the vertical distribution of lipids was first detected in coarse resolution sea ice cores, with typically more than 70% of the distribution of I occurring in the 0 – 5 cm (from the ice-water interface) section, while the 5 - 10 cm section yielded less than 30% (Figure 5.5-1). Determination of the relative (%) brine volume (Cox *et al.*, 1983; Golden *et al.*, 2007) over these horizons, provided justification for this significant bias in distribution, with increases in brine volume reflecting increased concentrations of I.

Further, more detailed, investigation on high resolution (1 cm horizons) sea ice cores, revealed significant variation in lipid distributions. From the data gathered, three, quite distinct, mechanisms through which lipids may become incorporated into the sea ice matrix are proposed (Figure 5.6-1).

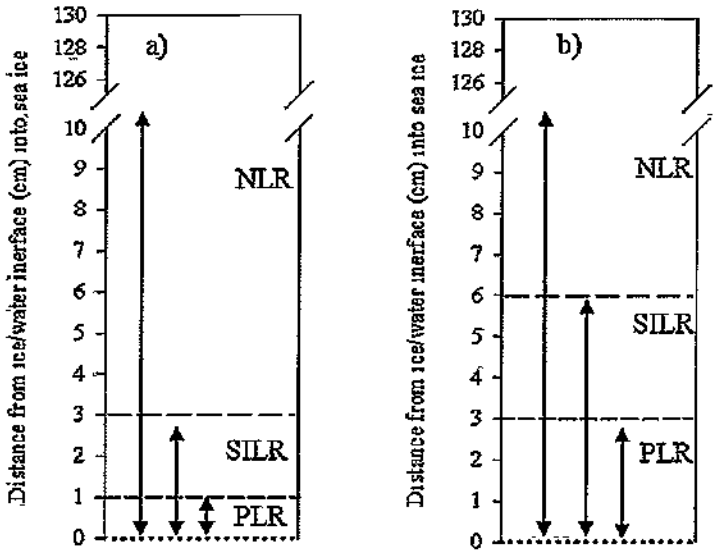

Figure 5 6-1. Schematic representation of observed early (a; D32) and mid bloom (b; D32) lipid distribution in the bottom 0 - 10 cm of Arctic sea ice cores collected during the IPY-CFL cruise. Dotted lines represent the ice-water interface. Short-dashed lines represent the upper limit of planktonic lipid distribution (Planktonic lipid region - PLR), while the long-dashed lines mark the upper limit of sea ice lipid distribution (Sea ice lipid region - SILR). While nonspecific lipids are distributed throughout (Non-specific lipid region - NLR).

5.6.2 Zonation of sea ice lipid incorporation

For the purpose of attempting to classify the sources of the various HBIs discussed in this study it was convenient to consider the ice as being divided into three regions As such, the results are presented according to the ability of each lipid to fit within one, or more, of three hypothetical sea ice regions.

i The planktonic-lipid-region (PLR), defined as the lower, porous region of sea ice that is characterised by the inclusion of lipids that appear unaffected by changes in the vertical permeability of sea ice.

ii. The sea-ice-lipid-region (SILR), defined as the vertical extension of the lower porous region of sea ice that has an apparent upper limit that is strongly influenced by changes in sea ice permeability above 5% brine volume.

iii. The non-specific-lipid-region (NSL) is, by definition non-specific and is characterised by lipids that show no distinct region of enhancement or depletion throughout the sea ice.

Identification of lipids considered characteristic of each region within sea ice is hypothesised to indicate the source of lipids, based on regions of significant enhancement. For example, the maximum concentration of lipids in the 0 – 1 cm horizon may be indicative of planktonic input from the water column. However, it is important to consider species specific production and their associated distribution within sea ice.

5.6.3 The Planktonic-Lipid-Region (PLR)

Variation in the distributions of some lipids in high resolution sea ice cores, collected both early in the Arctic sea ice algal bloom (D32; 22/3/08) and midway through the bloom (D38; 12/4/08), revealed distinct differences regarding the maximum concentration of some individual lipids. While the comparatively low temperature and salinity in the earlier sea ice core (D32) resulted in restricted vertical pore connectivity (above 0 – 3 cm), slight increases in temperature (ca. + 0.8°C) and salinity significantly extended the pore network in D38 to ca. 0 - 7 cm, from the ice-water interface. Irrespective of the marked increase in habitable area (Manes *et al.*, 2009), the distribution of some lipids, notably the fatty acids (**FI, FII, FIII, FIV** and **V**) and some sterols (**SI, SIII, SIV** and **SV**), remained virtually unchanged, both up-core and between cores. Further, maximum concentrations of these lipids continued to occur at the ice-

water interface (0 – 1 cm) in both cores. The vertical distribution of these widely produced lipids supports their substantial epontic and planktonic origins, proposed in the previous chapter. Furthermore, the vertical $\delta^{13}C$ isotope composition of fatty acids was indicative of carbon replenishment at the porous ice-water interface ($\delta^{13}C$ = -20 6 ± 1.1‰), compared to further up within the ice (1 – 2 cm, $\delta^{13}C$ = -18 2 ± 0.5‰), providing further evidence of the planktonic source of some lipids. Enhancement of the maximum occurrence of the ubiquitous epontic Arctic diatom, *Fragilariopsis cylindrus* (Grunow), in the bottom few millimetres in a similar high resolution study of cell distributions in sea ice produced similar conclusions (Mock *et al*, 2003) By culturing *F cylindrus* in artificial sea ice in the laboratory, Mock and co-workers recorded the greatest concentrations of chlorophyll *a* at the ice water interface (0 – 1 cm) with almost a 50% reduction in values within the adjacent 1 – 2 cm horizon. In further agreement with a PLR assignment, chlorophyll *a* concentrations were undetected for 5 – 10 cm in sea ice sampled during the early part of the IPY-CFL cruise.

In the early sea ice core (D32), **IIIa** was the only HBI isomer in agreement with this PLR distribution. In contrast, during the early bloom (D38), **IIa, IIIb** and **IIIc** all exhibited bottom enhancement, although **IIa** was the only one of these isomers to spread vertically to occupy all available habitat within the 5% permeability threshold. Conversely, none of the tri-unsaturated HBIs (**IIIa, IIIb, IIIc** and **IIId**) appeared, in significant concentration, to reach the upper limit of ice core pore permeability. The distribution of these tri-unsaturated HBIs was highly suggestive of their likely predominant planktonic production

5.6.4 The Sea-Ice-Lipid-Region (SILR)

In contrast to the distribution of lipids in the PLR, the HBIs **I** and **IIb** were not only distributed such that maximum concentration occurred away from the ice-water interface (at 2 – 3 cm), but that their significant internal distributions (90%) extended to the upper limit of ice core pore permeability in both cores. The presence of **I** and **IIb** throughout the entire region from the ice water interface to the 5% permeability threshold (D32; 0 – 3 cm, D38; 0 – 7 cm) was indicative of production within the sea ice, restricted by the brine channel connectivity. Of all the lipids analysed in sea ice, these two HBIs were the only ones that appeared to be particularly characteristic of internal sea ice production within the SILR. Furthermore, the relatively heavy $\delta^{13}C$ isotopic compositions observed in the fatty acids within the sea ice (1 – 4 cm; $\delta^{13}C$ -19.3 ±1.6‰; D38) support the internal depletion of ^{12}C that is considered indicative of carbon assimilation related to primary production in sea ice (Stein *et al.*, 2004). It is, however, noted that, despite the bottom enhancement (0 – 1 cm) of **IIa**, characteristic of the PLR, this HBI also extended well into the sea ice matrix in D38, providing strong evidence for both sea ice (SILR) and planktonic (epontic) biosynthesis. The suggested dual-source of **IIa** was further reflected in positive correlations with the characteristic PLR tri-unsaturated HBIs (**IIIb** $r = 0.86$; $p = < 0.002$ and **IIIc** $r = 0.92$; $p = < 0.001$) in addition to HBI **I** ($r = 0.75$; $p = < 0.001$).

The repeated appearance of the putative $\Delta^{7(20)}$ di-unsaturated HBI **IIc**, was again noted to correlate extremely well with all HBIs in the early, D32 core, while a specific association of **IIc** with the planktonic, tri-unsaturated HBIs in the later core, strengthened the assumption that this HBI may be produced by *Pleurosigma* spp. diatoms (e.g. Belt *et al.*, 2000a; Belt *et al.*, 2001a; Massé *et al.*, 2004a) whose lipids would be expected to present a PLR distribution.

Analysis (GC/MS) of large volumes (4 L) of sea ice surface material (combination of unconsolidated ice crystals and brine channel water) from meltponds also revealed the presence of HBIs **I** and **IIb** (< 0.72 pg mL^{-1} and < 0.69 pg mL^{-1} respectively), where they accounted for 64% - 85% of the HBIs present on the surface of the ice matrix The extremely low concentrations are a potential indication of the presence of HBI producing diatoms during sea ice formation, becoming entrapped in flocculating ice crystals. Detection of these lipids also demonstrates the potential presence of these compounds, in very low concentration, throughout the entire sea ice sheet.

5.6.5 The Nonspecific-Lipid-Region (NLR)

Some lipids (**SII, SVI, SVII** and **SVIII**) were found to be present throughout all sea ice core horizons, in some cases reaching maximum concentration above the 5% permeability threshold (e.g. **SVI** and **SVIII**). In contrast to PLR and SILR lipids, the diversity in sources of these sterols was supported by their ubiquitous presence and varied distributions in the sea ice cores Numerous studies have accounted for significant incorporation of terrigenous organic carbon within drifting sea ice, especially from shallow coastal regions (Stein *et al.*, 2004 and references therein), with additional consideration of aeolian and riverine lipid input also being important The presence of *n*-alkanes (Figure 4.5-18) with distinctive terrestrial stable carbon isotope signatures observed in this study further support this

5.6.6 Lipid biomarker covariance in sea ice

To better realise any potential covariance between HBIs, fatty acids and sterols, PCA was used to transform the concentration data into a smaller, more manageable coordinate set of data.

The low concentration and narrow vertical distribution of lipids in the early D32 sea ice core reduced the potential for reliable spatial projection of compounds in the PCA model (Figure 5.5-5, Figure 5.5-7 and Figure 5.5-9). The distinctly different vertical distributions of **IIIa** and **SII** are, however, reflected in the respective HBI and sterol PCA projections, while the fatty acid and sterol projections demonstrate further the reduced association of these lipids to the sea ice HBI, **I**.

Consideration of the correlation coefficients in association with the 2 dimensional PCA projection, aided in the interpretation of assigning some HBI sources (Figure 5.5-13). The HBIs **I**:**IIb** correlated well ($r = 0.96$; $p = < 0.001$), providing further evidence for the co-production of these two HBIs in sea ice diatoms. Conversely, the planktonic and epontic biosynthesis of the tri-unsaturated HBIs (**IIIa**, **IIIb**, **IIIc** and **IIId**) was reflected in less significant correlations to **I**, while the high p values indicate a significant probability of a false correlation being detected. The potential of poor HBI correlations being a result of the reliability of the PCA model is rejected following analysis of the fatty acids and sterols. Both fatty acids and sterols were found to respond as expected in the PCA with reasonably clear distinctions being possible regarding significant differences in abundant isomers, such as the animal (**SII**) and terrestrial sterols (**SVIII**).

While the similar sources of fatty acid production found in sea ice are again evident in D38 (Figure 5.5-17), the varied range of sterol sources is also further indicated (Figure

5 5-15) with the marine phytosterols (**SI, SIII, SIV** and **SV**) grouped independently of the animal (**SII**) and terrestrial sterols (**SVI, SVII** and **SVIII**). These provide further evidence of the reliability of the PCA projections for interpretation of HBI sources

5.7 Conclusion

The distributions of HBIs, fatty acids and sterols in two different high resolution (1 cm; 0 – 10 cm) sea ice cores has provided further evidence for the determination of the respective sources of these chemicals. In particular, the characteristically variable concentration of these lipids has facilitated the proposed classification of the biomarkers used in this study into three spatial groups:

- Planktonic-lipid-region (PLR): Region of Arctic sea ice extending from the permeable ice-water interface to the point within the ice that planktonic infiltration ceases. Characteristic lipids include the fatty acids and tri-unsaturated HBIs (**IIIa, IIIb, IIIc** and **IIId**).
- Sea-ice-lipid-region (SILR): Region of Arctic sea ice extending from close to the ice-water interface, to the upper limit of pore permeability, (defined as 5% brine volume). Characteristic lipids include the HBI **I** and **IIb**.
- Nonspecific-lipid-region (NLR): Entire region within the ice, from the ice-water interface to the ice-snow interface. Characteristic lipids include the terrestrial sterols (**SVI, SVII** and **SVIII**)

The distribution in sea ice of some lipids prevented confident allocation into a single region. The di-unsaturated HBI **IIa** for example, exhibited significant concentration at the ice-water interface, characteristic of PLR, yet was present up to the pore permeability threshold indicative of the SILR.

The proposed source assignment for these lipids in Arctic sea ice further isolates **I** as a distinctive sea ice biomarker, while exposing the reduced specificity of the fatty acids and sterols as biomarkers.

CHAPTER SIX

6 IP_{25} and other HBIs in the water column and macrobenthos of the Amundsen Gulf

6.1 Introduction

Chapter six describes a preliminary investigation into some processes that may influence the transfer of IP_{25} and other HBIs from Arctic sea ice into the underlying marine sediments in the Amundsen Gulf region of the CAA. In particular, implications of the presence of IP_{25} and numerous other HBIs in the lipids of a suite of micro- and macroscopic plankton and a variety of benthic organisms are discussed.

Interpretations of the presence of IP_{25} in sediments as a sea ice proxy necessitates a better understanding of the physical and biological processes capable of influencing its distribution. Consideration of (amongst other things) diatom transport from sea ice, through the water column is therefore crucial. Since the majority of previous studies that attempt to determine some of the complex processes involved are few and focus mainly on the Antarctic, these are included alongside investigations from the Arctic (where possible), to illustrate potential considerations for the transport of lipids from Arctic sea ice. An overview of the most commonly cited mechanisms for particle transport is also described here.

Primary production in many regions of the Arctic, including the CAA, is influenced by seasonal environmental changes such as ocean currents, photosynthetically active radiation (PAR), sea ice cover, temperature and salinity (e.g. Neal *et al.*, 1969; Stein *et*

al, 2004; Dunton *et al.*, 2005; Mundy *et al.*, 2009; Dieckmann *et al*, 2010). The southeast Canadian Beaufort Sea and Amundsen Gulf are considered oligotrophic (Boetius *et al.*, 1998; Mundy *et al*, 2009). It is estimated that phytoplankton provides more than 90% of the total primary production, with growth of sea ice algae only being significant during a short period in the spring (Hill *et al*, 2005). Hill and Cota (2005) observed primary production rates of less than 0.3 g C m^{-2} d^{-1} associated with ice cover, while values of up to 8 g C m^{-2} d^{-1} were recorded during sea ice break up (Sukhanova *et al*, 2009). Similarly, Arrigo and van Dijken (2004) used remote sensing (SeaWIFS) to determine mean annual carbon production in the Cape Bathurst region of the Amundsen Gulf of 90 to 175 g C m^{-2} yr^{-1} for the period 1998 to 2002. Forest and co-workers (2009) also determined the quantity of carbon production that reached the lower water column in the Amundsen Gulf (ca. 6 g C m^{-2} yr^{-1} at 100 m and 3.3 g C m^{-2} yr^{-1} at 210 m), estimating that ca. 75% of the carbon flux was present at 100 m, while just 55% of the surface carbon production was present at 210 m. This significant removal of carbon from vertical export in the pelagic environment is thought to reflect the retention and export of carbon in Arctic food chains (Wassmann, 1998) One mechanism responsible for some of this decline in carbon flux is grazing Significant grazing of algae is known to occur throughout the year, with copepod grazing responsible for the removal of up to ca. 30% of the phytoplankton production in Lancaster Sound (CAA) (Welch *et al*, 1992). Indeed, pelagic-benthic coupling is also evident from analysis of the carbon isotope composition of some copepod faecal pellets collected from 13 stations in the Barents Sea (Tamelander *et al*, 2008) The marginal ice zone signal ($\delta^{13}C$ = -21‰) recorded in some faecal pellets reflected enrichment of ^{13}C in comparison to the mean composition ($\delta^{13}C$ = -25.4‰) recorded in particulate organic carbon (Tamelander *et al.*, 2008). A similar difference was also recorded for organic matter obtained from sediment traps collected in Prydz Bay, East Antarctica with $\delta^{13}C$ of -15‰ and -20‰

respectively (Gibson *et al.*, 1999). These relatively few findings suggest that copepods are capable of grazing primarily on the abundant autotrophic biomass during peak bloom phase, thus demonstrating the episodic nature of Arctic carbon flux (Wassmann *et al.*, 1996).

Understanding the concept of particle transport from sea ice is critical to the application of IP_{25} as a useful tool in sediment core analysis, where the vertical transport of particles could influence the sedimentary distribution of the biomarker. Current knowledge of particle transport originates largely from sediment trap experiments (Gersonde *et al.*, 2002; Leventer, 2003; O'Brien *et al.*, 2006). In the Arctic O'Brien *et al.* used this approach to determine the primary sources of sediment flux in the Beaufort Sea; marine biological production; the Mackenzie River Plume; coastal and seabed erosion. A further study on the vertical transport of *Haslea* spp. diatoms by Brown (2007) involved the analysis of both IP_{25} and *Haslea* spp. diatom cells from an under-ice sediment trap (ArcticNet, 2005) where it was observed that both IP_{25} and *Haslea* spp. diatom cells reached maximum concentrations coincident with both each other and the timing of sea ice melt. This observation helped confirm the origin of *Haslea* spp. and IP_{25} in sea ice and ultimately, the mechanism of their transport from the sea ice (vertical sedimentation). In other studies vertical transport has been proposed to be responsible for up to 50% (Smith *et al.*, 1986), 60% (Legendre *et al.*, 1992), or more (Arrigo *et al.*, 2010) of carbon flux to the benthos in ice covered waters.

Water depths in the Amundsen Gulf typically range from 60 - 500 m. As such the potential for descending particles, including diatoms, to undergo dispersion and lateral transport is considerable. Although cells of sea ice endemic diatoms (e.g. *Haslea* spp.) potentially responsible for biosynthesis of IP_{25} are generally quite large (ca. 100 x 15

μm; Figure 6.1-1) compared to other abundant sea ice diatoms (e.g. *Fragilariopsis cylindrus*. ca. 10 x 2 μm; Figure 6.1-2), their microscopic size exposes them to a number of biotic and abiotic influences in the passage from sea ice to sediments (e.g. zooplankton grazing and ocean currents).

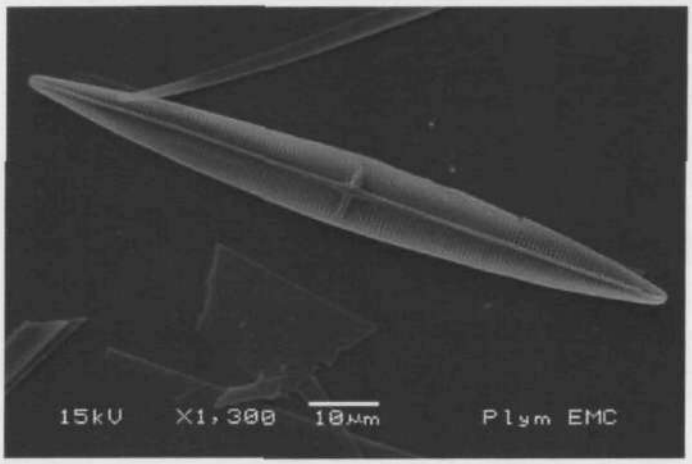

Figure 6.1-1. Scanning electron micrograph of *Haslea crucigeroides* and diatom fragments isolated from sediment trap CA20 during the ArcticNet cruise 2005 (Brown, 2007).

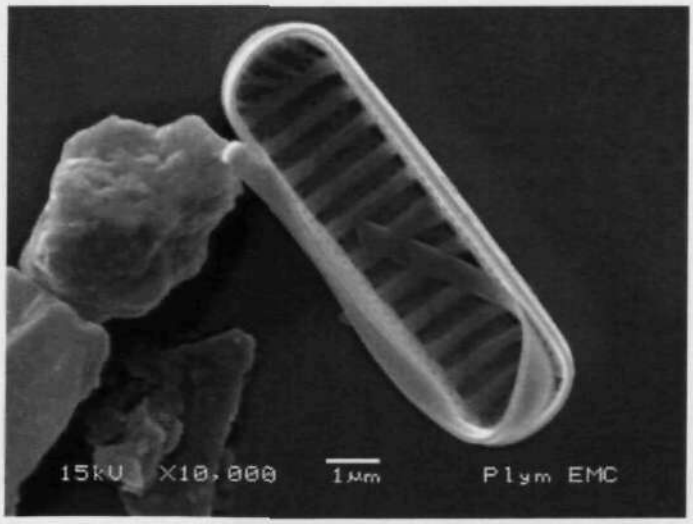

Figure 6.1-2. Scanning electron micrograph of *Fragilariopsis cylindrus* and sediment grains isolated from sediment trap CA20 during the ArcticNet cruise 2005 (Brown, 2007).

The general ballasting effect of senescent diatom cells is predicted, by Stokes's Law, to generate insufficient velocities to enable regionally representative sedimentation (Waite *et al.*, 1997). Stokes's Law states that particles falling under their own mass will achieve a terminal velocity in viscous fluid when frictional and buoyant forces balance gravitational force (Batchelor, 2000). Since Arctic sea water has a mean specific density of 1.026 g cm^{-3} (Kogeler *et al.*, 1987), the greater density of biogenic diatom silica (ca. 2-2.5 g cm^{-3} (Mackenzie, 2005; Brown, 2007)) is suggestive of sinking rates capable of providing sufficient export to the sediments to enable accumulation of cells. However, the density of intact cells of *H. crucigera*, retaining biological membranes and lipids (ca. 1.16 ± 0.02 g cm^{-3}) is lower than this mean value and is much closer to that of Arctic sea water.

As such, additional mechanisms for the sinking of sea ice diatoms need to be considered, especially since diatom sinking rates of up to 100 m d^{-1} have been reported (Smetacek, 1985). One such possible mechanism to explain increased diatom sinking rates may arise from the aggregation of diatom cells in zooplankton faecal pellets (Figure 6.1-3). Zooplankton grazing on the underside of sea ice in the Greenland Sea, (1994), produced faecal pellets at frequencies ranging from 1 - 15 pellets d^{-1}, providing 0.7 mg C m^{-2} d^{-1}, or almost 2% of the ice-bound carbon being transferred to the pelagic system (Gradinger *et al.*, 1999; Werner, 2000). Peperzak *et al.* (2003) therefore proposed that sinking rates are predominantly determined by cell or colony density, rather than cell size, so inclusion of cells into faecal pellets could result in net enhancements in sinking rates.

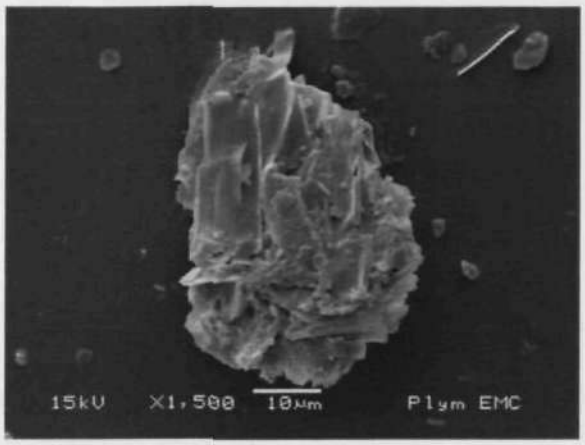

Figure 6.1-3. Scanning electron micrograph of a faecal pellet containing visible diatom fragments, isolated from sediment trap CA20 during the ArcticNet cruise 2005 (Brown, 2007).

This is similar to the aggregation of diatom cells (in the absence of zooplankton grazing) (Riebesell *et al.*, 1991), where aggregate sinking rates of up to three orders of magnitude greater than single algal cells have been reported (Riebesell *et al.*, 1991). Coagulation theory has also been used to explain the sudden decline of a phytoplankton bloom (e.g. Tiselius *et al.*, 1996). Some Arctic sea ice diatoms produce exopolymeric substances (EPS) (Krembs *et al.*, 2002b) which form sticky sheaths around diatoms within the brine channels of sea ice. Increased mucous (Billett *et al.*, 1983) and gelatinous secretions (Riemann, 1989) observed in post bloom phytoplankton stocks of the North Atlantic and temperate latitudes support the suggestions that diatoms would remain encased in EPS. During part of the investigation by Brown (2007) on the concentrations of *Haslea* spp. diatoms and IP_{25} in sediment traps it was noted that an intercellular bond, apparently occurring as part of the cell membrane, rather than siliceous frustule, appeared to be responsible for binding individual diatoms together (Figure 6.1-4).

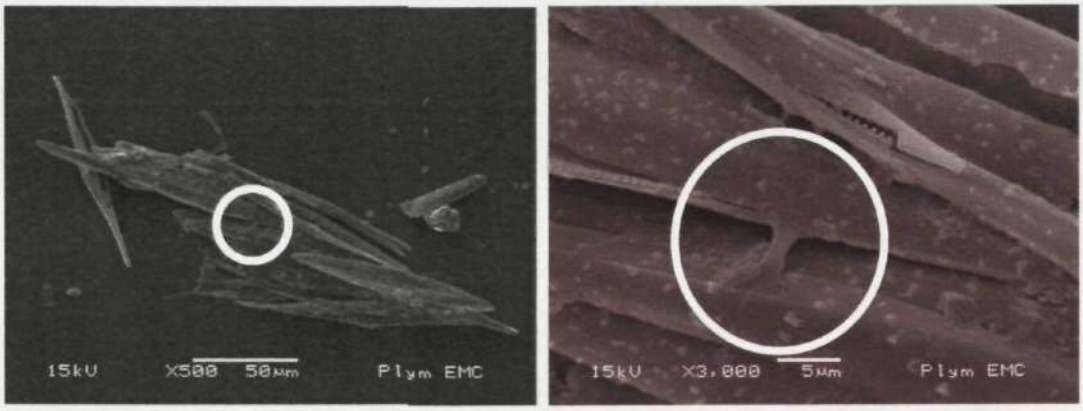

Figure 6.1-4. Scanning electron micrograph of non-acid digested *Haslea crucigera* cells obtained from culture. White circles indicate unidentifiable adhesion between cells.

Thermally stratified water columns in the Arctic are common (Neal *et al.*, 1969; Dieckmann *et al.*, 2010) and are often responsible for restricting convection to the upper sections (ca. 50 - 100 m) of the water column. Stratification provides a degree of vertical stability in the water column, resulting in enhanced vertical sinking rates through convection (Margalef, 1978; Smith *et al.*, 1986; Peperzak *et al.*, 2003), with increases of up to 50% in some cases (Peperzak *et al.*, 2003). Wind-driven mixing in combination with vertical convection, observed at the Northeast Water Polynya, east of Greenland, was observed to cause further enhancement of diatom sinking rates (Pesant, 2002). Additionally, the commonly stratified surface waters of the Arctic are sometimes underlain by separate water bodies that can be subject to lateral advection (Dieckmann *et al.*, 2010) that can also result in dispersion.

A number of studies carried out in the Southern Ocean demonstrate the susceptibility of allochtonous sediment inputs to lateral advection (Sachs *et al.*, 2003; Sicre *et al.*, 2005; Mollenhauer *et al.*, 2006). Lateral marine transportation of this nature was evident in a number of alkenone-based sea surface temperature reconstructions, (e.g. Benthien *et al.*, 2000). Further, a decoupling of ocean surface and sea-floor conditions was apparent in one multiproxy investigation, where it was found that while microfossil analyses

(diatoms and foraminifera) were representative of local climate, the allochtonous suites of *n*-alkanes and alkenones were shown to have originated from distant areas via oceanic and aeolian transport, respectively (Kim *et al.*, 2009). Conversely, some further studies in the Southern Ocean at depths of 4100 m provided evidence for the displacement of diatoms over large distances in Antarctic bottom waters resulting from isotherm displacement (Burckle, 1981; Jones *et al.*, 1984). The significance for biomarker redistribution is clear following calculation of the range of diatom redistribution resulting from this lateral displacement of suspended particles and sediments, caused by strong surface and bottom currents, benthic storms, and downslope processes which have generated estimates of up to 1000 km in 1500 m of water (Benthien *et al.*, 2000). Although the occurrence of lateral displacement does not appear in Arctic studies, for the CAA at least, the severity of biomarker redistribution is not expected to be as significant. Combining the maximum current velocity within the archipelago (50 cm s^{-1}) (Hell Gate, between Ellesmere and Devon Islands) (Hannah *et al.*, 2009) and average water depth of the Amundsen Gulf (ca. 300 m) with typical diatom sinking rates (< 100 m d^{-1} (Smetacek, 1985)), lateral excursion from any point of origin is estimated to reach no more than ca. 130 km. However, more localised currents, such as up-slope and down-slope currents (Schubert *et al.*, 1997 and references therein; Hannah *et al.*, 2009) may have more significant effects on redistribution, with additional complications arising from the episodic input from sea ice (Benthien *et al.*, 2000).

6.2 Arctic sea floor organisms

Particulates reaching the bottom of the water column in the CAA form the basis of many benthic macrofaunal diets (reviewed by Cusson *et al.*, 2007). It is noted, however, that the distribution of both benthic flora and fauna in the CAA is variable (Macdonald

et al., 1998), most likely resulting from concentrated nutrient replenishment from upwelling events found for Cape Bathurst (Hannah *et al.*, 2009). Cusson *et al.*, (2007) reported increases in species diversity towards the eastern CAA over 200 stations while a further study of 52 stations in 2002 - 2004 revealed abundances of 490 macrobenthic (> 0.4 mm) organisms m^{-2} in the eastern Amundsen Gulf, increasing to over 17,000 organisms m^{-2} off Cape Bathurst in the western Gulf (Conlan *et al.*, 2008), while Kröncke (1994) recognized a link between organic matter and macrobenthic biomass in the Arctic. The episodic release of organic carbon from seasonal algal blooms further affects the supply of carbon to the benthos, resulting in a dual component supply of autochthonous carbon; sea ice and planktonic (Wheeler *et al.*, 1996).

Yi-Sun *et al.*, (2009) investigated the diets of two common Arctic macrobenthic species; a bivalve *(Macoma baithica)* and crustacean *(Monoporeia affinis),* by adding phytoplankton and ^{13}C-labelled ice algae to sediments. They found that while the crustacean consumed both varieties of algae, the bivalve discriminated against the phytoplankton, preferring to ingest the labelled ice algae (Yi-Sun *et al.*, 2009). Some macrobenthic infaunal biomass abundance can be quite large (exceeding 360 g m^{-2} (Dunton *et al.*, 2005) and even reaching 4000 g m^{-2} in select regions of the nearby Chukchi Sea (Grebmeier *et al.*, 2007)) resulting in the potential for sequestration and redistribution of IP_{25} which requires consideration when interpreting the sedimentary abundance of this biomarker. Dietary distinctions between different sources of carbon (e.g. sea ice; plankton) can therefore potentially enable predictions of the distribution of ice originated lipids, such as IP_{25}, in sympagic, pelagic and benthic macrofaunal species, creating the potential for the presence of IP_{25} to act as a food web tracer across trophic levels.

The majority of the sampling program for the current research project was anticipated to involve sea ice collection. However, exceptionally poor Arctic sea ice cover during the winter in 2007, in conjunction with south-easterly winds in 2008, resulted in an unanticipated early retreat of sea ice from the study region during the cruise in 2008. This absence of sea ice for part of the planned sampling interval provided the unexpected opportunity for the collection of plankton samples. While this was not the primary objective of the main research goal, this additional sampling provided the opportunity to investigate, albeit using a suite of samples beyond the complete control of the author, the lipid content of the water column following sea ice melt. Therefore, the data presented in this chapter are considered to represent a preliminary, yet important and opportunistic study into the distribution and concentration of IP_{25} and other HBIs in Arctic water column flora and fauna.

6.3 Aims and objectives of pelagic HBI investigations

Arctic sea ice supports a highly complex marine sympagic system capable of imposing physical and biological influences on the underlying water column. The release of sea ice organisms, including diatoms containing IP_{25}, from melting sea ice to the water column exposes IP_{25} to a number of potential removal mechanisms. A better understanding of these processes is necessary to further improve the interpretations of *sedimentary occurrences of this sea ice biomarker. Therefore, the main aims of the work* described in this chapter were to:

i. Determine concentrations of IP_{25} (and other HBIs), fatty acids and sterols in pelagic communities of the Amundsen Gulf during spring to identify differences between sea ice and pelagic lipid concentrations.

ii. Determine correlations between each of the biomarkers identified in i. and compare these against results obtained from analysis of sea ice samples collected from the same region (chapters 4 and 5).

iii. Quantify, or estimate the dispersal of IP_{25} following release from Arctic sea ice to the water column.

iv. Carry out a qualitative investigation on the content of IP_{25} and other HBIs in macrofaunal organisms within the water column and benthos.

6.3.1 Selection of filtered seawater samples

Collection of filtered seawater samples using plankton net tows was carried out during the Canadian Circumpolar Flaw Lead System Study, as part of the International Polar Year (IPY-CFL) during legs 7, 8 and 9 (March — July 2008) (Chapter 4). Operational time restrictions prevented the collection of replicates. Vertical plankton net tows were collected from varying depths, determined by the approximate depth of maximum chlorophyll *a* measured by analysis of water samples collected using the conductivity, temperature and depth (CTD) profiler from 17 stations. Plankton net tow conditions are summarised in Table 6-1 Sampled water volumes were estimated by combining the area of the net mouths with the depths of each tow.

Table 6-1. Arctic Ocean plankton tow collection data from legs 7 to 9 of the IPY-CFL cruise, 2008.

Date	Tow type	Tow depth (m)	Estimated volume of water (m^3)	Station ID	Location			
11-Apr	Vertical	0-50	28.5	Under ice	71 ° 15	N	124 °37,	W
19-May	Vertical	0-20	2.8	St.405b	70 ° 39	N	122 ° 50	W
21-May	Vertical	0-80	11.2	St.1011	70 ° 42	N	123 ° 58	W
23-May	Vertical	0-80	11.2	St.1806	72 ° 39	N	127 ° 23	W
27-May	Vertical	0-95	17.5	St.9008	74 ° 19	N	127 °03	W
10-Jun	Vertical	0-40	2.8	St.405b	70 ° 39	N	123 ° 01	W
16-Jun	Vertical	0-20	1.4	FB00	70 ° 00	N	125 ° 50	W
18-Jun	Vertical	0-40	2.8	F7	69 °48	N	123 °49	W
23-Jun	Vertical	0-35	2.4	C.Bathurst	70 ° 36	N	127 ° 35	W
24-Jun	Vertical	0-40	2.8	F7	69 ° 49	N	123 ° 41	W
25-Jun	Vertical	0-40	2.8	FB07	69 ° 57	N	125 ° 53	W
27-Jun	Vertical	0-40	2.8	St.1200	71 ° 32	N	124 ° 19	W
28-Jun	Vertical	0-40	2.8	St.1208	71 ° 04	N	126 ° 06	W
30-Jun	Vertical	0-30	2.1	St.434	70 ° 10	N	133 ° 33	W
03-Jul	Vertical	0-40	2.8	St.6006	72 °39	N	128 °21	W
08-Jul	Vertical	0-40	2.8	St.410	71 ° 42	N	126 ° 29	W
10-Jul	Vertical	0-40	2.8	St.416	71 ° 17	N	127 ° 46	W
12-Jul	Vertical	0-40	2.8	D34	70 ° 18	N	124 ° 49	W

The spatial distribution of water column samples (Figure 6.3-1) was governed by other ship-based activities resulting in a relatively wide geographic range, rather than a localised study, yet sampling remained with the Amundsen Gulf and south eastern Beaufort Sea.

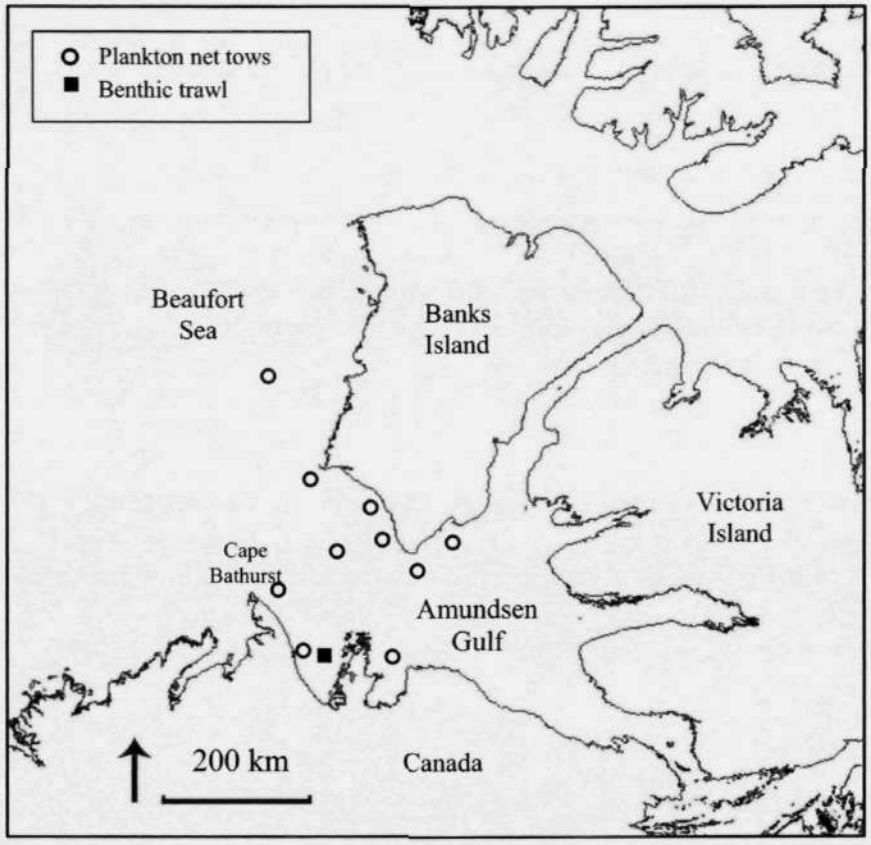

Figure 6.3-1. Spatial distribution of plankton net tow and benthic trawl collection sites from within the Amundsen Gulf region of the CAA during the IPY-CFL cruise, 2008.

The presence of sea ice until mid-March restricted the operation of plankton tows, with regular collection of filtered seawater coinciding with sufficient ice break-up to provide regular access to open water conditions (Figure 6.3-2).

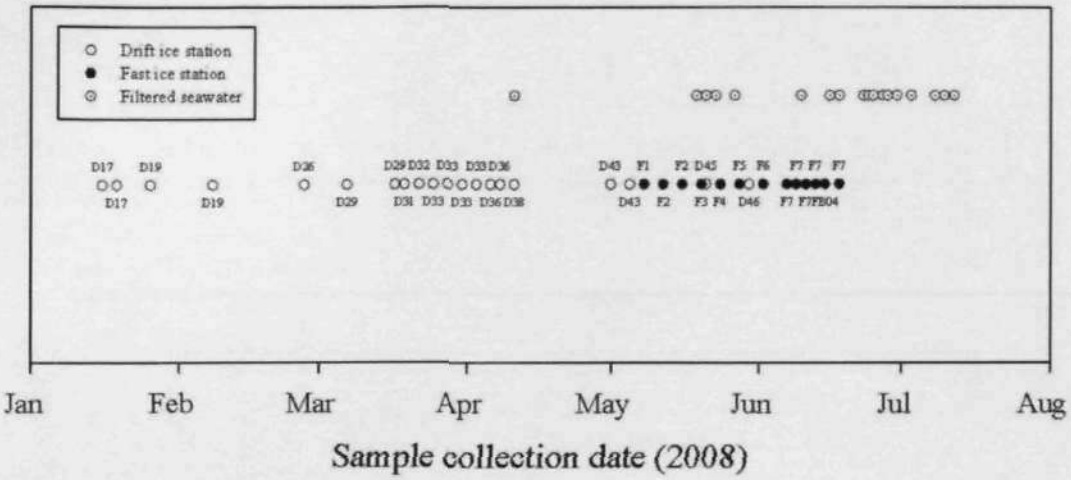

Figure 6.3-2. Temporal distribution of filtered seawater sample collection sites, compared to sea ice core collection (Chapter 4) from within the Amundsen Gulf region of the CAA during the IPY-CFL cruise, 2008.

Vertical plankton net tows were collected using either a small circular net (30 cm Ø) with 20 µm mesh (Figure 6.3-3) towed at ca. 50 cm s^{-1} by hand using a bow mounted derrick, or with a larger (75 cm Ø) net also with 20 µm mesh towed in the same way.

Figure 6.3-3. One of the plankton nets used for collecting vertical water column samples from the chlorophyll *a* maximum region to the surface; Diameter; 30 cm, length; 50 cm, mesh; 20 μm.

Water samples containing plankton were rinsed (ca. 200 mL; 0.2 μm filtered seawater) from the mesh into the cod-end (externally) and transferred (ca. 100 mL; 0.2 μm filtered seawater) into a plastic container *in situ* before being sieved (20 μm; 0.2 μm filtered seawater) in the laboratory to remove excess water. All filtered seawater samples were finally transferred (ca. 10 mL; 0.2 μm filtered seawater) into 15 mL sterile Corning centrifuge tubes and frozen (-20°C).

Copepods were collected by colleagues (IPY-CFL) using large (ca. 4 x 1 m^2) Tucker nets (200 μm) towed at ca. 1 knot at varying depths (ca. 200 m to < 50 m). Once retrieved, nets were washed externally using pumped seawater with samples being retrieved from the cod-end (ca. 500 mL; 0.2 μm filtered seawater) followed by isolation.

Copepods remained in filtered seawater for ca. 10 h before freezing (-20°C) in the laboratory to provide time to empty their guts.

Additional plankton net tows were carried out as part of an exploratory expedition to the North Pole by Antony Jinman and Eric Larsen (http://www.antonyjinman.com) within a comparable time window to those collected during the IPY-CFL cruise; 24/3/10 to 22/4/10 (Figure 6.3-4 and Table 6-2).

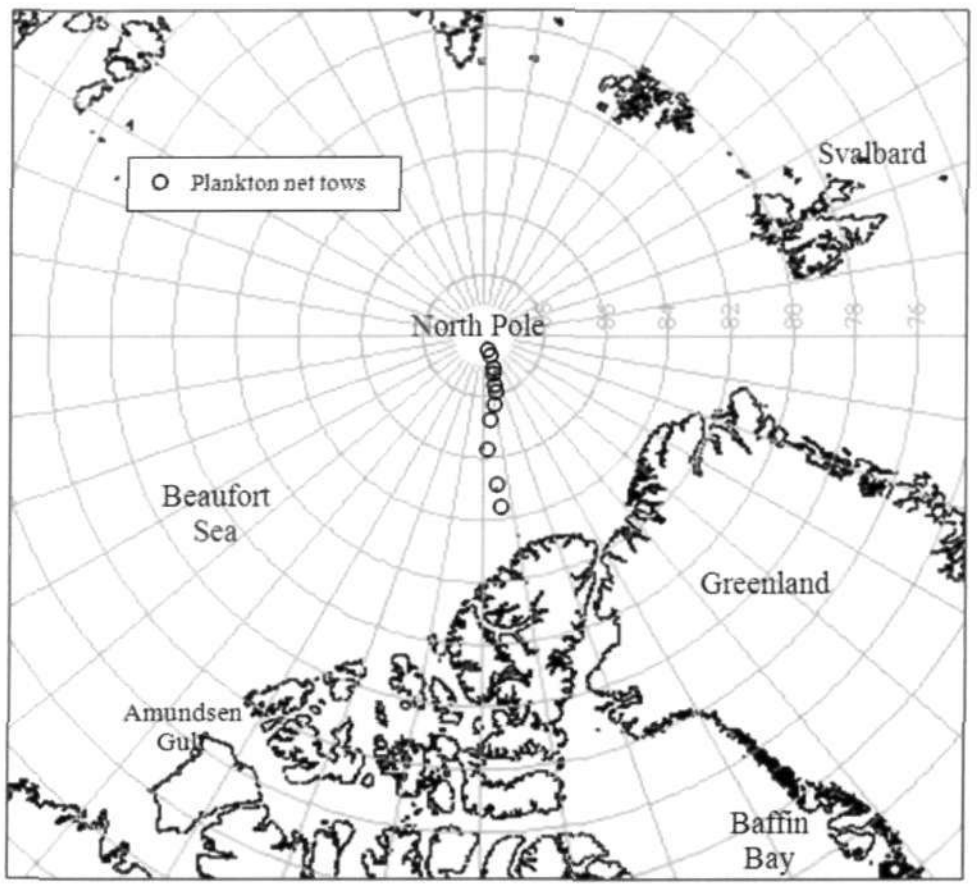

Figure 6.3-4. Spatial distribution of plankton net tow collection sites (open circles) north of Ellesmere Island to the North Pole region of the Arctic Ocean collected by Anthony Jinman and Eric Larsen in spring 2010.

Table 6-2. Arctic Ocean plankton tow collection data from north of Ellesmere Island to the North Pole, 2010.

Date	Tow type	Tow depth (m)	Estimated volume of water (m^3)	Station ID	Location			
24-Mar	Vertical	0-48	2.36	AJ VNT 9	85° 06	N	77° 03	W
24-Mar	Vertical	0-48	2.36	AJ VNT 3	85° 06	N	77° 04	W
29-Mar	Vertical	0-48	2.36	AJ VNT 19	85° 51	N	79° 06	W
7-Apr	Vertical	0-48	2.36	AJ VNT 4	87° 20	N	82° 40	W
13-Apr	Vertical	0-48	2.36	AJ VNT 15	88° 13	N	73° 59	W
14-Apr	Vertical	0-48	2.36	AJ VNT 11	88° 28	N	69° 14	W
15-Apr	Vertical	0-48	2.36	AJ VNT 17	88° 46	N	65° 06	W
16-Apr	Vertical	0-48	2.36	AJ VNT 2	88° 57	N	62° 54	W
17-Apr	Vertical	0-48	2.36	AJ VNT 1	89° 06	N	57° 24	W
17-Apr	Vertical	0-48	2.36	AJ VNT 21	89° 06	N	57° 24	W
19-Apr	Vertical	0-48	2.36	AJ VNT 16	89° 27	N	51° 02	W
20-Apr	Vertical	0-48	2.36	AJ VNT 8	89° 33	N	48° 31	W
21-Apr	Vertical	0-48	2.36	AJ VNT 12	89° 47	N	39° 23	W
22-Apr	Vertical	0-48	2.36	AJ VNT 20	89° 58	N	35° 42	W

While every effort was taken to ensure that filtered seawater samples collected by Anthony Jinman and Eric Larsen were collected using similar equipment (30 cm Ø; 20 µm mesh net) and techniques (hand drawn ca. 50 cm s^{-1} vertical tows) to those from the CFL expedition, some differences in approach were inevitable. Notably, in the absence of CTD measurements and chlorophyll *a* data, each net tow was carried out from ca. 48 m depth. In further contrast to CFL sampling, instead of washing the cod end, the end-mesh of the net was instead removed and stored in centrifuge tubes at ambient temperature (< 0°C) to combat difficulties of working in the extreme cold without laboratory facilities.

6.4 Selection of macrofaunal samples

A representative range of individual macrofaunal specimens was collected from four different phylas (5 echinoderms, 1 crustacean, 1 gastropod and a cnidarian) by towing a

benthic Agassiz sled (ca. 250 cm x 40 cm; 1 cm mesh: Figure 6.4-1) behind the *CCGS* Amundsen at ca. 1 - 2 knots on the seafloor for varying time intervals (typically ca. 15 mins, covering 40 - 100 m). Once retrieved, loose sediment was washed from the net using pumped seawater and the organisms spread on the deck for isolation of species.

Figure 6.4-1. Agassiz sled used for collecting macrofaunal (> 1 cm) specimens from sea floor sediments; Length 250 cm; width 40 cm; mesh size 1 cm.

Macrofaunal specimens were kept alive (ca. 24 - 48 h) in 20 L containers of flowing seawater in the absence of food before being frozen and stored (-20°C). Additional collection of the temperate sea urchin species *Echinus esculentus* (3 specimens) was carried out by SCUBA divers (Greta Vont; University of Plymouth) at Porth Kerris on the Lizard Peninsula in Cornwall, South West England on May 12th 2010. Urchins were transported live to Plymouth where they were frozen and stored (-20°C) prior to analysis. Accurate identification of Arctic and temperate sea urchins was achieved by

comparison of the respective Aristotle's lanterns (complex of oral bones and teeth) and general structural features of the test (shell), to taxonomic keys provided by the Natural History Museum and Marine Life Information Network (MarLIN) websites (www.nhm.ac.uk and www.marlin.ac.uk respectively).

6.5 Experimental

Each of the biomarkers of interest (hydrocarbons, sterols and fatty acids) required extraction from the sample matrix and separation into individual fractions prior to analysis by GC/MS. Partitioning of lipid fractions was achieved using a combination of chromatographic techniques (see below).

6.5.1 Extraction of filtered seawater samples

For a detailed description of the extraction and purification procedures shown in Figure 6.5-1, refer to Chapter 3 (Methods).

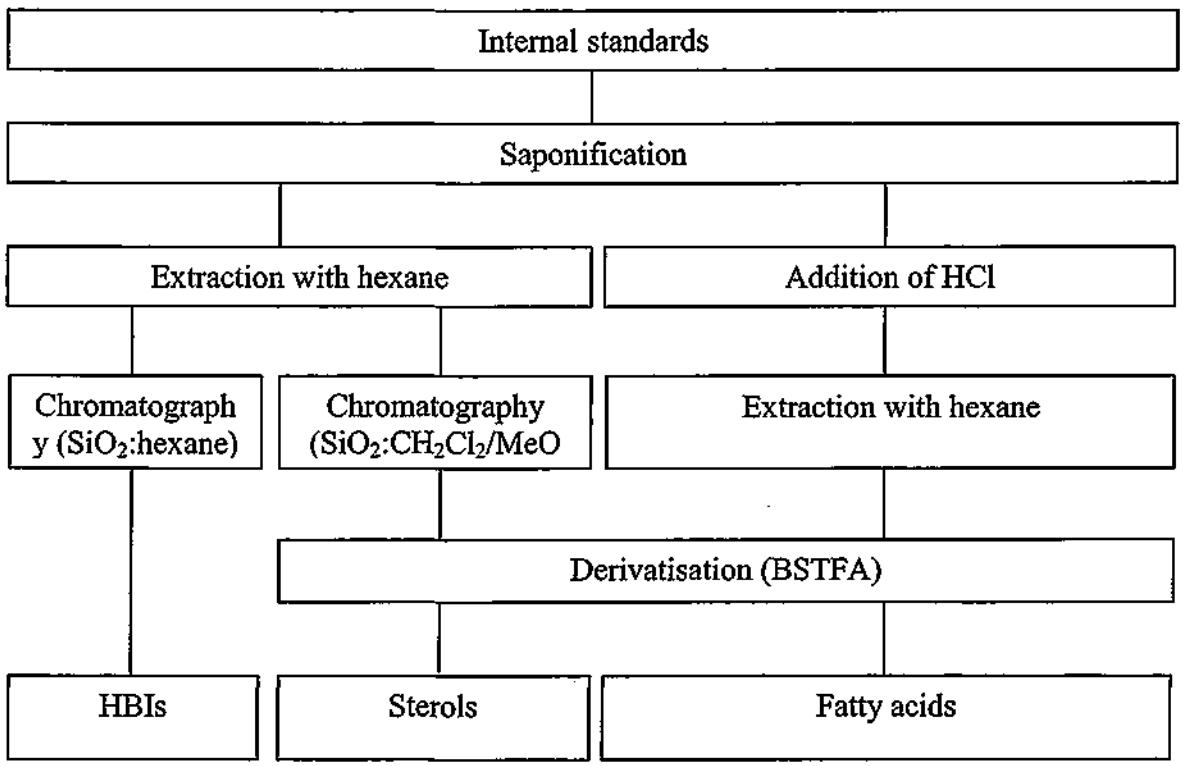

Figure 6.5-1. Sample extraction flow diagram for lipid biomarkers.

Briefly, upon defrosting, water column samples were filtered onto pre-weighed GF/F (0.7 µm) filters using artificial seawater (100 mL deionised water; 2.4g NaCl, 0.4 g anhydrous $NaSO_4$) to reduce osmotic stress (Garrison and Buck 1986). Filtered water and bulk zooplankton samples (> 710 µm) were then freeze dried and re-weighed to determine biomass prior to extraction. Following the addition of appropriate internal standards for quantification (see Chapter 3), GF/F filters containing filtered seawater samples were saponified (5 mL; 5% KOH, CH_3OH/H_20 (80/20 v/v)) at 80°C for 60 min Non-saponifiable lipids (NSLs) were then extracted into hexane (3 x 1 mL) and purified by open column silica chromatography (50.1 SiO_2 NSLs) with hexane mobile phase (5 column volumes) used to yield apolar lipids. Dichloromethane, followed by methanol (3 column volumes each) were used to elute sterols. Fatty acids were obtained by the addition of concentrated HCl (1 mL) to the saponified filters followed by re-extracting with hexane (3 x 1 mL). Prior to analysis by GC/FID or GC/MS, fatty acids and sterols were derivatised (50 µL BSTFA, 30 min, 70°C).

6.5.2 Extraction of macrofaunal specimens

A more detailed description of these procedures can be found in Chapter 3 (Methods). Briefly, following freeze drying, weighed specimens were ground using a solvent cleaned pestle and mortar (30 mL; DCM/MeOH; 50/50 v/v) before being soxhlet extracted (ca. 250 mL; dichloromethane; 24 h). The TOE was then purified using open column silica chromatography (50:1 SiO_2: TOE) with hexane used to yield apolar lipids (5 column volumes). Sterols were obtained from one echinoderm specimen (*Strongylocentrotus* sp.) using dichloromethane/methanol (5 column volumes; 50:50 v/v).

Another *Strongylocentrotus* sp. specimen was also saponified (5 mL; 5% KOH; CH_3OH/H_20 (80/20 v/v)) at 80°C for 60 min, with fatty acids obtained by the addition of concentrated HCl (1 mL) to the saponified extracts followed by re-extracting with hexane (3 x 1 mL).

Prior to analysis by GC/FID or GC/MS, fatty acids and sterols were derivatised (50 µL BSTFA, 30 min; 70°C).

Where stable isotope ($\delta^{13}C$) analysis of individual lipids was also required, the samples were purified using high performance liquid chromatography (HPLC; Ag^+ Chromospher 5 lipids). A mobile phase gradient of hexane-dichloromethane-acetone (Table 6-3) was used to isolate apolar hydrocarbons and individual HBIs at 1 mL min^{-1} using an Agilent 1100 series HPLC system. Fractions were collected manually over various time intervals necessary to isolate compounds of interest (0.2 — 1 min).

Table 6-3. High performance liquid chromatography mobile phase gradient of increasing polarity used to separate HBI isomers using Ag^+ (Chromospher 5 lipids).

Time (min)	Mobile phase	Solvent composition
0.00	Hexane	100%
4.00	Hexane	100%
4.01	DCM	100%
10.00	DCM	100%
16.00	DCM/Acetone	50/50%
16.01	Acetone	100%
28.00	Acetone	100%

The lipid content of the temperate sea urchin *Echinus esculentus* was also analysed using GC/MS and GCxGC/ToF MS to resolve co-eluting HBI isomers before the parent structure of the lipids was structurally confirmed by hydrogenation and re-analysis by GC/MS with co-injection of a C_{25} HBI alkane standard.

6.6 Results

Considerable ice cover prevented routine plankton collection coincident with all of the sea ice sampling, with initial collection commencing on 11/4/08 and continuous plankton collection beginning on 19/5/08 (30 days before the end of ice sampling). The initiation of more routine sample collection coincided with sufficient ice melt that provided limited access to the water and enabled collection of plankton net tows to continue until 12/7/08 (24 days after the end of sea ice sampling). Collection of water column samples terminated following the end of available ship accommodation (12/7/08)

Lipid concentrations in filtered seawater samples were converted to a volume seawater basis providing data that could be compared to values found in sea ice samples (Chapter 4).

6.6.1 Highly branched isoprenoids in the water column

All of the HBIs detected in sea ice (**I – IIId**) were detected in all 19 filtered seawater samples, although **IIa** was only detected in three of these (Figure 6.6-1). The earliest filtered seawater sample, collected from under sea ice (Station D38; 11/4/08), yielded the greatest concentration of HBIs in filtered seawater (**I – IIId**: 1.3 x 10^{-6} mg m^{-3} water), with the latest filtered seawater sample yielding the lowest HBI concentration (12/07/08· 3.2 x 10^{-8} mg m^{-3} water). The mean combined individual HBI concentrations measured in filtered seawater for the period 11/4/08 to 12/7/08 was ca 2.3 x 10^{-7} ± 2.7 x 10^{-7} mg m^{-3} water.

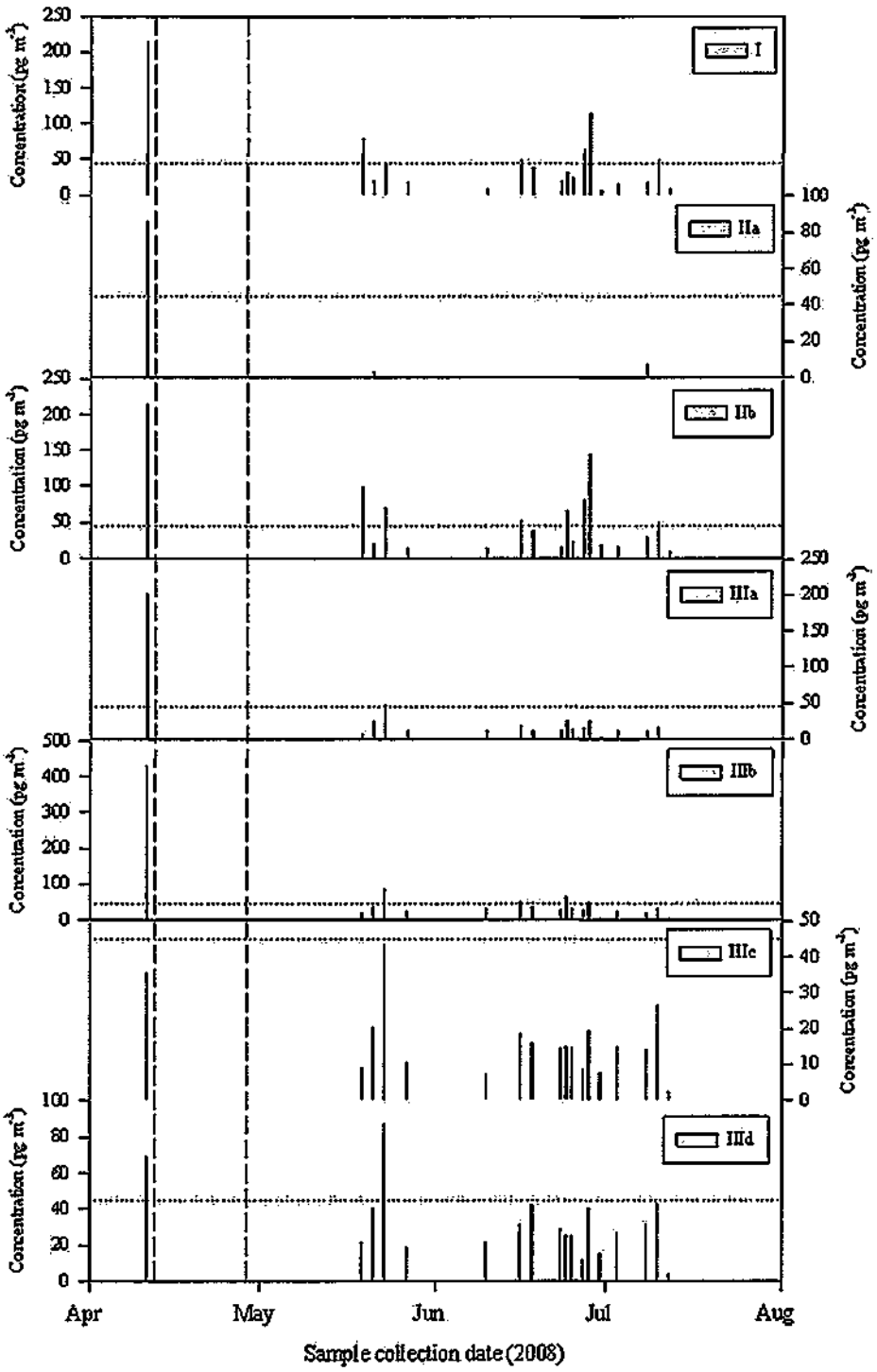

Figure 6.6-1. Temporal concentrations of individual HBIs (**I, IIa, IIb, IIIa, IIIb, IIIc** and **IIId**) per m^3 of water observed in filtered seawater (> 20 μm) during the IPY-CFL cruise (1/4/08 to 1/8/08); Vertical grey dashed lines represent a temporary break in sampling, horizontal dotted lines represent the mean concentration of **I** in the water column (45 ng m^{-3}).

Comparison of HBI concentrations between sea ice (Chapter 4) and filtered seawater samples indicate that combined individual HBI concentrations in Arctic seawater were

ca. 6 x 10^5 times less than was previously measured in sea ice (Table 6-4), with **I** being ca. 8 x 10^5 times less concentrated in the water than in sea ice.

Table 6-4. Mean HBI (**I – IIId**) lipid concentrations in sea ice (from Chapter 4) and filtered seawater samples.

		I	**Total HBIs**
Sea ice	Mean concentration (mg m^{-3})	3.7 x 10^{-2}	1.5 x 10^{-1}
	Relative to **I**	1	4
Filtered seawater	Mean concentration (mg m^{-3})	4.5 x 10^{-8}	2.3 x 10^{-7}
	Relative to **I**	1	5
$\left(Sea\ ice/_{Filtered\ seawater}\right)$		8.2 x 10^5	6.5 x 10^5

Noticeably, HBI concentrations measured in filtered seawater samples in the Amundsen Gulf were variable both between samples and through time from April to July (Figure 6.6-1) Despite this variability, the relative distributions of individual HBI isomers remained somewhat similar to those recorded for sea ice (Table 6-5) with a strong correlation, also observed in sea ice, evident between **I** and **IIb** ($r = 0.97$; $p = < 0.001$).

Table 6-5. Mean concentration (mg m^{-3}) and relative distribution (%) of HBI isomers observed in filtered seawater samples (> 20 μm) and sea ice (from Chapter 4) during the IPY-CFL cruise.

	I	**IIa**	**IIb**	**IIIa**	**IIIb**	**IIIc**	**IIId**
Mean concentration (mg m^{-3})	4.5×10^{-8}	5.1×10^{-9}	5.3×10^{-8}	2.5×10^{-8}	5.4×10^{-8}	1.6×10^{-8}	3.2×10^{-8}
Relative distribution (%) of HBI concentrations in filtered seawater	19.7	2.2	23.1	11.0	23.4	6.9	13.7
Relative distribution (%) of HBI concentrations in sea ice	27.2	1.7	31.4	1.0	28.1	0.8	9.8

However, some variation was present in the distribution of individual HBI isomers, relative to each other, between sea ice and the water column. In particular, the relative distribution of **IIIa** and **IIIc** increased by ca. an order of magnitude from sea ice to the water column. In contrast the contribution of **I** and **IIb** were observed decreasing from 27.2% and 31.4% to 19.7% and 23.1% respectively, from sea ice to the water column (Table 6-5). In contrast to the presence of HBIs in the Amundsen Gulf, analysis of filtered water samples using comparable techniques collected during the bloom period (March and April) in 2010 from north of Ellesmere Island, to near the North Pole (89°53N), yielded no detectable concentrations of any of the HBIs used in this study within the top 50 m of the water column beneath multiyear sea ice.

6.6.2 Fatty acids in the water column

The fatty acid content of the 19 filtered seawater samples obtained from the water column between 11/4/08 and 12/7/08 were measured (GC/MS), with fatty acids present in all samples. Each of the fatty acids detected in sea ice samples (Chapter 4) were also detected in filtered seawater samples, in addition to a range of other fatty acids that were also present in low concentrations (Figure 6.6-2).

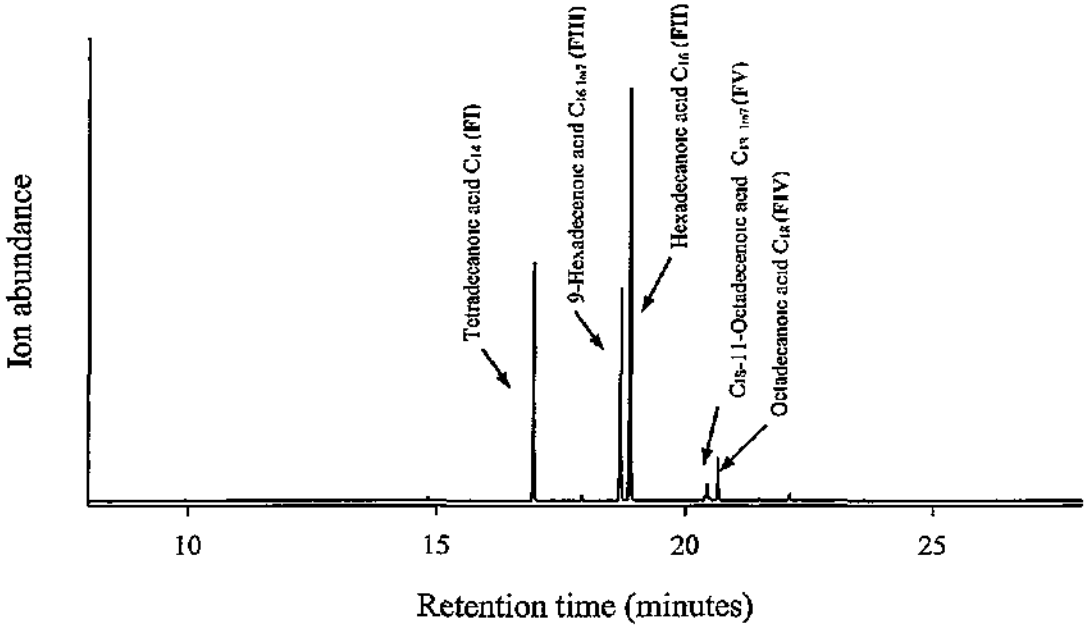

Figure 6.6-2 Partial mass chromatogram (*m/z* 117) GC/MS chromatogram of fatty acids (TMS) detected in filtered seawater collected during the spring bloom (St 405b, 10/06/2008) from the Amundsen Gulf during the IPY-CFL cruise 2008.

The maximum combined concentration of the fatty acids previously determined to be of largely diatom origin (**FI – FV**) for the period was observed in filtered seawater collected from ice-free water on 16/06/08 (7 7 x 10^{-2} mg m^{-3} water). The lowest fatty acid concentration (**FI – FV**) coincided with the lowest HBI concentration in the latest sample collected on the 12/07/08 (7.0 x 10^{-4} mg m^{-3} water). Overall, the mean combined individual concentrations of the fatty acids (**FI – FV**) from all 19 samples was 2 1 x 10^{-2} ± 2.2 x 10^{-2} mg m^{-3} water, making these fatty acids ca 9 x 10^{3} less concentrated than the same fatty acids in sea ice (Table 6-6). This difference in concentration between sea ice and seawater was far less than that observed for the HBIs (6 5 x 10^{5}). As such, collectively, the individual fatty acids (**FI – FV**) in the water column are 5 orders of magnitude greater than the HBIs, (and 6 orders of magnitude greater than **I**) whereas in sea ice fatty acids were only 3 orders of magnitude greater than HBIs (and 4 orders of

magnitude greater than I) measured in sea ice (Table 6-6), indicating a lesser dilution, or increased biological production, of the fatty acids than HBIs in the water column compared to the sea ice.

Table 6-6. Mean HBI (**I – IIId**) and fatty acid (**FI – FV**) lipid concentrations in sea ice (from Chapter 4) and filtered seawater samples

		I	**Total HBIs**	**Total fatty acids**
Sea ice	Mean concentration (mg m^{-3})	3.7×10^{-2}	1.5×10^{-1}	2×10^{2}
	Relative to **I**	1	4	5.4×10^{2}
Filtered seawater	Mean concentration (mg m^{-3})	4.5×10^{-8}	2.3×10^{-7}	2.1×10^{-2}
	Relative to **I**	1	5	4.6×10^{5}
$\left(Sea\ ice/_{Filtered\ seawater}\right)$		8.2×10^{5}	6.5×10^{5}	9.5×10^{3}

The fatty acid concentrations, like HBIs, also varied both between samples and through time (Figure 6.6-3), although importantly, not proportionally to the HBIs ($r = < 0.3$), suggesting either the production of fatty acids or absence of HBI production in the water column both during and following sea ice melt.

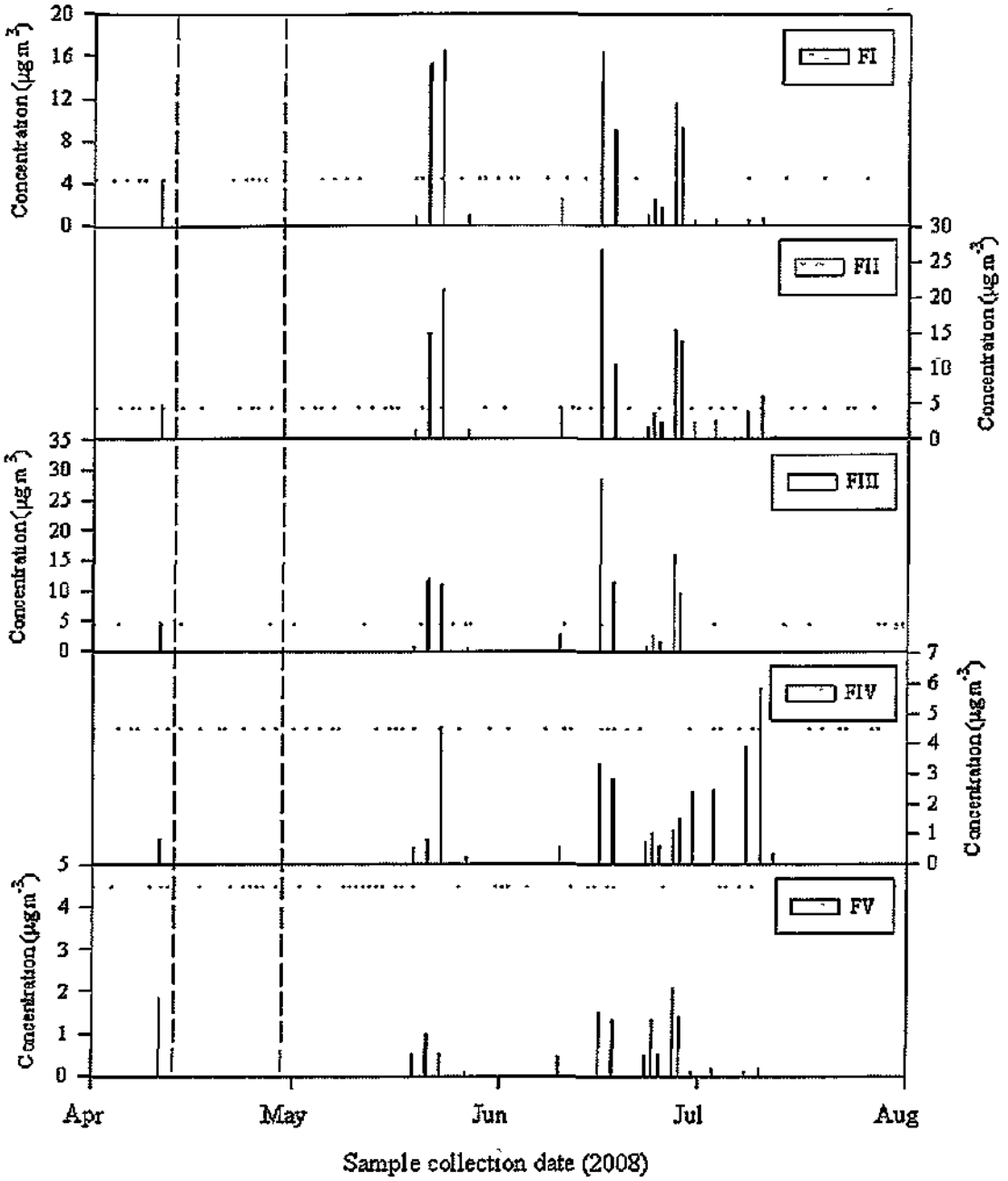

Figure 6.6-3. Temporal concentrations of individual fatty acids (**FI, FII, FIII, FIV** and **FV**) per m^3 of water observed in filtered seawater (> 20 µm) during the IPY-CFL cruise (1/4/08 to 1/8/08), Vertical grey dashed lines represent a temporary break in sampling, horizontal dotted lines represent 100,000 times the mean concentration of I in plankton (45 ng m^{-3}).

Further, minor variations in the relative fatty acid distributions were also observed. **FI** was found to increase, relative to the other fatty acids, by ca. 33% from sea ice to the water column, while the remaining fatty acids varied by less than 15% between sea ice

and the water column, with **FII** and **FIII** remaining the most abundant fatty acids in both sea ice and the water column (Table 6-7). The frequently reported diatom fatty acid ($C_{20:5}$) represented only a minor and highly variable contribution in filtered seawater samples (0.6 ± 0.8%) and, alongside other minor components, was not included in the calculations of total fatty acid concentrations

Table 6-7. Mean concentrations (mg m^{-3}) and relative distributions (%) of fatty acids observed in filtered water samples (> 20 μm) and sea ice (from Chapter 4) during the IPY-CFL cruise.

	FI	**FII**	**FIII**	**FIV**	**FV**
Mean concentration (mg m^{-3})	5.2×10^{-3}	7.5×10^{-3}	5.7×10^{-3}	1.8×10^{-3}	7.7×10^{-4}
Relative distribution (%) of fatty acid concentrations in filtered seawater	24.5	35.9	27.0	8.9	3.7
Relative distribution (%) of fatty acid concentrations in sea ice	16.6	38.5	32.6	7.6	4.7

The same fatty acids reported in the Amundsen Gulf samples were also present in pooled filtered seawater samples collected during the spring bloom (March – April 2010) from the high Arctic, north of Ellesmere Island to near the North Pole (89°53N). In addition to a comprehensive suite of fatty acids ranging C_8 to C_{28} and their unsaturated homologues (Figure 6.6-4), the fatty acids **FI**, **FII**, **FIII** and **FIV** were the most abundant (1.3×10^{-4} mg m^{-3} water) yet remained lower in concentration than those of the Amundsen Gulf (maximum; 4.8×10^{2} mg m^{-3} water).

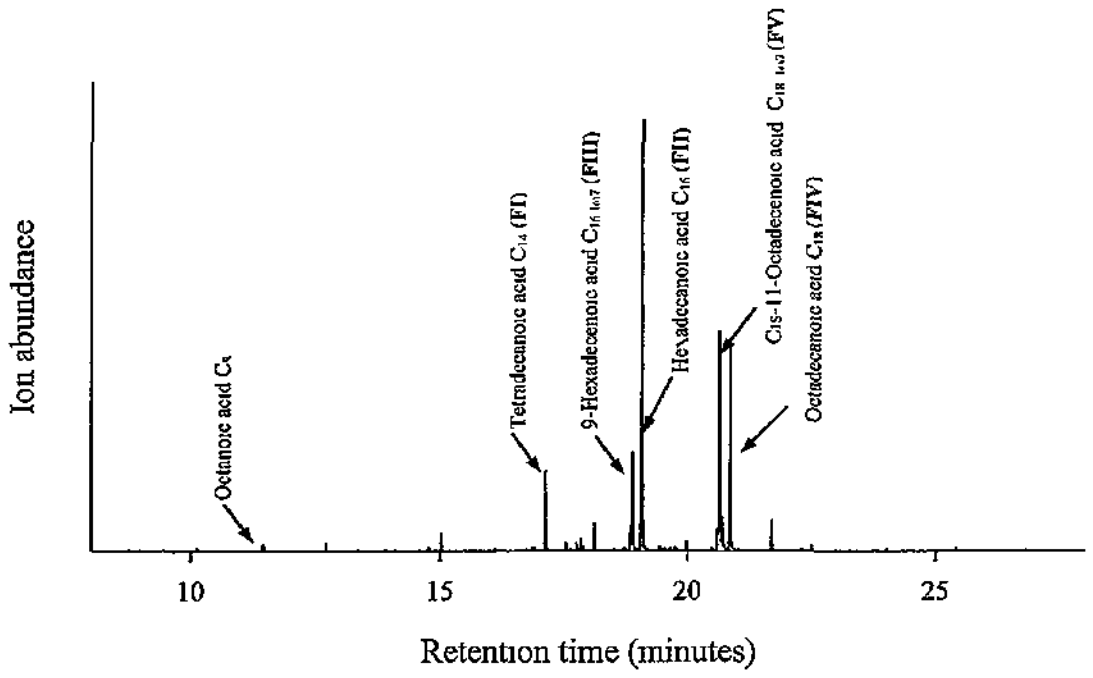

Figure 6 6-4 Partial TIC (*m/z* 117) GC/MS chromatogram of fatty acids (TMS) detected in filtered seawater collected during the spring bloom (March – April, 2010) from the high Arctic, north of Ellesmere Island to near the North Pole (89°53N).

6.6.3 Sterols in the water column

The sterol content of the 19 filtered seawater samples obtained from the Amundsen Gulf water column between 11/4/08 and 12/7/08 were measured (GC/MS), with sterols present in each sample Each of the sterols detected in sea ice samples (Chapter 4) were also detected in filtered seawater samples, except for **SVII**, which was not present in any seawater samples. The maximum combined concentration of the quantifiable detected sterols (**SII, SIII, SIV, SVI** and **SVIII**) for the period was observed in filtered seawater collected from ice-free water on 10/07/08 (4.1 x 10^{-3} mg m^{-3} water). The lowest sterol concentration (**SII, SIII, SIV, SVI** and **SVIII**) coincided with the lowest HBI and fatty acid concentrations in the latest sample collected on the 12/07/08 (1.3 x 10^{-4} mg m^{-3} water). Overall, the mean combined individual concentrations of the sterols (**SII, SIII, SIV, SVI** and **SVIII**) from all 19 samples was 1.5 x 10^{-3} ± 1 2 x 10^{-3} mg m^{-3}

water, making these sterols ca. 2 x 10^3 less concentrated in seawater than the same sterols in sea ice (Table 6-8). Consequently, of the HBIs, fatty acids and sterols, the latter represented the least change in concentration between sea ice and seawater. As such, sterol concentrations in sea ice and seawater are only ca. 2 orders of magnitude greater than **I** in sea ice and only ca. 4 orders of magnitude greater than **I** in the water column respectively (Table 6-8).

Table 6-8. Mean HBI (**I – IIId**), fatty acid (**FI – FV**) and sterol (**SII, SIII, SIV, SVI** and **SVIII**) lipid concentrations in sea ice (from Chapter 4) and filtered seawater samples.

		IP_{25}	Total HBIs	Total fatty acids	Total sterols
Sea ice	Mean concentration (mg m^{-3})	3.7×10^{-2}	1.5×10^{-1}	2×10^{2}	3.5
	Relative to **I**	1	4	5.4×10^{2}	95
Filtered seawater	Mean concentration (mg m^{-3})	4.5×10^{-8}	2.3×10^{-7}	2.1×10^{-2}	1.5×10^{-3}
	Relative to **I**	1	5	4.6×10^{5}	3.3×10^{4}
$\left({}^{Sea\ ice}/_{Filtered\ seawater}\right)$		8.2×10^{5}	6.5×10^{5}	9.5×10^{3}	2.3×10^{2}

Similar to HBI and fatty acid concentrations, sterol concentrations also fluctuated both between samples and through time with no visible parallel to HBIs or fatty acids ($r = < 0.4$) (Figure 6.6-5).

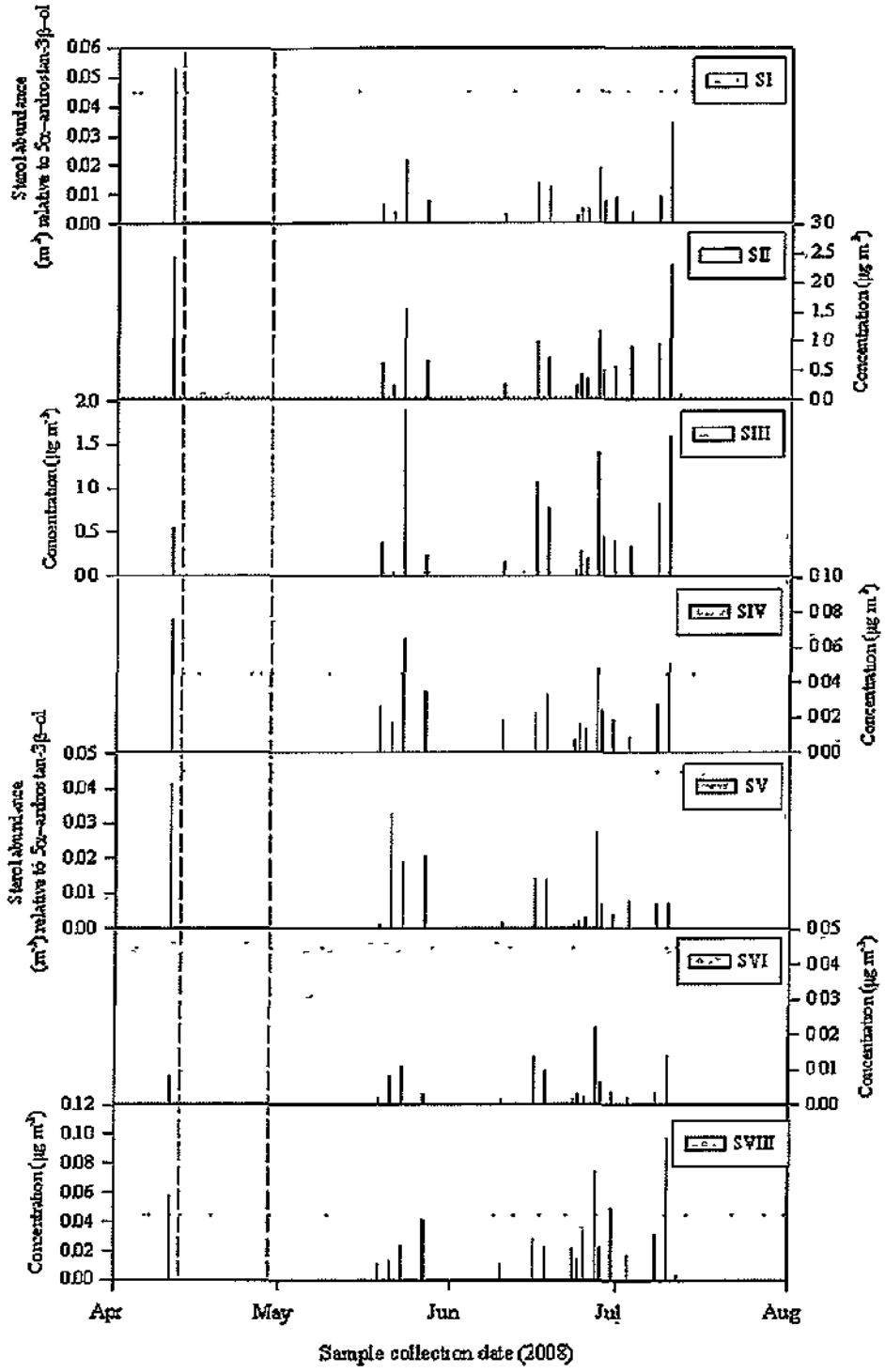

Figure 6.6-5. Temporal concentration of individual sterols (**SI, SII, SIII, SIV, SV, SVI** and **SVIII**) per m^3 of water observed in filtered seawater (> 20 µm) during the IPY-CFL cruise (1/4/08 to 1/8/08); Vertical grey dashed lines represent a temporary break in sampling, horizontal dotted lines represent 1000 times the mean concentration of **I** in plankton (45 ng m^{-3}).

The distribution of the recorded, quantified sterols, relative to each other, differed between sea ice and seawater with a minor increase (ca. 13%) in **SII** from sea ice to the water column (Table 6-9). Larger differences were apparent with the remaining sterols where **SIII**, increased ca. 77%, while **SIV**, **SVI** and **SVIII** decreased by ca. 69%, 76% and 95% respectively from sea ice to the water column. Despite these considerable changes, **SII** remained the most abundant sterol in both sea ice and seawater.

Table 6-9. Mean concentrations (mg m^{-3}) and relative distribution s (%) of sterols observed in filtered water samples (> 20 μm) and sea ice (from Chapter 4) during the IPY-CFL cruise.

	SII	**SIII**	**SIV**	**SVI**	**SVIII**
Mean concentration (mg m^{-3})	8.1×10^{-4}	5.7×10^{-4}	2.8×10^{-5}	6.3×10^{-6}	3.1×10^{-5}
Relative distribution (%) of sterol concentrations in filtered seawater	45.3	31.9	1.6	0.4	1.8
Relative distribution (%) of sterol concentrations in sea ice	51.5	7.4	5.16	1.7	34.0

Importantly, the ratio of total fatty acids (**FI – FV**) to total sterols, (**SII, SIII, SIV, SVI** and **SVIII**) measured in both sea ice (ca. 57) and seawater (ca. 13) reflected those previously reported by others in Antarctic sea ice (in sea ice = 15 - 66; Nichols *et al.*, 1993) and Arctic seawater during Spring (in seawater = 1 - 10; Yunker *et al.*, 1995), adding confidence to assigning the predominantly seawater, rather than sea ice source of fatty acids and sterols detected in seawater during this study.

As with the fatty acids, all sterols used in this study (**SI - SVIII**) were also present in the high Arctic (Ellesmere to the North Pole) filtered seawater samples, with the exception

of SV, that were collected during the bloom period (March – April) in 2010. The combined concentration of which was 1.5 x 10^{-3} mg m^{-3}, similar to the Amundsen Gulf which was also 1.5 x 10^{-3} mg m^{-3}.

6.6.4 Comparison of water column lipids

Multivariate analysis of lipids in the water column was carried out on HBIs, fatty acids and sterols using PCA in an attempt to classify compounds according to their primary source, e.g. marine, terrestrial, animal etc. (Figure 6.6-6). The PCA model was reasonably robust, using 10 variables and 18 observations. However, sufficient variation was not accounted for in the first two PCs (51%), requiring three axes (accounting for 68% of the variation) to enable better interpretation

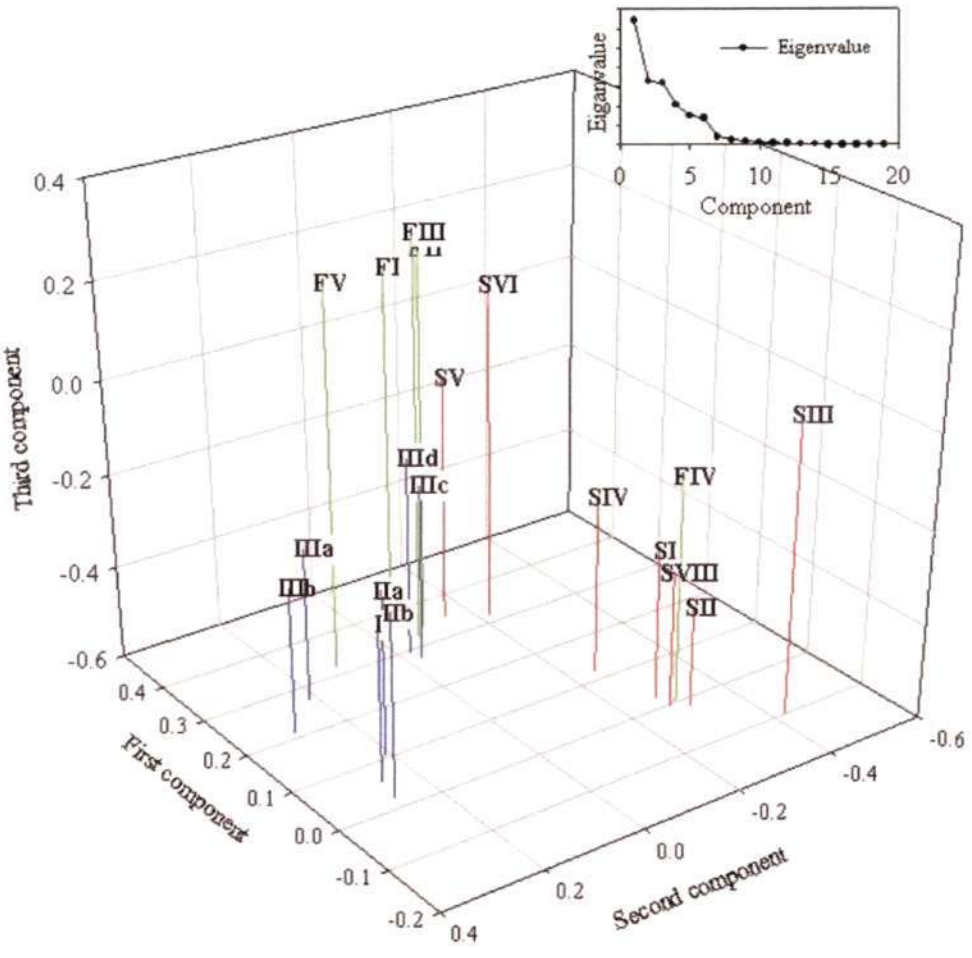

Figure 6.6-6. First, second and third component variable (loadings) plot of the principal components analysis for biomarkers recorded in filtered seawater (> 20 µm) during the IPY-CFL cruise 2008. Proximity of compounds in three dimensions is a function of *covariance*. *Red = sterols (**SI** to **SVIII**), green = Fatty acids (**FI** to **FV**), blue = HBIs (**I** to **IIId**)*. Inset: Eigenvalue plot showing the proportion of variability accounted for by the first three components (68%).

Distinct grouping was evident in both the sterols and fatty acids, with vertical spread reflecting variation within each group. While sterols **SV** and **SVI** were grouped in close proximity to the main abundant fatty acids (**FI**, **FII** and **FIII**), the remaining sterols (**SI**, **SII**, **SIII**, **SIV** and **SVIII**) were positioned near to each other and **FIV**. Further grouping was evident in the HBIs with three groups forming: (**I**, **IIa**, **IIb**), (**IIIa**, **IIIb**) and (**IIIc**, **IIId**) where the latter was nearest to the fatty acids and phytosterols. It is worth noting that the low concentration of some compounds, especially, **IIa** (2% of the total HBI concentration) may have resulted in poor spatial representation in the PCA model.

Additionally, the inability of the model to represent a preferred proportion (> 70%) of the data within two or three components suggests that interpretations should be considered with caution.

6.6.5 Highly branched isoprenoids in bulk zooplankton

Collection of *Calanus* sp. copepods on four dates (16th and 21st April and 17th and 30th May 2008) enabled determination (GC/MS) of the HBI lipid content of these heterotrophic zooplankton in the Amundsen Gulf water column coincident with the presence of sea ice and collection of seawater samples. Analyses of *Calanus* sp. revealed the presence of each HBI previously detected in sea ice and seawater during this study (**I – IIId**) in all four samples. Concentrations of the combined individual HBIs (**I - IIId**) in *Calanus* sp. zooplankton (> 710 μm) were determined for dry mass and ranged from 15 ng g^{-1} on 16/4/08 to 30 ng g^{-1} on 17/5/08 (Figure 6.6-7). The distribution of HBIs, relative to one another, in zooplankton (Table 6-10) show an overall decrease of **I** compared to filtered seawater and sea ice, yet further analysis revealed that **I** increased in concentration through time, most likely following ingestion by pelagic or sympagic zooplankton (Figure 6.6-8).

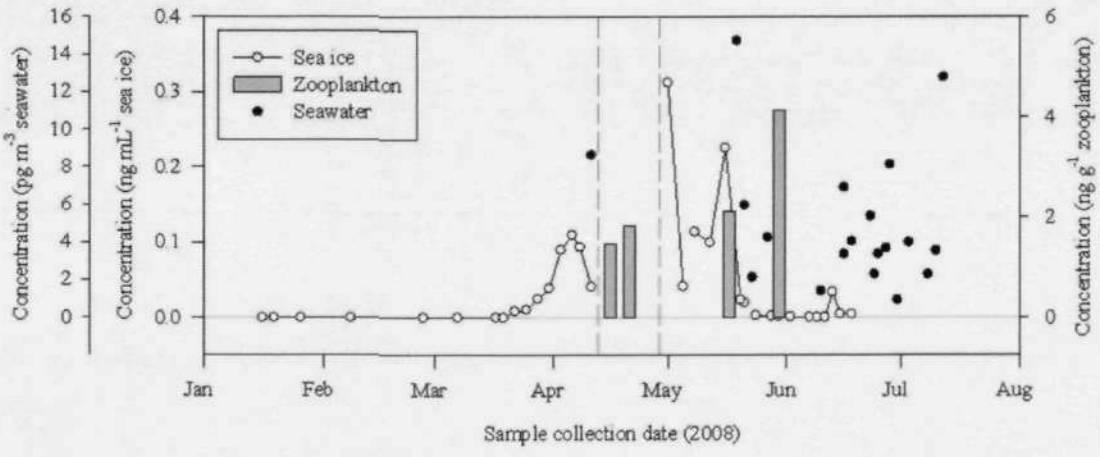

Figure 6.6-7. Temporal concentration of total HBIs (**I** to **IIId**) observed in Arctic sea ice (ng mL^{-1}), phytoplankton (ng g^{-1}) and zooplankton (ng g^{-1}) observed in filtered seawater (> 20 μm; > 710 μm respectively) during the IPY-CFL cruise (1/1/08 to 1/8/08); Vertical grey dashed lines represent a temporary break in some sampling.

Table 6-10. Relative distribution of HBI isomers observed in zooplankton (> 710 μm), filtered seawater (> 20 μm) and sea ice (from Chapter 4) during the IPY-CFL cruise 2008.

	I	**IIa**	**IIb**	**IIIa**	**IIIb**	**IIIc**	**IIId**
Relative distribution (%) of HBI concentrations in zooplankton	11.0	8.9	15.4	0.0	44.4	11.8	8.5
Relative distribution (%) of HBI concentrations in filtered seawater	19.7	2.2	23.1	11.0	23.4	6.9	13.7
Relative distribution (%) of HBI concentrations in sea ice	27.2	1.7	31.4	1.0	28.1	0.8	9.8

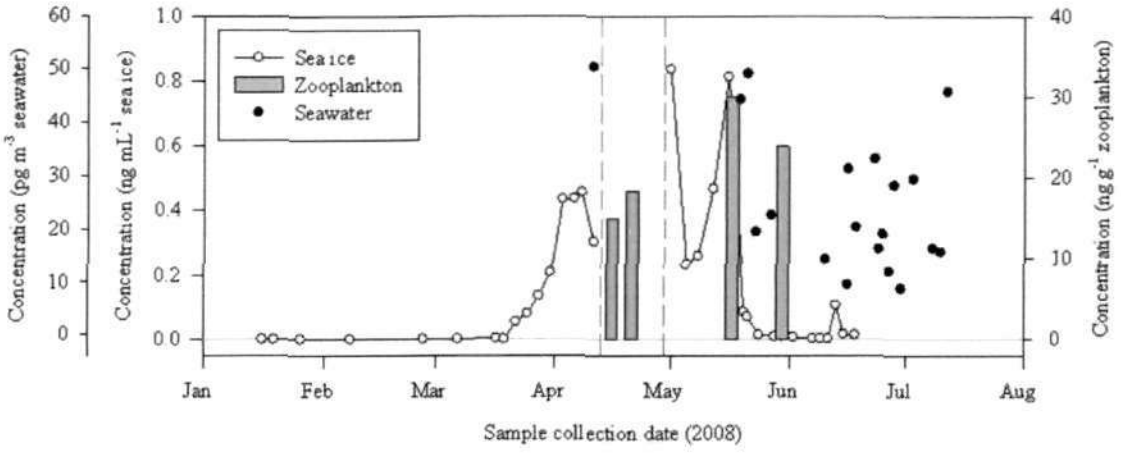

Figure 6.6-8. Temporal concentration of **I** observed in Arctic sea ice (ng mL^{-1}), phytoplankton (ng g^{-1}) and zooplankton (ng g^{-1}) observed in filtered seawater (> 20 µm; > 710 µm respectively) during the IPY-CFL cruise (1/1/08 to 1/8/08); Vertical grey dashed lines represent a temporary break in some sampling.

In contrast to sea ice and seawater distributions of individual HBIs, relative to one another, HBIs detected in zooplankton comprised greater proportions of **IIa**, **IIIb** and **IIIc** (9%, 44% and 12%) while **I** and **IIb** became less dominant (11% and 15% respectively) compared to distributions previously recorded in sea ice (27% and 31% respectively; Table 6-10). N.B. Fatty acids and sterols were not determined for *Calanus* sp. since many published data reveal a ubiquitous suite of these lipids that are biosynthesised within the organisms that would consequently mask any diatomaceous contribution (e.g. Fraser *et al.*, 1989).

6.6.6 Highly branched isoprenoids in macrofaunal specimens

A qualitative assessment of the HBI content of specimens from a range of macrofaunal organisms (Figure 6.6-9 and Figure 6.6-10) revealed detectable (GC/MS) contributions of the HBIs previously detected in sea ice, seawater and zooplankton in seven of the nine animals (Table 6-11).

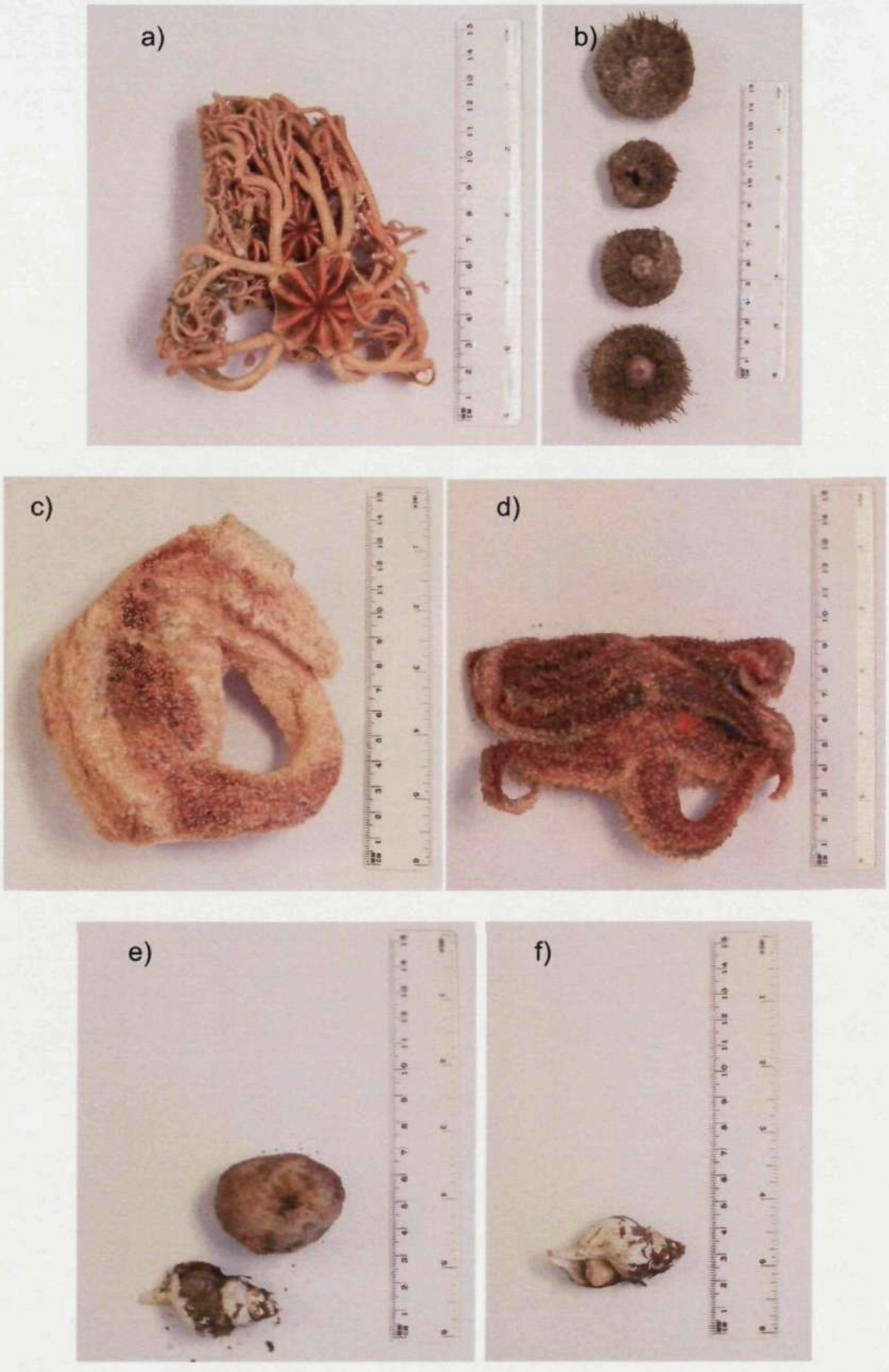

Figure 6.6-9. Macrofaunal specimens collected for lipid analysis from Agassiz net trawls in Franklin Bay during the IPY-CFL cruise 2008. a) basket star, b) Arctic sea urchins (*Strongylocentrotus sp.)*, c) starfish-a, d) starfish-b, e) anemone, f) snail collected from South West England by divers, 2010.

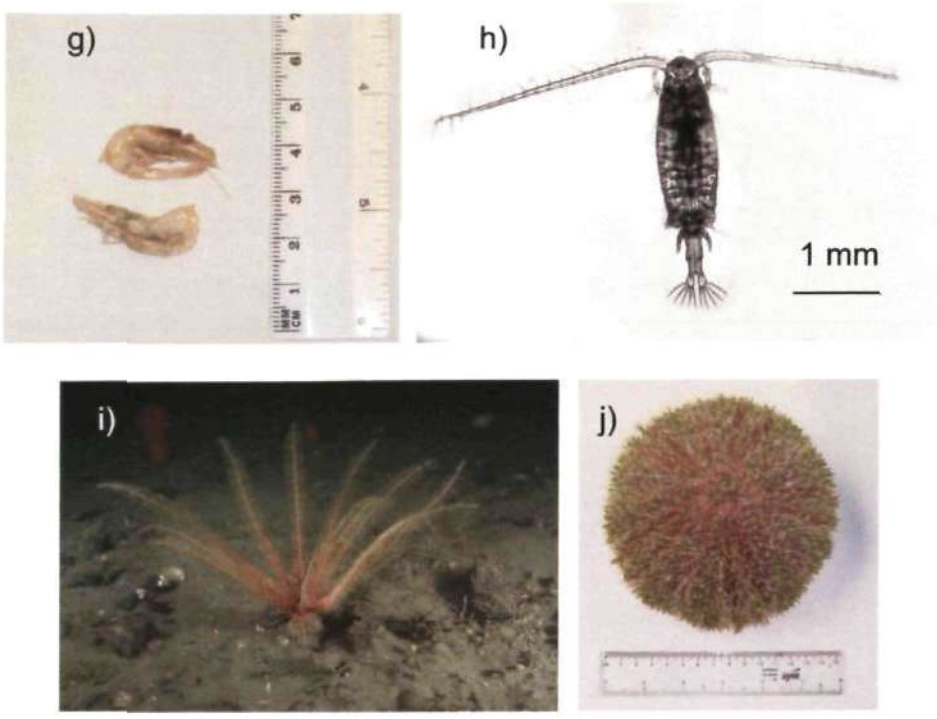

Figure 6.6-10. Macrofaunal specimens collected for lipid analysis from Agassiz net trawls in Franklin Bay during the IPY-CFL cruise 2008. g) shrimp, h) copepod, i) feather star and j) temperate water sea urchin, *Echinus esculentus* collected from South West England by divers, 2010.

Table 6-11. Distribution (%) of HBIs in macrofaunal specimens collected for lipid analysis from Agassiz net trawls in Franklin Bay and Darnley Bay during the IPY-CFL cruise 2008.

HBI distribution (%)	I	IIa	IIb	IIIa	IIIb	IIIc	IIId
Basket star	*	*	*	*	*	*	*
Arctic sea urchin	47.2	3.8	33	2.3	6.8	3.2	3.8
Starfish a	28.8	14.0	24.4	5.8	11.9	6.7	8.4
Starfish b	36.5	4.9	46.6	2.1	4.8	2.5	2.6
Anemone	*	*	*	*	*	*	*
Snail	34.3	3.9	22.4	7.7	12.5	8.4	10.7
Shrimp	41.4	4.1	33.6	2.6	13.3	1.7	3.3
Epibenthic Copepod	35.2	10.6	30.0	3.8	9.5	5.8	5.1
Featherstar	21.0	2.0	18.6	10.4	29.6	9.9	8.5
Mean distribution % ± 1 s.d.	34.9 ± 8.4	6.2 ± 4.4	29.8 ± 9.3	5 ± 3.2	12.6 ± 8.1	5.5 ± 3.1	6.1 ± 3.1

* No HBIs detected.

In contrast, neither the echinoderm (basket star; Figure 6.6-10a) nor the cndarian (anemone; Figure 6.6-10e) contained any detectable HBIs. In specimens containing

HBIs the distribution of these lipids, relative to one another varied between specimens, with either **I**, **IIb** or **IIIb** being the most abundant in each specimen analysed (Table 6-11). Overall, the mean distribution of HBIs, relative to each other, for all macrofaunal specimens analysed was dominated by **I** and **IIb** (ca. 35% and 30% respectively), representing HBI distributions more comparable with those measured in sea ice rather than those in zooplankton or seawater (Table 6-12).

Table 6-12. Relative distribution of HBI isomers observed in macrofaunal specimens, zooplankton (> 710 μm), filtered seawater (> 20 μm) and sea ice (from Chapter 4) during the IPY-CFL cruise (1/4/08 to 1/8/08).

	I	**IIa**	**IIb**	**IIIa**	**IIIb**	**IIIc**	**IIId**
Relative distribution (%) of HBI concentrations in the macrobenthos	34.9	6.2	29.8	5.0	12.6	5.5	6.1
Relative distribution (%) of HBI concentrations in zooplankton	11.0	8.9	15.4	0.0	44.4	11.8	8.5
Relative distribution (%) of HBI concentrations in filtered seawater	19.7	2.2	23.1	11.0	23.4	6.9	13.7
Relative distribution (%) of HBI concentrations in sea ice	27.2	1.7	31.4	1.0	28.1	0.8	9.8

Statistical comparison of the HBI distributions, relative to each other, in sea ice and filtered seawater ($r = 0.93$) and sea ice and zooplankton ($r = 0.59$) revealed a decreasing similarity to HBI distributions initially measured in sea ice (Table 6-13). In contrast, comparison of these relative HBI distributions in sea ice to macrofaunal specimens ($r = 0.83$), indicates an increased similarity of the HBI distributions found in sea ice.

Table 6-13. Correlation matrix of HBI distribution, relative to each other, in macrofaunal specimens, zooplankton (> 710 µm), filtered seawater (> 20 µm) and sea ice (from Chapter 4) during the IPY-CFL cruise (1/4/08 to 1/8/08). Correlations in bold are significant (10%) where n = 7.

	Relative distribution (%) of HBI concentrations in the **macrobenthos**	Relative distribution (%) of HBI concentrations in **zooplankton**	Relative distribution (%) of HBI concentrations in **filtered seawater**
Relative distribution (%) of HBI concentrations in **zooplankton**	R = 0.14; $p = 0.8$		
Relative distribution (%) of HBI concentrations in **filtered seawater**	R = **0.69**; $p = 0\ 08$	R = **0.58**; $p = 0.17$	
Relative distribution (%) of HBI concentrations in **sea ice**	R = **0.83**, $p = 0\ 02$	R = **0.59**; $p = 0\ 16$	R = **0.93**; $p = 0.002$

More detailed analysis (GC/MS) of the Arctic sea urchin (*Strongylocentrotus* sp. Figure 6.6-9b) revealed a range of compounds not previously observed in sea ice, filtered seawater or zooplankton during this study. Retention time and mass spectral analysis, combined with hydrogenation and co-injection of C_{25} HBI alkane and alkene standards suggested these were also HBIs, with comparison to published data confirming the structures of some, while others appeared to be previously unreported In addition to the HBIs recorded throughout this study (**I – IIId**), an extra 5 di-unsaturated HBIs (**II**) with *m/z* 348, 1 tri-unsaturated HBI (**III**) with *m/z* 346, 2 tetra-unsaturated HBIs (**IV**) with *m/z* 344 and a penta-unsaturated HBI (**V**) with *m/z* 342 were observed (Figure 6.6-11).

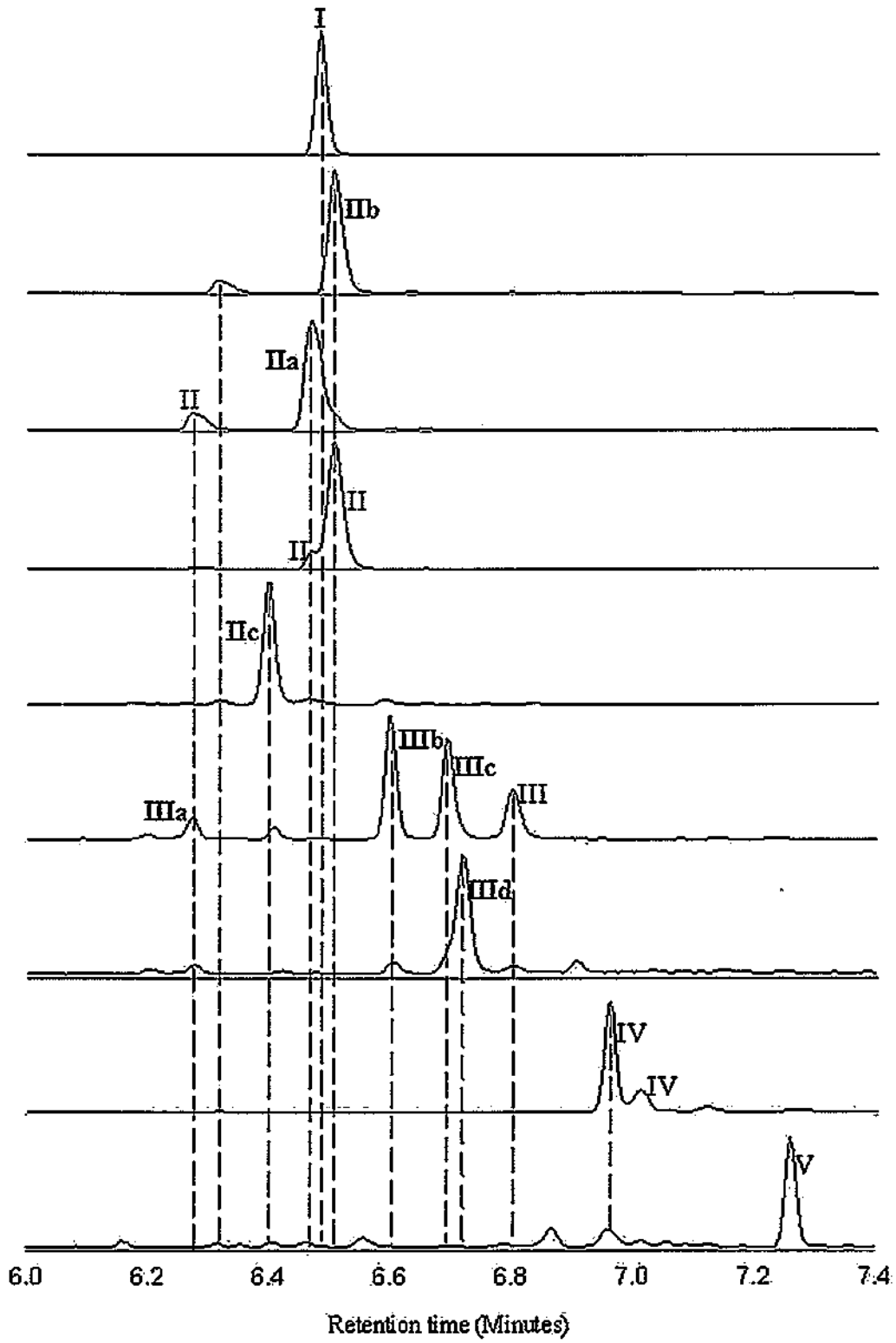

Figure 6.6-11. Partial TIC chromatograms of fractions obtained from Ag^+ (ChromSpher 5 lipids) prep. HPLC of the apolar hydrocarbon fraction of Arctic sea urchin (*Strongylocentrotus* sp.) collected during the IPY-CFL cruise 2008. HBIs used throughout this study are in bold, with some abundant additional HBIs labelled according to unsaturation; di-unsaturated II, tri-unsaturated III, tetra- unsaturated IV and penta- unsaturated V.

HPLC purification (Ag^+ Chromospher 5 lipids) of some of the HBIs isolated from *Strongylocentrotus* sp. yielded sufficient quantities of these lipids (ca. 0.5 - 5 μg) for ^{13}C stable isotope analysis (Table 6-14) where **I**, **IIa**, **IIb** and **IIc** were all found to be relatively enriched in ^{13}C in comparison to ^{12}C, with **I** and **IIa** the most and **IIc** the least.

Table 6-14 Summary of main HBIs (and respective $\delta^{13}C$) isolated by Ag^+ (Chromspher 5 lipids) preparatory HPLC from Arctic sea urchins collected during the IPY-CFL cruise 2008.

HBI	$\delta^{13}C$ (‰)
I	-17 1 ± 0 5
IIa	-17 1 ± 0 6
IIb	-17 9 ± 0 2
IIc	-19 8 ± 0 6

Determination of the fatty acid content of *Strongylocentrotus* sp. also revealed a range of saturated, mono- and polyunsaturated fatty acids (Figure 6.6-12) with considerable proportions of the fatty acids **FI**, **FII** and **FIII** present (13%, 20% and 32% respectively, of total fatty acids detected). Cholesterol was also present as the dominant sterol.

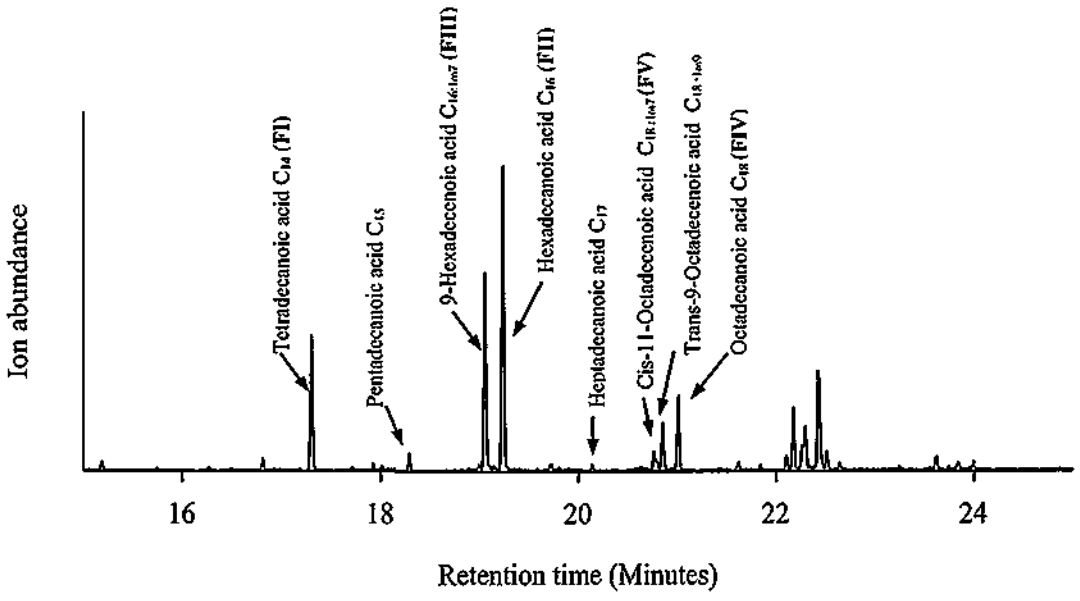

Figure 6.6-12. Partial selective ion monitoring (*m/z* 117) chromatogram of the hexane extractable lipids obtained from the hydrolysed, saponified fraction, of sea urchins collected during the IPY-CFL cruise 2008. Abundant fatty acids are identified with those used in the current study suffixed with **FI, FII, FIII, FIV, FV** and **FVI**.

An analogous approach to the lipid analysis of the Arctic sea urchin, *Strongylocentrotus* sp. was carried out on the temperate water sea urchin, *Echinus esculentus* (Figure 6.6-10j) to establish the uniqueness of the range of HBIs observed in the Arctic Species. While it was found that *E. esculentus* did contain a similar 'extended' suite of HBIs beyond those routinely used in this study, the sea ice diatom biomarker **I** was not present. However, **IIb, IIc, IIIa, IIIb** and **IIIc** were all present and although quantification was not possible, they appeared to make an important contribution to the overall HBI distribution in this species (Figure 6.6-13).

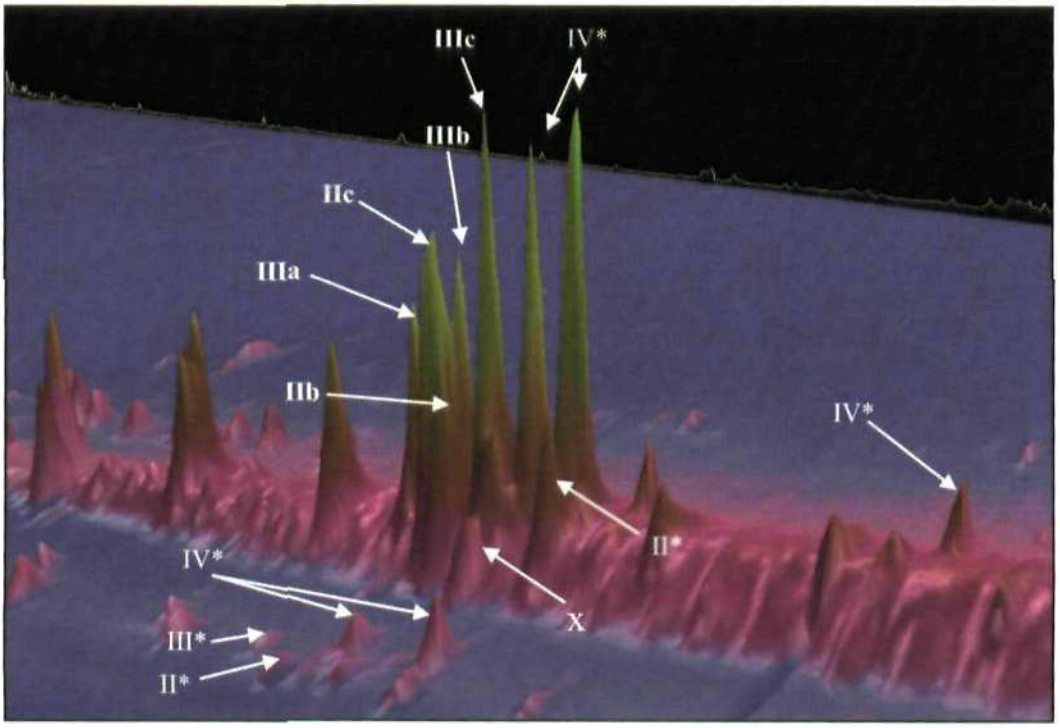

Figure 6.6-13. Partial GC-GC/ToF MS TIC chromatogram of the apolar hydrocarbon fraction of the temperate sea urchin *Echinus esculentus,* collected from South West England, 2010. HBIs used throughout this study are in bold (**I** – **IIIc**), with some abundant additional HBIs labelled according to unsaturation; saturated alkane – **x**, di-unsaturated – **II***, tri-unsaturated - **III***, tetra-unsaturated - **IV*** and penta-unsaturated **V***, based on mass spectral similarities to published HBIs and hydrogenation to parent $C_{25:0}$ structure.

Importantly, the presence of a saturated C_{25} HBI ($C_{25:0}$) was confirmed by co-injection of a standard, along with GC retention and mass spectral comparison, representing the first documented appearance of this HBI in the environment (Figure 6.6-13). Further, the presence of previously unidentified HBIs was also confirmed by interpretation of mass spectral data prior to hydrogenation and co-injection of the C_{25} HBI alkane standard (Figure 6.6-14).

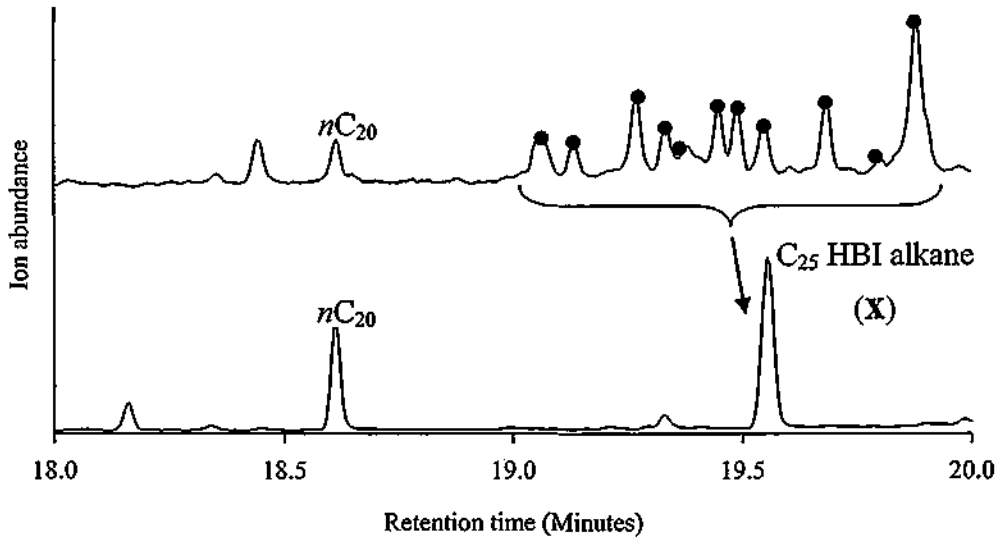

Figure 6.6-14. Partial GC/MS TIC chromatogram of the apolar hydrocarbon fraction of the temperate sea urchin *Echinus esculentus,* collected from South West England, 2010. Top: C_{25} HBIs (black dots). Bottom: the resulting hydrogenation product; C_{25} HBI alkane (X), following hydrogenation of the mixture of HBIs (top).

6.7 Discussion

6.7.1 Presence and distribution of lipids in filtered seawater samples

Initial collection of filtered seawater samples was restricted by the presence of sea ice in the Amundsen Gulf with the first sample being collected through a hole made by divers in the ice intended for other sampling (11/4/08). Later in the spring some areas of sea ice began breaking and drifting northwest into the Beaufort Sea presenting areas of both sea ice and open water from 19/5/08. While providing the opportunity to sample the water column, this mix of sea ice and open water could have been a factor responsible for the irregular distribution of lipids in the water column. While the distribution of planktonic algae in the water column has previously been observed by some to be sporadic (Michel *et al.*, 2006), fluctuations in overall lipid concentrations may also have resulted from ship mobility, or potential modification or mobility of the pre-measured chlorophyll *a* maximum depth within the water column due to the complexity of the environment at this time. Although concentrations of each class of lipid varied greatly through time on a localised scale (Figure 6.6-1, Figure 6.6-3 and Figure 6.6-5) the presence of all HBIs (except **IIa** in some samples), fatty acids and sterols (except **SVII**) that were also detected in sea ice reveal the extent of interconnectivity between sea ice and seawater habitats in this region of the Arctic at least, consistent with the finding of previous studies (Brown, 2007). In contrast, filtered seawater samples collected from the high Arctic during the sea ice bloom period in 2010 revealed the presence of only fatty acids and sterols in the water column beneath multiyear sea ice north of Ellesmere Island to the North Pole The absence of HBIs beneath thicker (ca 2 – 5 m) multiyear sea ice was not surprising since significant light attenuation, most likely resulting from thicker ice that is often covered in snow, will restrict PAR required by diatoms for photosynthesis and therefore existence. Interestingly, the presence of fatty acids and

sterols, in the absence of HBIs, in the high Arctic help validate the likely non-sea ice diatom sources of many of these lipids suggested in previous chapters (Chapters 4 and 5).

In the Amundsen Gulf however, differences in lipid concentrations between sea ice and the water column were anticipated to reflect the relative source (ice/water) contribution of each lipid class, with HBIs displaying the greatest relative change between sea ice and seawater (6.5×10^5) and sterols the least (2×10^3) (Table 6-8). The greater difference in sea ice and seawater concentrations of HBIs is therefore believed to indicate the reduced production of these lipids in seawater compared to sea ice. Although some HBIs are known to have planktonic sources (Belt *et al.*, 2001c) that may bias this approach, the even greater change in concentration between sea ice and seawater of **I** (8.2×10^5) adds further confidence in assigning this biomarker, at least, as being exclusive to sea ice. It is therefore hypothesised that there is little to no contribution of **I** from the water column other than that originating from the sea ice itself following melting. In contrast, the comparably reduced differences observed in the fatty acids and sterols between sea ice and seawater concentrations suggested a significant presence of these lipids already in the water column. The concentration of these lipids relative to each other (Fatty acid/Sterol) is also representative of previously reported planktonic distributions (Nichols *et al.*, 1993; Yunker *et al.*, 1995). In further support of the hypothesis generated in Chapter 5 (the presence of many fatty acids and sterols in some parts of the sea ice was a result of seawater intrusion to the porous bottom few centimetres of sea ice), the relative differences between lipid classes in both sea ice and seawater (Table 6-6) reveal increased relative concentrations of these lipids of at least two orders of magnitude, relative to **I**, from sea ice to the water column. Finally, the apparent differences in contribution of HBIs, fatty acids and sterols was implied by the grouped PCA projection where seawater fatty acids, sterols and

seemingly planktonic HBIs are positioned apart from the other HBIs (**I**, **IIb** and **IIIb**) that displayed a relative decrease in distribution from sea ice to seawater.

6.7.2 Presence and distribution of lipids in zooplankton samples

Determination of the relative distribution of HBIs in pelagic zooplankton (Table 6-10) was achieved over four dates coincident with sea ice and filtered seawater samples (Figure 6.6-7). The lipid content of zooplankton was analysed to establish the grazing and HBI bioaccumulation potential in the early stages of the Arctic food web with consideration to dispersal or removal of the sea ice biomarker **I** With the exception of **IIIa**, each of the HBIs, including **I**, recorded in sea ice and seawater were present in the lipids of *Calanus* sp. zooplankton indicating a mixed sea ice/seawater diet of these organisms. Interestingly, the contribution of **I**, relative to other HBIs, in zooplankton decreased further, in addition to the decrease previously recorded from sea ice to seawater (Sea ice, 27.2%, seawater; 19 7% and zooplankton; 11%; Table 6-10), with **IIb** also decreasing further (Sea ice, 31.4%, seawater; 23.1% and zooplankton; 15.4%, Table 6-10). The resulting distribution of the HBIs, relative to one another, in *Calanus* sp. therefore represented more closely the HBI distribution observed in seawater than sea ice (Table 6-10) In contrast, **IIa**, **IIIb** and **IIIc** increased in distribution, relative to the other HBIs, from sea ice, to seawater, to zooplankton (Table 6-10). These changes in relative HBI distribution may provide important information on the diet of some Arctic heterotrophs, enabling determination of dietary preferences between sea ice and planktonic algae in some organisms at least The potential increase of **I** in the lipids of *Calanus* sp. through time (Figure 6.6-8) suggests some potential for bioaccumulation in this organism, yet the mixed contribution of the HBIs most likely indicates a non-

selective diet for this species at least. The potential for accumulation in these organisms and redistribution of either diatoms and potentially **I** is however clear.

6.7.3 Presence and distribution of lipids in macrofaunal specimens

Collection of macrofaunal organisms was carried out coincident with collection of sea ice, filtered seawater and zooplankton (16/6/08) to assess the relative distribution of HBIs in a representative suite of individual macrofaunal specimens in the Amundsen Gulf (5 echinoderms, 1 crustacean, 1 gastropod and a cnidarian; Figure 6.6-9 and Figure 6.6-10). While HBIs were not detected in all of the Arctic specimens collected (Table 6-11), those that did contain HBIs were found to have each isomer previously identified in sea ice, seawater and zooplankton, suggesting a non-selective means of accumulation. In one specimen (*Strongylocentrotus* sp.) a number of additional HBIs were also detected (Figure 6.6-11). Typically, the distribution of HBIs relative to each other, in the seven specimens that did contain these lipids, was most closely comparable to sea ice distributions ($r = 0.83$ $p = 0.02$), being dominated by **I** and **IIb** (ca. 34.9% and 29.8% respectively; Table 6-12). The remaining HBI distributions, relative to one another, were variable, with contributions of **IIIa**, **IIIb**, **IIIc** and **IIId** appearing as a composite of sea ice, seawater and zooplankton distributions (Table 6-12). Variation in the HBI distributions between organisms was also evident (Table 6-11). Some specimens appeared biased towards the more unsaturated HBIs where, for example, the featherstar comprised 58% tri-unsaturated HBIs (**IIIa**, **IIIb**, **IIIc** and **IIId**), while others appeared to favour the more saturated HBIs (e.g. *Strongylocentrotus* sp., shrimp and epibenthic copepod), with 84% of the HBIs in *Strongylocentrotus* sp. comprised of **I**, **IIa** and **IIb**. In addition to the HBIs common to sea ice, seawater and zooplankton, *Strongylocentrotus* sp. also contained 4 di-unsaturated HBIs, another tri-unsaturated

HBI, two tetra-unsaturated HBIs and a penta-unsaturated HBI (Figure 6.6-11) With the potential for biosynthesis of HBIs by *Strongylocentrotus* sp. ruled out following determination of the distinctive sea ice carbon isotope composition of some of the HBIs (Table 6-14), an alternative was suggested, the presence of these additional HBIs was hypothesised to indicate the potential ability of this organism to bioaccumulate HBIs through ingestion, with the consequence that HBI concentrations previously below the limit of GC/MS detection became sufficiently concentrated for detection in the lipids of this organism. In support of this, the fatty acid content of *Strongylocentrotus* sp. was also determined, exposing a suite of fatty acids containing fewer varieties, compared to those of sea ice or seawater. Importantly, these comprised mainly of fatty acids considered to be of diatom origin (65%; **FI, FII** and **FIII**), and therefore indicative of diatom ingestion (Figure 6.6-14). This hypothesis was further supported by HBI analysis of the lipid content of a temperate marine sea urchin (*Echinus esculentus*; Figure 6.6-10j) which also contained a varied suite of readily detectable HBIs (Figure 6.6-13). Further, microscopic analysis of the stomach content of *Strongylocentrotus* sp. and *Echinus esculentus* showed the diet of these organisms involved diatoms of both planktonic and benthic varieties (including sea ice diatom species for the Arctic *Strongylocentrotus* sp.) Finally, the presence of some hitherto unidentified HBIs (structurally confirmed by GC mass spectral analysis, hydrogenation and co-injection of HBI standards, Figure 6.6-14) in both *Strongylocentrotus* sp and *Echinus esculentus* indicate the significance of these organisms in the accumulation and possible redistribution of HBIs in both Arctic and temperate environments.

6.8 Conclusion

The ubiquitous presence of all HBIs (**I** – **IIId**) in at least some filtered seawater samples was determined during sea ice break-up. The distribution of HBIs, relative to each other, in the water column revealed similarities to those observed for sea ice, with **I** and **IIb** being slightly less prominent than in sea ice, yet remaining highly abundant and well correlated to each other, while increases in the relative abundance of **IIIa**, **IIIc** and **IIId** also occurred.

Differences in HBI concentrations between sea ice and the water column resulting, most probably from dispersion following sea ice melt, was quantified at approximately 6.5 x 10^5. This value appears reasonable assuming a degree of dispersion and dilution in the water column in comparison to the concentrated colonisation of sea ice brine channels. Of all the lipids measured, **I** was also found to be the most diluted lipid in the water column compared to sea ice (8.2 x 10^5), providing further evidence for the sea ice specificity of this biomarker. Fatty acids and sterols were also found to become more dilute in the water column, although the probable planktonic source of at least some of these lipids in sea ice appeared to attenuate the magnitude of this during comparisons.

Finally, the presence of numerous HBIs in pelagic fauna, in addition to readily detectable quantities of these lipids in some benthic fauna revealed a previously unknown extent of bioaccumulation that also presented numerous novel HBIs for detection in both polar and temperate regions. The extent to which this bioaccumulation results in removal or redistribution of HBIs remains unknown at this point.

CHAPTER SEVEN

7 HBI preservation in Arctic sediments

7.1 Introduction

Chapter 7 investigates the short term (< 500 yrs) preservation of IP_{25} and other HBIs following the deposition of these lipids in marine sediments of the Amundsen Gulf region of the CAA. The detailed sedimentary analysis of IP_{25} and other HBIs carried out on a pair of box cores (St 405b and St 1216) obtained from the Amundsen Gulf is discussed. Cores were selected to represent regions of both deep, offshore, reduced biological activity, and shallow, near shore, high biological activity environments respectfully. A variety of geochemical approaches were adopted to investigate the possible influences capable of supplementing either preservation or decomposition of IP_{25} and polyunsaturated HBIs in both locations. Four additional sediment cores were also analysed to complement the initial findings.

7.1.1 Biomarker preservation in Arctic sediments

The preserved lipid component of many biological organisms can be unambiguously linked to their source, providing a proxy for historical observations (e.g. Eglinton *et al.*, 1967; Brassell *et al.*, 1986; Killops *et al.*, 1993; Smart, 2002; Eglinton *et al.*, 2008). However, many biomarkers, such as chlorophylls and fatty acids posses functional groups or are unsaturated (Armstrong *et al.*, 1991; Killops *et al.*, 1993). Consequently, biomarkers in sediments often undergo diagenesis which usually entails a degree of defunctionalisation and either reduction (hydrogenation) or aromatisation. The sustained

utility of these diagenetic products is, however, evident in the number of successful Arctic climate studies based on marine sediment geochemical analysis over many years (e.g. Scalan *et al.*, 1970; Wen-Yen *et al* , 1976; Billett *et al* , 1983; Calvert *et al.*, 1993; Schubert *et al* , 1996, Belt *et al* , 2007, Andrews *et al* , 2009; Vare *et al* , 2009; Belt *et al.*, 2010, Vare *et al.*, 2010) The reliability of the biomarker approach to climate reconstruction through sediment analysis is further strengthened by the development and application of multi-proxy methods including techniques such as X-ray fluorescence (XRF and ITRAX) that enable precise scrutiny of the inorganic sediment composition (Rothwell *et al.*, 2006; Rolland *et al.*, 2009). For example, effective use of this non-destructive approach to geochemical analysis (Croudace *et al.*, 2006) was carried out by Vare *et al* , (2009), who successfully adopted ITRAX to determine the consistency of the sedimentary profile in a high resolution (5 mm) investigation of IP_{25} in the Barrow Strait region of the CAA

The interpretation of biomarkers in sediments is ideally carried out on a chronological sequence dictated by sedimentation. This process of sediment and biomarker deposition and subsequent burial occurs in Arctic marine sediments, sometimes generating a largely undisturbed record of biomarkers such as IP_{25} (Belt *et al.*, 2000b; Belt *et al* , 2007, Belt *et al.*, 2008, Massé *et al.*, 2008; Vare *et al* , 2009; Belt *et al.*, 2010; Vare *et al* , 2010). However, physical interactions of the land and ocean, often resulting from the geographical features of a region such as the CAA, can limit the ability of sediments to consistently record accurate palaeo signals. Ocean currents, terrestrial runoff, biological disturbances and glaciation are all examples of geographically inferred biotic and abiotic influences capable of removing, redistributing or disturbing the sedimentary record.

7.1.2 Arctic sedimentation rates and lipid burial

The Arctic Ocean is considered semi closed and subject to significant terrigenous inputs from erosion, water runoff and fluvial inputs (Stein *et al.*, 2004). Marine sedimentary contributions also account for a varied volume and distribution of organic input (Drenzek *et al.*, 2007). However, since the Arctic is generally considered to be oligotrophic (e.g. Boetius *et al.*, 1998; Mundy *et al.*, 2009), this is not as significant as riverine input. Since the Arctic Ocean is surrounded by the large continents of North America, Canada and Eurasia, it receives a far greater volume of riverine suspended particulate matter than that of the Antarctic Ocean (Holmes *et al.*, 2002). However, the Arctic only accounts for ca. 11% (227 $x10^6$ t^{-1} yr^{-1}) of global river runoff (Shiklomanov, 1998) and ca. 1% of the global riverine sedimentary input (Gordeev, 2006). A number of factors are responsible for this low sediment input, such as frozen permafrost and relatively low levels of anthropogenic activities. Towards the high Arctic, further reductions in sedimentation are evident (Backman *et al.*, 2004), potentially preventing accurate high resolution (decadal to annual) sediment core analysis.

7.1.3 Ocean currents in the Canadian Arctic Archipelago

The numerous islands of the CAA result in narrow channels ranging from ca. 50 – 150 km which direct ocean tides through the region in an easterly direction from the Beaufort Shelf (Williams *et al.*, 2008). Currents are observed ranging up to 130 cm s^{-1} in some narrow straits of the archipelago such as Fury and Hecla Strait (< 2 km wide) and Hells gate (< 7 km wide), with the majority (ca. 95 %) of the region exposed to currents < 20 m s^{-1} (Hannah *et al.*, 2009). Variations in tidal currents within confined straits may result in lateral transportation and redistribution of particles, such as

diatoms. Strong currents also provide an increased potential for redistribution of previously deposited, loosely consolidated, sediments, potentially creating regions depleted in organic matter.

Analysis of the established palaeo-sea-surface temperature proxy U^{K}_{37} in 87 surface sediment samples from the western south Atlantic exposed this issue of lateral transport of biomarkers. Deviations in temperature, from contemporary observations, were recorded from sedimentary alkenones of -2°C to -6°C (Benthien *et al*, 2000, Mollenhauer *et al*, 2006) leading the authors to claim strong lateral displacement of suspended particles was responsible for the temperature anomalies

7.1.4 Sources of organic carbon in Arctic marine sediments

Organic Carbon (OC) in the Arctic can be broadly classified as either marine or terrestrial (e.g. Venkatesan *et al.*, 1983; Macdonald *et al.*, 1998, Stein *et al*, 2004) Marine bio-production in the Arctic is, in general, dominated by photosynthetic fixation of carbon by phytoplankton and sea ice algae (Sakshaug, 2004). In contrast, dominant terrestrial OC sources in the Arctic are generally considered as. river discharge, coastal erosion, sea ice input and aeolian transport of dusts (e.g. Rachold *et al.*, 2004, Stein *et al*, 2004 and references therein)

Carbon/nitrogen (C/N) ratios of organic matter have been used to estimate the relative contribution of either marine or terrestrial OC (Schubert *et al*, 1996), where values of 5 - 8 are considered representative of marine sources. In contrast, terrigenous organic matter generally has values of > 15, caused by reduction of organic nitrogen (ON) following, for example, sequestration by terrestrial nitrogen fixing prokaryotes (Meyers, 1997; Stein *et al*, 2004).

Observation of suites of *n*-alkanes can provide evidence for the terrestrial or marine assignment of OC (Bray *et al.*, 1961). While the source of modern *n*-alkanes is varied, being produced by numerous plants and animals for a multitude of specific functions, their ubiquity can be exploited to determine the origin of OC in the Arctic. Decarboxylation of fatty acids in photosynthetic plants of marine and terrestrial origin imposes a characteristic enhancement of the odd numbered (i.e. nC$_{27}$, nC$_{29}$ . . .) *n*-alkanes, creating, an often distinctive, odd-over-even predominance (Schubert *et al.*, 1996) and is referred to as the carbon preference index or CPI. Marine OC production is generally recorded in the relatively short chain *n*-alkanes (nC$_{15}$, nC$_{17}$ and nC$_{19}$), while terrestrial plant waxes produce a similar enhancement in long chain compounds (nC$_{27}$, nC$_{29}$, and nC$_{31}$). While these long chain hydrocarbons are relatively specific to terrestrial higher plants, short chain *n*-alkanes are not so specific, being produced by either marine or fresh water phytoplankton. Further, following the observed possible algal origin of long chain odd *n*-alkanes in sediments, (Lichtfouse *et al.*, 1994), it has become clear that the interpretation of ratios between short and long chain *n*-alkanes can not always be considered wholly conclusive.

7.1.5 The effect of particle size on organic carbon retention

The particle size of sediments is commonly divided into at least two size fractions based around 63 μm. This approach is especially common in micropalaeontological studies, where the size fraction of interest determines the ecological significance of the assemblages being studied (Smart, 2002). In sedimentological studies, a slightly more detailed classification is often required, where the accurate distinction of sediment grain size can provide evidence of specific geological and environmental processes (Eisenhauer *et al.*, 1999). A common classification of sediment grain size used by

sedimentologists and geologists divides sediment material into three main fractions; clay: < 2 μm; silt: 2 – 63 μm; sand (coarse): 63 μm – 2 mm (Friedman *et al.*, 1978). Sediment grain size can also be significant in terms of the retention of OC (Stein *et al*, 2004). For example, the sorting of organic rich Peruvian sediments into nine size fractions demonstrated how increases in sedimentary OC can sometimes be attributed to the larger surface area offered by smaller sediment grains (Bergamaschi *et al*, 1997) The mechanisms of sedimentary particle distribution are varied Terrestrial inputs, derived from river plumes or weathering can significantly influence the particulate matter of a region (Gordeev, 2006), sometimes obscuring marine signals in sediments. The enclosure of the Amundsen Gulf within a coastal region highlights the importance of identifying the major rivers of this region.

7.1.6 Impact of bioturbation on lipids in Arctic marine sediments

In biomarker studies, the undisturbed preservation of seasonal particle flux is highly desirable Preservation of the sequential seasonal sedimentation in a marine system is essential if information on short duration events (ca. 1 – 100 years), are required However, bioturbation is capable of restricting accurate sedimentary reconstructions in many oxic sediments (Maire *et al.*, 2008). Sediment reworking and bio-irrigation (transport of interstitial pore water) is caused by the activities (locomotion, feeding, burrowing etc.) of numerous benthic and some pelagic faunal species (e.g Pearson, 2001 and references therein). Bioturbation can significantly affect the physical and chemical properties of the sediment (Lohrer *et al*, 2004), along with redistribution and mixing of seasonal biomarker laminations imposing considerable difficulties on sediment core analysis (Maire *et al*, 2008).

The large scale investigation of the distribution patterns of the macrobenthos on the Canadian Beaufort Shelf by Conlan and co-workers (2008) exposed considerable variation in species diversity. A vast range of crustaceans, polychaetes and molluscs were found to vary locally, apparently in accordance to regional changes in productivity. Additionally, the shallow (< 40 m) Cape Bathurst region was also observed to exhibit a ten-fold increase in biomass in relation to other shelf regions, an increase that was mostly attributed to the amphipod, *Ampelisca macrocephala* and the polychaete, *Barantolla Americana* that were not abundant elsewhere. Furthermore, the deeper (> 100 m) part of the Cape Bathurst region was considered representative of the Beaufort Shelf, of similar depth, and was dominated by the deep burrowing polychaete, *Maldane sarsi* (4 - 15 cm; Dufour *et al.*, 2008).

In an attempt to determine the extent of bioturbation in marine sediments, Maire and co-workers (2008) reviewed a range of approaches, concluding that the most widely adopted technique involved analysis of naturally occurring radionuclide tracers. Early applications of ^{210}Pb as a tracer was for geochronological analysis of marine sediments (Koide *et al.*, 1972). The presence of ^{210}Pb (half-life 22.3 yrs) in marine sediments stems from a series of rapid decays from ^{226}Ra (half life 1622 years) to ^{222}Rn (half-life 3.8 days) in the atmosphere before falling out with precipitation and aerosols (Weiss *et al.*, 1986). While the measurement of ^{210}Pb in sediments was initially propagated as a means of chronological dating, it is also useful as a measure of bioturbation.

The effectiveness of the ^{210}Pb isotope approach in determining reworking in the upper (< 30 - 40 years old) sections of sediment cores was evident in a study of Arctic bioturbation rates (Clough *et al.*, 1997). A transect of more than fifteen shallow (< 15 cm) sediments were sampled from the Chukchi Shelf, across the Lomonosov Ridge through to East Greenland. Reworking was of greatest significance in the shallow Chukchi Shelf, with mixed layers evident up to 10 cm in depth.

7.1.7 Biological and chemical alteration of biomarkers during diagenesis

Once sedimented, organic matter in marine sediments is often degraded (Killops *et al*, 1993, Arnosti *et al*, 2006), with functional groups and unsaturation commonly being susceptible (Armstrong *et al*, 1991; Killops *et al.*, 1993) For example, as part of an investigation into the sedimentary stability of HBI alkenes the addition of mild acids (K-10 Montmorillonite clay and tosic acid-acetic acid) to lipids **IIa** and **IIb** revealed geometric isomerism (*E/Z*) in addition to migration of the $\Delta^{6(17)}$ double bond in **IIb** to the $\Delta^{5(6)}$ position, characteristic of **IIa** (Belt *et al*, 2000b). Additionally, the tri-unsaturated HBIs, **IIIc** and **IIId** revealed similar geometric isomerisation (*E/Z*), with the same migration of the $\Delta^{6(17)}$ double bond to the $\Delta^{5(6)}$ position Spectroscopic analysis of product mixtures also revealed the presence of penta-substituted cyclohexenes and other minor products. In all cases the double bond at $\Delta^{23(24)}$ remained unreacted (Belt *et al*, 2000b).

The formation of organic sulphur compounds, more common of anoxic conditions, is an alternative diagenetic pathway proposed by some for HBIs (Sinninghe Damsté *et al.*, 2007). In contrast to the presence of mild acids, the absence of reactive iron and oxohydroxide coatings on clay particles in the presence of anoxic sediments can lead to the incorporation of sulphur into organic matter (Canfield, 1989; Sinninghe Damsté *et al*, 2007). Indeed, Werne and co-workers (2000) observed that the dominant mechanism of inorganic sulphur incorporation in the anoxic Cariaco Basin entailed inorganic sulphides reacting with the most accessible pair of double bonds in the isoprenoid side chain of a tri-unsaturated tricyclic triterpenoid, creating a thiane ring The potential for sulphur incorporation into HBIs is, therefore, a potential concern in regions of high primary production, where permanent, or temporary, anoxic conditions

may occur. Formation of a C_{25} thiane from a $C_{25:2}$ HBI in Ellis Fjord sediments in Antarctica adds credence to sulphurisation as a potential diagenetic pathway for HBIs in some anoxic sediments (Sinninghe Damsté *et al.*, 2007).

The absence of functional groups in typical HBIs, and the presence of reduced unsaturation in IP_{25} and di-unsaturated HBIs (**IIa** and **IIb**) may explain the ease of detection of these biomarkers in Holocene sediments (e.g. Vare *et al.*, 2009; Belt *et al.*, 2010; Gregory *et al.*, 2010; Vare *et al.*, 2010) and, in some cases, in sediments up to ca. 1.5 Ma years old (unpublished data). This ease of detection is most likely due to the occurrence of a single relatively unreactive double bond in IP_{25} ($\Delta^{23(24)}$) that probably limits the diagenetic reactions of this biomarker in sediments, including the incorporation of sulphur.

7.1.8 Reduction and oxidation of lipids in Arctic marine sediments

While inorganic sulphurisation in anoxic sediments is a potential limitation to the preservation of some HBIs, the occurrence of organic metabolism in oxic sediments also needs to be considered. The sedimentation of OC to the seafloor drives the benthic and infaunal food web, with microbes forming the foundation. Boetius and Damm (1998) observed that microbial activity and oxygen penetration in the Laptev Sea were controlled by organic matter input over a water depth gradient (50 – 3500 m). Maximum activities were observed at the sediment-water interface resulting from the accumulation of fresh particles. Additionally, in a bioturbated mixed zone, usually in the upper 5 – 10 cm, OC was enriched compared to deeper sediments, suggesting that OC can be degraded by microbes under oxic conditions. Experimentation with squalene and marine denitrifying bacteria confirmed the ability of microbes to degrade isoprenoid compounds under oxic conditions, observing up to a 77% decrease in the hydrocarbon

over 120 days, with targeted breakdown of the double bonds (Rontani *et al.*, 2002). The significance of this degradation in terms of biomarkers is evident in the anoxic/oxic comparison of the established palaeothermometers U^{K}_{37} and TEX_{86} where preferential degradation of isomers resulted in inaccurate temperatures in contemporary environments (Huguet *et al.*, 2009).

The importance of determining the extent of oxic/anoxic exposure, or redox gradient (Stein *et al* , 2004), in surface sediments consequently becomes more important Redox interactions commonly occur at a point where, under the influence of labile OC metabolism, the drawdown, or withdrawal of oxygen occurs in sediments Changes in oxygen concentration in the sediment are subsequently recorded in the oxidative states of certain reactive element species such as manganese, arsenic, rhenium, cadmium, silver phosphorous and iron (Jakobsson *et al* , 2004; Macdonald *et al.*, 2004; Gilbert *et al.*, 2006, Katsev *et al.*, 2006).

A number of studies have determined the redox depths of the Amundsen Gulf and Beaufort sediments (e.g. Gilbert *et al.*, 2006), with depths ranging from 1 – 7 cm in response to persistent or episodic changes in the deposition flux of degradable organic matter and the concentrations of oxygen in the overlying bottom water (Katsev *et al.*, 2006). In addition to observations in the Amundsen Gulf, simulated sediment experiments revealed that organic-poor sediments were more sensitive to rapid changes in oxygen penetration depth, resulting from increased OC, that can result in multiple redox boundary excursions evident in Mn mobility within the sediments (Katsev *et al.*, 2006)

7.1.9 Use of inorganic elements in palaeo-sediment reconstruction

Exposure of OC to the various potential diagenetic processes in marine sediments renders biomarkers susceptible to inaccurate interpretation as discussed (e.g. Huguet *et*

al., 2009). A common approach to verifying trends in biomarkers is the multiproxy approach, where independent measures are observed in parallel. Important sedimentary features, such as sedimentation rate, grain size analysis and inorganic elemental analysis are invaluable in determining sedimentary (e.g. Vare *et al.*, 2009). In particular, complementary elemental analysis of marine sediments exposes changes in the geochemistry necessary to determine lithogenic (Ti/Rb and Al) and biogenic (Ca/Fe) sources, with Mn indicating redox mobility, within a sediment core (Croudace *et al.*, 2006; Vare *et al.*, 2009). The imbalance of individual elements, evidenced by ratio decline or enhancement, can be used to identify changes in source lithogenic material, which in itself can be an indication of changes in the palaeo-climate.

7.2 Aims and objectives of sedimentary HBI and geochemical analysis

The production and subsequent transportation of IP_{25} from within sea ice, to the water column and underlying sediments has been observed in this study (Chapters 4, 5 and 6). Previously, quantities of IP_{25} and sometimes other HBIs have been determined for sediments and used for palaeo-sea ice reconstructions without major consideration of the potential impacts of diagenesis (e.g. Belt *et al.*, 2007; Andrews *et al.*, 2009; Müller *et al.*, 2009; Vare *et al.*, 2009; Belt *et al.*, 2010). While the potential diagenetic pathways of some $C_{25:2}$ and $C_{25:3}$ HBI alkenes have been investigated in laboratory experiments (Belt *et al.*, 2000b) some have begun to explore the degradation of IP_{25} also. Vare *et al.*, (2009) for example observed an increase in the ratio of a di-unsaturated HBI compared to IP_{25}, inconsistent with significant diagenesis, while Muller *et al.*, (2009) observed the greatest quantities of IP_{25} in the oldest sediments (ca. 30 kyr) of a core, also challenging the occurrence of significant degradation in this biomarker over time. Despite this, much work remains to be carried out on the *in situ* preservation or

degradation of IP_{25} and related HBIs in Arctic marine sediments to further improve the sedimentary interpretation of the sea ice biomarker. Therefore the main aims of this chapter were to investigate factors capable of altering IP_{25} concentration and distribution in shallow marine sediments by

i. Investigating the geochemistry of near surface marine sediments within the CAA
ii. Determining if any geochemical relationships exist between IP_{25} and other analytes measured as part of i.
iii. Establishing the effect, if any, of bioturbation in the relatively shallow Arctic marine sediments of the CAA

7.3 Selection of sediment samples

Collection of sediment samples was carried out over two expeditions (IPY-CFL 2008 and ArcticNet 2005/7). Two box cores (St 405b and St 1216) were collected during the Canadian Circumpolar Flaw Lead System Study, as part of the International Polar Year (IPY-CFL), and a further four box cores were obtained by Dr. Lindsay Vare, Prof Simon Belt and Dr. Guillaume Massé during the ArcticNet cruises (August/September 2005/2007). All cruises were carried out onboard the class 1200 Canadian Coast Guard Ship, Amundsen with all box cores being < ca 45 cm in depth. The spatial distribution of these sediment cores is shown in Figure 7.3-1.

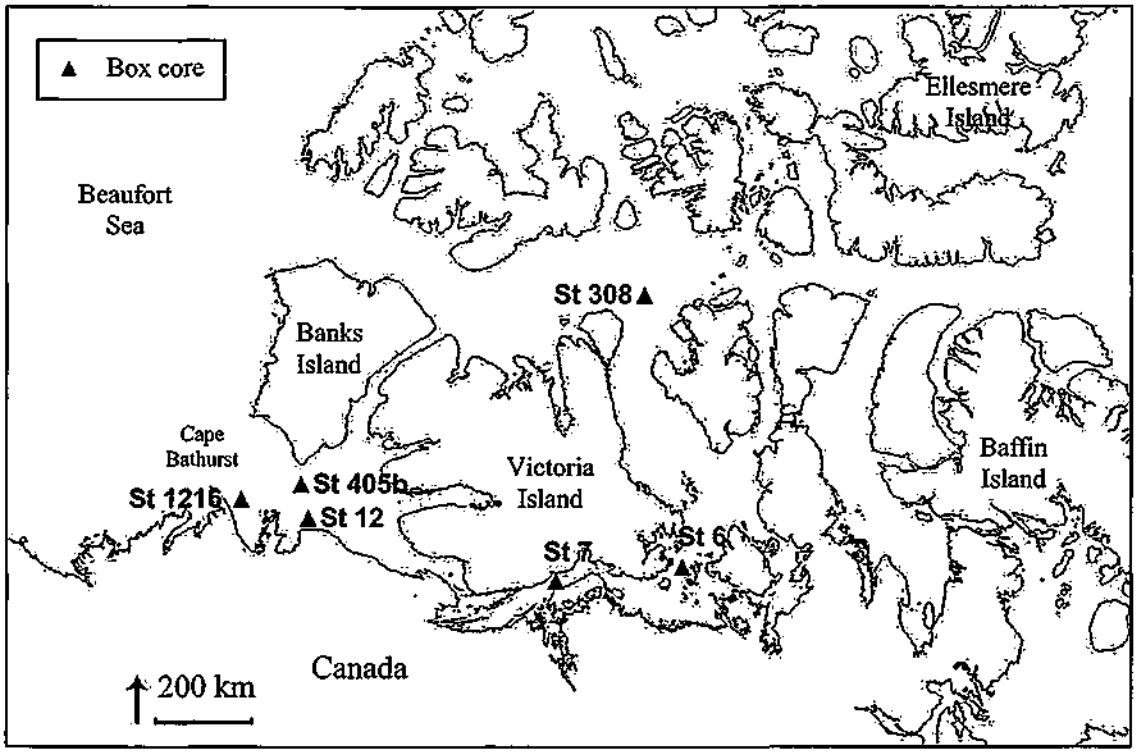

Figure 7.3-1. Spatial distribution of Arctic marine sediment box cores (Triangles) collected from within the Amundsen Gulf during the CFL-IPY cruise, 2008, and in transect throughout the western CAA during the ArcticNet cruise 2005/7.

A Precision Enterprise box corer was used to collect short sediment box cores from areas with water depths between 60 m and 500 m (Table 7-1). The box corer (50 x 50 x 50 cm) removed intact surface sediments (0.25 m^2) of various depths (< ca 45 cm) from the sea floor, preserving the sediment-water interface enabling accurate, fine resolution determination of sediment characteristics. Following sediment retrieval, 20 cm Ø metal tubes were driven into the sediment by hand and dug out, preserving the sediment within the tube. The cores were then sectioned using metal plates on a custom made jig at the required resolution (0.2 – 5 cm). The outer edge of the sediment horizon that came into contact with the metal tube was discarded to avoid mixed horizons and contamination with the remaining sediment being stored (Whirl-Pak, -20°C).

Table 7-1 Arctic marine box core collection data from the IPY-CFL cruise, 2008 and ArcticNet cruises 2005 and 2007.

Cruise/Date	Station ID	Core type	Core length (cm)	Water depth (m)	Sedimentation rate (cm yr^{-1})	Location			
ArcticNet 2005	St6	Box	30	61	0 16	69°9	N	100°41	W
ArcticNet 2005	St7	Box	40	117	0.08	69°00	N	106°34	W
ArcticNet 2005	St12	Box	45	219	*	69°54	N	122°57	W
ArcticNet 2007	St308	Box	20	341	0.09	74°07	N	103°04	W
IPY-CFL 2008	St405b	Box	21	500	0 08	70°40	N	123°00	W
IPY-CFL 2008	St1216	Box	20	100	*	70°36	N	127°36	W

* Mixed sediment prevented determination of sedimentation rate.

7.4 Experimental

The determination of the sediment geochemistry involved a range of techniques which are summarised below and described in greater detail in chapter 3 (Methods).

7.4.1 Extraction of HBIs from Arctic marine sediments

Briefly, St 405b and St 1216 sediments were weighed before and after freeze drying to determine the water content of the sediments. Following addition of the internal standard (7-hexylnonadecene, 10 µL; 10 µg mL^{-1}) required for later quantification of HBIs, sediments were sonicated in dichloromethane/methanol (15 mins; ca 3 mL; 2:1 v/v) and transferred to a clean vial where solvents were evaporated with nitrogen to obtain a TOE. The TOE was then dissolved in methanol (1 mL) and extracted using hexane (3 x 1 mL) and milli-Q water (1 mL) to isolate apolar lipids Once isolated, apolar lipids were purified by open column silica chromatography (50·1; SiO_2:lipids), with hexane mobile phase (3 column volumes), to yield apolar lipids. The other 4 box core sediments (St 6, St 7, St 12 and St 308) were extracted by Dr Lindsay Vare using

the same method. Where $\delta^{13}C$ analyses were required after initial GC/MS analysis, the samples were further chromatographically purified (5% $AgNO_3$).

In the absence of replicates to determine sample variability, ten replicates of a control sediment obtained from Franklin Bay in the Amundsen Gulf were extracted, resulting in < 10% inter-sample variability being established.

7.4.2 Isolation of diatom frustules from Arctic marine sediments

LST Fastfloat (specific gravity (SG) 2.21), was used to isolate diatoms from freeze dried sediment. Following gentle agitation, the samples were left to settle (24 h) before transferring the surface layer (ca. 0.2 mL) of LST and material < 2.21 SG into a centrifuge tube. Once diluted with water to < ca. 1.5 SG the solution was centrifuged, where diatom frustules formed pellets that were recovered for subsequent LM and SEM slide mounting and HBI extraction using the method described in previous chapters (Chapter 3).

7.4.3 Determination of sediment geochemistry

In addition to lipid analysis of marine sediments, the total organic carbon (TOC), inorganic elemental compositions and ^{210}Pb content were determined for all cores as described in Chapter 3. Sediment grain size analysis was carried out on selected sediments from St 405b and St 1216.

7.5 Results

7.5.1 Deep water Arctic marine sediment cores

7.5.1.1 St 405b box core

7.5.1.1.1 HBI distributions in sediments

The lipid content of sediments from St 405b was determined for each 5 mm sediment horizon from 0 – 210 mm (43 horizons), where each of the HBIs previously found in sea ice, seawater and macrofauna (**I – IIId**) were present in all horizons. Examination of the sediment concentration profile of **I** (Figure 7.5-1) revealed three distinct features Firstly, from the sediment-water interface to ca 40 mm, I had the highest concentration of all of the analysed HBIs with relatively little variation in concentration (ca. 12 ± 1.5 ng cm^{-3}). Secondly, the concentration decreased, steadily, to < 5 times the surface concentration, from 40 mm, reaching 2.1 ng cm^{-3} at 80 mm. Thirdly, the concentration of I remained reasonably constant throughout the lower section (> 80 mm) of the core (80 – 210 mm = ca. 2.6 ± 0.8 ng cm^{-3}) with no significant positive or negative excursions.

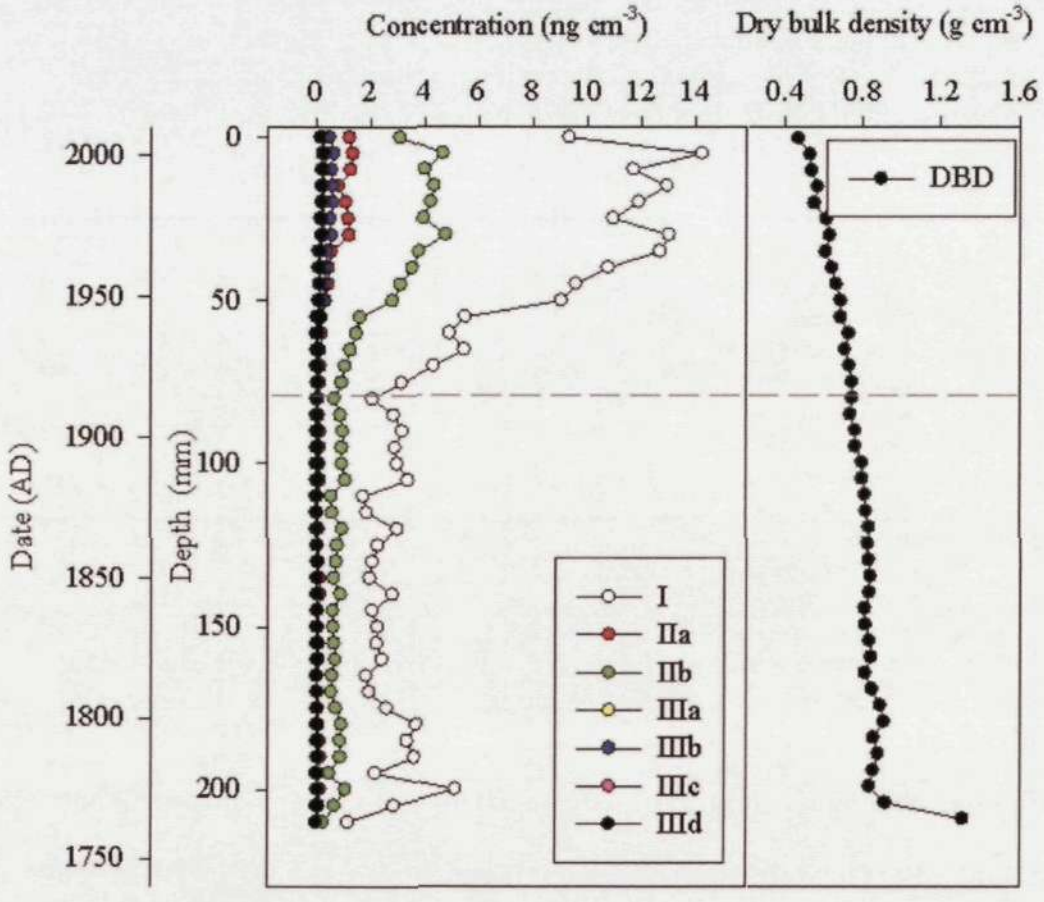

Figure 7.5-1. Vertical profiles of individual HBI lipids and dry bulk density in the sediments of St 405b (0 cm = water-sediment interface). Grey dashed line represents approximate position of the redox boundary determined by Mn oxidative state *vs.* Ti (Mn/Ti).

Overall the relative distribution of HBIs in sediments did not closely resemble those observed in sea ice, filtered seawater or macrofauna (Chapters 4, 5 and 6) (Table 7-2) although consistent with the HBIs in sea ice and macrobenthos, **I** also dominated in all sediment horizons, with **IIb** correlating highly to **I** ($r = 0.99$ $p = <0.0001$).

Table 7-2. Relative distribution of HBI isomers observed in St 405b sediments (0 - 210 mm) compared to macrofaunal specimens (from Chapter 6), zooplankton (> 710 μm) (from Chapter 6), filtered seawater (> 20 μm) (from Chapter 6) and sea ice (from Chapter 4) during the IPY-CFL cruise (1/4/08 to 1/8/08).

	I	**IIa**	**IIb**	**IIIa**	**IIIb**	**IIIc**	**IIId**
Relative distribution (%) of HBI concentrations in St 405b sediments	65.7	5.7	22.2	1.2	2.9	1.4	1.0
Relative distribution (%) of HBI concentrations in the macrobenthos	34.9	6.2	29.8	5.0	12.6	5.5	6.1
Relative distribution (%) of HBI concentrations in zooplankton	11.0	8.9	15.4	0.0	44.4	11.8	8.5
Relative distribution (%) of HBI concentrations in filtered seawater	19.7	2.2	23.1	11.0	23.4	6.9	13.7
Relative distribution (%) of HBI concentrations in sea ice	27.2	1.7	31.4	1.0	28.1	0.8	9.8

The tri-unsaturated HBIs, **IIIa**, **IIIb**, **IIIc** and **IIId**, collectively represented only 6.5% of the total HBIs (**I** – **IIId**) in the surface, reducing to 4.3% in the deeper sediments (Figure 7.5-2).

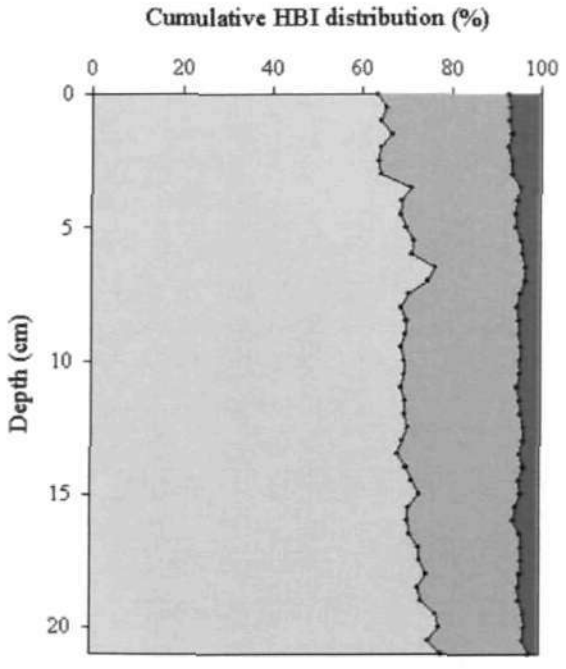

Figure 7.5-2. Cumulative distribution (%) of **I** (light grey), **IIa** and **IIb** (grey) and **IIIa**, **IIIb**, **IIIc** and **IIId** (dark grey) in St 405b box core sediments.

Additionally, while currently unquantifiable, the presence of the tentatively assigned $\Delta^{7(20)}$ HBI, **IIc** previously observed in numerous Arctic samples from this study was also recorded in sediments, in good agreement to both **I** and **IIb** ($r = 0.98$; $p = < 0.001$ and $r = 0.99$; $p = < 0.001$ respectively) as well as correlating well to all other HBIs ($r = > 0.96$).

7.5.1.1.2 Relative distribution of HBIs in diatoms isolated from St 405b sediments

Diatom frustules were isolated from St 405b sediments (LST Fastfloat; 2.21 specific gravity) from a surface horizon (0 – 5 mm; diatom mass = 2.8 ± 0.6 mg; n = 4) and below surface horizon (80 – 85 mm; diatom mass = 0.6 ± 0.3 mg; n = 4) (Figure 7.5-3).

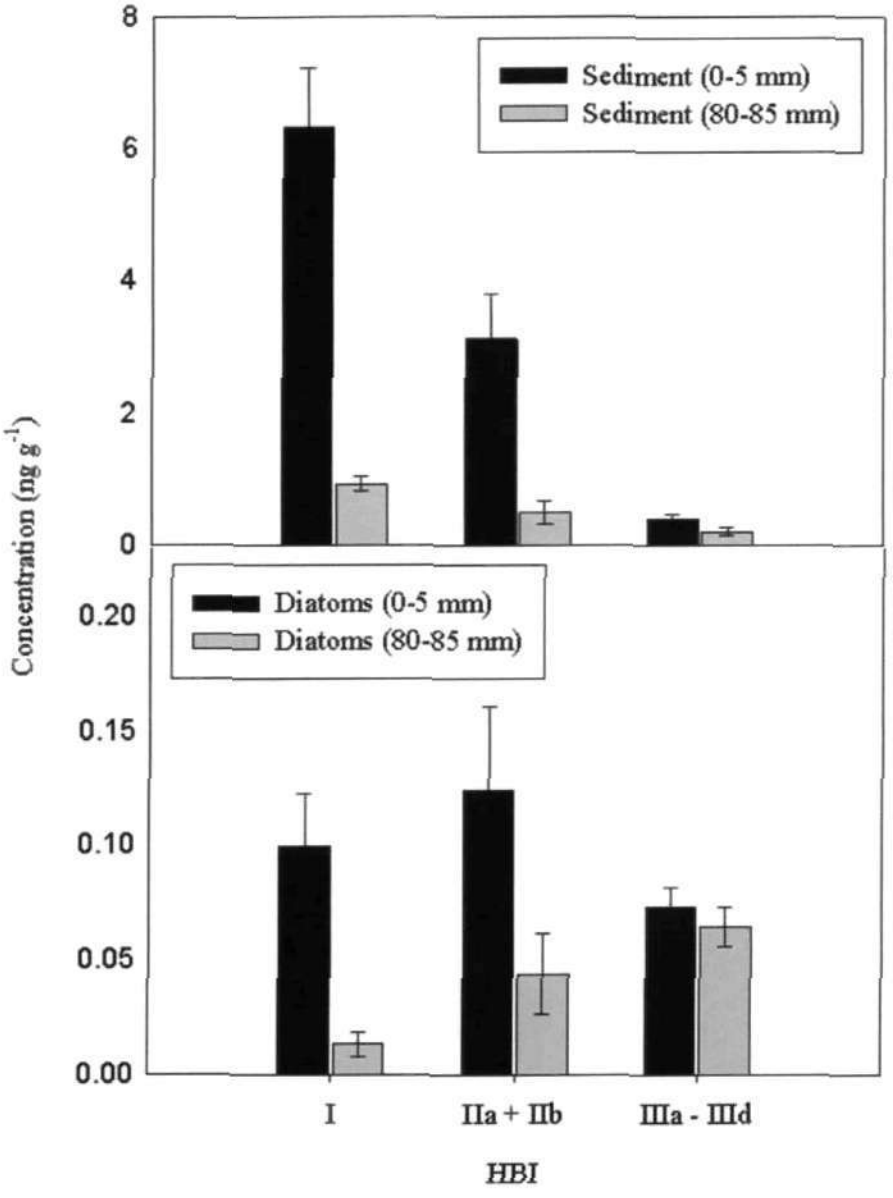

Figure 7.5-3. Distribution of mono- di- and tri-unsaturated HBIs detected in sediments (top) and diatom frustules (bottom) from two sediment horizons (0 – 5 mm and 80 – 85 mm) in St 405b box core.

Each of the HBIs used throughout this study (**I** – **IIId**) were detected in lipid extracts from all diatom frustule and sediment replicates (n = 4) in each horizon. The mass of diatom frustules isolated from 0.25 g freeze dried sediment represented 1.6 ± 0.4% (0 - 5 mm) and 0.4 ± 0.2% (80 – 85 mm) of the total sediment mass (diatom frustules + sediment mass) from the surface and below surface sediments respectfully (Table 7-3).

Table 7-3. Diatom and sediment masses (relative to each other; %) obtained following isolation of diatom frustules from freeze dried sediment (0 – 5 mm and 80 – 85 mm) from St 405b with the distribution (%) of **I** and **IIIa – IIId** measured in both diatom frustules and diatom free sediments.

	Diatom mass (% total mass)	Sediment mass (% total mass)	Diatom **I** (% total **I**)	Sediment **I** (% total **I**)	Diatom **IIIa – IIId** (% total **IIIa – IIId**)	Sediment **IIIa – IIId** (% total **IIIa – IIId**)
0 – 5 mm	1.6 ± 0.4	98.4 ± 0.4	1.6 ± 0.6	98.4 ± 0.6	15.6 ± 2.9	85.8 ± 3.7
80 – 85 mm	0.4 ± 0.2	99.6 ± 0.4	1.4 ± 0.4	98.6 ± 0.4	24.6 ± 7.5	75.4 ± 7.5

Notably, there were almost 5 times fewer diatom frustules in the lower (80 – 85 mm) sediment horizons than at the surface (0 – 5 mm), consistent with HBI concentrations previously measured in St 405b (Figure 7.5-1).

For mass corrected HBI concentrations in sediment fractions, the distribution of mono- di- and tri-unsaturated HBIs was observed to change over depth with **I** reducing by 87%, **IIa + IIb** collectively reducing by 84% and **IIIa – IIId** reducing by 48% overall from 0 – 5 mm to 80 – 85 mm. In contrast, mass corrected HBI concentrations in isolated diatom frustules did not decrease so significantly with **I** also reducing by 87%, while **IIa + IIb** collectively reduced by 64% and **IIIa – IIId** reduced by 11% overall from 0 – 5 mm to 80 – 85 mm (Figure 7.5-3).

Interestingly, the relative distribution of I across sediments and diatom frustules appears to represent an unbiased distribution equivalent to the mass of each fraction (total mass = 0.4 – 1.6% diatom frustules and ca 99% sediment) with no affinity for particular particles (e.g. diatom or sediment) being evident (Table 7-3). In contrast, the distribution of tri-unsaturated HBIs **IIIa – IIId** appear more biased, with 16 – 25% of the total tri-unsaturated HBIs being associated with the total mass of diatom frustules (0.4 – 1.6%) (Table 7-3). In further contrast to HBI distributions observed in sediments following diatom isolation, the tri-unsaturated HBIs represent the greatest concentration of HBIs measured in diatom frustules, an observation not previously seen in sea ice, filtered seawater, macrofaunal organisms or sediments in this study.

7.5.1.1.3 Box core sediment geochemistry

A chronology for St 405b was constructed from determination of $^{210}Pb_{xs}$ from 8 sediment horizons (between 0 - 14 cm) (Figure 7.5-4) yielding a mean linear sedimentation rate of 0.09 cm yr^{-1}. Examination of the $^{210}Pb_{xs}$ data suggested the presence of mixed sediments between 0 – 1 cm.

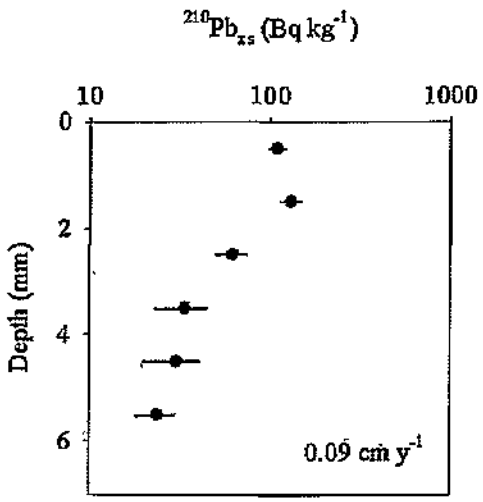

Figure 7.5-4. $^{210}Pb_{xs}$ data obtained from St 405b box core with mean sediment accumulation rate.

Extrapolation of the sediment accumulation rate over the length of the core presented an age model spanning 258 years over 21 cm (ca. 11 yr cm^{-1}). With the exception of the final horizon, the dry bulk density profile showed a gradual overall increase with depth (Figure 7.5-5).

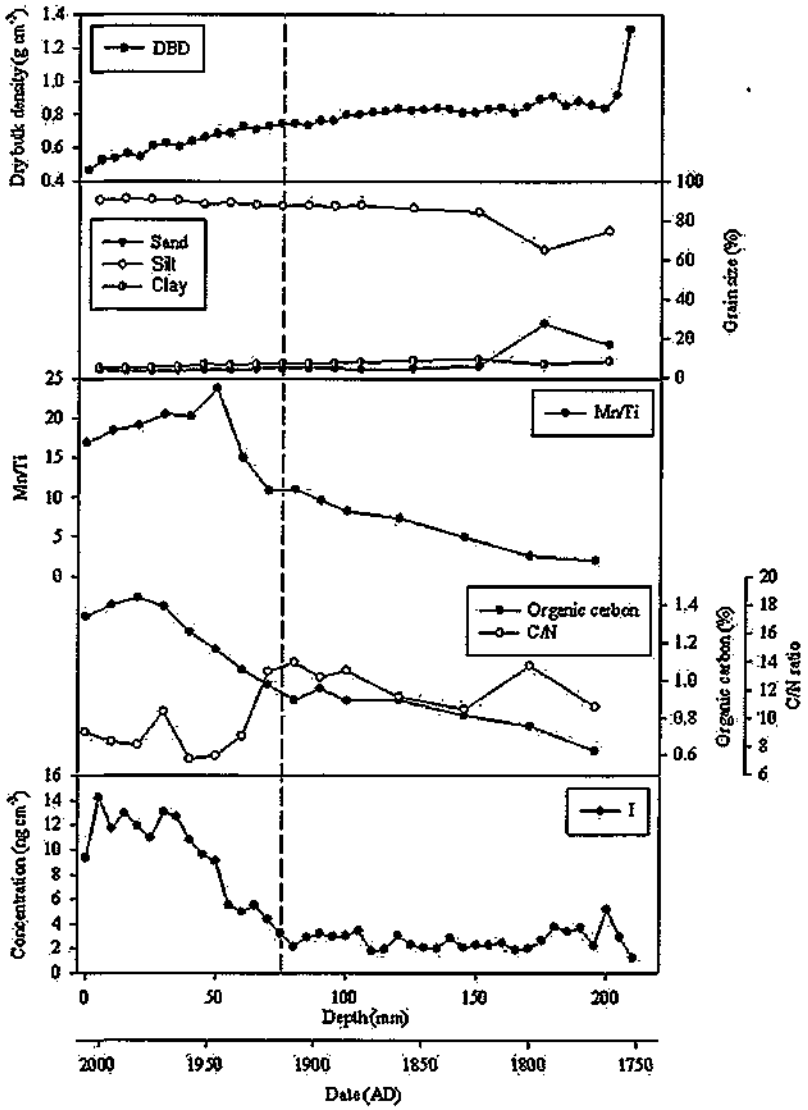

Figure 7.5-5. Vertical profiles of biomarker **I** and organic carbon with C/N and Mn/Ti ratios, with sediment grain size and dry bulk density in the sediments of St 405b (0 cm = water-sediment interface). Grey dashed line represents approximate position of the redox boundary determined by Mn oxidative state *vs.* Ti (Mn/Ti).

The downcore profile of the ratio of labile, solid state, manganese (Mn) against the relatively refractory titanium (Ti) in St 405b revealed similarities to that of **I** ($r = 0.89$; p

= < 0.001), in sediments (Figure 7.5-5). The decrease in the Mn/Ti ratio, presumably as a response to the vertical migration of reduced Mn in sediment pore water, was interpreted as reflecting the position of the redox boundary, with a reduction in oxygen penetration occurring below ca. 75 mm (Figure 7.5-5; grey dashed line). The sub-surface Mn maximum at ca 50 mm most likely reflected a response to the vertical migration of oxygen penetration resulting from fluctuations in OC flux to the sediment (Katsev *et al* , 2006).

The corresponding pristane/phytane (Pr/Ph) downcore profile varied through depth in the box core with a distribution analogous to that of I ($r = 0.79$; $p = < 0.001$) as the ratio decreased from characteristically oxic surface values of 2.2 (Brooks *et al* , 1969; Ten Haven *et al.*, 1987) (Figure 7.5-6)

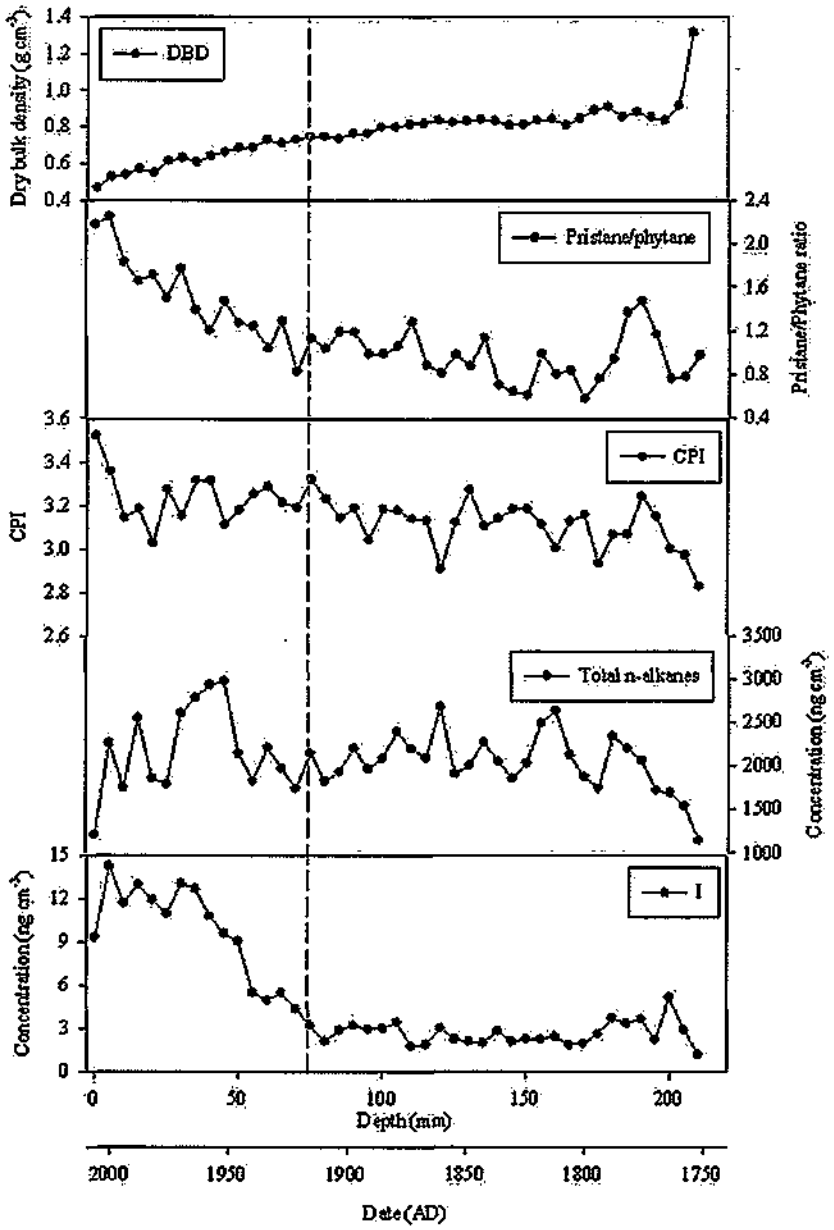

Figure 7.5-6. Vertical profiles of biomarker **I** and *n*-alkanes with CPI and pristine/phytane ratios, with dry bulk density in the sediments of St 405b (0 cm = water-sediment interface). Grey dashed line represents approximate position of the redox boundary determined by Mn oxidative state *vs.* Ti (Mn/Ti).

Between ca. 50 – 80 mm the ratio generated values indicative of less oxic conditions (ca. 1.2), before remaining relatively stable at 0.9 ± 0.2, being suggestive of a marginally anoxic depositional environment. The pr/ph and Mn/Ti ratios were also correlated ($r = 0.68$; $p = 0.005$) in further support of the presence of a redox boundary. However, the reliability of using the pr/ph ratio is not completely clear since numerous

rationales have been proposed for additional sources of phytane that cause difficulties in interpreting the environmental significance of this ratio (discussed by Ten Haven *et al.*, 1987; Powell, 1988; Ten Haven *et al* , 1988)

To complement lipid biomarker observations, organic carbon and nitrogen (C/N) profiles were also measured in the sediments (Figure 7.5-5). The OC composition also correlated significantly with I (r – 0.95; p - < 0.001), with the relative distribution being consistent with numerous published data for the south-eastern Beaufort Sea and Amundsen Gulf (mean = 1 06% ± 0.3%) (e.g Stein *et al* , 2004 and references therein). Additionally, the surface, to sub-surface (0 – 60 mm) C/N ratio of ca. 8.4 ± 1.1, indicated a marine origin (ca 5 - 8, Meyers, 1997; Stein *et al* , 2004), with lower sediment horizons (70 – 195 mm) approaching values more representative of terrestrial origin (> 15) at 12.5 ± 1 3 OC values measured on the box core also correlated well with Mn/Ti (r = 0.91, p = < 0.001)

Further, calculation of the carbon preference index (CPI) (Equation 17) revealed no distinct change in the contribution of either odd or even *n*-alkanes throughout the core, with a mean CPI of 3 2 ± 0.1, characteristic of more recently deposited biological material (Bray *et al* , 1961, Scalan *et al.*, 1970, Peters *et al* , 2007)

Equation 17

$$CPI_{25-32} = 0.5 \times \frac{(nC_{25} + nC_{27} + nC_{29} + nC_{31})}{(nC_{24} + nC_{26} + nC_{28} + nC_{30})} + \frac{(nC_{25} + nC_{27} + nC_{29} + nC_{31})}{(nC_{26} + nC_{28} + nC_{30} + nC_{32})}$$

The sediment concentration profile of the combined *n*-alkanes (nC_{15}-nC_{33}) was also relatively refractory in distribution (Figure 7.5-6), with significantly (ca. 90 times) greater concentrations than I (2.1 ± 0 4 μg cm^{-3}).

Finally, determination of the sediment grain sizes revealed a relatively consistent composition throughout, with silt comprising 86% ± 7%. The dominance of silts at the surface of the core (92%) was consistent with contour observations of a band of fine sediments (> 90% silt/clay) extending from near Cape Bathurst, and entering the Amundsen Gulf (Stein *et al.*, 2004 and references therein), as well as studies by Vare *et al.*, (2009) and Belt *et al.*, (2010).

7.5.1.2 St 308 box core

7.5.1.2.1 IP_{25} distribution

Examination of HBI lipid concentrations at 1 mm resolution from 0 – 2.5 cm and at 10 mm resolution from 2.5 – 19.5 cm (41 horizons in total), revealed the presence of each of the HBIs (**I** – **IIId**) in all sediments from 0 – 16 cm and only **I**, **IIa** and **IIb** in sediments from 16 – 19.5 cm with **I** most abundant in all horizons (Figure 7.5-7).

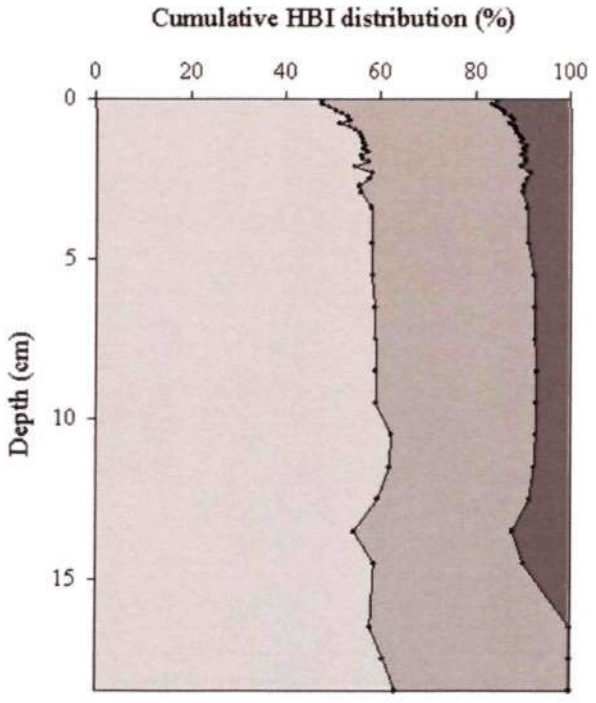

Figure 7.5-7. Cumulative distribution (%) of **I** (light grey), **IIa** and **IIb** (grey) and **IIIa**, **IIIb**, **IIIc** and **IIId** (dark grey) in St 308 box core sediments.

The downcore profile of **I** in St 308 sediments (Figure 7.5-8) revealed similarities to the distribution of **I** in St 405b (r = 0.94; $p = < 0.001$) with maximum concentrations of **I** at the surface followed by a mid-depth decline before reaching minimum concentrations in the lower sections of the core.

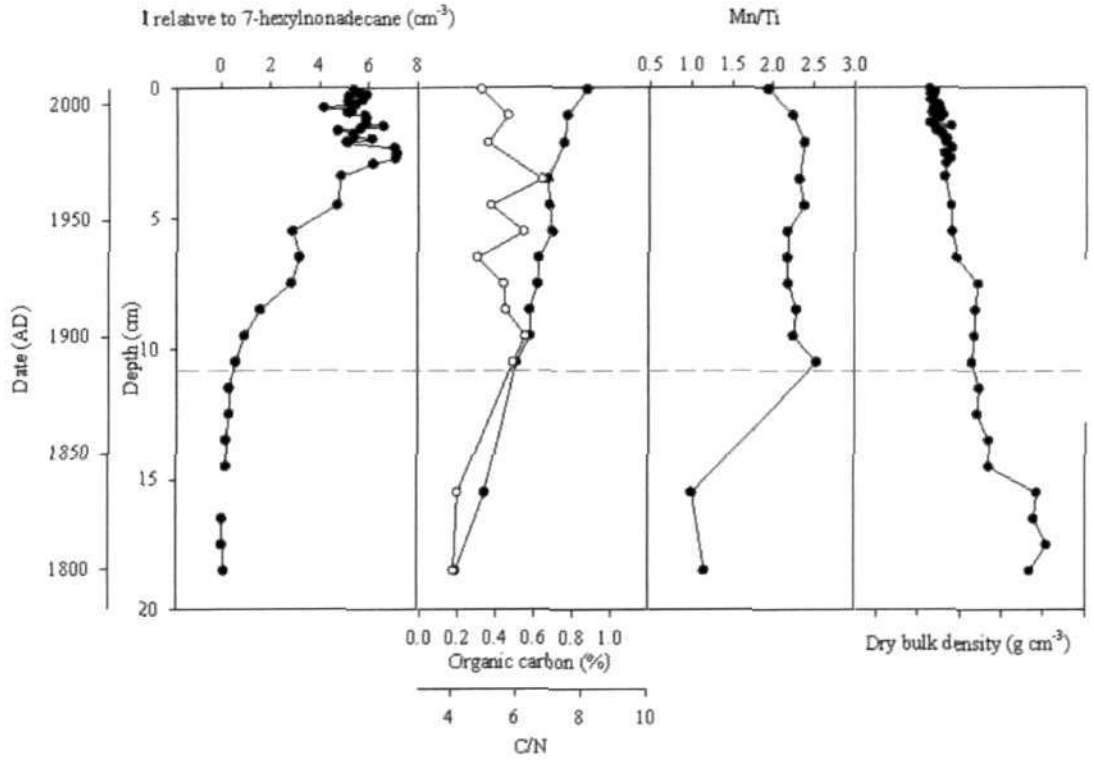

Figure 7.5-8. Vertical profiles of dry bulk density corrected biomarker **I**, with organic carbon (black)and C/N ratio (white), Mn/Ti ratio and dry bulk density for the sediments of St 308 (0 cm = water-sediment interface). Grey dashed line represents approximate position of the redox boundary determined by Mn oxidative state *vs.* Ti (Mn/Ti).

The distributions of the mono- di- and tri-unsaturated HBIs relative to each other in St 308 (Figure 7.5-7) showed, like St 405b, that **I** represented the greatest relative distribution of the HBIs (ca. 56%), with tri-unsaturated HBIs disappearing below ca. 16 cm.

7.5.1.2.2 Box core sediment geochemistry

A chronology was constructed for St 308 based on the determination of $^{210}Pb_{xs}$ in 5 sediment horizons (between 0 - 9 cm) (Figure 7.5-9) yielding a mean linear sedimentation rate of 0.08 cm yr^{-1}, almost identical to that of St 405b. From the $^{210}Pb_{xs}$ data it was determined that a shallow mixed layer was present between 0 – 0.5 cm.

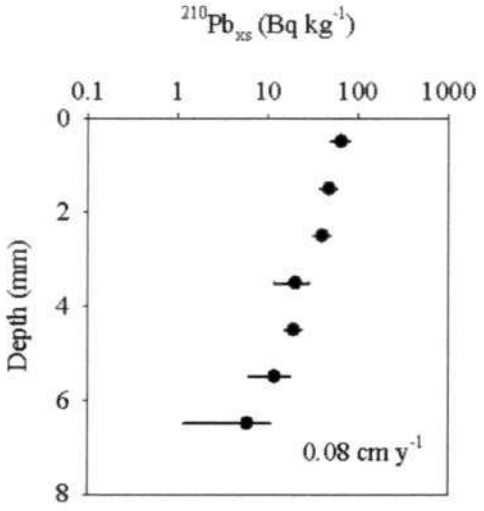

Figure 7.5-9. $^{210}Pb_{xs}$ data obtained from St 308 box core with mean sediment accumulation rate.

Extrapolation of the sediment accumulation rate over the length of the core generated an age model spanning 207 years over 19 cm (ca. 11 yr cm^{-1}). Like St 405b, dry bulk density showed little change throughout the core (0.9 g cm^{-3} ± 0.2 g cm^{-3}), with a gradual increase in density with depth (Figure 7.5-8).

The Mn/Ti ratio revealed a surface maximum, and subsequent reduction lower down the sediment profile in St 308 in good correlation to that of **I** ($r = 0.88$; $p = < 0.001$).

The mean OC composition of the core was 0.6% ± 0.3%, with a decline from a surface maximum, to minimum abundance in the lower sections with strong correlation being evident in St 308 between **I** and OC ($r = 0.95$; $p = < 0.001$) and Mn and OC

(r = 0.89 ; p = < 0.001). The OC measured in St 308 was about 50% of that found for St 405b, yet of similar distribution (r = 0.89; p = < 0.001).

The C/N ratio of the St 308 sediment core showed little correlation to the other geochemical data from either St 308 or St 405b, most likely as result of variation in terrigenous nitrogen supply given the spatial distribution of the two sites in the CAA.

7.5.2 Intermediate water depth Arctic marine sediment cores

7.5.2.1 St 6 box core

7.5.2.1.1 IP_{25} distribution

Measurement of HBI lipid concentrations for each 1 cm resolution sediment horizon from 0 – 29 cm (29 horizons), revealed the concentration of **I** (Figure 7.5-10).

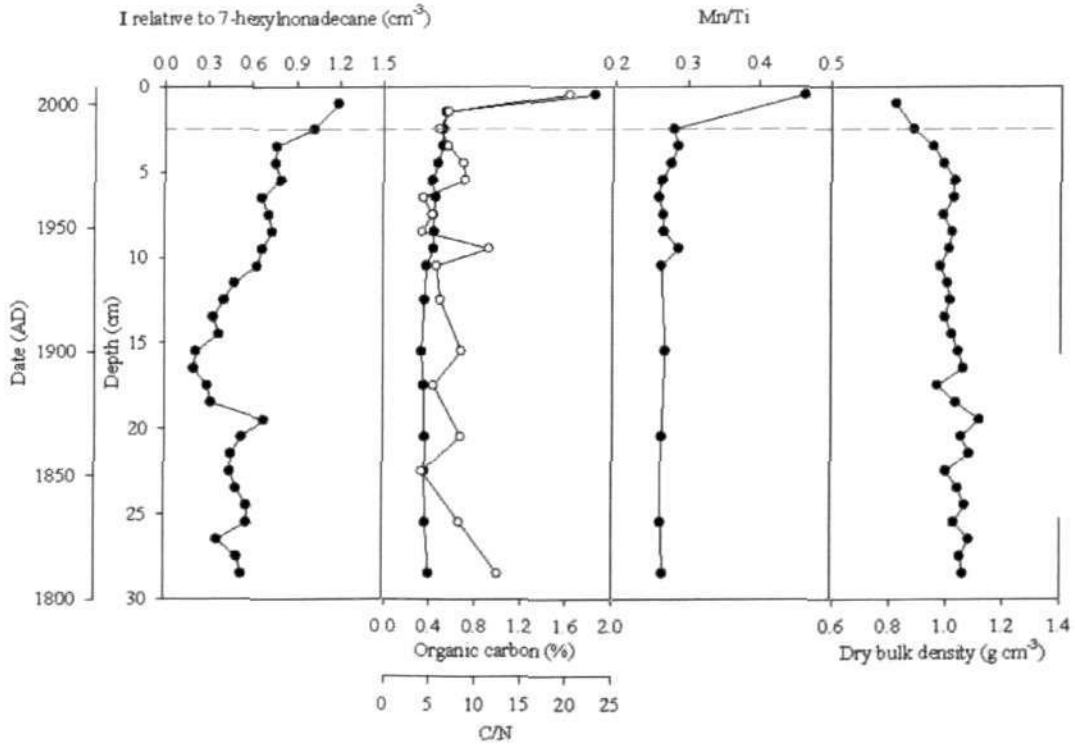

Figure 7.5-10. Vertical profiles of dry bulk density corrected biomarker **I**, with organic carbon (black) and C/N ratio (white), Mn/Ti ratio and dry bulk density for the sediments of St 6 (0 cm = water-sediment interface). Grey dashed line represents approximate position of the redox boundary determined by Mn oxidative state *vs.* Ti (Mn/Ti).

Each of the HBIs (**I** – **IIId**) used in this study were also detected in every sample (Figure 7.5-11).

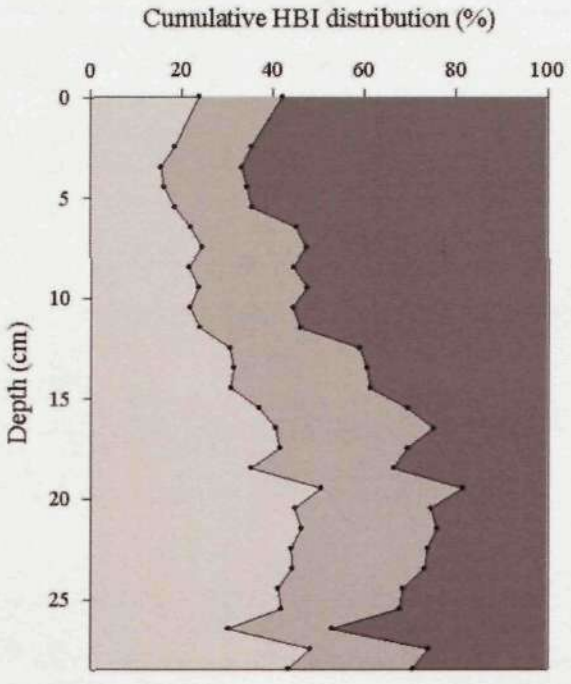

Figure 7.5-11. Cumulative distribution (%) of **I** (light grey), **IIa** and **IIb** (grey) and **IIIa**, **IIIb**, **IIIc** and **IIId** (dark grey) in St 6 box core sediments.

The downcore concentration profile of **I** in St 6 was variable, with a surface maximum, followed by a steady decrease in concentration to ca. 16 cm (Figure 7.5-10). Similarly, the di- and tri-unsaturated HBIs also decreased in relative abundance from ca. 80% near the surface to ca. 40% towards the bottom of the core (Figure 7.5-11).

7.5.2.1.2 Box core sediment geochemistry

As for previous cores, a chronology was constructed for St 6 based on the measured $^{210}Pb_{xs}$ content of 11 sediment horizons (between 0 - 13 cm) yielding a mean linear sedimentation rate of 0.16 cm yr^{-1}, almost twice as great as for the deep water cores

St 405b and St 308 (Figure 7.5-12). Examination of the $^{210}Pb_{xs}$ data suggested the presence of a shallow mixed layer at 0 – 0.5 cm.

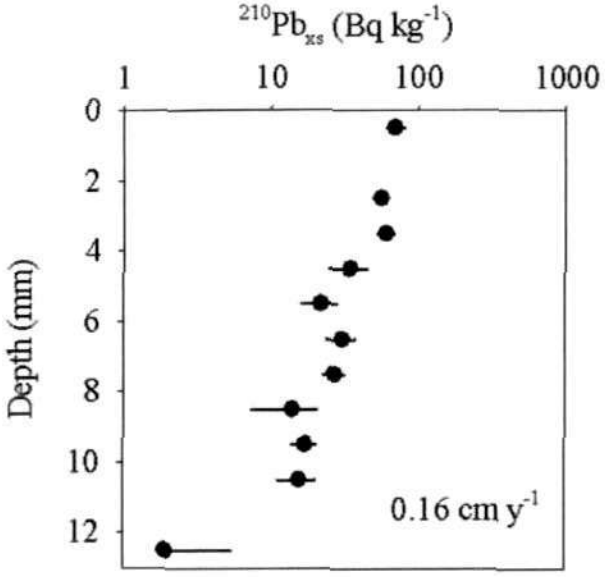

Figure 7.5-12. $^{210}Pb_{xs}$ data obtained from St 6 box core with mean sediment accumulation rate.

Extrapolation of the chronology over the length of the box core presented an age model spanning 202 years over 30 cm (ca. 6.7 yr cm^{-1}). Dry bulk density remained relatively unchanged throughout the core (1.01 ± 0.06 g cm^{-3}), with a slight overall increase with depth.

The Mn/Ti ratio also showed a surface maximum (0 – 1 cm) before declining steeply from 1 – 2 cm where it remained at ca. 0.28 throughout the rest of the box core (Figure 7.5-10). The OC content and C/N ratio profiles in St 6 reflect that for Mn/Ti with surface maxima and both declining in the adjacent (1 – 2 cm) sediment horizon where OC remained refractory to the bottom of the core while C/N varied slightly (7.8 ± 3.9), but remained indicative of marine source organic matter (Stein *et al.*, 2004).

7.5.2.2 St 7 box core

7.5.2.2.1 IP_{25} distribution

Measurement of HBI lipid concentrations for each 1 cm resolution sediment horizon from 0 – 38 cm (38 horizons), revealed the concentrations of **I** (Figure 7.5-13).

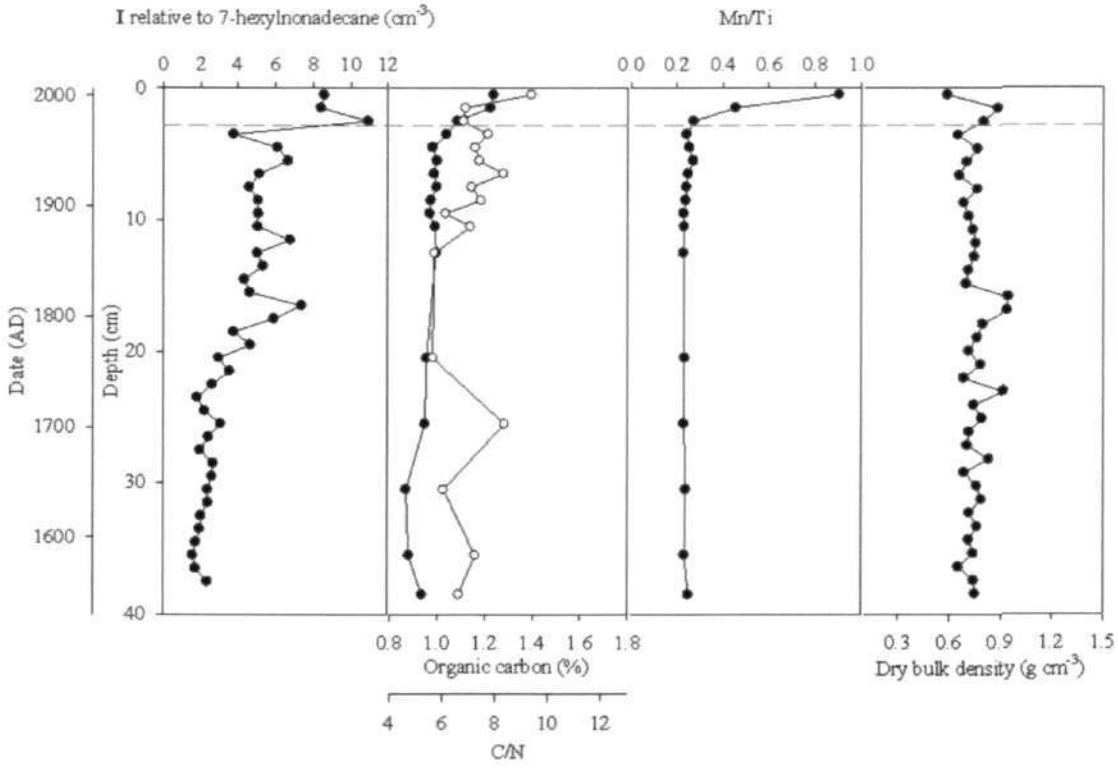

Figure 7.5-13. Vertical profiles of dry bulk density corrected biomarker **I**, with organic carbon (black) and C/N ratio (white), Mn/Ti ratio and dry bulk density for the sediments of St 7 (0 cm = water-sediment interface). Grey dashed line represents approximate position of the redox boundary determined by Mn oxidative state *vs.* Ti (Mn/Ti).

Each of the HBIs (**I** – **IIId**) used in this study were also detected in every sample (Figure 7.5-14).

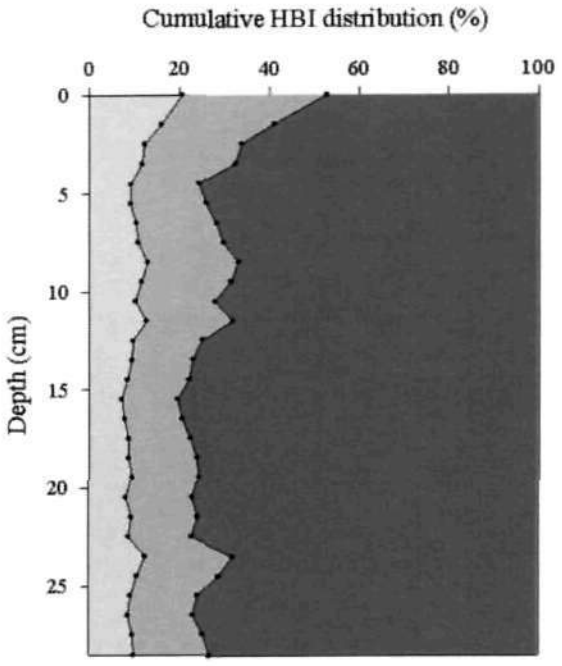

Figure 7.5-14. Cumulative distribution (%) of **I** (light grey), **IIa** and **IIb** (grey) and **IIIa**, **IIIb**, **IIIc** and **IIId** (dark grey) in St 7 box core sediments.

The downcore concentration profile of **I** in St 7 illustrated a near-surface (2 – 3 cm) maximum, followed by a steady decrease in concentration to the bottom of the core (Figure 7.5-13). In contrast, the combined relative distribution of the di- and tri-unsaturated HBIs increased from ca. 80% near the surface to ca. 90% towards the bottom of the core (Figure 7.5-14).

7.5.2.2.2 Box core sediment geochemistry

As for previous cores, a chronology was constructed for St 7 based on the measured $^{210}Pb_{xs}$ content of 9 sediment horizons (between 0 - 13 cm) (Figure 7.5-15) yielding a mean linear sedimentation rate of 0.08 cm yr^{-1}, ca. half as much as St 6 and almost equal to the deep water cores St 405b and St 308. Analysis of the $^{210}Pb_{xs}$ data suggested the presence of a mixed layer penetrating from 0 – 3.5 cm.

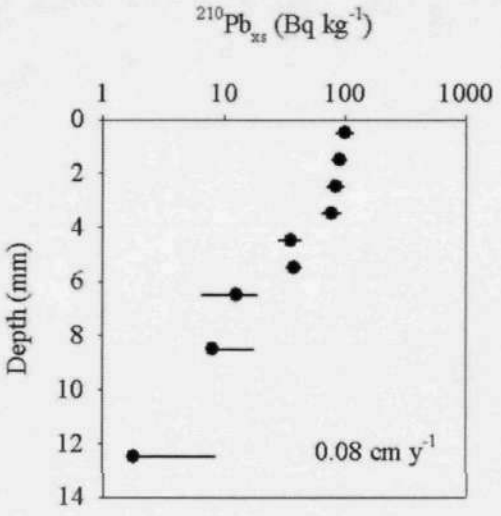

Figure 7.5-15. $^{210}Pb_{xs}$ data obtained from St 7 box core with mean sediment accumulation rate.

Extrapolation of the chronology over the length of the core presented an age model spanning 462 years over 40 cm (ca. 12 yr cm^{-1}). Dry bulk density showed little variation throughout the core (0.75 ± 0.08 g cm^{-3}). The distribution of Mn/Ti had a distinct surface (0 – 2 cm) maximum followed by decreasing values. The OC continent of St 7 at the surface was 1.2, declining to ca. 1.0 by ca. 4 cm with a mean C/N ratio of 7.1 ± 0.9.

7.5.3 Shallow water Arctic marine sediment cores

7.5.3.1 St 1216 box core

7.5.3.1.1 Highly branched isoprenoid distributions

The HBI lipid content of St 1216 sediments was determined for each 2 mm resolution sediment horizon with each of the HBIs (**I** – **IIId**) being present in all cases from 0 - 198 mm (99 horizons). Examination of the downcore concentration profile of **I**

(Figure 7.5-16) revealed variation throughout the length of the St 1216 core (16 ± 2.7 ng cm^{-3}).

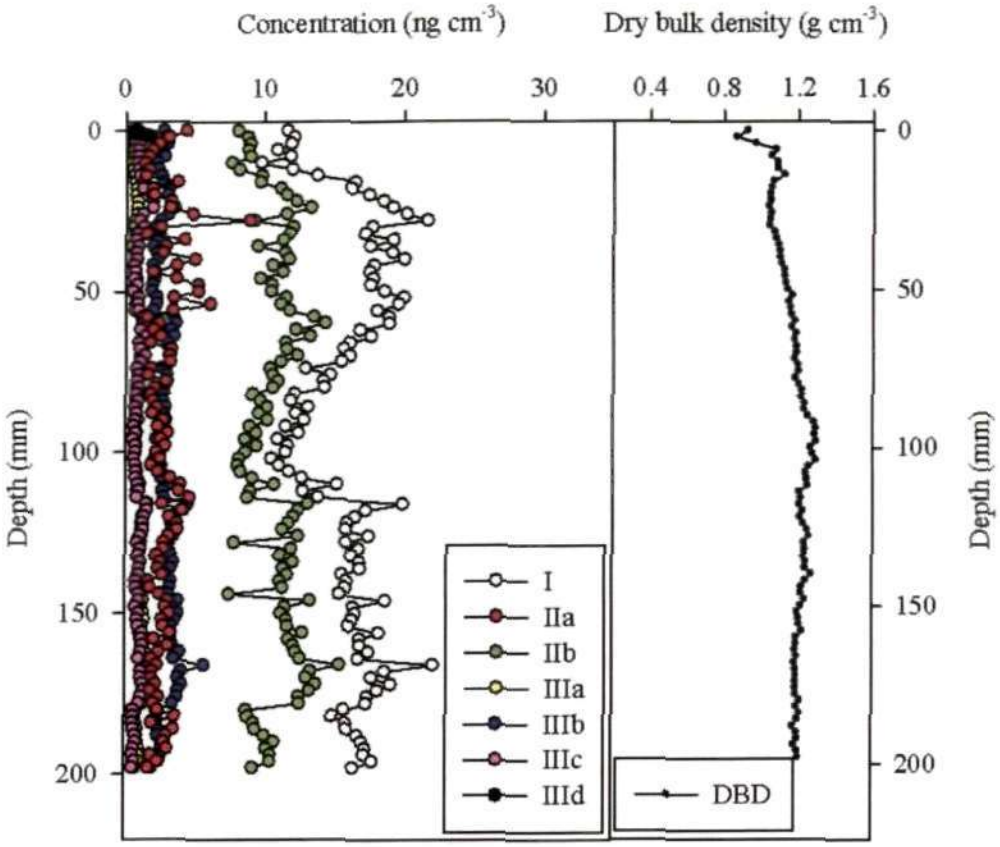

Figure 7.5-16. Vertical profiles of individual HBI lipids and dry bulk density in the sediments of St 1216 (0 cm = water-sediment interface).

Like St 405b, **I** was the most dominant HBI in St 1216 (ca. 45%) (Table 7-4), yet in contrast to St 405b, the lowest concentration of **I** occurred in surface to sub-surface sediments with 9.7 ng cm^{-3} at 10 mm.

Table 7-4. Relative distribution of HBI isomers observed in St 1216 (0 – 198 mm) and St 405b sediments (0 – 210 mm) compared to macrofaunal specimens (from Chapter 6), zooplankton (> 710 μm) (from Chapter 6), filtered seawater (> 20 μm) (from Chapter 6) and sea ice (from Chapter 4) during the IPY-CFL cruise (1/4/08 to 1/8/08).

	I	**IIa**	**IIb**	**IIIa**	**IIIb**	**IIIc**	**IIId**
Relative distribution (%) of HBI concentrations in St 1216 sediments	44.7	8.0	30.4	2.8	8.3	2.9	2.9
Relative distribution (%) of HBI concentrations in St 405b sediments	65.7	5.7	22.2	1.2	2.9	1.4	1.0
Relative distribution (%) of HBI concentrations in the macrofauna	34.9	6.2	29.8	5.0	12.6	5.5	6.1
Relative distribution (%) of HBI concentrations in zooplankton	11.0	8.9	15.4	0.0	44.4	11.8	8.5
Relative distribution (%) of HBI concentrations in filtered seawater	19.7	2.2	23.1	11.0	23.4	6.9	13.7
Relative distribution (%) of HBI concentrations in sea ice	27.2	1.7	31.4	1.0	28.1	0.8	9.8

Below ca. 118 mm concentrations of **I** became relatively stable at 17 ± 1.2 ng cm^{-3}, almost 7 times greater than in St 405b. The relative distribution of mono- di- and tri-unsaturated HBIs in St 1216 sediments was dominated, by **I** (Figure 7.5-17), with **IIa** and **IIb** contributing rather more than in St 405b (Figure 7.5-17 and Table 7-4). It was also observed that while the tri-unsaturated HBIs, (**IIIa – IIId**), collectively still only represented a minor fraction (ca. 17%) of the total HBIs (**I – IIId**), the contribution was consistent throughout the deeper sediments.

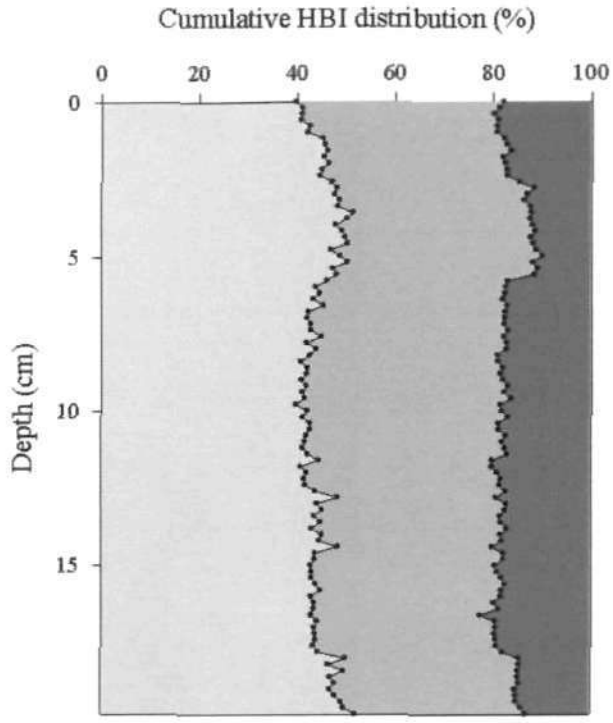

Figure 7.5-17. Cumulative distribution (%) of **I** (light grey), **IIa** and **IIb** (grey) and **IIIa**, **IIIb**, **IIIc** and **IIId** (dark grey) in St 1216 box core sediments.

Overall, the distribution of HBIs relative to each other in St 1216 most closely reflected those previously observed in macrofaunal specimens (Table 7-4) and St 405b.

7.5.3.1.2 Box core sediment geochemistry

A chronology based on the $^{210}Pb_{xs}$ measured in St 1216 sediments was attempted for 2 sediment horizons (between 0 - 3 cm) (Figure 7.5-18).

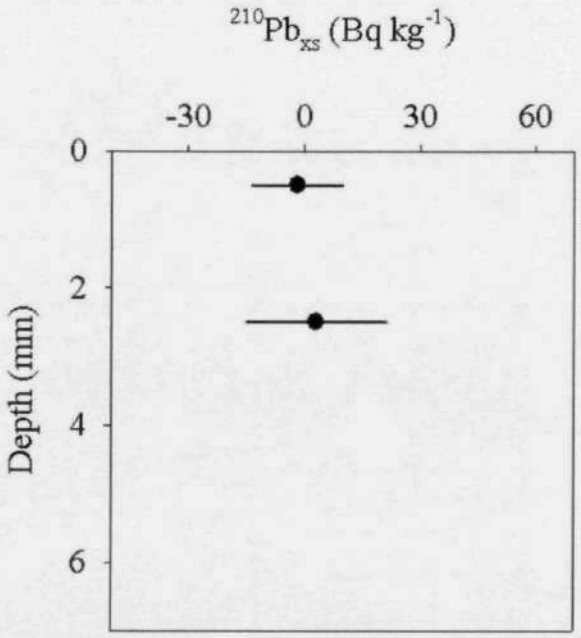

Figure 7.5-18. $^{210}Pb_{xs}$ data obtained from St 1216 box core with mean sediment accumulation rate.

Trial analysis of two surface horizons (0 - 1 cm and 2 – 3 cm) revealed considerable sediment mixing throughout, potentially resulting from bioturbation, which prevented estimation of a useable age model for this core. Dry bulk density remained relatively unchanged throughout at 1.2 ± 0.08 g cm^{-3} (Figure 7.5-16).

In St 1216 the downcore ratio profile of the labile, solid state, Mn against the relatively refractory Ti was highly variable (3.1 ± 1.1) and did not reflect the profiles of **I**, OC or the pr/ph ratio (Figure 7.5-19 and Figure 7.5-20).

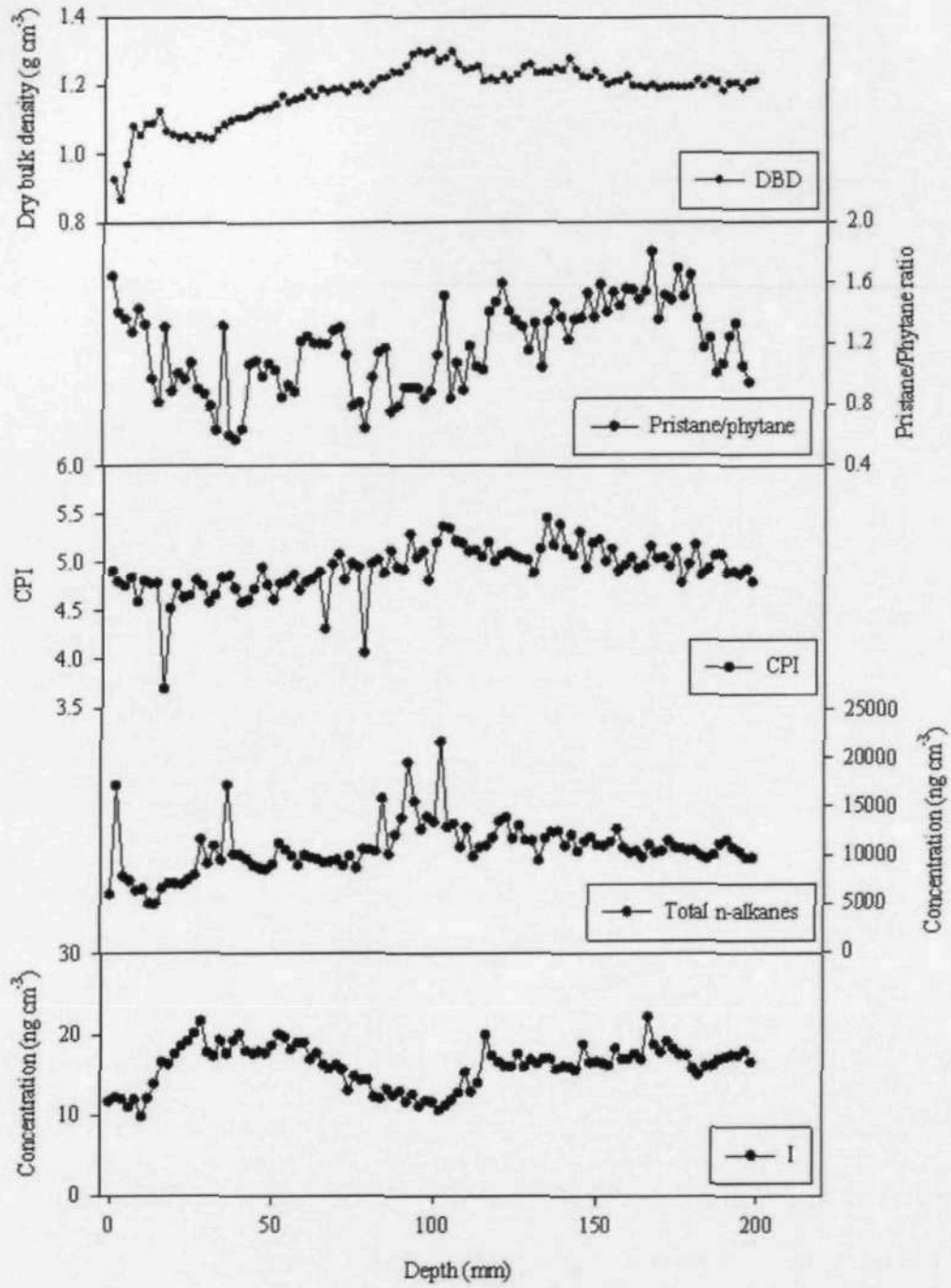

Figure 7.5-19. Vertical profiles of biomarker **I** and *n*-alkanes with CPI and pristine/phytane ratios, with dry bulk density in the sediments of St 1216 (*0 cm* = water-sediment interface).

The pr/ph ratio also did not indicate any significant enhancement or decline as it fluctuated near unity (1.2 ± 0.3). However, the lithogenic indicator ratio, Al/Ti did correlate to **I** ($r = 0.81$; $p = < 0.001$) and, to a far lesser extent, OC ($r = 0.56$; $p = 0.04$)

(Figure 7.5-20). Given the coastal immediacy of this core (< 14 km) and proximity of the nearby Horton River (< 80 km), increases and indeed fluctuations of likely terrestrially derived aluminium in sediments were justified (Stoffyn *et al.*, 1982; Middag *et al.*, 2009 and references therein).

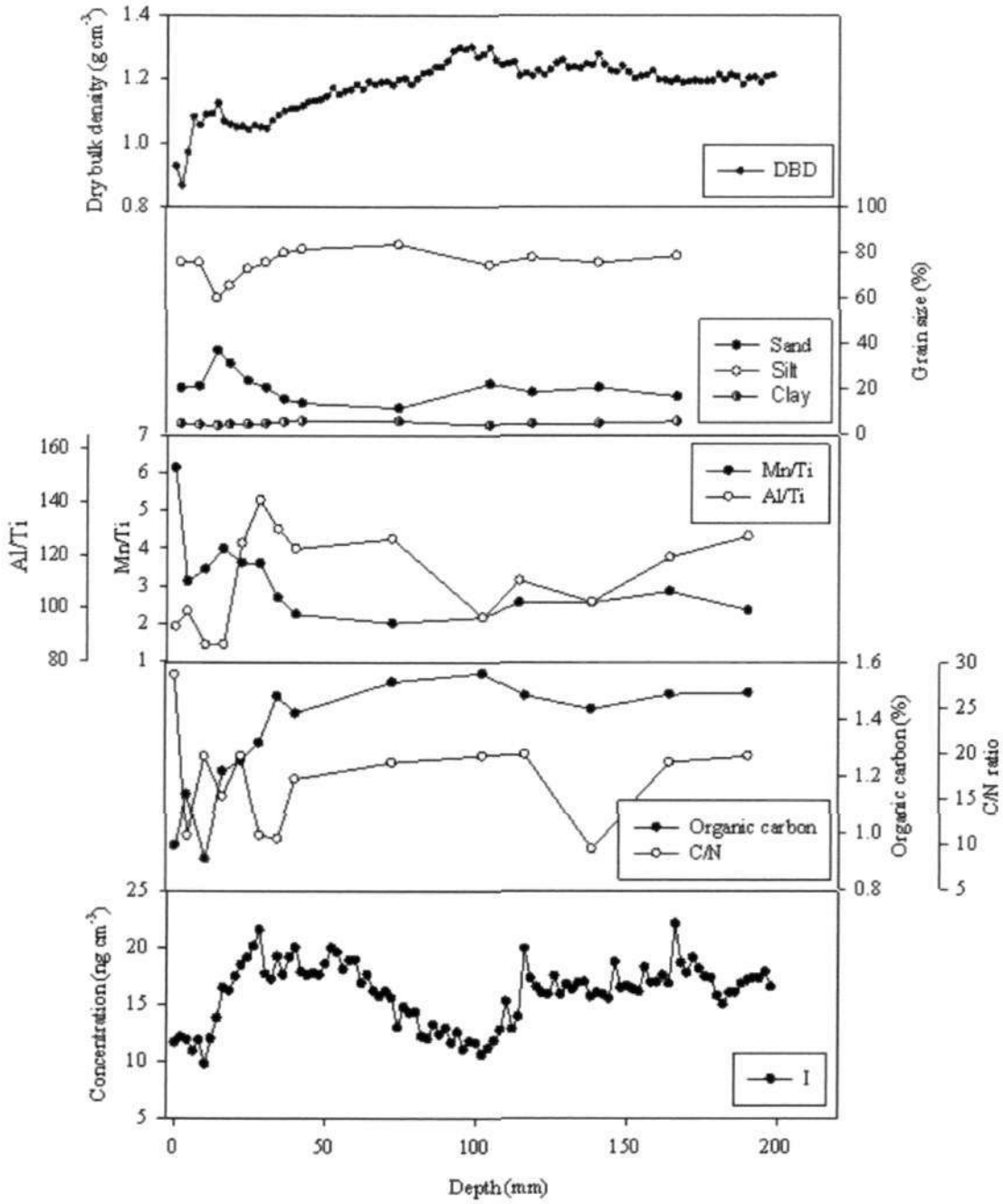

Figure 7.5-20. Vertical profiles of biomarker **I** and organic carbon (black) with C/N (white), Mn/Ti (black) and Al/Ti ratios (white), with sediment grain size and dry bulk density in the sediments of St 1216 (0 cm = water-sediment interface).

An enhancement of OC composition (Figure 7.5-20), compared to St 405b, comprising 1.3% ± 0.2% remained consistent with numerous published data for the south-eastern Beaufort Sea and Amundsen Gulf (e.g. Stein *et al.*, 2004 and references therein) and was potentially suggestive of increased primary production in this region.

A mean C/N ratio in St 1216 sediments of 17.1 ± 5.2 was indicative of terrestrial input (Figure 7.5-20), with the variation in the surface to sub-surface (0 – ca. 40 mm) distributions of OC and the C/N ratio supporting the notion of mixing suggested by the $^{210}Pb_{xs}$ distribution (Figure 7.5-18).

The *n*-alkanes (nC_{15}-nC_{33}) also had a relatively linear distribution (Figure 7.5-19), with far greater (ca. 600 times) concentrations than **I** (10.6 ± 2.6 μg cm^{-3}) consistent with steady terrestrial input. Indeed, stable carbon isotope analysis of the surficial (0 – 2 mm) *n*-alkanes (nC_{17} – nC_{33}) revealed a typical terrestrial signal ($\delta^{13}C$ = -32.1 ± 0.7 ‰). Calculation of the CPI (Equation 17) revealed no distinct change in the contribution of either odd or even *n*-alkanes, throughout the core, with a mean CPI of 4.9 ± 0.3, characteristic of more recently deposited biological material (e.g. > ca. 3; Bray *et al.*, 1961; Scalan *et al.*, 1970; Peters *et al.*, 2007).

Finally, determination of sediment grain sizes revealed a variable composition throughout, with silt comprising 75% ± 6.4% (Figure 7.5-20). The increased presence of coarse grain sand particles (20.6% ± 6.9%) likely reflected terrestrial erosion given the coastal location of the core and was consistent with grain sizes observed near Cape Bathurst compiled by Stein and Macdonald (2004).

7.5.3.2 St 12 box core

7.5.3.2.1 IP_{25} distribution

Measurement of HBI lipid concentrations for each 1 cm resolution sediment horizon from 0 – 45 cm (45 horizons), revealed the presence of each HBI (**I** – **IIId**) previously described in sea ice, filtered seawater and macrofauna in this study in every sample. The downcore concentration profile of **I** in St 12 was variable between sediment horizons (11.8 ± 3.4 ng cm^{-3}), but showed no significant enhancement or decline overall (Figure 7.5-21), similar to that described for **I** in St 1216 (Figure 7.5-16).

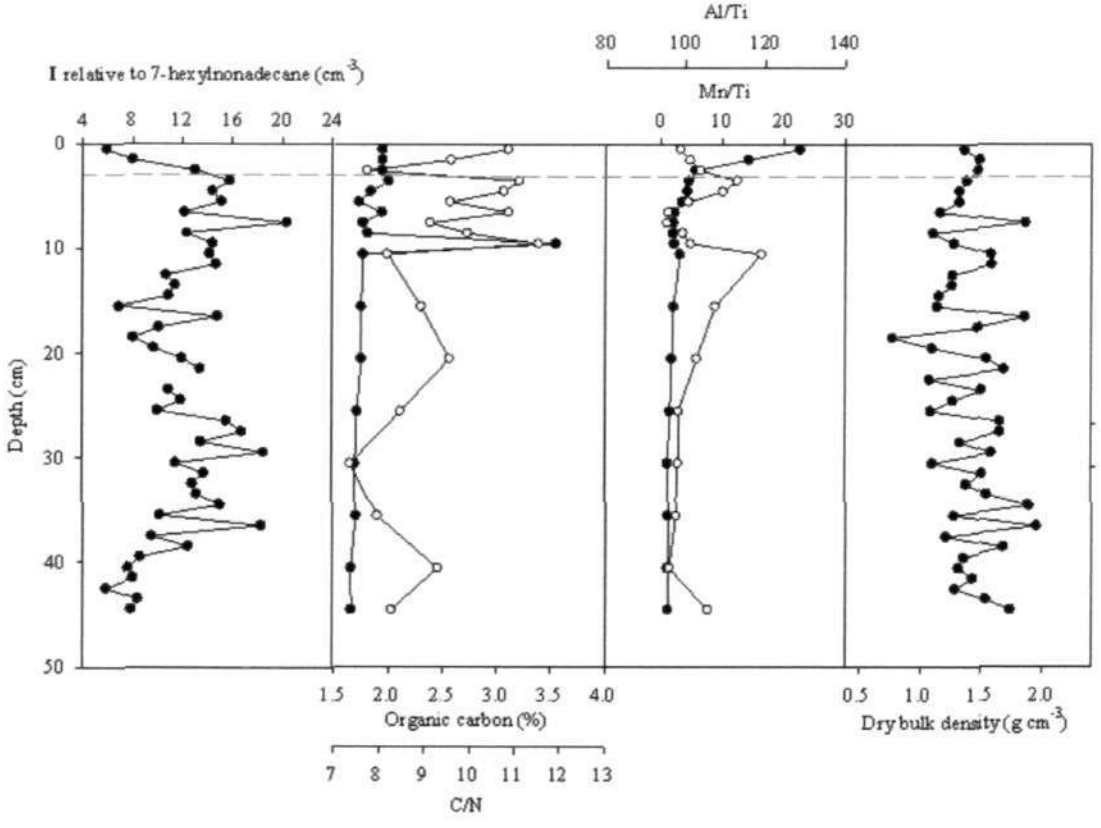

Figure 7.5-21. Vertical profiles of dry bulk density corrected biomarker **I**, with organic carbon (black) and C/N ratio (white), Mn/Ti (black) and At/Ti (white) ratios and dry bulk density for the sediments of St 12 (0 cm = water-sediment interface). Grey dashed line represents approximate position of the redox boundary determined by Mn oxidative state *vs.* Ti (Mn/Ti).

The relative distribution of mono- di- and tri-unsaturated HBIs in St 12 also showed little variation, with **I** contributing far less than in the previous cores (< 25%) (Figure 7.5-22).

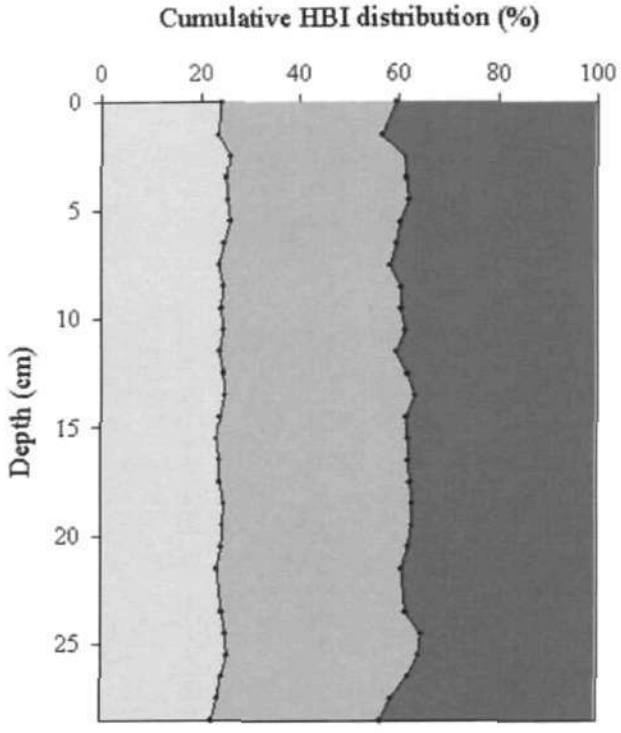

Figure 7.5-22. Cumulative distribution (%) of **I** (light grey), **IIa** and **IIb** (grey) and **IIIa**, **IIIb**, **IIIc** and **IIId** (dark grey) in St 12 box core sediments.

7.5.3.2.2 Box core sediment geochemistry

As for previous cores, a chronology for St 12 was attempted based on the determination of $^{210}Pb_{xs}$ in 3 sediment horizons (between 1 - 9 cm) (Figure 7.5-23).

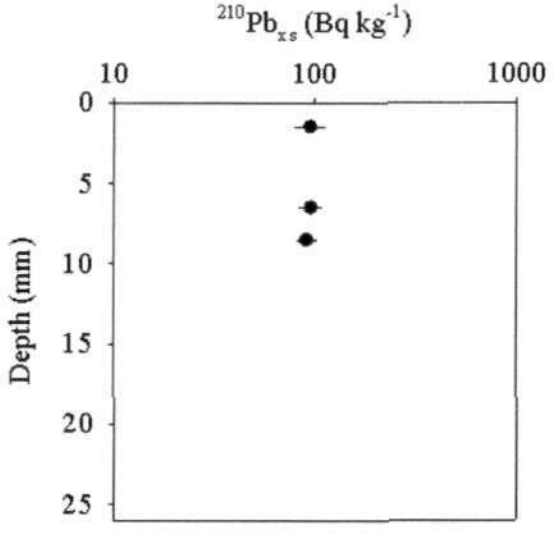

Figure 7.5-23. $^{210}Pb_{xs}$ data obtained from St 12 box core with mean sediment accumulation rate.

Trial analysis of three surface sediment horizons provided evidence for the occurrence of considerable sediment mixing in the surface horizons at least, which prevented construction of a useable age model.

Additionally, a highly variable (0.7 g cm^{-3} to 1.9 g cm^{-3}) dry bulk density was measured with a modal density of 1.3 g cm^{-3} (Figure 7.5-21).

The sediment profile of the ratio of Mn/Ti in St 12 showed a surface maximum before declining towards 2 cm where the ratio became constant throughout the rest of the core. The Mn/Ti profile did not reflect that of **I** or other geochemical observations (Figure

7.5-21). In contrast, the Al/Ti ratio revealed a variable, or potentially mixed, contribution of aluminium, similar to that found for St 1216 (Figure 7.5-21).

Calculation of the OC and C/N ratios, revealed variable compositions, analogous to those recorded in St 1216; 1.9% ± 0.4% (Figure 7.5-21), potentially as a result of variation in terrigenous nitrogen supply given the different riverine inputs of St 12 and St 1216 in the CAA, with St 12 receiving sediments from the nearby (< 50 km) Hornaday River.

7.6 Discussion

A better understanding of the physiochemical properties of Arctic marine sediments is desired if the interpretation of **I** in this medium is to be used for palaeo-sea ice reconstructions. The ability to accurately deduce the significance of **I** in sediments relies entirely on the prolonged, accurate, representation of this lipid following deposition.

The observation of sub-surface (< 10 cm) decreases in concentration of HBIs in some sediment box cores analysed here exposed a potential caveat to this approach. Analysis of organic/inorganic geochemical data obtained from a range of sediments, from the Amundsen Gulf, established three potential trends in HBI preservation in surficial sediments; 1) labile, with surface maximum followed by rapidly decreasing concentrations, 2) intermediate, exhibiting a surface maximum concentration with gradually declining concentrations with depth, 3) refractory, with no distinct maximum or minimum concentrations. An apparent dependence of the preservation of **I** and other HBIs on OC flux and oxygen penetration is proposed.

7.6.1 Labile lipid profiles

Sediments collected from St 405b and St 308 were collected from deep water sites (500 m and 341 m respectively), more than 50 km offshore, with neither station being reported as being exceptionally abundant in terms of macrofaunal organisms (Conlan *et al.*, 2008). Measurement of the $^{210}Pb_{xs}$ decay rate in surface sediments from both stations supported the presence of undisturbed sedimentation at a relatively slow rate ca. 0.08 – 0.09 cm y^{-1} in support of a low productivity environment. Isolation of diatoms from the sediment matrices of two horizons in St 405b (Figure 7.5-3) revealed that sediments, rather than diatoms retained the majority (ca. 98%) of **I** detected in samples. Having established the limited ability of diatoms to retain this HBI following deposition

at this site, attention was instead focused on the sediments. Further geochemical analysis of these sediments enabled estimation of the redox depth based on the ratio of Mn/Ti in sediments from both St 405b and St 308 (ca. 75 mm). The measured redox depth was found to correlate strongly with sediment lipid profiles in each case ($r = > 0.88$, $p = <0.0001$), suggesting the potential for redox associated diagenesis of HBIs in these sediments, at least. Further, determination of the OC content of the sediments, known to influence oxygen penetration in the sediments by stimulating biological activity (Thomson *et al.*, 1996; Gobeil *et al.*, 1997; Katsev *et al.*, 2006) also reflected the concentration profile of **I** in both sediment cores, further supporting the hypothesis of redox associated HBI diagenesis.

In these two deep water offshore sediment box cores from different regions of the CAA, it was observed that the mean relative distribution of mono- di- and tri-unsaturated HBIs were similar to each other, with **I** accounting for 65.7% and 55.9% of the total HBIs in St 405b and St 308 respectively (Table 7-5), while the remaining di- and tri-unsaturated HBIs accounted for less than 33% and less than 12% respectively.

Table 7-5. Mean relative distributions (%) of mono- di- and tri-unsaturated HBIs detected in sediment cores from the CAA.

	I	**IIa + IIb**	**IIIa - IIId**
St 405b	65.7	27.9	6.5
St 308	55.9	32.1	11.4
St 1216	44.7	38.4	16.9
St 12	24.1	34.8	41.1
St 6	25.8	22.2	51.9
St 7	10.6	17.3	72.0

The mean relative distribution of the individual HBIs recorded in St 405b (Table 7-2) were found to most closely represent the distribution measured in macrofaunal

specimens (r = 0.89 p = < 0.001) (Chapter 6) rather than sea ice (Chapters 4 and 5), filtered seawater or zooplankton (Chapter 6).

7.6.2 Intermediate lipid profiles

Sediments collected from St 6 and St 7 were collected from intermediate water depths at two sites (61 m and 117 m respectively), no more than 15 km offshore, with neither station being reported as being exceptionally biologically productive (Conlan *et al.*, 2008). Measurement of the $^{210}Pb_{xs}$ decay rate in surface sediments from both stations supported the presence of undisturbed sedimentation at relatively high rates (St 6 ca. 0.16 cm y^{-1} and a lower rate; St 7 ca. 0.08 cm y^{-1}), suggesting the potential of varied marine and terrestrial input sources in these environments resulting from the coastal proximity.

Further geochemical analysis of these sediments enabled estimation of the redox depth based on the ratio of Mn/Ti in sediments from both St 6 and St 7 (ca. 2 cm). Unlike for the deeper water cores (St 405b and St 308), the measured redox depth was not found to correlate strongly with sediment lipid profiles in either core, although the steepest decline in concentration of **I** does occur within the top 2 cm of each core (Figure 7.5-13 and Figure 7.5-16). Combined, these data suggest that redox associated diagenesis of HBIs in these sediments at least is potentially still present, although less significant than in St 405b and St 308.

Further, determination of OC content and C/N ratio reflected the Mn/Ti ratio, supporting the connectivity of carbon content and oxygen penetration in Arctic marine sediments.

In these two intermediate water, near shore sediment cores, it was observed that the mean relative distribution of mono- di- and tri-unsaturated HBIs were similar to each

other, yet differed from the deepwater cores, with **I** accounting for 25.8% and 10.6% of the total HBIs in St 6 and St 7 respectively (Table 7-5), while the remaining di- and tri-unsaturated HBIs were < 23% and < 72% respectively. While it is difficult to attribute these differences to a particular cause, it is hypothesised that the relative increase in poly-unsaturated HBIs is the result of increased phytoplankton production rather than degradation of **I** in this region.

7.6.3 Refractory lipid profiles

Box core sediments were collected at St 1216 and St 12 from intermediate water depths (100 m and 219 m respectively), less than 10 km offshore. St 1216 is a particularly biologically productive site (Conlan *et al.*, 2008) receiving cold water upwelling and with it, nutrient replenishment (Williams *et al.*, 2008). In addition, both St 1216 and St 12 receive a terrestrial sediment contribution from the Horton and Hornaday Rivers respectively. In agreement with a biologically active region, linear decay rates in the measured $^{210}Pb_{xs}$ were not observed in surface sediments from either station, suggesting that sediments were mixed (Schmidt *et al.*, 2007). Further geochemical analyses of these sediments were used to attempt to estimate the redox depth based on the ratio of Mn/Ti in sediments with limited success. Determination of the Al/Ti ratio, to provide information on the detrital constituent of the sediment, revealed a highly variable contribution in both cores, indicating a degree of inconsistency in sediment source that is mirrored in the concentration of **I** in St 1216 at least ($r = 0.81$; $p = < 0.001$). Combined, these data provide evidence for assigning a mixed sediment profile and therefore inaccurate representation of palaeo-sea ice conditions. Importantly, unlike the non-mixed sediment profiles of **I** observed in this study (St 405b, St 308, St 6 and St 7), concentrations of **I** did not decrease with depth in St 1216 or St 12.

In these two intermediate water depth, near-shore sediment cores, it was observed that the mean relative distribution of mono- di- and tri-unsaturated HBIs were not that similar to each other, with **I** accounting for 44.7% and 24.1% of the total HBIs in St 1216 and St 12 respectively (Table 7-5), while the remaining di- and tri-unsaturated HBIs were < 39% and < 41% respectively. The mean relative distribution of the individual HBIs recorded in St 1216 (Table 7-4) were found to most closely represent the distribution measured in macrofaunal specimens (Chapter 6) ($r = 0.98$ $p = < 0.001$) rather than sea ice (Chapters 4 and 5), filtered seawater or zooplankton (Chapter 6). Since macrofaunal specimens were collected from near St 1216, this potentially suggests that HBIs in the benthos reflect that of the sediments they inhabit.

7.6.4 Distribution of mono- di- and tri-unsaturated HBIs in sediments

Measurement of the mono- di- and tri-unsaturated HBIs in all six shallow (< 45 cm) Arctic box cores revealed that sediments collected from similar environments, although not necessarily adjacent to each other, contained HBIs in similar distributions (Figure 7.6-1).

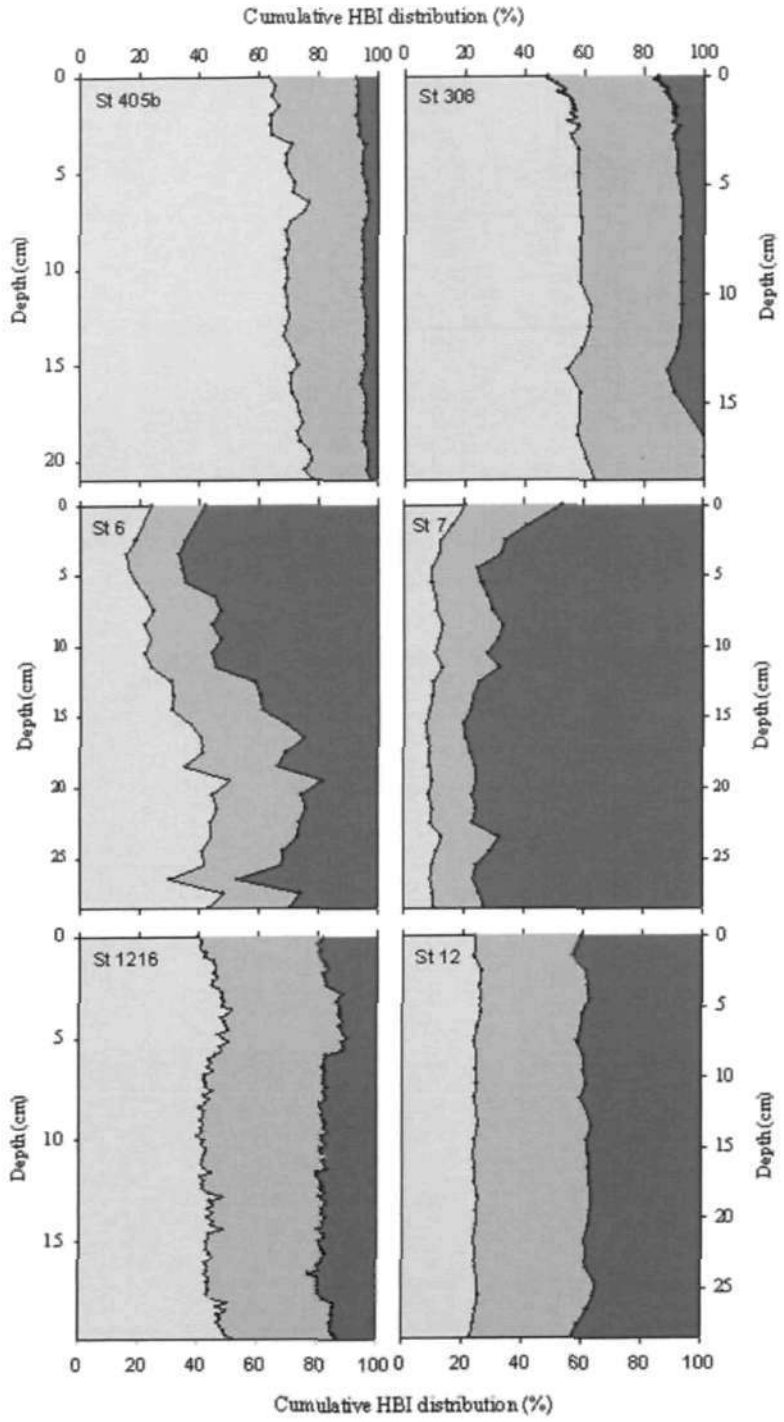

Figure 7.6-1. Cumulative distribution (%) of **I** (light grey), **IIa** and **IIb** (grey) and **IIIa**, **IIIb**, **IIIc** and **IIId** (dark grey) in box core sediments.

St 405b and St 308 collected from deep water environments contained a greater distribution of **I** than other HBIs, while St 6 and St 7, collected from the shallowest water depths, contained a greater distribution of tri-unsaturated HBIs. While it is

therefore hypothesised that HBI distributions in shallow surface and sub-surface Arctic box cores will be influenced by water depth, it is anticipated that water depth alone is not the controlling factor. Since water depth can be associated with many physical and biological factors such as coastal proximity, light attenuation, upwelling and terrestrial inputs for example. It is therefore hypothesised that these considerations are more likely to be responsible for the HBI distributions observed rather than water depth alone.

Finally, the distributions of mono- di- and tri-unsaturated HBIs in these six sediment box cores did not indicate any preferential degradation in association with unsaturation through depth with, in most cases, the distribution of HBIs, relative to one another, remaining fairly constant throughout.

7.7 Conclusion

Diatom analysis and the distributions of biogeochemical indicators have provided some evidence for the diagenetic potential of a range of shallow surface and sub-surface Arctic marine sediments. Through statistical analysis it was determined that oxygen penetration, measured *via* Mn mobility, was most likely influential in the preservation of IP_{25} in deep water non-mixed sediments at least While the precise chemistry involved in HBI diagenesis remains unknown, it would appear that reactions in the presence of oxygen, rather than sulphur, could be the primary mechanism for HBI degradation in some surface Arctic marine sediments.

In addition, the role of OC appears central to controlling the depth of oxygen penetration, and therefore HBI degradation, in these sediments. The annual episodic pulse input of sea ice bloom originated carbon may have significant implications for an otherwise reduced productivity region, providing material for microbial decomposition in oxic sediments.

Further, regions of the Arctic Ocean where carbon flux to the sediment is sufficient to support macrofaunal communities are likely to experience considerable sediment reworking. The requirement of nutrients, oxygen and carbon for many of these organisms often means these regions are confined to shallow, marginal shelf seas where upwelling and terrestrial runoff supply nutrients and seasonal sea ice provides much of the carbon (Clough *et al.*, 1997). It is observed that bioturbation in these regions (St 1216 and St 12) is considerably more severe than in deeper, less productive water (St 405b and St 308). The implication for attenuation of decadal or millennial scale events recorded in sediments however has not been addressed, but is expected to vary with benthic productivity rates and dominant species type. With a 50% attenuation of a 4 kyr event in moderately mixed sediments with accumulation of ca 0.001 cm yr^{-1} (Anderson, 2001) the potential for well mixed Arctic sediment attenuation requires consideration.

Finally, the distinctive characteristics of the sediment and lipid profiles discussed in this chapter may aid predictions of the extent of preservation of IP_{25} in new sediments based on water depth, coastal proximity and the biological productivity of the region.

CHAPTER EIGHT

8 Conclusions and future work

This chapter outlines the main findings of the work described in this thesis and summarises the key conclusions. In particular, the combined experimental outcomes have provided new information regarding the production and fate of the Arctic sea ice biomarker IP_{25} and these will assist in the interpretation of sedimentary distributions in the future..

8.1 Objectives of this research

The presence of HBIs in the marine environment has long been known, with diatoms having been identified as the source of these ubiquitous lipids (Robson *et al*, 1986; Rowland *et al.*, 1990; Hird *et al*, 1995; Wraige *et al*, 1998b; Sinninghe Damsté *et al.*, 1999; Belt *et al.*, 2001c; Rowland *et al*, 2001a) One mono-unsaturated C_{25} HBI, termed IP_{25}, identified as being specific to some sea ice endemic diatoms (Belt *et al*, 2007) has since been isolated and quantified in a variety of Arctic marine sediments facilitating palaeo-sea ice extent reconstructions (e.g. Belt *et al.*, 2007; Andrews *et al.*, 2009; Müller *et al.*, 2009; Vare *et al*, 2009; Belt *et al*, 2010).

Despite this, little was known previously about the specific environmental conditions in which the sea ice diatoms produced IP_{25} (or other HBIs), or the process of sedimentation and preservation in shallow surface and sub-surface sediments.

To this end, the specific objectives of this study were to:

1 Determine the temporal and spatial restrictions on the production of IP_{25} and other HBIs in diatoms within Arctic sea ice.

ii. Determine concentrations of IP_{25} (and other HBIs), fatty acids and sterols in pelagic communities of the Amundsen Gulf during spring to identify differences between sea ice and pelagic lipid concentrations.

iii. Carry out a qualitative investigation on the content of IP_{25} and other HBIs in macrofaunal organisms within the water column and benthos.

iv. Investigate relationships that may exist between IP_{25} and any other geochemical parameters measured in shallow surface marine sediments within the CAA.

In order to fully investigate these objectives, it was necessary to collect a time series of Arctic sea ice cores, water-column and benthic samples containing various micro- and macrofaunal biota and marine surface sediment cores. Each sample was analysed for IP_{25} and other HBIs with some also being analysed for a suite of lipids commonly used to represent algal productivity in marine environments.

8.2 Conclusions of this research

The first aim of this study was to identify the timing of IP_{25} and other HBI production in Arctic sea ice. Analysis of replicate sea ice samples collected from January through to July provided sea ice lipid distributions during spring in 2008 (Chapter 4), with a distinct increase in concentrations of IP_{25} and other HBIs evident from mid to late March through to early May. Additional analysis of established diatom productivity indicator lipids (e.g. fatty acids), along with diatom cell concentrations and chlorophyll *a* concentrations, provided compelling evidence in favour of IP_{25} (and some other HBI) concentrations representing an Arctic sea ice diatom bloom.

A similar multiproxy technique was adopted (Chapter 5) using the same lipid biomarkers to establish the limitations of internal sea ice production of IP_{25} and other HBIs. Higher resolution sectioning of sea ice cores (1 cm) containing early and mid-

bloom lipid concentrations provided a greater insight into the sea ice specificity of the HBIs investigated in this study Comparison of these lipids to the porosity of the ice, estimated by calculation of brine volume, provided the basis for classification of lipids into three regions; 1) Planktonic lipid region (PLR) 2) Sea ice lipid region (SILR) and 3) Non-specific lipid region (NLR).

As a result, at least some of the temporal and spatial controls on the production of IP_{25} and other HBIs in Arctic sea ice were established, the findings of which can now be incorporated into both existing and future sedimentary interpretations of palaeo-sea ice conditions of the region.

The second aim of this work was to investigate some of the processes that occurred subsequent to the production of IP_{25} and other HBIs in Arctic sea ice. Following sea ice melt, diatoms containing IP_{25} and other HBIs were released to the water column and were found to experience considerable decreases in concentration compared to sea ice, with dilution factors quantified at approximately 8.2×10^5 and 6.5×10^5 respectively (Chapter 6). Other Lipids, such as fatty acids and sterols, were also found at lower concentrations in the water column, compared to sea ice, although this was probably due to water column enhancement of at least some of these lipids from planktonic sources since these lipids were comparably less dispersed than IP_{25} or the other HBIs in the water column.

Once dispersed in the underlying water column IP_{25} and other lipids became susceptible to numerous physical and biological interactions of which biological removal was investigated qualitatively. By collecting and analysing the lipid content of eight species of Arctic marine macrofauna from four phyla it was found that many of these pelagic and benthic organisms contained IP_{25} and some other HBIs. The sea urchin *Strongylocentrotus* sp. contained in excess of 5µg IP_{25} per specimen, that indicated the

potential for a significant interruption of the transport of this biomarker from sea ice to the sediments. Rudimentary microscopic investigation of the stomach of *Strongylocentrotus* sp. also revealed the presence of sea ice diatoms, providing evidence for assigning ingestion as the mechanism of inclusion, while stable carbon isotope data for individual lipids confirmed a sea ice origin.

The fourth aim of the study was to consider the short-term preservation of IP_{25} (and to a lesser extent other HBIs) in Arctic surface marine shelf sediments. Previously, sedimentary distributions of IP_{25} often (although not always) included a surface (0 – 1 cm) maximum in concentration before rapidly declining within the first few centimetres of the core. It was unclear if the cause of this near surface decline in concentration was a reflection of recent sea ice conditions or of potential early diagenesis of the biomarker.

For this study, the collection of six sediment cores from three distinctly different regions (e.g. water depth, biological productivity and coastal proximity) were used as a basis for investigating this phenomenon. Multiproxy geochemical analyses were adopted to determine the sediment geochemistry in each case. For non-bioturbated sediments at least, significant statistical correlations indicated a connection between concentrations of IP_{25} and the organic carbon content, as well as Mn mobility in the sediments. Combined, the data suggested that the near surface decreases measured in IP_{25} concentrations more likely reflected the geochemistry of the sediments than an accurate record of recent sea ice conditions.

As a result, further investigations are required before this important finding can be confirmed, but in the mean time it is recommended that care be taken in interpreting short cores. Regarding previously published longer sediment cores, the main focus seldom involves the surface sediments, yet this should be a consideration in terms of fluctuations in overall concentrations of IP_{25} throughout the core.

To summarise, while some objectives of this thesis were addressed in full and have provided important information on the temporal and spatial production of IP_{25} and other HBIs in Arctic sea ice, other objectives remain either qualitatively or inconclusively addressed at this point. However, it is important to realise that they represent the initial exploration of what is a highly complex system in a highly demanding environment. Despite this, IP_{25} and other HBIs in the Arctic have never been studied in such detail and as such it is hoped that much of the work carried out in this thesis will form the foundation for future studies of this important sea ice diatom biomarker and its continued application as a useful sea ice proxy.

8.3 Future work

The data presented here have provided detailed information on the production, distribution and preservation of IP_{25} and other HBIs in the Arctic. The interpretation of these findings is however based on measurements and observations from one year in the Arctic. To ensure these findings are reliably interpreted, continued attempts to further refine observations relating to the timing and distribution of IP_{25} and other HBIs in sea ice are desirable from subsequent years Whilst it is anticipated that the production of these HBIs in other Arctic regions will also be coincident with sea ice diatom blooms, other influences, such as the local geography or oceanography, may result in some differences.

A highly important, yet relatively simple, experiment that should be carried out at the nearest opportunity would attempt to answer a fundamental question relating to the

production of IP_{25} in sea ice; how do sea ice specific diatoms become seeded into the sea ice each year? The hypothesis suggested in Chapter 6 indicates that these sea ice diatoms may reside on the seafloor in shallow regions where they act as nuclei for ice crystal growth which subsequently float to the surface to form sea ice. Collection of box core sediments from shallow (< ca. 50m) coastal bays could be used to investigate this. The application of a microscope slide cover slip in the presence of light would encourage live benthic diatoms to adhere to the glass, while senescent or dead cells would remain in sediment. Microscopic identification of these glass adhered cells could be used to study the diatom assemblage for the presence of sea ice diatoms.

Since some samples (e.g. filtered seawater column samples) were not obtained as part of a pre-planned sampling schedule (c.f. sea ice sampling), it would be desirable that further attention be focused on establishing a more stationary, long-term sampling strategy in the Arctic that may provide temporal concentration data associated with sea ice melt from one region to eliminate the effects of ship mobility to improve this data, providing a more accurate account of the timing, concentration and rate of transport of IP_{25} and other HBIs to the water column and seafloor.

As a result of identifying IP_{25} and other HBIs in opportunistic macrobenthos samples of the Amundsen Gulf, the reliability of existing and future sedimentary analyses of IP_{25} may require greater consideration of the potential for biological removal of this biomarker. As such, it is recommended that, where possible, the biology of a region is noted. Further, it is proposed that the sea ice specificity, along with significant biological accumulation in some organisms of IP_{25}, may result in a subsequent application of this biomarker as a food web tracer of sea ice diet to assist in rapid determination of carbon budget distributions in the Arctic.

Further investigation of IP_{25} within the stomach of *Strongylocentrotus* sp. at least should continue following the detection of the biomarker in a selection of 15 specimens from north east Greenland Since Bluhm *et al*, (1998) observed an average 3.6 *Strongylocentrotus pallidus* individuals m^{-2} in the Northern Barents Sea, the continued investigation of this species is considered important Indeed, the global distribution of echinoids, combined with their apparent ability to accumulate HBIs may provide scientists with some novel HBIs. Further, a recent collaboration with the British Antarctic Survey has led to the collection of a further 20 echinoid specimens from the Adelaide Island on the Antarctic Peninsula. Specimens are being collected in replicates of 5 spanning the Antarctic sea ice diatom bloom period in an effort to establish whether or not HBI concentrations are temporarily associated with the bloom or are more permanently accumulated in these organisms.

Future investigations relating to the potential oxic degradation of IP_{25} and other HBIs in surface marine sediments will be difficult since the marine sediment geochemistry of natural sediments is notoriously complex and difficult to interpret. The extent of oxic degradation on IP_{25} and other HBIs would need to be further investigated in controlled laboratory experiments. Examples of anoxic experiments from Antarctic sediments revealed an exceptional case where some HBIs were transformed into cyclic lipids Conversely oxic experiments should be less complicated than anoxic and it is therefore considered imperative that such experiments be carried out in the laboratory on a range of sediments using combinations of spiked lipids, including IP_{25} and cultures of Arctic HBI producing diatoms

REFERENCES

Albaigés, J., Grimalt, J., Bayona, J. M., Riseborough, R. W., de Lappe, B. and Walker II, W. (1984). Dissolved, particulate and sedimentary hydrocarbons in a deltaic environment. Advances in Organic Geochemistry. Schenk, P. A., de Leeuw, J. W. and Lijmbach, G. W. M., Organic Geochemistry. **6:** 237-48.

Aleksandrov, I. A. (1994). The classification of sea-ice according to the type of its underside profiles and the reflection of sound from rough ice of various types. *Acoustical physics* **40**: 654-57.

Aletsee, L. and Jahnke, J. (1992). Growth and productivity of the psychrophilic marine diatoms *Thalassiosira antarctica* Comber and *Nitzschia frigida* Grunow in batch cultures at temperatures below the freezing point of sea water. *Polar biology* **11**: 643-47.

Andersen, O. (1977). Primary production associated with sea ice at Godhavn, Disko, West Greenland. *Ophelia* **16**: 205-20.

Anderson, D. M. (2001). Attenuation of millennial-scale events by bioturbation in marine sediments. *Paleoceanography* **16**: 352-57.

Andreas, K., Dietmar, F., Ina, P., Uwe, J. and Gerhard, D. (2007). Regulation of proline metabolism under salt stress in the psychrophilic diatom *Fragilariopsis cylindrus* (Bacillariophyceae). *Journal of Phycology* **43**: 753-62.

Andrews, J. T., Belt, S. T., Olafsdottir, S., Massé, G. and Vare, L. L. (2009). Sea ice and marine climate variability for NW Iceland/Denmark Strait over the last 2000 cal. yr BP. *The Holocene* **19**: 775-84.

Anna, C. P., Janice Beeler, S. and Cornelius, W. S. (1985). Photosynthesis-irradiance relationships in sea ice microalgae from McMurdo Sound, Antarctica. *Journal of Phycology* **21**: 341-46.

Arao, T., Kawaguchi, A. and Yamada, M. (1987). Positional distribution of fatty acids in lipids of the marine diatom *Phaeodactylum tricornutum*. *Phytochemistry* **26**: 2573-76.

Arctic-ROOS. (2009, 14/08/09). Daily Updated Time series of Arctic sea ice area and extent derived from SSMI data provided by NANSEN. Nansen Environmental and Remote Sensing Center Retrieved 14/08/09, 2009, from http://arctic-roos.org/observations/satellite-data/sea-ice/ice-area-and-extent-in-arctic.

Armstrong, D. W., Tang, Y. and Zukowski, J. (1991). Resolution of enantiomeric hydrocarbon biomarkers of geochemical importance. *Analytical Chemistry* **63**: 2858-61.

Arndt, C. E. and Swadling, K. M. (2006). Crustacea in Arctic and Antarctic sea ice: Distribution, diet and life history strategies. *ADVANCES IN MARINE BIOLOGY, VOL 51* **51**: 197-315.

Arnosti, C. and Jorgensen, B. B. (2006). Organic carbon degradation in arctic marine sediments, Svalbard: A comparison of initial and terminal steps. *Geomicrobiology journal* **23**: 551-63.

Arrigo, K. R., Mock, T. and Lizotte, M. P. (2010). Primary producers and sea ice. Sea ice: second edition. Thomas, D. N. and Dieckmann, G. S. Oxford, Blackwell Publishing Ltd: 283-325.

Arrigo, K. R. and Sullivan, C. W. (1992). The influence of salinity and temperature covariation on the photophysiological characteristics of Antarctic sea ice microalgae. *Journal of Phycology* **28**: 746-56.

Arrigo, K. R. and van Dijken, G. L. (2004) Annual cycles of sea ice and phytoplankton in Cape Bathurst polynya, southeastern Beaufort Sea, Canadian Arctic. *Geophysical Research Letters* **31**.

Assur, A. (1960). Composition of sea ice and its tensile strength. AIPRE Research Report. **44**.

Backman, J., Jakobsson, M , Lovlie, R., Polyak, L. and Febo, L. A (2004). Is the central Arctic Ocean a sediment starved basin? *Quaternary science reviews* **23**. 1435-54.

Barenholz, Y. (2002). Cholesterol and other membrane active sterols: from membrane evolution to "rafts". *Progress in Lipid Research* **41**: 1-5.

Barrett, S M., Volkman, J. K and Dunstan, G A. (1995). Sterols of 14 species of marine diatoms (Bacillariophyta) *Journal of Phycology* **31**. 360-69

Batchelor, G. K. (2000). An introduction to fluid dynamics. Cambridge, Cambridge University Press.

Bechtel, A and Schubert, C. J. (2009). A biogeochemical study of sediments from the eutrophic Lake Lugano and the oligotrophic Lake Brienz, Switzerland. *Organic Geochemistry* **40**: 1100-14.

Belt, S. T., Allard, W. G., Johns, L., König, W. A., Massé, G., Robert, J.-M. and Rowland, S. (2001a). Variable stereochemistry in highly branched isoprenoids from diatoms. *Chirality* **13**: 415-19.

Belt, S. T., Allard, W. G., Massé, G., Robert, J. M. and Rowland, S. J. (2000a). Highly branched isoprenoids (HBIs): Identification of the most common and abundant sedimentary isomers. *Geochimica et Cosmochimica Acta* **64**: 3839-51.

Belt, S. T., Allard, W. G., Massé, G., Robert, J. M. and Rowland, S. J (2001b). Structural characterisation of C_{30} highly branched isoprenoid alkenes (rhizenes) in the marine diatom *Rhizosolenia setigera Tetrahedron Letters* **42**. 5583-85.

Belt, S T., Allard, W G , Rintatalo, J., Johns, L A , van Duin, A C T. and Rowland, S. J. (2000b). Clay and acid catalysed isomerisation and cyclisation reactions of highly branched isoprenoid (HBI) alkenes: Implications for sedimentary reactions and distributions. *Geochimica et Cosmochimica Acta* **64**: 3337-45.

Belt, S. T , Massé, G., Allard, W. G., Robert, J. M. and Rowland, S J. (2001c). C_{25} highly branched isoprenoid alkenes in planktonic diatoms of the *Pleurosigma* genus. *Organic Geochemistry* **32**: 1271-75

Belt, S. T., Massé, G., Allard, W. G., Robert, J. M. and Rowland, S. J. (2001d). Identification of a C_{25} highly branched isoprenoid triene in the freshwater diatom *Navicula sclesvicensis Organic Geochemistry* **32**: 1169-72.

Belt, S. T., Massé, G., Allard, W. G., Robert, J. M. and Rowland, S. J (2002). Effects of auxosporulation on distributions of C_{25} and C_{30} isoprenoids alkenes in *Rhizosolenia setigera. Phytochemistry* **59**. 141-48

Belt, S. T., Massé, G., Rowland, S. J., Poulin, M., Michel, C. and LeBlanc, B (2007). A novel chemical fossil of palaeo sea ice: IP_{25} *Organic geochemistry* **38**: 16-27.

Belt, S T , Massé, G., Vare, L. L., Rowland, S J , Poulin, M , Sicre, M.-A., Sampei, M. and Fortier, L. (2008) Distinctive ^{13}C isotopic signature distinguishes a novel sea ice biomarker in Arctic sediments and sediment traps. *Marine Chemistry* **112**: 158-67

Belt, S. T., Vare, L. L., Massé, G., Manners, H., Price, J , MacLachlan, S., Andrews, J. T. and Schmidt, S. (2010). Striking similarities in temporal changes to seasonal sea ice conditions across the central Canadian Arctic Archipelago during the last 7,000 years *Quaternary Science Reviews* **29**: 3489-504.

Benthien, A. and Muller, P. J. (2000) Anomalously low alkenone temperatures caused by lateral particle and sediment transport in the Malvinas Current region,

western Argentine Basin. *Deep Sea Research Part I: Oceanographic Research Papers* **47**: 2369-93.

Bergamaschi, B. A., Tsamakis, E., Keil, R. G., Eglinton, T. I., Montluçon, D. B. and Hedges, J. I. (1997). The effect of grain size and surface area on organic matter, lignin and carbohydrate concentration, and molecular compositions in Peru Margin sediments. *Geochimica et cosmochimica acta* **61**: 1247-60.

Billett, D. S. M., Lampitt, R. S., Rice, A. L. and Mantoura, R. F. C. (1983). Seasonal sedimentation of phytoplankton in the deep sea benthos. *Nature* **302**: 520-22.

Bischof, K., Hanlet, D. and Wiencke, C. (2007). UV Radiation and Arctic marine Microalage. UV Radiation and Arctic ecosystems. Hessen, D. O. London, Springer.

Blasco, S., Rochon, A., St-Onge, G., Schell, T. and Scott, D. B. (2009). Foraminiferal assemblage changes over the last 15,000 years on the Mackenzie-Beaufort Sea Slope and Amundsen Gulf, Canada: Implications for past sea ice conditions. *Paleoceanography* **24**.

Bluhm, B. A., Piepenburg, D. and von Juterzenka, K. (1998). Distribution, standing stock, growth, mortality and production of *Strongylocentrotus pallidus* (Echinodermata: Echinoidea) in the northern Barents Sea. *Polar Biology* **20**: 325-34.

Boetius, A. and Damm, E. (1998). Benthic oxygen uptake, hydrolytic potentials and microbial biomass at the Arctic continental slope. *Deep Sea Research Part I: Oceanographic Research Papers* **45**: 239-75.

Booth, B. C. and Horner, R. A. (1997). Microalgae on the Arctic Ocean section, 1994: species abundance and biomass. *Deep-sea research. Part II, Topical studies in oceanography* **44**: 1607.

Brassell, S. C., Eglinton, G., Marlowe, I. T., Pflaumann, U. and Sarnthein, M. (1986). Molecular stratigraphy - A new tool for climatic assessment. *Nature* **320**: 129-33.

Bray, E. E. and Evans, E. D. (1961). Distribution of n-paraffins as a clue to recognition of source beds *Geochimica et Cosmochimica Acta* **22**: 2-15.

Brooks, J. D., Gould, K. and Smith, J. W. (1969). Isoprenoid Hydrocarbons in Coal and Petroleum. *Nature* **222**: 257-59.

Brown, T. A. (2007). Identification of Arctic Sea ice diatoms: B.Sc dissertation, University of Plymouth.

Budge, S., Wooller, M., Springer, A., Iverson, S., McRoy, C. and Divoky, G. (2008). Tracing carbon flow in an arctic marine food web using fatty acid-stable isotope analysis. *Oecologia* **157**: 117-29.

Bunt, J. (1970). Seasonal primary production in Antarctic sea ice at McMurdo Sound in 1967. *Journal of marine research* **28**: 304.

Burckle, L. H. (1981). Displaced Antarctic diatoms in the Amirante Passage. *Marine Geology* **39**: M39-M43.

Calvert, S. E. and Pedersen, T. F. (1993). Geochemistry of Recent oxic and anoxic marine sediments: Implication for the geological record. *Marine Geology* **113**: 67-88.

Canfield, D. E. (1989). Reactive iron in marine sediments. *Geochimica et cosmochimica acta* **53**: 619-32.

Casey, R. E., Weinheimer, A. L. and Nelson, C. O. (1990). Cenozoic radiolarian evolution and zoogeography of the pacific. *Bulletin of Marine Science* **47**: 221-32.

Christodoulou, S., Joux, F., Marty, J -C., Sempéré, R and Rontani, J.-F. (2010) Comparative study of UV and visible light induced degradation of lipids in non-axenic senescent cells of *Emiliania huxleyi*. *Marine chemistry* **119**: 139-52.

Clough, L. M , Ambrose, J W G., Kirk Cochran, J , Barnes, C., Renaud, P. E. and Aller, R. C (1997) Infaunal density, biomass and bioturbation in the sediments of the Arctic Ocean *Deep Sea Research Part II: Topical Studies in Oceanography* **44**· 1683-704.

Conlan, K., Aitken, A., Hendrycks, E., McClelland, C. and Melling, H. (2008). Distribution patterns of Canadian Beaufort Shelf macrobenthos. *Journal of Marine Systems* **74**: 864-86.

Cota, G F (1985). Photoadaptation of high Arctic ice algae. *Nature* **315**: 219-22.

Cox, G. F. N. and Weeks, W. F. (1975). Brine drainage and Initial salt entrapment in sodium chloride ice *U.S. Cold regions research and and engineering laboratory Research report* **345**.

Cox, G F. N. and Weeks, W. F. (1983). Equations for determining the gas and brine volumes in sea-ice samples. *The Journal of Glaciology* **29**: 306-16

Croudace, I. W., Rindby, A. and Rothwell, R. G. (2006). ITRAX: description and evaluation of a new multi-function X-ray core scanner. New Techniques in Sediment Core Analysis. Rothwell, R. G. London, Geological Society. **267**: 51-63.

Cusson, M., Archambault, P. and Aitken, A. (2007) Biodiversity of benthic assemblages on the Arctic continental shelf: historical data from Canada. *Marine ecology progress series* **331**. 291-304

Darby, D. A., Bischof, J. F. and Jones, G. A (1997) Radiocarbon chronology of depositional regimes in the western Arctic Ocean. *Deep-Sea Research Part Ii-Topical Studies in Oceanography* **44**: 1745-57.

de Vernal, A., Eynaud, F., Henry, M., Hillaire-Marcel, C , Londeix, L., Mangin, S., Matthiessen, J , Marret, F , Radi, T., Rochon, A., Solignac, S and Turon, J. L (2005). Reconstruction of sea-surface conditions at middle to high latitudes of the Northern Hemisphere during the Last Glacial Maximum (LGM) based on dinoflagellate cyst assemblages *Quaternary Science Reviews*. **24**: 897-924.

de Vernal, A., Henry, M., Matthiessen, J., Peta, J. M , André, R., Karin, P. B., Frédérique, E., Kari, G , Joel, G., Dominique, H., Rex, H , Martin, J. H., Martina, K -P., Elisabeth, L , Virginie, L., Odile, P., Vera, P., Taoufik, R., Jean-Louis, T. and Elena, V (2001). Dinoflagellate cyst assemblages as tracers of sea-surface conditions in the northern North Atlantic, Arctic and sub-Arctic seas: the new n = 677 data base and its application for quantitative palaeoceanographic reconstruction. *Journal of Quaternary Science* **16**. 681-98.

Decho, A. W (1990). Microbial exopolymer secretions in ocean environments: their role(s) in food webs and marine processes *Oceanography and marine biology* **28** 73-153

Dieckmann, G. and Hellmer, H. (2003). The Importance of Sea Ice: An Overview Sea Ice, An Introduction to its physics, chemistry, biology and geology. Thomas, D and Dieckmann, S. Oxford, Blackwell publishing: 1-21.

Dieckmann, G S. and Hellmer, H. H. (2010) The importance of sea ice: an overview. Sea ice (second edition). Thomas, D. and Dieckmann, S. Chichester, Blackwell Publishing Ltd: 1-22.

Dieckmann, G. S., Rohardt, G., Hellmer, H and Kipfstuhl, J. (1986) The occurrence of ice platelets at 250 m depth near the Filchner ice shelf and it's significance for sea ice biology. *Deep-sea research. Part A, Oceanographic research papers* **33**: 141-48.

Drenzek, N. J., Montlucon, D. B., Yunker, M. B., Macdonald, R. W. and Eglinton, T. I. (2007). Constraints on the origin of sedimentary organic carbon in the Beaufort Sea from coupled molecular C-13 and C-14 measurements. *Marine Chemistry* **103**: 146-62.

Dufour, S. C., White, C., Desrosiers, G. and Juniper, S. K. (2008). Structure and composition of the consolidated mud tube of Maldane sarsi (Polychaeta: *Maldanidae*). *Estuarine, Coastal and Shelf Science* **78**: 360-68.

Dunstan, G. A., Volkman, J. K., Barrett, S. M., Leroi, J. M. and Jeffrey, S. W. (1994). Essential polyunsaturated fatty acids from 14 species of diatom (Bacillariophyceae). *Phytochemistry* **35**: 155-61.

Dunton, K. H., Goodall, J. L., Schonberg, S. V., Grebmeier, J. M. and Maidment, D. R. (2005). Multi-decadal synthesis of benthic-pelagic coupling in the western arctic: Role of cross-shelf advective processes. *Deep Sea Research Part II: Topical Studies in Oceanography* **52**: 3462-77.

Dyke, A. S., Dale, J. E. and McNeely, R. N. (1996a). Marine molluscs as indicators of environmental change in glaciated North America and Greenland during the last 18,000 years. *Geographie Physique et Quaternaire* **50**: 125-84.

Dyke, A. S., England, J., Reimnitz, E. and Jette, H. (1997). Changes in Driftwood Delivery to the Canadian Arctic Archipelago: The Hypothesis of Postglacial Oscillations of the Transpolar Drift. *Arctic* **50**: 1-16.

Dyke, A. S., Hooper, J. and Savelle, J. M. (1996b). A history of sea ice in the Canadian Arctic Archipelago based on postglacial remains of the bowhead whale (*Balaena mysticetus*). *Arctic* **49**: 235-55.

Dyson, N. (1998). Chromatographic integration methods (Second edition). Cambridge, Royal Society of Chemistry.

Eddie, B., Krembs, C. and Neuer, S. (2008). Characterization and growth response to temperature and salinity of psychrophilic, halotolerant *Chlamydomonas* sp ARC isolated from Chukchi Sea ice. *Marine ecology progress series* **354**: 107-17.

Eglinton, G. and Calvin, M. (1967). Chemical fossils. *Scientific American* **216**: 32-43.

Eglinton, T. I. and Eglinton, G. (2008). Molecular proxies for paleoclimatology. *Earth and planetary science letters* **275**: 1-16.

Eicken, H. (2003). Chapter 2 - From the microscopic, to the macroscopic, to the regional scale: Growth, microstructure and properties of sea ice. Sea Ice, An Introduction to its physics, chemistry, biology and geology. Thomas, D. N. and Dieckmann, G. S. Oxford, Blackwell publishing.

Eicken, H., Krouse, H. R., Kadko, D. and Perovich, D. K. (2002). Tracer studies of pathways and rates of meltwater transport through Arctic summer sea ice. *Journal of geophysical research* **107**.

Eicken, H., Lange, M. A. and Dieckmann, G. S. (1991). Spatial variability of sea ice properties in the Northwestern Weddell Sea. *Journal of Geophysical Research* **96**: 10603-15.

Eisenhauer, A., Meyer, H., Rachold, V., Tütken, T., Wiegand, B., Hansen, B. T., Spielhagen, R. F., Lindemann, F. and Kassens, H. (1999). Grain size separation and sediment mixing in Arctic Ocean sediments: evidence from the strontium isotope systematic. *Chemical Geology* **158**: 173-88.

England, J. H., Furze, M. F. A. and Doupé, J. P. (2009). Revision of the NW Laurentide Ice Sheet: implications for paleoclimate, the northeast extremity of Beringia, and Arctic Ocean sedimentation. *Quaternary science reviews* **28**: 1573-96.

Estrada, M., Bayer-Giraldi, M., Felipe, J., Marrase, C., Sala, M. M. and Vidal, M. (2009). Light and nutrient effects on microbial communities collected during spring and summer in the Beaufort Sea. *Aquatic microbial ecology* **54**: 217-31.

Forest, A., Bélanger, S., Sampei, M , Sasaki, H , Lalande, C. and Fortier, L (2009). Three-year assessment of particulate organic carbon fluxes in Amundsen Gulf (Beaufort Sea): Satellite observations and sediment trap measurements. *Deep Sea Research Part I. Oceanographic Research Papers* **57**: 125-42.

Fraser, A. J., Sargent, J. R. and Gamble, J. C. (1989). Lipid class and fatty acid composition of Calanus finmarchicus (Gunnerus), Pseudocalanus sp. and Temora longicornis Muller from a nutrient-enriched seawater enclosure. *Journal of experimental marine biology and ecology* **130**: 81-92.

Friedman, G M. and Sanders, J. E. (1978). Principles in Sedimentology. New York, Wiley.

Garrison, D. L., Ackley, S. F. and Buck, K. R. (1983). A physical mechanism for establishing algal populations in frazil ice *Nature* **306**: 363-65

Garrison, D. L. and Buck, K. R (1986). Organism losses during ice melting: A serious bias in sea ice community studies *Polar Biology* **6**: 237-39.

Gersonde, G. R , Wefer, G. G and Fischer, G. G. (2002) Organic carbon, biogenic silica and diatom fluxes in the marginal winter sea-ice zone and in the Polar Front Region· interannual variations and differences in composition. *Deep-sea research. Part II, Topical studies in oceanography* **49**: 1721-45

Gibson, J A E , Trull, T., Nichols, P. D., Summons, R E. and McMinn, A. (1999). Sedimentation of ^{13}C-rich organic matter from Antarctic sea-ice algae: A potential indicator of past sea-ice extent. *Geology* **27**· 331-34.

Gilbert, C., Mucci, A. and Sundby, B. (2006). Sediment Geochemistry in the Canadian Arctic. *McGill Science Undergraduate Research Journal* **1**: 5-6.

Gillan, F. T , McFadden, G. I., Wetherbee, R. and Johns, R. B. (1981). Sterols and fatty acids of an Antarctic sea ice diatom, *Stauroneis amphioxys*. *Phytochemistry* **20**: 1935-37.

Gobeil, C., Macdonald, R. W. and Sundby, B. (1997). Diagenetic separation of cadmium and manganese in suboxic continental margin sediments. *Geochimica et cosmochimica acta* **61**: 4647-54

Golden, K. M., Eicken, H , Heaton, A. L., Miner, J., Pringle, D. J. and Zhu, J. (2007). Thermal evolution of permeability and microstructure in sea ice. *Geophysical Research Letters* **34**.

Gordeev, V. V. (2006). Fluvial sediment flux to the Arctic Ocean. *Geomorphology* **80**· 94-104.

Gosselin, M., Legendre, L., Therriault, J -C. and Demers, S. (1990a). Light and nutrient limitation of sea-ice microalgae (Hudson Bay, Canadian Arctic). *Journal of Phycology* **26**: 220-32.

Gosselin, M., Legendre, L., Therriault, J. C. and Demers, S. (1990b). Light and nutrient limitation of sea ice microalgae (Hudson-Bay, Canadian Arctic). *Journal of Phycology* **26**· 220-32.

Gosselin, M , Legendre, L., Therriault, J. C., Demers, S. and Rochet, M. (1986) Physical control of the horizontal patchiness of sea ice microalgae. *Marine Ecology Progress Series* **29**. 289-98.

Gosselin, M., Levasseur, M., Wheeler, P A., Horner, R. A. and Booth, B C. (1997). New measurements of phytoplankton and ice algal production in the Arctic Ocean *Deep Sea Research Part II* **44**· 1623-44.

Gradinger, R., Friedrich, C and Spindler, M. (1999). Abundance, biomass and composition of the sea ice biota of the Greenland Sea pack ice. *Deep Sea Research Part II. Topical Studies in Oceanography* **46**: 1457-72.

Gradinger, R., Spindler, M. and Weissenberger, J. (1992). On the structure and development of Arctic pack ice communities in Fram Strait: a multivariate approach. *Polar biology* **12**: 727-33.

Grant, W. S. and Horner, R. A. (1976). Growth responses to salinity variations in four Arctic Ice Diatoms. *Journal of Phycology*: 180-85.

Grebmeier, J. M. and Barry, J. P. (2007). Benthic processes in polar polynyas. Polynyas: Windows into Polar Oceans. Halpern, D., Elsevier Oceanography Series: 262-90.

Gregory, T. R., Smart, C. W., Hart, M. B., Massé, G., Vare, L. L. and Belt, S. T. (2010). Holocene palaeoecology and dissolution of foraminifera in Barrow Strait. *Journal of Quaternary Science*

Grossi, V., Beker, B., Geenevasen, J. A. J., Schouten, S., Raphel, D., Fontaine, M.-F. and Sinninghe Damsté, J. S. (2004). C_{25} highly branched isoprenoid alkene from the marine benthic diatom *Pleurosigma strigosum*. *Phytochemistry* **65**: 3049-55.

Hannah, C. G., Dupont, F. and Dunphy, M. (2009). Polynyas and tidal currents in the Canadian Arctic Archipelago. *Arctic* **62**: 83-95.

Hasle, G. R. and Syvertsen, E. E. (1997). Marine diatoms. Identifying marine phytoplankton. Tomas, C. R. San Diego, Academic Press: 5-385.

Haslett, S. K. (2002a). Palaeoceanographic applications of planktonic sarcodine protozoa: Radiolaria and foraminifera. Quaternary environmental micropalaeontology. Haslett, S. K. Ofxord, Arnold.

Haslett, S. K. (2002b). Quaternary environmental micropalaeontology. London, Arnold.

Heide-Jørgensen, M. P., Laidre, K. L., Logsdon, M. L. and Nielsen, T. G. (2007). Springtime coupling between chlorophyll a, sea ice and sea surface temperature in Disko Bay, West Greenland. *Progress in Oceanography* **73**: 79-95.

Hill, V. and Cota, G. (2005). Spatial patterns of primary production on the shelf, slope and basin of the Western Arctic in 2002. *Deep Sea Research Part II: Topical Studies in Oceanography* **52**: 3344-54.

Hird, S. J. (1992). Origins and short-term sedimentary fate of globally distributed biological marker hydrocarbons: Ph.D thesis, Univeristy of Plymouth.

Hird, S. J. and Rowland, S. J. (1995). An investigation of the Sources and Seasonal Variations of Highly Branched Isoprenoid Hydrocarbons in Intertidal Sediments of the Tamar Estuary, UK. *Marine Environmental Research* **40**: 423-37.

Holmes, R. M., McClelland, J. W., Peterson, B. J., Shiklomanov, I. A., Shiklomanov, A. I., Zhulidov, A. V., Gordeev, V. V. and Bobrovitskaya, N. N. (2002). A circumpolar perspective on fluvial sediment flux to the Arctic Ocean. *Global biogeochemical cycles* **16**.

Hop, H., Falk-Petersen, S., Svendsen, H., Kwasniewski, S., Pavlov, V., Pavlova, O. and Søreide, J. E. (2006). Physical and biological characteristics of the pelagic system across Fram Strait to Kongsfjorden. *Progress in oceanography* **71**: 182-231.

Hoppema, M. and Anderson, L. G. (2007). Biogeochemistry of polynyas and their role in sequestration of anthropogenic constituents. Polynyas: windows to teh world. Smith, W. O. and Barber, D. G., Elsivier.

Huguet, C., Kim, J.-H., de Lange, G. J., Sinninghe Damsté, J. S. and Schouten, S. (2009). Effects of long term oxic degradation on the TEX_{86} and BIT organic proxies. *Organic Geochemistry* **40**: 1188-94.

IPY-CFL. (2010). Arctic Climate Change - Circumpolar Flaw Lead System Study. Retrieved 01/02, 2010, from http://www.ipy-cfl.ca/.

Irwin, B. D. (1990). Primary production of ice algae on a seasonally ice-covered, continental-shelf. *Polar biology* **10**: 247-54.

Jakobsson, M., Grantz, A., Kristoffersen, Y. and Macnab, R. (2004). The Arctic Ocean: Boundary conditions and background information. The organic carbon cycle in the Actic Ocean. Macdonald, R. W. and Stein, R. London, Springer.

Jan-Gunnar, W., Kåre, E., Sebastian, G. and Børge, H (2004). Surface reflectance of sea ice and under-ice irradiance in Kongsfjorden, Svalbard. *Polar Research* **23**: 115-18

Jiang, S., Stamnes, K., Li, W and Hamre, B. (2005). Enhanced solar irradiance across the atmosphere-sea ice interface: a quantitative numerical study. *Applied optics-OT* **44**: 2613-25.

Johns, L., Wraige, E. J., Belt, S. T., Lewis, C A., Massé, G , Robert, J. M. and Rowland, S J. (1999) Identification of a C_{25} highly branched isoprenoid (HBI) diene in Antarctic sediments, Antarctic sea-ice diatoms and cultured diatoms. *Organic Geochemistry* **30**: 1471-75.

Jolliffe, I. T. (2002). Principal components analysis (Second edition). New York, Springer.

Jones, G. A. and Johnson, D. A. (1984) Displaced Antarctic diatoms in Vema Channel sediments· Late Pleistocene/Holocene fluctuations in AABW flow. *Marine geology* **58**. 165-86.

Katsev, S , Sundby, B and Mucci, A. (2006) Modelling vertical excursions of the redox boundary in sediments: Application to deep basins of the Arctic Ocean. *Limnology and oceanography* **51**: 1581-93.

Kennedy, H., Thomas, D. N , Kattner, G., Haas, C. and Dieckmann, G. S. (2002). Particulate organic matter in Antarctic summer sea ice: concentration and stable isotopic composition *Marine Ecology Progress Series.* **238**: 1-13.

Killops, S. D. and Killops, V. J. (1993). An introduction to organic geochemistry. London, Longman

Kim, J. H., Crosta, X , Michel, E., Schouten, S., Duprat, J and Damste, J. S. S (2009). Impact of lateral transport on organic proxies in the Southern Ocean. *Quaternary Research* **71**: 246-50.

Koc, C N., Moros, C M. and Andersen, C. C. (2004). A highly unstable Holocene climate in the subpolar North Atlantic: evidence from diatoms. *Quaternary science reviews* **23** 2155-66

Kogeler, J. W., Falk-Petersen, S , Kristensen, A , Pettersen, F and Dalen, J (1987). Density and sound speed contrasts in sub-Arctic zooplankton. *Polar biology* **7**: 231-35.

Koide, M., Soutar, A and Goldberg, E. D. (1972) Marine geochronology with ^{210}Pb. *Earth and planetary science letters* **14**: 442-46

Kottachchi, N., Schröder-Adams, C. J., Haggart, J. W. and Tipper, H. W. (2002). Jurassic foraminifera from the Queen Charlotte Islands, British Columbia, Canada: biostratigraphy, paleoenvironments and paleogeographic implications. *Palaeogeography, palaeoclimatology, palaeoecology* **180**. 93-127.

Kovacs. (2010) Mark II coring system. Retrieved 15/02, 2010, from http://www.kovacsicedrillingequipment.com/mark_ii.html.

Krembs, C., Deming, J. W. and Eicken, H. (2002a). Can microorganisms, especially *Melosira arctica*, significantly alter the physical properties of sea ice and to what biological advantage 53rd Arctic Science Conference, connecting northern waters, Fairbanks, Alaska, American Association for the Advancement of Science, Arctic Division.

Krembs, C , Eicken, H., Junge, K. and Deming, J. W. (2002b). High concentrations of exopolymeric substances in Arctic winter sea ice: implications for the polar

ocean carbon cycle and cryoprotection of diatoms. *Deep Sea Research Part I: Oceanographic Research Papers* **49**: 2163-81.

Krembs, C., Tuschling, K. and v. Juterzenka, K. (2002c). The topography of the ice-water interface" - its influence on the colonization of sea ice by algae. Polar biology, Springer Science & Business Media B.V. **25:** 106-17.

Kröncke, I. (1994). Macrobenthos composition, abundance and biomass in the Arctic Ocean along a transect between Svalbard and the Makarov Basin. *Polar biology* **14**: 519-29.

Kurt, R. B., Patricia, A. B., Wilfred, N. B. and David, L. G. (1992). A Dinoflagellate cyst from Antarctic sea ice. *Journal of Phycology* **28**: 15-18.

Lee, S. H., Whitledge, T. E. and Kang, S. H. (2008). Spring time production of bottom ice algae in the landfast sea ice zone at Barrow, Alaska. *Journal of Experimental Marine Biology and Ecology* **367**: 204-12.

Legendre, L., Ackley, S., Diekmann, G., Gulliksen, B., Horner, R., Hoshiai, T., Melnikov, I., Reeburgh, W., Spindler, M. and Sullivan, C. (1992). Ecology of sea ice biota 2. Global significance. *Polar biology* **12**: 429-44.

Leventer, A. (2003). Chapter 10 – Particulate flux from sea ice in polar waters. Sea Ice, An Introduction to its physics, chemistry, biology and geology. Thomas, D. N. and Dieckmann, G. S. Oxford, Blackwell publishing.

Lichtfouse, E., Derenne, S., Mariotti, A. and Largeau, C. (1994). Possible algal origin of long-chain odd *n*-alkanes in immature sediments as revealed by distributions and carbon-isotope ratios. *Organic Geochemistry* **22**: 1023-27.

Linda, S.-G., Mila, S. S., Diane, L. and Janet, H. (1988). Effect of light cycle on diatom fatty acid composition and quantitative morphology. *Journal of Phycology* **24**: 1-7.

Lizotte, M. P. (2001). The contributions of sea ice algae to Antarctic marine primary production. *American Zoologist* **41**: 57-73.

Lizotte, M. P. and Sullivan, C. W. (1992). Biochemical composition and photosynthate distribution in sea ice algae of McMurdo Sound, Antarctica - Evidence for nutrient stress during the spring bloom. *Antarctic Science* **4**: 23-30.

Lohrer, A. M., Thrush, S. F. and Gibbs, M. M. (2004). Bioturbators enhance ecosystem function through complex biogeochemical interactions. *Nature* **431**: 1092-95.

Lund, J. W. G., Kipling, C. and Cren, E. D. (1958). The inverted microscope method of estimating algal numbers and the statistical basis of estimations by counting. *Hydrobiologia* **11**: 143-70.

Macdonald, L. R., Yunker, L. M., Harvey, L. H. and Belicka, L. L. (2004). The role of depositional regime on carbon transport and preservation in Arctic Ocean sediments. *Marine Chemistry* **86**: 65-88.

Macdonald, R. W., Solomon, S. M., Cranstone, R. E., Welch, H. E., Yunker, M. B. and Gobeil, C. (1998). A sediment and organic carbon budget for the Canadian Beaufort Shelf. *Marine Geology* **144**: 255-73.

Mackenzie, F. T. (2005). Sediments, Diagenesis, and Sedimentary Rocks: Treatise on Geochemistry, Elsevier.

Maire, O., Lecroart, P., Meysman, F., Rosenberg, R., Duchêne, J.-C. and Grémare, A. (2008). Quantification of sediment reworking rates in bioturbation research: a review. *Aquatic Biology* **2**: 219-38.

Manes, S. S. and Gradinger, R. (2009). Small scale vertical gradients of Arctic ice algal photophysiological properties. *Photosynthesis research* **102**: 53-66.

Mann, M. E., Bradley, R. S. and Hughes, M. K. (1998). Global-scale temperature patterns and climate forcing over the past six centuries *Nature* **392**: 779-87.

Marco Vincenzo, P., Giampiero, P., Laurita, B., Rossella, P., Maurizio, D. and Teresa, G (1997). Investigation of 4-methyl sterols from cultured dinoflagellate algal strains. *Journal of Phycology* **33**: 61-67

Margalef (1978). Life-forms of phytoplankton as survival alternatives in an unstable environment. *Oceanology. Acta* **1**: 493–509.

Massé, G. (2003). Highly Branched Isoprenoid Alkenes from Diatoms. A Biosynthetic and Life Cycle Investigation: Ph.D thesis. Department of Environmental Sciences. Plymouth, University of Plymouth.

Massé, G , Belt, S. T., Allard, G. W , Lewis, C. A., Wakeham, S. G. and Rowland, S. J. (2004a). Occurrence of novel monocyclic alkenes from diatoms in marine particulate matter and sediments *Organic Geochemistry* **35**: 813-22.

Massé, G , Belt, S. T. and Rowland, S. J. (2004b). Biosynthesis of unusual monocyclic alkenes by the diatom *Rhizosolenia setigera* (Brightwell). *Phytochemistry* **65**: 1101-06.

Massé, G , Rowland, S. J., Sicre, M.-A., Jacob, J., Jansen, E. and Belt, S T (2008). Abrupt climate changes for Iceland during the last millennium. Evidence from high resolution sea ice reconstructions. *Earth and Planetary Science Letters* **269**: 565-69.

Matthiessen, J., Turon, J. L , Rochon, A and De Vernal, A. (1997). Organic-walled dinoflagellate cysts: Palynological tracers of sea-surface conditions in middle to high latitude marine environments. *Geobios* **30**: 905-20.

Mayewski, P. A., Rohling, E E , Stager, J. C., Karlen, W., A, M K., Meeker, L. D., Meyerson, E. A., Gasse, F., van Kreveld, S., Holmgren, K., Lee-Thorp, J., Rosqvist, G., Rack, F , Staubwasser, M., Schneider, R. R and Steig, E. J (2004). Holocene climate variability. *Quaternary Research* **62**: 243-55.

McMinn, A , Skerratt, J , Trull, T., Ashworth, C and Lizotte, M. (1999) Nutrient stress gradient in the bottom 5 cm of fast ice, McMurdo Sound, Antarctica *Polar biology* **21** 220-27.

McPhee, M. G., Morison, J. H. and Nilsen, F. (2008) Revisiting heat and salt exchange at the ice-ocean interface: Ocean flux and modeling considerations. *Journal of geophysical research* **113**.

Medlin, L K. and Hasle, G. R. (1990a). Some *Nitzschia* and related diatom species from fast ice samples in the Arctic and Antarctic. *Polar Biology* **10**: 451-79.

Medlin, L K. and Priddle, J. (1990b). Polar marine diatoms Cambridge, British Antarctic Survey

Melnikov, I (1997). Arctic sea ice ecosystem. Luxemburg, Taylor and Francis Ltd.

Melnikov, I. A. and Bondarchuk, L. L (1987). Ecology of mass accumulation of colonial diatom algae under drifting Arctic ice. *Oceanology* **27**: 233-36

Meyers, P. A. (1997). Organic geochemical proxies of paleoceanographic, paleolimnologic, and paleoclimatic processes. *Organic Geochemistry* **27**: 213-50.

Michel, C., Ingram, R. G and Harris, L. R. (2006). Variability in oceanographic and ecological processes in the Canadian Arctic Archipelago. *Progress in Oceanography* **71**: 379-401.

Middag, R., de Baar, H J. W., Laan, P and Bakker, K (2009). Dissolved aluminium and the silicon cycle in the Arctic Ocean *Marine chemistry* **115**: 176-95.

Mikkelsen, D M , Rysgaard, S and Glud, R N. (2008) Microalgal composition and primary production in Arctic sea ice: a seasonal study from Kobbefjord (Kangerluarsunnguaq), West Greenland *Marine ecology progress series* **368**: 65-74.

Mock, T., Kruse, M. and Dieckmann, G. S. (2003). A new microcosm to investigate oxygen dynamics at the sea ice water interface. *Aquatic Microbial Ecology* **30**: 197-205.

Molina-Cruz, A. (1977). Radiolarian assemblages and their relationship to the oceanography of the sub tropical southeastern Pacific. *Marine micropaleontology* **2**: 315-52.

Mollenhauer, G., McManus, J. F., Benthien, A., Müller, P. J. and Eglinton, T. I. (2006). Rapid lateral particle transport in the Argentine Basin: Molecular ^{14}C and $^{230}Thxs$ evidence. *Deep Sea Research Part I: Oceanographic Research Papers* **53**: 1224-43.

Morley, J. J. and Stepien, J. C. (1984). Siliceous microfauna in waters beneath Antarctic sea ice. *Marine ecology progress series* **19**: 207-10.

Mudie, P. J., Harland, R., Matthiessen, J. and De Vernal, A. (2001a). Marine dinoflagellate cysts and high latitude Quaternary paleoenvironmental reconstructions: an introduction. *Journal of Quaternary Science* **16**: 595-602.

Mudie, P. J. and Rochon, A. (2001b). Distribution of dinoflagellate cysts in the Canadian Arctic marine region. *Journal of Quaternary Science* **16**: 603-20.

Müller, J., Massé, G., Stein, R. and Belt, S. T. (2009). Variability of sea-ice conditions in the Fram Strait over the past 30,000 years. *Nature Geoscience* **2**: 772-76.

Mundy, C. J., Barber, D. G. and Michel, C. (2005). Variability of snow and ice thermal, physical and optical properties pertinent to sea ice algae biomass during spring. *Journal of Marine Systems* **58**: 107-20.

Mundy, C. J., Gosselin, M., Ehn, J., Gratton, Y., Rossnagel, A., Barber, D. G., Martin, J., Tremblay, J.-Ã. r., Palmer, M., Arrigo, K. R., Darnis, G. r., Fortier, L., Else, B. and Papakyriakou, T. (2009). Contribution of under-ice primary production to an ice-edge upwelling phytoplankton bloom in the Canadian Beaufort Sea. *Geophys. Res. Lett.* **36**.

Murray, J. W. (2002). Introduction to benthic foraminifera. Quaternary environmental micropalaeontology. Haslett, S. K. Oxford, Arnold: 5-14.

NASA. (2009). SeaWiFS Project. Retrieved 14/08, 2009, from http://oceancolor.gsfc.nasa.gov/SeaWiFS/.

Neal, V. T., Neshyba, S. and Denner, W. (1969). Thermal Stratification in the Arctic Ocean. *Science* **166**: 373-74.

Nichols, D. S., Nichols, P. D. and Sullivan, C. W. (1993). Fatty acid, sterol and hydrocarbon composition of Antarctic sea ice diatom communities during the spring bloom in McMurdo Sound. *Antarctic Science* **5**: 271-78.

Nicolaus, M., Hudson, S. R., Gerland, S. and Munderloh, K. (2010). A modern concept for autonomous and continuous measurements of spectral albedo and transmittance of sea ice. *Cold Regions Science and Technology* **62**: 14-28.

Nigrini, C. (1970). Radiolarian assemblages in the North Pacific and thier application to a study of Quaternary sediments. *Memoir of the Geological Society of America* **126**: 139-83.

Nihashi, S. and Ohshima, K. I. (2001). Relationship between ice decay and solar heating through open water in the Antarctic sea ice zone. *Journal of geophysical research* **106**: 16767-82.

O'Brien, M. C., Macdonald, R. W., Melling, H. and Iseki, K. (2006). Particle fluxes and geochemistry on the Canadian Beaufort Shelf: Implications for sediment transport and deposition. *Continental Shelf Research* **26**: 41-81.

Okada, K., Kasahara, H., Yamaguchi, S., Kawaide, H., Kamiya, Y., Nojiri, H. and Yamane, H. (2008). Genetic evidence for the role of isopentenyl diphosphate

isomerases in the mevalonate pathway and plant development in arabidopsis. *Plant & Cell Physiology* **49**: 604-16.

Olli, K., Wassmann, P., Reigstad, M., Ratkova, T N., Arashkevich, E., Pasternak, A., Matrai, P. A., Knulst, J., Tranvik, L., Klais, R. and Jacobsen, A (2007). The fate of production in the central Arctic Ocean - top-down regulation by zooplankton expatriates? *Progress in oceanography* **72**: 84-113.

Opute, F I. (1974). Lipid and fatty-acid composition of diatoms. *Journal of Experimental Botany* **25**: 823-35.

Parsons, T., Maita, Y. and Lalli, C. (1984). A manual of chemical and biological methods for seawater analysis. Totronto, Pergamon Press.

Pearson, T H. (2001). Functional group ecology in soft sediment marine benthos: The role of bioturbation. *Oceanography and Marine Biology: An Annual Review* **39**: 233-67.

Peperzak, L., Colijn, F., Koeman, R., Gieskes, W. W. and Joordens, J. C. (2003). Phytoplankton sinking rates in the Rhine region of freshwater influence *Journal of Plankton Research* **25**: 365-83.

Perovich, D. K., Grenfell, T. C., Richter-Menge, J. A., Light, B., Tucker, W. B. and Eicken, H. (2003). Thin and thinner Sea ice mass balance measurements during SHEBA. *Journal of geophysical research* **108**.

Pesant, S. (2002) Wind-triggered events of phytoplankton downward flux in the Northeast Water Polynya. *Journal of Marine Systems* **31**: 261

Peter, J. R , Andrew, M., Ken, G. R and Chris, A. (2005). Short term effect of temperature on the photokinetics of microalgae from the surface layers of Antarctic pack ice. *Journal of Phycology* **41**: 763-69.

Peters, K. E., Walters, C. C. and Moldowan, J. M. (2007). The biomarker guide. volume 1, biomarkers and isotopes in the environment and human history. New York, Cambridge University Press.

Petrich, C. and Eicken, H. (2010). Growth, structure and properties of sea ice. Chichester, Blackwell publishing ltd

Polyak, L., Alley, R. B., Andrews, J. T., Brigham-Grette, J., Cronin, T. M., Darby, D A., Dyke, A S , Fitzpatrick, J. J., Funder, S , Holland, M , Jennings, A. E., Miller, G. H , O'Regan, M., Savelle, J , Serreze, M., St John, K., White, J W C. and Wolff, E. (2010). History of sea ice in the Arctic. *Quaternary Science Reviews* **29** 1757-78.

Poulin, M. (1990a). Family Naviculaceae: Arctic species Polar marine diatoms Medlin, L. K. and Priddle, J. Cambridge, British Antarctic Survey: 137-49.

Poulin, M. (1990b). Ice diatoms: the Arctic. Polar Marine Diatoms. Medlin, L K. and Priddle, J. Cambridge, British Antarctic Survey: 15-18.

Poulin, M. (1993) *Craspedopleura* (Bacillariophyta), a new diatom genus of arctic sea ice assemblages. *Phycologia* **32**: 223-33.

Poulin, M. and Cardinal, A (1982a). Sea ice diatoms from Manitounuk Sound, Southeastern Hudson Bay (Quebec, Canada). I. Family *Naviculaceae*. *Canadian Journal of Botany* **60**: 1263-78.

Poulin, M and Cardinal, A. (1982b). Sea ice diatoms from Manitounuk Sound, Southeastern Hudson Bay (Quebec, Canada). II Family *Naviculaceae*, genus *Navicula*. *Canadian Journal of Botany* **60** 2825-45.

Poulin, M and Cardinal, A. (1983). Sea ice diatoms from Manitounuk Sound, Southeastern Hudson Bay (Quebec, Canada). III *Cymbellaceae, Entomoneidaceae, Gomphonemataceae*, and *Nitzschiaceae*. *Canadian Journal of Botany* **61**: 107-18.

Powell, T. G. (1988). Scientific correspondance: Pristane/phytane ratio as environmental indicator. *Nature* **333**: 604.

Prahl, F. G., Muehlhausen, L. A. and Zahnle, D. L. (1988). Further evaluation of long-chain alkenones as indicators ofurther paleoceanographic conditions. *Geochimica et cosmochimica acta* **52**: 2303-10.

Prahl, F. G. and Wakeham, S. G. (1987). Calibration of unsaturation patterns in long-chain ketone compositions for palaeotemperature assessment. *Nature* **330**: 367-69.

Qiang, H., Hanesiak, J., Savelyev, S., Papakyriakou, T. and Taylor, P. A. (2008). Visibility during Blowing Snow Events over Arctic Sea Ice. Weather & Forecasting, American Meteorological Society. **23:** 741-51.

Rachold, V., Eicken, H., Gordeev, V. V., Grigoriev, M. N., Hubberton, H.-W., Lipsitin, A. P., Shevchenco, V. P. and Schirrmeister, L. (2004). Modern terrigenous organic carbon input to the Arctic Ocean. The organic carbon cycle in the Arctic Ocean. Stein, R. and Macdonald, E. W. London, Springer.

Rampen, S. W., Abbas, B. A., Schouten, S. and Sinninghe Damsté, J. S. (2010). A comprehensive study of sterols in marine diatoms (Bacillariophyta): Implications for their use as tracers for diatom productivity. *Limnology and oceanography* **55**: 91-105.

Reimnitz, E., Kempema, E. W., Weber, W. S., Clayton, J. R. and Payne, J. R. (1990). Suspended matter scavenging by rising frazil ice. *CRREL Monographs* **90**: 97-100.

Reuss, N. and Poulsen, L. K. (2002). Evaluation of fatty acids as biomarkers for a natural plankton community. A field study of a spring bloom and a post-bloom period off West Greenland. *Marine Biology* **141**: 423-34.

Richerol, T., Rochon, A., Blasco, S., Scott, D. B., Schell, T. M. and Bennett, R. J. (2008). Distribution of dinoflagellate cysts in surface sediments of the Mackenzie Shelf and Amundsen Gulf, Beaufort Sea (Canada). *Journal of Marine Systems* **74**: 825-39.

Riebesell, U., Schloss, I. and Smetacek, V. (1991). Aggregation of algae released from melting sea ice - Implications for seeding and sedimentation. *Polar biology* **11**: 239-48.

Riederer, M. and Muller, C. (2006). Biology of the plant cuticle. London, Blackwell.

Rieley, G. (1994). Derivatization of organic compounds prior to gas-chromatographic combustion-isotope ratio mass spectrometric analysis - identification of isotope fractionation processess. *The Analyst* **119**: 915-19.

Riemann, F. (1989). Gelatinous phytoplankton detritus aggregates on the Atlantic deep-sea bed - Structure and mode of formation. *Marine biology* **100**: 533-39.

Robock, A. (1980). The seasonal cycle of snow cover, sea ice and surface albedo. *Monthly Weather Review* **108**: 267-85.

Robson, J. N. and Rowland, S. J. (1986). Identification of novel widely distributed sedimentary acyclic sesterterpenoids. *Nature* **324**: 561-63.

Robson, J. N. and Rowland, S. J. (1988). Biodegradation of highly branched isoprenoid hydrocarbons: A possible explanation of sedimentary abundance. *Organic Geochemistry* **13**: 691-95.

Rochon, A. (2009). The ecology and biological affinity of Arctic dinoflagellates and their paleoceanographical significance in the Canadian High Arctic. From Deep-sea to Coastal Zones: Methods and Techniques for Studying Paleoenvironments, doi: 10.1088/1755-1307/5/1/012003.

Rolf, G., Michael, S. and Detlev, H. (1991). Development of Arctic sea-ice organisms under graded snow cover. *Polar Research* **10**: 295-308.

Rolland, N , Larocque, I., Francus, P., Pienitz, R and Laperrière, L. (2009). Evidence for a warmer period during the 12th and 13th centuries AD from chironomid assemblages in Southampton Island, Nunavut, Canada *Quaternary Research* **72**: 27-37

Rontani, J.-F., Koblizek, M., Beker, B , Bonin, P. and Kobler, Z. (2003). On the origin of *cis*-vaccenic acid photodegradation products in the marine environment *Lipids* **38**. 1085-92.

Rontani, J.-F., Mouzdahir, A., Michotey, V and Bonin, P (2002). Aerobic and anaerobic metabolism of squalene by a denitrifying bacterium isolated from marine sediment. Archives of Microbiology, Springer Science & Business Media B.V. **178:** 279-87

Rothwell, R G., Hoogakker, B., Thomson, J , Croudace, I. W. and Frenz, M (2006). Turbidite emplacement on the southern Balearic Abyssal Plain (western Mediterranean Sea) during Marine Isotope Stages 1-3: an application of ITRAX XRF scanning of sediment cores to lithostratigraphic analysis. New Techniques in Sediment Core Analysis. Rothwell, R G. London, The Geological Society of London. **267:** 79-98

Round, F E (2008). Personal communications Brown, T. A. Bristol.

Round, F E , Crawford, R. M. and Mann, D. G. (1990) The Diatoms: Biology and morphology of the genera. Cambridge, Cambridge University Press.

Rowland, S. J., Allard, W G., Belt, S. T., Massé, G., Robert, J M., Blackburn, S , Frampton, D., Revill, A T and Volkman, J. K. (2001a) Factors influencing the distribution of polyunsaturated terpenoids in the diatom, *Rhizosolenia setigera*. *Phytochemistry* **58**: 717-28

Rowland, S. J., Belt, S. T , Wraige, E J , Masse, G., Roussakis, C. and Robert, J M (2001b). Effects of temperature on polyunsaturation in cytostatic lipids of *Haslea ostrearia Phytochemistry* **56**: 597-602

Rowland, S. J. and Robson, J N (1990). The widespread occurence of highly branched acyclic C_{20}, C_{25} and C_{30} hydrocarbons in recent sediments and biota - a review *Marine Environmental Research* **30**. 191-216.

Rózanska, M , Gosselin, M., Poulin, M., Wiktor, J. M and Michel, C. (2009). Influence of environmental factors on the development of bottom ice protist communities during the winter-spring transition. *Marine Ecology Progress Series* **386**: 43-59

Rueda, G., Rosell-Melé, A., Escala, M., Gyllencreutz, R. and Backman, J. (2009). Comparison of instrumental and GDGT-based estimates of sea surface and air temperatures from the Skagerrak. *Organic Geochemistry* **40**. 287-91.

Ruhland, K., Priesnitz, A. and Smol, J P (2003). Paleolimnological evidence from diatoms for recent environmental changes in 50 lakes across Canadian Arctic treeline. *Arctic, Antarctic and Alpine Research* **35**: 110-23.

Sachs, J. P. and Anderson, R. F. (2003). Fidelity of alkenone paleotemperatures in southern Cape Basin sediment drifts. *Paleoceanography* **18**. 1082

Sakai, H , Ahagon, N., Narita, H., Ito, M and Itaki, T. (2003). Depth distribution of radiolarians from the Chukchi and Beaufort seas, western Arctic. *Deep-sea research Part I, Oceanographic research papers* **50** 1507-22.

Sakshaug, E. (2004). Primary and secondary production the Arctic Seas. The organic carbon cycle in the Arctic ocean. Stein, R. and Macdonald, R W. London, Springer.

Savelle, J. M., Dyke, A. S. and McCartney, A. P. (2000). Holocene bowhead whale (*Balaena mysticetus*) mortality patterns in the Canadian Arctic Archipelago. *Arctic* **53**. 414-21.

Scalan, E. S. and Smith, J. E. (1970). An improved measure of the odd-even predominance in the normal alkanes of sediment extracts and petroleum. *Geochimica et cosmochimica acta* **34**: 611-20.

Schell, T. M., Moss, T. J., Scott, D. B. and Rochon, A. (2008). Paleo-sea ice conditions of the Amundsen Gulf, Canadian Arctic Archipelago: Implications from the foraminiferal record of the last 200 years. *Journal of Geophysical Research* **113**: C03S02, doi:10.1029/2007JC004202.

Schmidt, S., Howa, H., Mouret, A., Lombard, F., Anschutz, P. and Labeyrie, L. (2009). Particle fluxes and recent sediment accumulation on the Aquitanian margin of Bay of Biscay. *Continental Shelf Research* **29**: 1044-52.

Schmidt, S., Jouanneau, J.-M., Weber, O., Lecroart, P., Radakovitch, O., Gilbert, F. and Jézéquel, D. (2007). Sedimentary processes in the Thau Lagoon (France): From seasonal to century time scales. *Estuarine, Coastal and Shelf Science* **72**: 534-42.

Schouten, S., Sinninghe Damste, J. S., Herfort, L., Schefuss, E., Weijers, J. W. H. and Hopmans, E. C. (2004). A novel proxy for terrestrial organic matter in sediments based on branched and isoprenoid tetraether lipids. *Earth and planetary science letters* **224**: 107-16.

Schubert, C. J. and Stein, R. (1996). Deposition of organic carbon in Arctic Ocean sediments: Terrigenous supply *vs.* marine productivity. *Organic Geochemistry* **24**: 421-36.

Schubert, C. J. and Stein, R. (1997). Lipid distribution in surface sediments from the eastern central Arctic Ocean. *Marine geology* **138**: 11-25.

Shiklomanov, I. A. (1998). comprehensive assessment of the freshwaterresources of the World: Assessment of eater resources and water availability in the World. WMO, UNDP, UNED, FAO et al., WMO. Geneva.

Sicre, M. A., Labeyrie, L., Ezat, U., Duprat, J., Turon, J. L., Schmidt, S., Michel, E. and Mazaud, A. (2005). Mid-latitude Southern Indian Ocean response to Northern Hemisphere Heinrich events. *Earth and planetary science letters* **240**: 724-31.

Sinninghe Damsté, J. S., Muyzer, G., Abbas, B., Rampen, S. W., Massé, G., Allard, W. G., Belt, S. T., Robert, J. M., Rowland, S. J., Moldowan, J. M., Barbanti, s. m., Fago, F. J., Denisevich, P., Dahl, J., Trindade, L. A. F. and Schouten, S. (2004). The Rise of the Rhizosolenid Diatoms. *Science* **304**: 584-87.

Sinninghe Damsté, J. S., Rijpstra, W. I., Schouten, S., Peletier, H., van der Maarel, M. J. E. C. and Gieskes, W. W. C. (1999). A C_{25} highly branched isoprenoid alkene and C_{25} and C_{27} *n*-polyenes in the marine diatom *Rhizosolenia setigera*. *Organic Geochemistry* **30**: 95-100.

Sinninghe Damsté, S., Rijpstra, W. I. P., Coolen, M. J. L., Schouten, S. and Volkman, J. K. (2007). Rapid sulphurisation of highly branched isoprenoid (HBI) alkenes in sulphidic Holocene sediments from Ellis Fjord, Antarctica. *Organic Geochemistry* **38**: 128-39.

Smart, C. W. (2002). Environmental application of deep-sea benthic foraminifera. Quaternary Environmental Micropalaeontology. Haslett, S. K. London, Oxford University Press.

Smetacek, V. S. (1985). Role of sinking in diatom life-history cycles: ecological, evolutionary and geological significance. *Marine biology* **84**: 239-51.

Smith, I. R. (2002). Diatom-based Holocene paleoenvironmental records from continental sites on Northeastern Ellesmere Island, high Arctic, Canada. *Journal of Paleolimnology* **27**: 9-28.

Smith, R E H., Cavaletto, J F., Eadie, B J. and Gardner, W. S. (1993). Growth and lipid composition of high Arctic ice algae during the spring bloom at Resolute, Northwest Territories, Canada. *Marine Ecology Progress Series* **97**: 19-29.

Smith, W. and Barber, D. (2007). Polynyas: Windows to the World Elsevier Science Ltd

Smith, W. O. and Nelson, D. M. (1986) Importance of ice edge phytoplankton production in the Southern Ocean. *Bioscience* **36**: 251-57.

Stein, R. and Macdonald, R. W. (2004). The organic carbon cycle in the Arctic Ocean. London, Springer.

Stoffyn, M. and Mackenzie, F. T. (1982). Fate of dissolved aluminum in the oceans. *Marine chemistry* **11**: 105-27.

Stokes, C. R., Clark, C D. and Winsborrow, M. C. M. (2006). Subglacial bedform evidence for a major palaeo-ice stream and its retreat phases in Amundsen Gulf, Canadian Arctic Archipelago. *Journal of quaternary science* **21**. 399-412.

Stoll, H. M. (2006). Climate change - The Arctic tells its story. *Nature* **441**: 579-81.

Sturm, M., Holmgren, J. and Perovich, D. K. (2002a). Winter snow cover on the sea ice of the Arctic Ocean at the Surface Heat Budget of the Arctic Ocean (SHEBA): Temporal evolution and spatial variability. *Journal of geophysical research* **107**.

Sturm, M., Perovich, D. K. and Holmgren, J. (2002b). Thermal conductivity and heat transfer through the snow on the ice of the Beaufort Sea. *Journal of geophysical research* **107**.

Sukhanova, I. N., Flint, M. V., Pautova, L A , Stockwell, D. A., Grebmeier, J. M. and Sergeeva, V. M. (2009). Phytoplankton of the western Arctic in the spring and summer of 2002: Structure and seasonal changes. *Deep-sea research Part II, Topical studies in oceanography* **56**: 1223-36.

Suzuki, M. and Muranaka, T (2007) Molecular Genetics of Plant Sterol Backbone Synthesis. *Lipids* **42**: 47-54.

Tamelander, T., Reigstad, M , Hop, H., Carroll, M. L. and Wassmann, P. (2008). Pelagic and sympagic contribution of organic matter to zooplankton and vertical export in the Barents Sea marginal ice zone *Deep-sea research. Part II, Topical studies in oceanography* **55**: 2330-39.

Ten Haven, H. L , de Leeuw, J. W., Rullkotter, J. and Sinninghe Damsté, J. S. (1987). Restricted utility of the pristane/phytane ratio as a palaeoenvironmental indicator. *Nature* **330**: 641-42.

Ten Haven, H. L., Rullkotter, J., De Leeuw, J. W and Sinninghe Damste, J. S. (1988). Pristane/phytane ratio as environmental indicator *Nature* **333** 604-04.

Theberge, M.-C., Prevost, D and Chalifour, F. P. (1996). The Effect of Different Temperatures on the Fatty Acid Composition of *Rhizobium leguminosarum* bv. viciae in the Faba Bean Symbiosis *New Phytologist* **134**: 657-64.

Thomas, D , Papadimitriou, S. and Michel, C. (2010). Biogeochemistry of sea ice. Sea ice (Second edition). Thomas, D and Dieckmann, G. Chichester, Wiley: 425-68.

Thomsen, H A. (1992). Plankton i de indre danske farvande. Havforskning fra Miljøstyrelsen Copenhagen, Scantryk

Thomson, J., Higgs, N C. and Colley, S (1996). Diagenetic redistributions of redox-sensitive elements in northeast Atlantic glacial/interglacial transition sediments. *Earth and planetary science letters* **139**. 365.

Tiselius, P. and Kuylenstierna, B. (1996). Growth and decline of a diatom spring bloom phytoplankton species composition, formation of marine snow and the role of heterotrophic dinoflagellates. *Journal of Plankton Research* **18**: 133-55.

Untersteiner, N. (1968) natural desalination and equilibrium salinity profile of perennial sea ice *Journal of geophysical research* **73**: 1251-57

Vare, L. L., Massé, G. and Belt, S. T. (2010). A biomarker-based reconstruction of sea ice conditions for the Barents Sea in recent centuries. *The Holocène* **20**: 637-43.

Vare, L. L., Massé, G., Gregory, T. R., Smart, C. W. and Belt, S. T. (2009). Sea ice variations in the central Canadian Arctic Archipelago during the Holocene. *Quaternary Science Reviews* **28**: 1354-66.

Venkatesan, M. I., Kaplan, I. R. and Ruth, E. (1983). Hydrocarbon geochemistry in surface sediments of Alaskan outer continental shelf .1. C-15+ Hydrocarbons. *AAPG bulletin* **67**: 831-40.

Vieno, P., David, G. L., Tatu, A. M., Jari, T. and Anna-Maija, L. (2000). Plant sterols: biosynthesis, biological function and their importance to human nutrition. *Journal of the Science of Food and Agriculture* **80**: 939-66.

Vincent, J.-S. (1982). The Quaternary history of Banks Island, N.W.T., Canada. *Géographie physique et Quaternaire,* **36**: 209-32.

Vincent, J. S. (1990). Late Tertiary and early Pleistocene deposits and history of Banks Island, Southwestern Canadian Arctic Archipelago. *Arctic* **43**: 339-63.

Volkman, J. K. (1986). A review of sterol markers for marine and terrigenous organic matter. *Organic Geochemistry* **9**: 83-99.

Volkman, J. K., Barrett, S. M., Blackburn, S. I., Mansour, M. P., Sikes, E. I. and Gelin, F. (1998). Microalgal biomarkers: A review of recent research developments. *Organic Geochemistry* **29**: 1163-79.

Volkman, J. K., Barrett, S. M. and Dunstan, G. A. (1994). C_{25} and C_{30} highly branched isoprenoid alkenes in laboratory cultures of two marine diatoms. *Organic Geochemistry* **21**: 407-14.

Volkman, J. K., Jeffrey, S. W., Nichols, P. D., Rogers, G. I. and Garland, C. D. (1989). Fatty acid and lipid composition of 10 species of microalgae used in mariculture. *Journal of Experimental Marine Biology and Ecology* **128**: 219-40.

von Quillfeldt, C. H. (1997). Distribution of diatoms in the Northeast Water Polynya, Greenland. *Journal of Marine Systems* **10**: 211-40.

Waite, A., Fisher, A., Thompson, P. A. and Harrison, P. J. (1997). Sinking rate versus cell volume relationships illuminate sinking rate control mechanisms in marine diatoms. *Marine ecology progress series* **157**: 97-108.

Walker, N. P., Partington, K. C., Van Woert, M. L. and Street, T. L. T. (2006). Arctic sea ice type and concentration mapping using passive and active microwave sensors. *IEEE transactions on geoscience and remote sensing* **44**: 3574-84.

Wang, J., Cota, G. F. and Comiso, J. C. (2005). Phytoplankton in the Beaufort and Chukchi Seas: Distribution, dynamics, and environmental forcing. *Deep-Sea Research Part II* **52**: 3355-68.

Wassmann, P. (1998). Retention versus export food chains: processes controlling sinking loss from marine pelagic systems. *Hydrobiologia* **363**: 29-57.

Wassmann, P., Andreassen, I., Reigstad, M. and Slagstad, D. (1996). Pelagic-benthic coupling in the Nordic Seas: The role of episodic events. *Marine ecology* **17**: 447-71.

Weiss, H. V. and Naidu, A. S. (1986). ^{210}Pb flux in an Arctic Coastal Region. *Arctic* **39**: 59-64.

Welch, H. E., Bergmann, M. A., Siferd, T. D., Martin, K. A., Curtis, M. F., Crawford, R. E., Conover, R. J. and Hop, H. (1992). Energy Flow thorough the Marine Ecosystem of the Lancaster Sound Region, Arctic Canada. *Arctic* **45**: 343-57.

Wen-Yen, H. and Meinschein, W. G. (1976). Sterols as source indicators of organic materials in sediments. *Geochimica et cosmochimica acta* **40**: 323-30.

Werne, J. P., Hollander, D. J., Behrens, A., Schaeffer, P., Albrecht, P. and Sinninghe Damsté, J. S. (2000). Timing of early diagenetic sulfurization of organic matter:

a precursor-product relationship in Holocene sediments of the anoxic Cariaco Basin, Venezuela *Geochimica et cosmochimica acta* **64**. 1741-51.

Werner, I. (2000) Faecal pellet production by Arctic under-ice amphipods – transfer of organic matter through the ice/water interface. *Hydrobiologia* **426**: 89-96.

Werner, I., Ikavalko, J. and Schunemann, H. (2007). Sea-ice algae in Arctic pack ice during late winter *Polar Biology* **30**: 1493-504.

Wheeler, P. A., Gosselin, M., Sherr, E., Thibault, D., Kirchman, D. L., Benner, R. and Whitledge, T. E. (1996). Active cycling of organic carbon in the central Arctic Ocean. *Nature* **380** 697-99.

Williams, W J. and Carmack, E. C. (2008). Combined effect of wind-forcing and isobath divergence on upwelling at Cape Bathurst, Beaufort Sea. *Journal of marine research* **66**: 645-63.

Wraige, E. J., Belt, S. T., Lewis, C A , Cooke, D. A., Robert, J. M., Massé, G. and Rowland, S. J. (1997). Variations in structures and distributions of C_{25} highly branched isoprenoid (HBI) alkenes in cultures of the diatom, *Haslea ostrearia* (Simonsen). *Organic Geochemistry* **27**: 497-505.

Wraige, E. J., Belt, S T., Massé, G. and Robert, J. M (1998a). Variations in distributions of C_{25} highly branched isoprenoid (HBI) alkenes in the diatom, *Haslea ostrearia*: influence of salinity. *Organic Geochemistry* **28**: 855.

Wraige, E. J., Belt, S. T., Massé, G., Robert, J. M and Rowland, S. J. (1998b). Variations in distributions of C_{25} highly branched isoprenoid (HBI) alkenes in the diatom, *Haslea ostrearia*: influence of salinity. *Organic Geochemistry* **28**: 855-59.

Wuchter, C., Schouten, S., Coolen, M. J. L and Damste, J. S. S. (2004). Temperature-dependent variation in the distribution of tetraether membrane lipids of marine Crenarchaeota: Implications for TEX_{86} paleothermometry. *Paleoceanography* **19**.

Yamashita, H., Takahashi, K. and Fujitani, N. (2002). Zonal and vertical distribution of radiolarians in the western and central Equatorial Pacific in January 1999. *Deep Sea Research Part II. Topical Studies in Oceanography* **49** 2823-62.

Yi-Sun, M., Clough, L M., Carroll, M. L , Dai, J., Ambrose Jr, W. G. and Lopez, G R. (2009) Different responses of two common Arctic macrobenthic species (*Macoma balthica* and *Monoporeia affinis*) to phytoplankton and ice algae: Will climate change impacts be species specific? *Journal of experimental marine biology and ecology* **376**: 110-21.

Ying, L., Kang-san, M and Shi-chun, S. (2000) Total lipid and fatty acid composition of eight strains of marine diatoms *Chinese Journal of Oceanology and Limnology* **18**: 345-49

Yunker, M B., Macdonald, R. W , Veltkamp, D. J and Cretney, W. J. (1995). Terrestrial and marine biomarkers in a seasonally ice-covered Arctic estuary - integration of multivariate and biomarker approaches. *Marine Chemistry* **49**: 1-50.

Zhu, J , Jabini, A , Golden, K M., Eicken, H and Morris, M. (2006) A network model for fluid transport through sea ice. *Annals of Glaciology* **44**: 129-33.

Zhukova, N. V. and Aizdaicher, N A (1995). Fatty acid composition of 15 species of marine microalgae. *Phytochemistry* **39**: 351-56.

FOLD-OUT LIPID STRUCTURES

Frequently referenced chemical structures

Highly branched isoprenoids

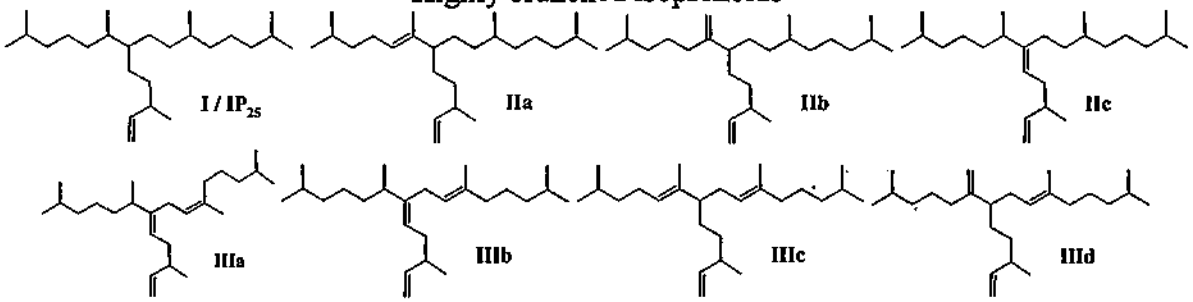

Fatty acids (Trimethylsilyl esters)

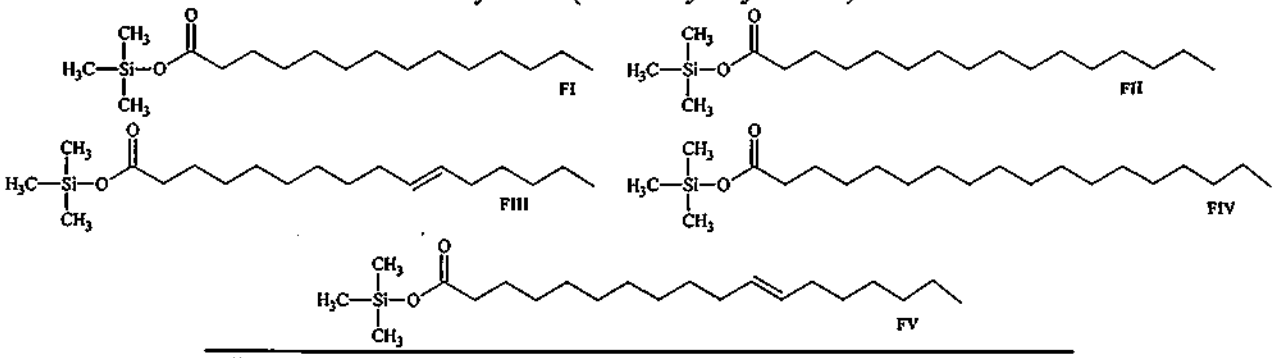

Identifier	IUPAC name	Trivial name
FI	Tetradecanoic acid	Myristic acid (C_{14})
FII	Hexadecanoic acid	Palmitic acid (C_{16})
FIII	*cis* -9-hexadecenoic acid	Palmitoleic acid ($C_{16:1\omega7}$)
FIV	Octadecanoic acid	Stearic acid (C_{18})
FV	*cis*-11-octadecenoic acid	*cis*-Vaccenic acid ($C_{18:1\omega7}$)

Sterols (Trimethylsilyl ethers)

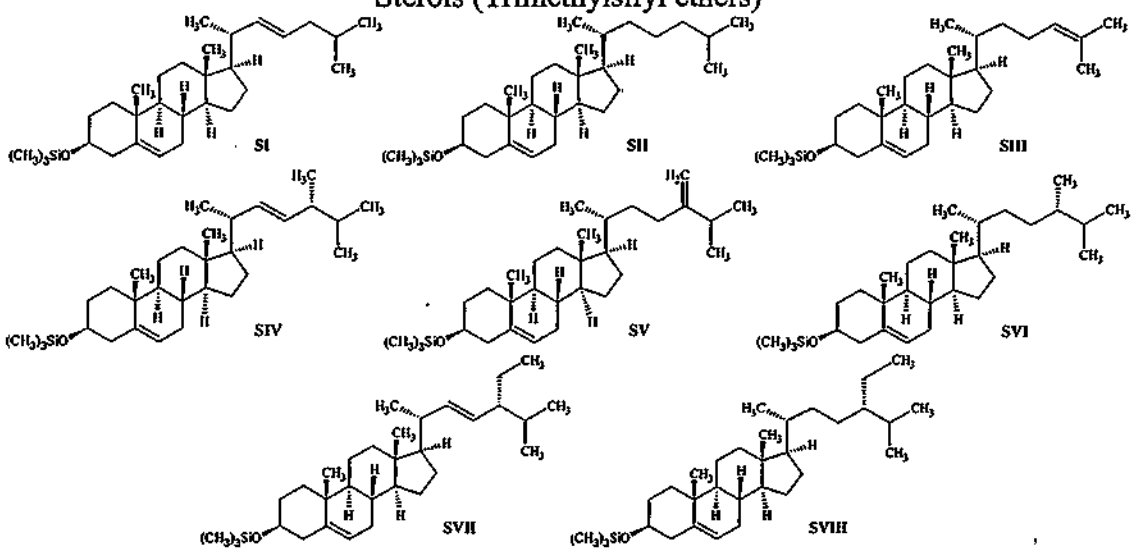

Identifier	IUPAC name	Trivial name
SI	Cholest-5,22*E*-dien-3β-ol	22-dehydrocholesterol
SII	Cholest-5-en-3β-ol	Cholesterol
SIII	Cholest-5,24-dien-3β-ol	Desmosterol
SIV	24-Methylcholesta-5,22*E*-dien-3β-ol	Brassicasterol
SV	24-Methylcholesta-5,24(28)-dien-3β-ol	Chalinasterol
SVI	24-Methylcholest-5-en-3β-ol	Campesterol
SVII	24-Ethylcholesta-5,22*E*-dien-3β-ol	Stigmasterol
SVIII	24-Ethylcholest-5-en-3β-ol	β-Sitosterol